ADA087051

LEVEL

SU-SEL-75-004
TR-3615-3

Second-Order Electromagnetic and Hydrodynamic Effects in High-Frequency Radio-Wave Scattering from the Sea

by

Donald E. Johnstone

March 1975

DTIC
ELECTE
JUL 2 1 1980
C

Technical Report No. 3615-3

DTIC FILE COPY

CENTER FOR RADAR ASTRONOMY

STANFORD ELECTRONICS LABORATORIES

STANFORD UNIVERSITY · STANFORD, CALIFORNIA

3 2 2 4 0 0   80 6 12 026

SEL-75-004

SECOND-ORDER ELECTROMAGNETIC AND HYDRODYNAMIC EFFECTS
IN HIGH-FREQUENCY RADIO-WAVE SCATTERING FROM THE SEA

by

Donald L. Johnstone

March 1975

DTIC
SELECTED
JUL 2 1 1980

C

Technical Report No. 3615-3

Prepared under

Radioscience Laboratory
Stanford Electronics Laboratories
Stanford University   Stanford, California

ABSTRACT

A theoretical analysis of high-frequency radio-wave scattering from the sea establishes relationships between the doppler continuum of observed radar echoes and the heights and propagation directions of ocean-surface waves. This provides new techniques for the remote sensing of sea-surface conditions by either monostatic or bistatic radars.

Integral expressions for the incremental surface radar cross section per unit frequency are derived, assuming a slightly rough time-varying random surface for the sea. These expressions are a function of surface-height directional spectra and contain electromagnetic and hydrodynamic effects to second order. First-order terms confirm that Bragg scattering from wave trains of a single frequency and direction is responsible for the discrete lines in observed doppler spectra; the second-order terms, which provide a continuum, are interpreted physically by a double Bragg-scattering process that involves an intermediate-scattered radio wave that may be either freely propagating or evanescent. A coordinate transformation provides paths of integration that can be related to specific features in observed doppler spectra and also results in a numerically efficient method for the evaluation of the second-order radar cross sections.

Doppler spectra calculated from model ocean wave-height directional spectra agree generally in shape, power content, and occurrence of swell with data from radar and oceanographic measurements. It is concluded that second-order effects and double Bragg scattering are responsible for most of the features in the continuum of doppler spectra of radar echoes from the sea. Parameters for estimating wind speed and direction, based on the variations of radar cross section with these conditions, are consistent with the available experimental data.

CONTENTS

CONTENTS (Cont)

ILLUSTRATIONS

ILLUSTRATIONS (Cont)

ILLUSTRATIONS (Cont)

TABLES

SYMBOLS

$A, A(t)$	collection of terms a constant
A_e	effective area of receive antenna
$A_1, A_2, \ldots, A_1$	antenna-pattern weighting factors
$A_{mn}, A_{mnI}, A(m,n,I,z)$	Fourier coefficients (may be superscripted to denote order)
$A_{zz}(\ )$	second partial derivative of $A(\ )$ with respect to z
a	wave number of the fundamental spatial period a constant defining directional distribution
$\hat{a}$	unit vector (may be subscripted by a coordinate reference)
$B, B(t)$	collection of terms
$B_{mn}, B_{mnI}, B(m,n,I)$	Fourier coefficients (may be superscripted to denote order)
$B_1(\ ), B_2(\ )$	integration constants
$b(\ )$	z-component of radio-wave propagation constant
$C, C(t)$	collection of terms
C	ocean-wave phase-velocity contour
C_o	ocean-wave phase-velocity cutoff
C_{mn}, C_{mnI}	Fourier coefficients (may be superscripted to denote order)
c	radio-wave propagation velocity
$c_1, \ldots, c_4$	integration constants
$\bar{c}$	contour
$D, D(t)$	collection of terms
d	differential operator distance (may be subscripted)
da, ds	incremental area (may be subscripted)

dv	incremental volume
$\overline{dc}$	incremental distance along contour
$\overline{ds}$	incremental area with direction $\overline{n}$
	incremental path length
E	electric field
$E(\ )$	exponential phase coefficient
$E(t), E(t+\tau)$	general function of time
E_i, E_s	incident and scattered electric fields
E_v, E_H	vertical and horizontal components of electric field
$E_x(\ ), E_y(\ ), E_z(\ ),$ $E_\theta(\ ), E_{\varphi}(\ )$	$x-$, $y-$, $z-$, $\theta-$, $\varnothing$-components of electric field (may appear without arguments)
$\overline{E}, \overline{E}(x,y,z)$	electric-field vector
$F(t)$	integration constant
$\mathscr{F}(t)$	Fourier transform
$f, f(\ )$	frequency
	surface height
	arbitrary function
f_B	Bragg frequency
f_o	transmitter frequency
f_x, f_y	partial derivatives of $f(x,y)$ with respect to x and y
f_{px}	x-component of pressure force per unit mass
$\overline{f}_g$	gravity force per unit mass
$\overline{f}_p$	pressure force per unit mass
G	antenna gain
$G(\Theta)$	directional distribution of wave-height spectrum
g	acceleration of gravity
H	height
H_x, H_y, H_z	x-, y-, z-components of magnetic field

$\bar{H}$		magnetic-field vector
h		depth
		wave height
h_o, h_1		z-component of radio-wave propagation constant in air and in conductor
I		summation index (may be subscripted or primed)
i		imaginary unit
J		summation index (may be subscripted or primed)
J, J_δ		Jacobians
$\bar{J}$		vector electric current density
K		partial integrand
k		ocean wave number (may be subscripted)
		summation index (may be subscripted or primed)
k_c		cutoff value of ocean wave number
k_m		mean wave number for swell
k_s		wave number for swell
k_{20}		ocean wave number fixed by doppler condition
$\bar{k}$		vector ocean wave number (may be subscripted)
L		surface spatial period
		ocean wavelength
		linear dimension
L(s)		ratio of gamma functions
L_x, L_y		x-, y-components of $\bar{L}$
$\bar{L}$		directional ocean wavelength
ℓ		summation index
m		summation index (may be subscripted or primed)
		integer variable
N, N(s)		directional distribution normalization constant
n		summation index (may be subscripted or primed)
		integer variable
		Bragg order

n_x, n_y, n_z	x-, y-, z-components of unit normal
$\bar{n}, \bar{n}_1$	unit normal vector
$P, P(\ )$	roughness coefficient (may be subscripted)
P_R, P_T	received and transmitted power
$\bar{P}$	general vector function
p	wave number (may be subscripted or primed) pressure
$Q(\ )$	product of two roughness coefficients
$\bar{Q}$	general vector function
q	wave number (may be subscripted or primed)
R	radial distance target-to-receiver distance
$R(\ )$	statistical autocorrelation or autocovariance function (may be subscripted)
R_1	transmitter-to-target distance integration region radius
R_2	target-to-receiver distance integration region radius
$R_{AA}, R_{AB}, \ldots$	autocorrelation of AA, BB, ...
$\mathcal{R}(\tau)$	time autocorrelation function (may be subscripted)
r	radial distance z-component of wave number
S, S_1	surfaces
S_i	incident power density at target
S_s	scattered power density at receiver
$S(\ ), S_{\omega,\Theta}(\ ),$ $S_{k_x, k_y}(\ )$	wave-height directional spectrum wave-height spectrum (one argument)
$S_w(\ )$	wind-generated wave-height directional spectrum
$S_s(\ )$	swell wave-height directional spectrum
$\bar{S}$	time-average power density

s	spread factor
T	Fourier-expansion time period
t	time variable (may be subscripted)
u	dummy integer or wave-number variable (may be primed) exponential phase factor (may be primed)
$u, u(z)$	wind speed
u_x, u_y, u_z	x-, y-, z-components of particle velocity
u_*	shear-stress (friction) velocity
$\bar{u}$	particle velocity
V	closed volume
v	dummy integer or wave-number variable (may be primed)
$\bar{v}$	ocean-wave velocity
$W, W(\ )$	surface roughness spectrum (may be superscripted to denote order, or subscripted)
$W_s, W_s(\ )$	swell-generated roughness spectrum
$W_w, W_w(\ )$	wind-generated roughness spectrum
w	fundamental time-harmonic in Fourier expansion
$X, X(\ )$	dummy variable
XI, XR	dummy argument of sinc function
x	dummy argument or variable rectangular coordinate (may be subscripted or primed)
$Y, Y(\ )$	dummy variable
YI, YR	dummy argument of sinc function
y	dummy argument or variable rectangular coordinate (may be subscripted or primed)
Z_s	conductor surface impedance
z	rectangular coordinate (may be subscripted or primed) position of fluid particle

α	sine of θ_i
β, β_i, β_r	radio-wave propagation constants
β_e	equilibrium range constant
$\beta_x, \beta_y, \beta_z$	x-, y-, z-components of vector wave number
$\bar{\beta}, \bar{\beta}_i, \bar{\beta}_r$	vector radio-wave numbers
$\hat{\beta}$	unit vector in direction of $\bar{\beta}$
$\Gamma, \Gamma(\ )$	gamma function kernel of cross-section integral
Γ_{EM}	electromagnetic kernel
Γ_H	hydrodynamic kernel
γ	cosine of θ_i
γ_0	x-component of radio-wave propagation constant in air
γ_1	x-component of radio-wave propagation constant in conductor
Δ	normalized surface impedance
Δk	maximum deviation of swell wave number
$\Delta\theta$	maximum deviation of swell direction
$\delta(\ )$	Dirac delta function
$\delta x, \delta y, \ldots$	incremental values of x, y, ...
ϵ	permittivity (may be subscripted) small constant (may be subscripted)
η	doppler shift characteristic impedance of free space
$\eta, \eta(\ )$	surface displacement or profile (may be superscripted to denote order)
η_x, η_y, η_z	partial derivative of surface displacement with respect to x, y, z (may have multiple subscripts or superscripted to denote order)
Θ	angle between ocean-wave and wind directions
Θ_r	resonance angle

θ	observation elevation angle (from zenith)
θ_i	incidence angle
θ_m	mean swell direction
θ_s	angle between radar and swell directions
θ_w	angle between radar and wind directions
κ	Karman's constant
Λ	constant relating Charnock's and Karman's constants
λ	wavelength
μ	permeability parameter relating wind and ocean-wave speeds
μ_o	cutoff value of μ-parameter
ν	integer variable Pierson-Moskowitz spectrum constant
ρ	charge density fluid density
$\bar{\rho}$	radial vector from origin to point on surface
$\sigma, \sigma_{VV}, \sigma_1, \sigma_2, \ldots, \sigma_i$	radar cross section incremental radar cross section (may appear with alternate upper-case subscripts)
$\sigma, \sigma_k, \sigma_\theta$	standard deviations
σ_c	conductivity
$\sigma(\omega), \sigma_{VV}(\omega), \sigma_{VV}(\eta)$	incremental radar cross section per unit frequency (may be superscripted to denote order or appear with alternate upper-case subscripts)
σ^o, σ_{VV}^o	incremental radar cross section for time-varying surfaces (may appear with alternate upper-case subscripts)
$\bar{\sigma}, \bar{\sigma}_{VV}$	statistical average incremental radar cross section for static surfaces (may be superscripted to denote order or appear with alternate upper-case subscripts)
τ	dummy time variable
Φ	scalar function

$\Phi(\omega)$	power spectral density (may be subscripted) wave-height (nondirectional) spectrum
$\Phi_{AA}, \Phi_{AB}, \cdots$	partial power spectral density for AA, AB, ...
$\emptyset$	observation azimuth angle (from x-axis)
φ	angle between wind and radar directions
$\varphi, \varphi_a, \varphi_b, \varphi(\ )$	velocity potential (may be superscripted to denote order)
$\varphi_x, \varphi_y, \varphi_z, \varphi_t$	partial derivatives of velocity potential with respect to x, y, z, t (may be superscripted to denote order or have multiple subscripts)
Ω	radian wave frequency (may be subscripted or primed)
ω	radian wave frequency (may be subscripted or primed)
ω_s, ω_w	swell and wind-generated radian wave frequencies
ω_B	Bragg radian frequency
ω_c	ocean-wave cutoff radian frequency
ω_d, ω_D	doppler radian frequencies
∇	gradient operator
$\nabla \cdot$	divergence operator
$\nabla \times$	curl operator
$\nabla \times \bar{u}$	vorticity

ACKNOWLEDGMENT

Chapter I

INTRODUCTION

In the mid-1950's, Crombie (1955) presented evidence indicating that radio waves reflected from the sea obey a Bragg-scattering law in which the ocean waves act as a diffraction grating. He argued that the sharp spectral lines observed in such radar echoes occur at precisely the doppler-shifted frequencies expected of signals scattered by ocean waves whose length is one-half the radio wavelength. The classical deep-water dispersion relationship where wave speed is proportional to the square root of the ocean wavelength explains the doppler shift. Because of the correspondence between ocean wavelength and observed doppler shift, Crombie suggested that ocean wave-height spectra could be studied by radar. From an experiment conducted at Wake Island, Teague et al (1973) determined the directional wave-height spectrum of 7 sec ocean waves by just such measurements of the discrete lines in the returned-signal doppler spectrum.

In addition to the sharp Bragg lines, the echo spectrum from ocean surfaces contains a continuum or sideband structure (Fig. 1) that cannot be explained by the simple Bragg theory originally proposed. Hasselmann
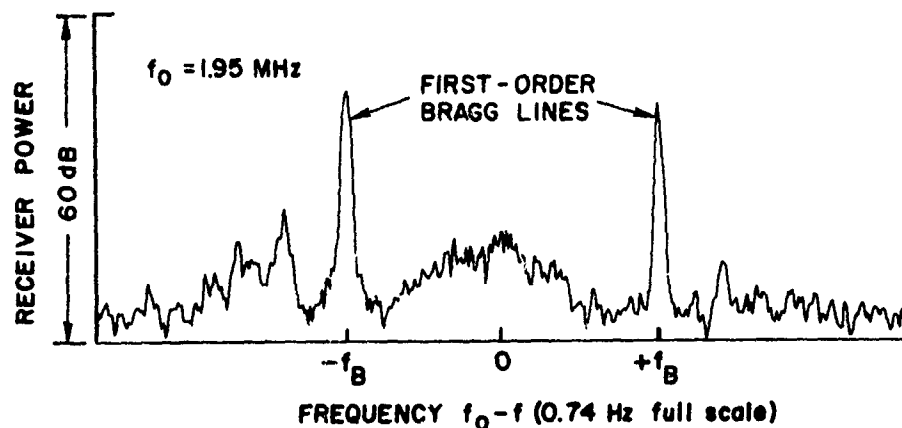
Fig. 1. BACKSCATTERED POWER VS DOPPLER SHIFT. Recorded at Wake Island in November 1972, this plot is typical of observed sea echo. The Bragg-line frequency is $f_B = 0.14$ Hz; transmitter frequency is f_o.

1

(1971) suggested that higher order wave-wave interactions, which can also produce surface periodicities of one-half the radar wavelength, are responsible for the continuum; however, his analysis indicates the presence of symmetrical sidebands about the first-order Bragg lines which is a contradiction to the observations presented in Fig. 1. In a more detailed analysis of the scattering problem, based on Rice's (1951) perturbation method, Barrick (1972) obtained an expression for the echo power spectrum (actually an expression for radar cross section per unit area per unit frequency) that produces a sideband structure more in accord with observations. An approach similar to Barrick's provides the starting point for the research presented here.

A. Motivation

Measurements at a single radio frequency [Tyler et al, 1973, 1974] have indicated that radar techniques can provide an order of magnitude improvement over conventional oceanographic methods in the determination of the directional distribution of ocean wave-height spectra; however, such techniques have utilized only the discrete Bragg lines to obtain this information. Because these lines represent radio-wave scattering from a single ocean-surface spectral component, multiple radio frequencies would be required to obtain data concerning additional components. The possibility of using the echo-spectrum continuum from a single radar frequency to determine a complete directional wave-height spectrum provides much of the stimulus for this research. In some applications, single-frequency coverage is a necessity. For example, remote sensing of ocean surfaces with high-frequency radio waves that propagate via the ionosphere is practical at only a few select radio frequencies that depend on the time of observation and the particular area of ocean surface to be covered. Additionally, at these high frequencies, the ocean waves producing the Bragg lines are often not indicative of the speed of the wind driving them (Appendix B) and, if remote tracking of wind velocity is of interest, the sidebands, which are a function of the entire wave-height spectrum (Chapter IV), become important.

The purpose of this research is to develop a theory to describe and predict doppler or echo spectra (with emphasis on the continuum) and to relate these spectra to the dynamics of the scattering surface. This would provide the means to eventually obtain directional wave-height spectra from the complete radar echo.

B. Organization

The electromagnetic theory for scattering from the perfectly conducting slightly rough surfaces proposed by Rice (1951) is developed in Chapter II. The scattered fields derived from Rice's perturbation solution to Maxwell's equations are applied to the Stratton-Chu integral [Stratton, 1941] to obtain second-order integral expressions, in terms of a surface-roughness spectrum for per unit area (or incremental) radar cross section per unit frequency. The impact of finitely conducting surfaces on radar cross section is also considered. Chapter III presents the hydrodynamic theory necessary to obtain a relationship for the second-order wave-height spectrum in terms of first-order spectra. Because of the nonlinearities in the ocean-surface boundary condition, perturbation techniques must again be employed, this time in the form of Tick's method [Kinsman, 1965]. Some of the proposed first-order wave-height spectral models are examined in preparation for the numerical evaluation of the integral expressions for radar cross section. A model for swell, which is expected to account for some of the unexplained features in observed radar spectra, is also developed. Attention has been restricted to deep-water ocean waves in which the effects of the ocean bottom and shorelines have been neglected. Chapters II and III contain basic derivations to accommodate the readers who are unfamiliar with either radar or oceanographic disciplines.

In Chapter IV, the scattering theory developed in Chapter II is combined with the hydrodynamic theory from Chapter III to produce second-order integral expressions for the incremental radar cross section per unit frequency for ocean surfaces. These expressions are interpreted in terms of a double Bragg-scattering process, and a transformation of coordinates leads to a numerically efficient method of evaluation.

Calculations of radar cross section for several of the first-order wave-height spectral models have also been included. Chapter V presents comparisons between predicted and measured radar doppler spectra, and Chapter VI provides a summary with recommendations for future research. Appendixes A and B are computational asides, and Appendix C is a collection of theoretical doppler-spectra plots for various wave-height spectral models.

C. Contributions

The major contributions produced by this work are as follows.

(1) Second-order integral expressions have been derived for the bistatic incremental radar cross section per unit frequency for ocean surfaces.

(2) Efficient methods have been specified and developed for evaluating the cross-section integrals.

(3) The relationship between the ocean-wave directional propagation constants, Bragg condition, and doppler theory that determines the sign of the doppler shift produced by individual ocean-wave trains has been physically interpreted.

(4) Swell has been included in the analyses of second-order spectra.

(5) Theoretical and observed doppler spectra for known oceanographic conditions have been compared in detail.

Chapter II

ELECTROMAGNETIC SCATTERING THEORY

The essence of any radar system is the ability of the system to provide information concerning a remote object or target, based entirely on how the object scatters electromagnetic waves. For example, the distance from the radar to a target can be determined from the time required for the radar signal to reach the target and return; the radial velocity of the target can be deduced from the returned radio-wave doppler shift, and its size can be estimated from the returned signal strength. The cause and effect relationship between object and scattered electromagnetic wave must be known, however, so as to relate a particular target characteristic to a characteristic of the scattered radio wave. This relationship is expressed by the radar cross section of the target.

Radar cross section σ is defined as that area which, when multiplied by the power density in the electromagnetic field incident on the scatterer, provides a power that, if reradiated isotropically, would produce the actual power density at the receive location. It is the connecting link between the physical attributes of the scatterer (such as size, shape, velocity, and electrical properties) and the scattered signal strength observed by the radar.

To understand this connection, consider a radar that is transmitting power P_T through an antenna with gain G with respect to an isotropic radiator (Fig. 2). The power density at an object some distance R_1 from the radar is

$$\frac{GP_T}{4\pi R_1^2}$$

By definition, the power

$$\sigma \times \frac{GP_T}{4\pi R_1^2}$$

if reradiated isotropically, results in a power density,

5

$$\sigma \times \frac{GP_T}{(4\pi)^2 R_1^2 R_2^2}$$

actually observed at the receiver a distance R_2 from the target. This power density multiplied by the effective area A_e of the receive antenna yields the radar received power P_R,

$$P_R = \sigma \times \frac{GP_T A_e}{(4\pi)^2 R_1^2 R_2^2}$$

As a result, the effect of the scatterer on received power is expressed through the radar cross section σ.
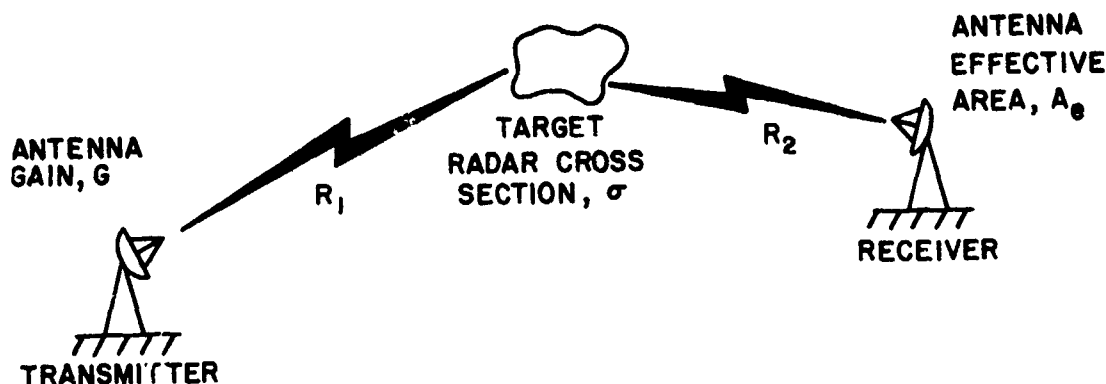
Fig. 2. RADAR GEOMETRY. Transmitting power P_T, this radar would receive scattered power $(P_T G \sigma A_e)/(4\pi R_1 R_2)^2$.

Generally, σ is a function of both the radar-target geometry and such target properties as size, shape, velocity, and electrical characteristics; therefore, a single measurement of received power is not sufficient to characterize the scattering properties of an object. Radar observers, however, usually seek information concerning the physical attributes of a target rather than its scattering properties. Although complete scattering properties may not be required to obtain the information desired, they may not be sufficient either; nevertheless, it is

from these properties, partial or complete, that this information must be extracted when radar techniques are employed.

The purpose of this chapter is to determine the scattering properties, in the form of an expression for radar cross section per unit area, for slightly rough time-varying surfaces. Because the results obtained here will be applied in Chapter IV to ocean surfaces, an equation for radar cross section is sought in terms of wave height, wavelength, and wave direction. These parameters are of interest to the ocean radar observer and are expressed conveniently in combined form as wave-height directional spectra.

The cross-section derivations that follow are approximate and obtained from first- and second-order perturbation solutions to Maxwell's equations. Such second-order expressions in terms of wave-height directional spectra have appeared previously [Barrick, 1970]; however, these were valid only for monostatic or backscatter (radar transmitter and receiver colocated) and grazing-incidence (mean target surface and radar transmitter coplanar) conditions; see Fig. 3a. Expressions valid for the arbitrary-incidence bistatic geometries illustrated in Fig. 3b will be derived here.

Section A discusses Rice's [1951] derivations for fields scattered by a time-invariant slightly rough random surface. Section B uses the Stratton-Chu integral [Stratton, 1941] to reformulate the Rice solutions in a form suitable for the calculation of incremental (per unit area) radar cross section. First- and second-order perturbation solutions for radar cross section in terms of random-surface spectra are derived in Section C. Sections D and E expand the Rice theory to include time-varying and finitely conducting surfaces, respectively. The specifics of ocean-surface radar cross section are described in Chapter IV after a discussion of hydrodynamic theory in Chapter III.

A. Rice's Scattering Theory

1. Surfaces and Statistics

Because ocean surfaces appear to be both random and regular (or periodic) depending on the height from which they are viewed

7

TRANSMITTER/RECEIVER

INCIDENT RAY
SCATTERED RAY
TARGET

a. Monostatic grazing-
incidence radar
(transmitter and
receiver colocated)

TRANSMITTER

INCIDENT
RAY

SCATTERED
RAY

RECEIVER

TARGET
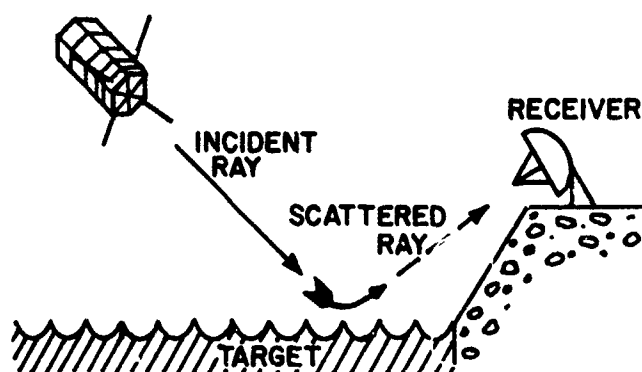
b. Bistatic radar
(transmitter and
receiver separated)

Fig. 3. MONOSTATIC AND BISTATIC RADARS. Grazing incidence occurs when
radar transmitter is pointed at horizon.

[Kinsman, 1965], it seems only natural that the mather tical model rep-
resenting them contains both features. Scattering   such a model
(Fig. 4) for time-invariant surfaces has been a: .e. by Rice [1951].

Following Rice, the surface height f(x,y) is represented by
a double Fourier series with gaussian-distributed complex ran   effi-
cients, where

$$f(x,y) = \sum_{mn} P(m,n) \, \exp[-ia(mx + ny)]^{\dagger} \qquad (2.1)$$

[†]Because up to eightfold summations will be encountered, the convention
of not repeating the Σ symbol for each sum will be maintained through-
out.

8
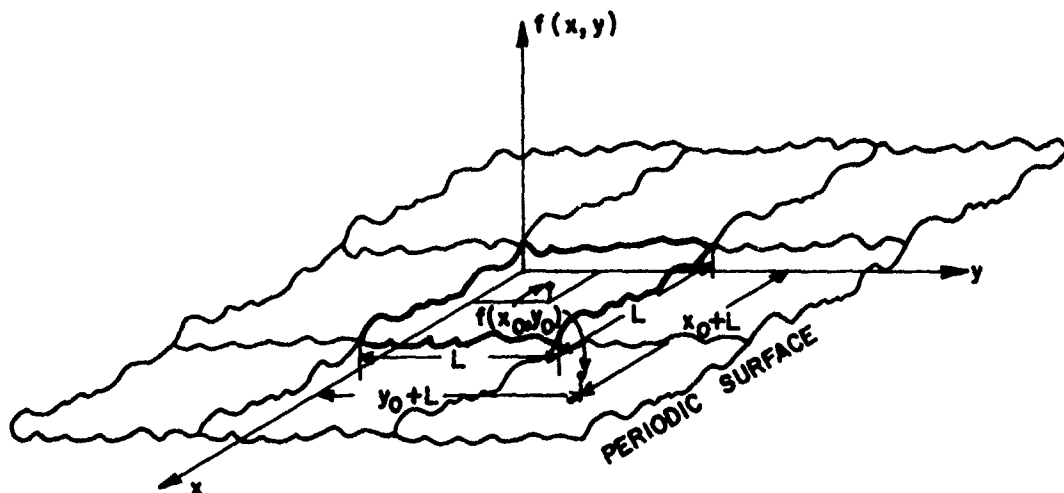
Fig. 4. PERIODIC ROUGH SURFACE. The surface profile at any point
(x_o, y_o) is duplicated at all points $(x_o + mL, y_o + nL)$, where
L is the spatial period and m and n are integers from $-\infty$ to
∞.

and

$a = 2\pi/L$ (L designates the spatial period of the surface)

$i = \sqrt{-1}$

$-\infty < m,n < \infty$

Because the surface height must be real, it is required that

$$P(m,n) = P^*(-m,-n)$$

where * denotes the complex conjugate.

Ocean wave-height measurements [Kinsman, 1965, Ch. 7] indicate
that a gaussian distribution closely represents actual wave-height dis-
tributions; however, there are obvious reasons why the actual distribu-
tion cannot be truly gaussian. One impressive reason is the small but
finite possibility of encountering ocean waves several hundreds of feet
high, or higher, if the wave-height distribution is exactly gaussian.
Backed by measurements and compelled by the need to simplify the ensuing
mathematics, a gaussian distribution will be assumed.

The statistics for $P(m,n)$ are summarized [Rice, 1951] as follows:

$$\langle P(m,n) \rangle = 0 \tag{2.2a}$$

$$\langle P(m,n)\ P(u,v) \rangle = 0 \qquad (u,v) \neq (-m,-n) \tag{2.2b}$$

$$\langle P(m,n)\ P^*(m,n) \rangle = \langle P(m,n)\ P(-m,-n) \rangle = \frac{\pi^2 W(p,q)}{L^2} \tag{2.2c}$$

where

$$p = am = 2\pi m/L$$

$$q = an = 2\pi n/L$$

$\langle \cdot \rangle$ = statistical average over the range of the argument for fixed m,n

$W(p,q)$ = surface-roughness spectrum

Condition (2.2a), the zero-mean assumption, simplifies the mathematics to follow without consequence to the results because each pectral component of the ocean surface is assumed to have the same mean level. Condition (2.2b), the independence assumption, is required for the following analysis but is not strictly valid for ocean surfaces. The nonbreaking deep-water ocean-wave profiles of interest here deviate slightly from true sinusoids [Kinsman, Ch. 5] and, therefore, contain higher order harmonics having related amplitudes in a Fourier representation. Nonlinear wave-wave interactions producing related harmonic terms also invalidate the independence assumption. Because a wave-profile deviation from a sinusoid can be interpreted as resulting from the wave-wave interaction of an ocean wave with itself [Stewart, 1974], a single phenomenon can be considered responsible for the violation of (2.2b). Fortunately, the effects of nonlinear wave interactions are small [Kinsman, 1965, Ch. 13] and can be represented as second-order perturbations to a first-order surface profile satisfying (2.2b). The roughness spectrum describes only this first-order profile, although second-order effects are examined in Chapter III and are included in the final expression for radar cross section (Chapter IV). Condition (2.2c) requires a more quantitative explanation.

10

The ocean wave-height spectra to be considered are obtained as the Fourier transform of the surface-height autocovariance function when the surface model is a wide-sense stationary process. The autocovariance of the Rice surface (2.1) is

$$R(x_1,x_2,y_1,y_2) = \left\langle f(x_1,y_1) \cdot f^*(x_2,y_2) \right\rangle$$

$$= \left\langle \sum_{mn} P(m,n) \exp\left[-ia(mx_1 + ny_1)\right] \right.$$

$$\left. \cdot \sum_{m'n'} P^*(m',n') \exp\left[ia(m'x_2 + n'y_2)\right] \right\rangle$$

Because $\langle P \cdot P^* \rangle = 0$, unless $m = m'$ and $n = n'$,

$$R(x,y) = R(x_1 - x_2, y_1 - y_2)$$

$$= \sum_{mn} \langle P(m,n) P^*(m,n) \rangle \exp\left\{-ia\left[m(x_1 - x_2) + n(y_1 - y_2)\right]\right\}$$

Use of the two-dimensional Fourier transform,

$$\frac{1}{(2\pi)^2} \iint_{-\infty}^{\infty} R(x,y) \exp\left[-ia(m_o x + n_o y)\right] dxdy$$

provides the surface spectrum

$$W(m_o,n_o) = \sum_{mn} \langle P(m,n) P^*(m,n) \rangle \frac{1}{(2\pi)^2} \iint_{-\infty}^{\infty} \exp\left\{-ia\left[x(m_o + m) + y(n_o + n)\right]\right\} dxdy$$

The above integrals are expressions of the Dirac delta function defined in one form [Bracewell, 1965, p. 357] by

11

$$\delta(k) = \frac{1}{2\pi} \int_{-\infty}^{\infty} e^{-ikx} \, dx$$

therefore,

$$W(m_o, n_o) = \sum_{mn} \langle P(m,n) \, P^*(m,n) \rangle \; \delta(am + am_o) \; \delta(an + an_o)$$

If the double summation is treated as a double integral,[†] then

$$W(m_o, n_o) = \iint_{-\infty}^{\infty} \langle P(m,n) \, P^*(m,n) \rangle \; \delta(p + p_o) \; \delta(q + q_o) \, dmdn$$

where $p = am$, $q = an$, $p_o = am_o$, $q_o = an_o$.

Changing variables from m to p, n to q, etc. leads to

$$W(p_o, q_o) - \iint_{-\infty}^{\infty} \left(\frac{L}{2\pi}\right)^2 \langle P(m,n) \, P^*(m,n) \rangle \; \delta(p + p_o) \; \delta(q + q_o) \, dpdq$$

which, with the aid of the delta-function sampling property, integrates to

$$W(p_o, q_o) = \left\langle P(m_o, n_o) \, P^*(m_o, n_o) \right\rangle \left(\frac{L}{2\pi}\right)^2$$

for any p_o and q_o. Generally, then, the average of $P(m,n) \, P^*(m,n)$, in terms of the surface-height spectrum, becomes

$$\langle P(m,n) \, P^*(m,n) \rangle = \left(\frac{2\pi}{L}\right)^2 W(p,q)$$

[†] Details of the limiting process for transition from summations to integrations can be found in many texts [Cheng, 1959, Ch. 5].

Rice's roughness spectrum is seen to be 2^2 larger (one factor of 2 for each dimension of the Fourier transform) than the surface-height spectrum as defined by the Fourier transform of the surface-height auto-covariance. To facilitate reference to Rice's work, the roughness-spectrum definition will be employed throughout the following derivations; when the alternate definition is used, the differences will be noted.

2. Electromagnetic-Field Expansion and Boundary Conditions

An initial step in determining the radar cross section for the surface in Eq. (2.1) is to relate the scattered electromagnetic field to the incident field. This can be simplified by assuming the surface to be perfectly conducting. Although ocean-surface conductivity is not infinite, it is sufficiently high for the effects of finite conductivity to be expressed as a perturbation to the perfectly conducting theory (Section E).

The incident field can be represented by a plane wave propagating in the x,z-plane (Fig. 5). Described by its electric-field vector $\overline{E} \exp[-i\beta(\alpha x - \gamma z) + i\omega t]$, the plane wave is considered either horizontally
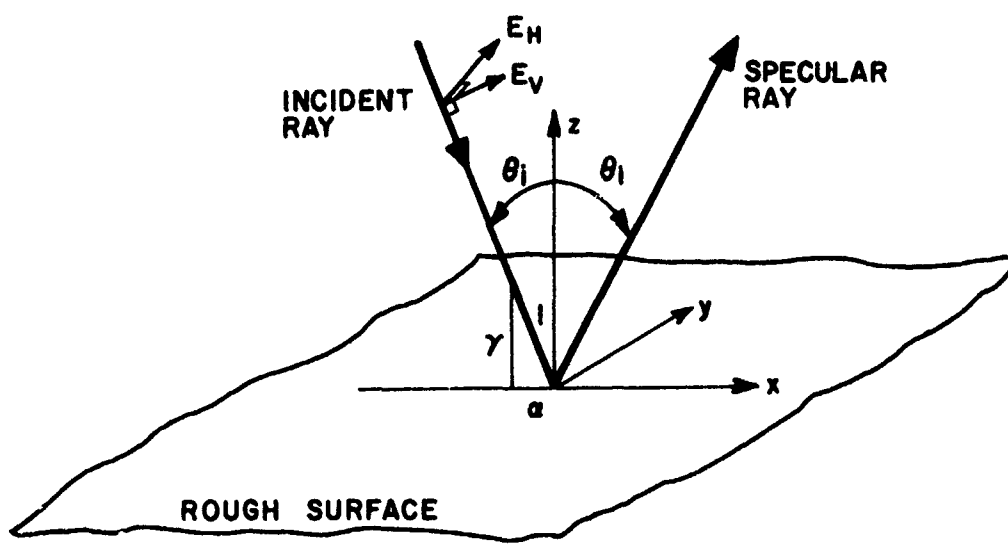
Fig. 5. INCIDENT FIELDS AND SPECULAR DIRECTION. E_V and E_H are vertically and horizontally polarized components of the incident electric field.

polarized ($\overline{E}$ perpendicular to the x,z-plane) or vertically polarized ($\overline{E}$ in the x,z-plane). Generally, $\overline{E}$ is a complex vector of the form $E\,\hat{a}$, where $\hat{a}$ is a unit vector in the direction of $\overline{E}$, and E is a complex quantity assumed here to have unity magnitude ($|E| = 1$). The coefficients α and γ are the sine and cosine of the incidence angle θ_i illustrated in Fig. 5, and β is the free-space propagation constant $2\pi/\lambda$, where λ is the wavelength of the incident wave. The time factor $\exp(i\omega t)$ will henceforth be assumed, where ω is the radian frequency of the wave.

Following Rice, the total electromagnetic field above the surface is expressed as a sum of the incident field, fields reflected in the absence of surface roughness, and those fields scattered because of surface roughness. Waves reflected in the absence of surface roughness propagate in a single direction (specular) determined by Snell's law (Fig. 5). Waves scattered by surface roughness can propagate in all directions, including specular, and will be referred to as nonspecular scattered waves. Total fields are used at this point to satisfy the boundary conditions at the surface. Later, scattered fields are obtained by removing the incident field from the total-field expressions.

Because surface roughness is periodic in the x,y-plane (Fig. 4), the nonspecular scattered fields will also be periodic, with the same period, in this plane and, therefore, can be expressed by a two-dimensional Fourier series. Solving for the coefficients of this series in terms of the roughness coefficients $P(m,n)$ produces the desired scattered-field expressions as a function of surface roughness.

For horizontally polarized incident waves, components (Fig. 6) of the total field $\overline{E}(x,y,z)$ are

$$E_x = \sum_{mn} A_{mn}\, E(m,n,z) \qquad\qquad (2.3a)$$

$$E_y = 2i \sin \beta\gamma z \, \exp(-i a \nu x) + \sum_{mn} B_{mn}\, E(m,n,z) \qquad (2.3b)$$

$$E_z = \sum_{mn} C_{mn}\, E(m,n,z) \qquad\qquad (2.3c)$$
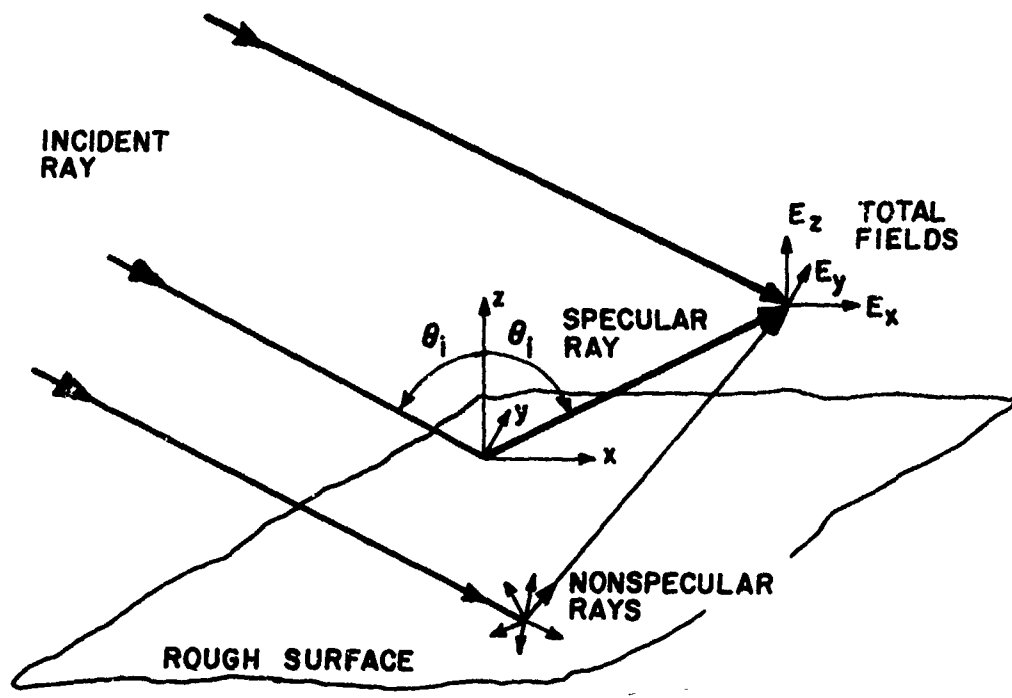
Fig. 6. TOTAL FIELDS ABOVE A SURFACE. The total electromagnetic field at any point above a surface is a vector sum of the specular and nonspecular scattered fields plus the incident field.

where

$$E(m,n,z) = \exp[-ia(mx + ny) - ib(m,n) z] \qquad (2.4)$$

and the summations are from $-\infty$ to ∞.

To satisfy the wave equation $\nabla^2 \overline{E} + \beta^2 \overline{E} = 0$,

$$b(m,n) = \begin{cases} \left(\beta^2 - a^2 m^2 - a^2 n^2\right)^{1/2} & a^2 m^2 + a^2 n^2 < \beta^2 \\ -i\left(a^2 m^2 + a^2 n^2 - \beta^2\right)^{1/2} & a^2 m^2 + a^2 n^2 > \beta^2 \end{cases} \qquad (2.5)$$

For $b(m,n)$ imaginary, the negative root is specified to provide the decaying, rather than the increasing, exponential solution to the wave equation that $\overline{E}(x,y,z)$ must satisfy.

15

The first term in the expression for E_y is the total field that would exist above a perfectly conducting flat plane. For any incidence angle θ_i, this term can be written as

$$\underbrace{\exp[-i\beta(\alpha x - \gamma z)]}_{\text{incident}} - \underbrace{\exp[-i\beta(\alpha x + \gamma z)]}_{\text{reflected}} = \underbrace{2i\ \sin\ (\beta\gamma z)\ \exp(-i\beta\alpha x)}_{\text{total}}$$

where $\alpha = \sin\theta_i$ and $\gamma = \cos\theta_i$ (Fig. 5).

To determine the Fourier coefficients A_{mn}, B_{mn}, and C_{mn}, the above term must be periodic, thereby restricting incidence angles to the discrete values given by $\beta\sin\theta_i = 2\pi\nu/L = a\nu$, where ν is an integer. Equation (2.3b) contains this restriction. For large L, almost any desired angle of incidence is permissible. Later, L is allowed to become infinite, thereby removing this restriction on θ_i. These coefficients are found by satisfying the tangential electric-field boundary condition to order $\beta^2 f^2(x,y)$; higher order terms are neglected.

The tangential electric field at any point on the surface can be written as

$$\overline{E} - \overline{n}(\overline{E}\cdot\overline{n}) = \overline{0} \qquad (2.6)$$

where $\overline{n}$ is the unit vector normal to the surface at this point (Fig. 7), and $\overline{0}$ is the null vector. Expanded into its components, Eq. (2.6) becomes

$$E_x - n_x(E_x n_x + E_y n_y + E_z n_z) = 0$$

$$E_y - n_y(E_x n_x + E_y n_y + E_z n_z) = 0 \qquad (2.7)$$

$$E_z - n_z(E_x n_x + E_y n_y + E_z n_z) = 0$$

The unit normal components can be written [Sokolnikoff and Redheffer, 1958] as

16

$$n_x = -f_x \left(1 + f_x^2 + f_y^2\right)^{-1/2}$$

$$n_y = -f_y \left(1 + f_x^2 + f_y^2\right)^{-1/2} \qquad (2.8)$$

$$n_z = \left(1 + f_x^2 + f_y^2\right)^{-1/2}$$

where f_x and f_y are the partial derivatives of $f(x,y)$ with respect to x and y and are assumed to be of order f.
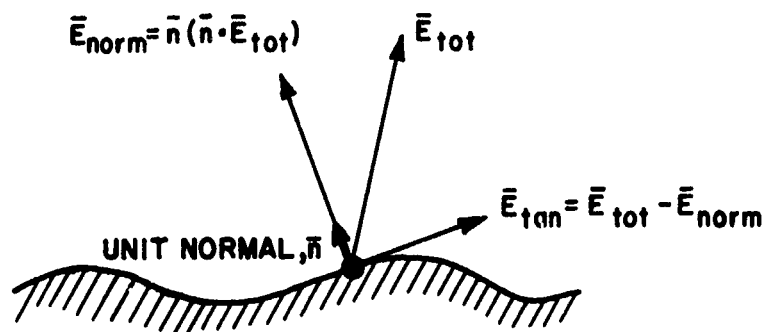
Fig. 7. FIELD COMPONENTS AT SURFACE BOUNDARY.

Writing the first two boundary conditions in Eqs. (2.7) in terms of the unit normal components and retaining only terms of order $\beta^2 f^2$ provides the boundary conditions to second order,

$$E_x + f_x E_z = 0$$

$$\qquad (2.9)$$

$$E_y + f_y E_z = 0$$

Expansion of the field components in Eqs. (2.3) in increasing orders of f at the surface yields

$$\sin \beta\gamma f = \beta\gamma f + \text{order } (f^3)$$

$$E(m,n,f) = [1 - ib(m,n) \; f + \ldots] \; E(m,n,o)$$

$$A_{mn} = A_{mn}^{(1)} + A_{mn}^{(2)} + \ldots$$

where $A_{mn}^{(1)}$ is of order βf and $A_{mn}^{(2)}$ is of order $\beta^2 f^2$. Similar expressions exist for B_{mn} and C_{mn}. The boundary conditions (2.9) for horizontal polarization now become

$$\sum_{mn} \left[A_{mn}^{(1)} + A_{mn}^{(2)} + f_x C_{mn}^{(1)} \right] [1 - ib(m,n) \; f] \; E(m,n,o) = 0$$

and

$$2i \exp(-ia\nu x) \cdot \beta\gamma f + \sum_{mn} \left[B_{mn}^{(1)} + B_{mn}^{(2)} + f_y C_{mn}^{(1)} \right] [1 - ib(m,n)f] \; E(m,n,o) = 0$$

$$(2.10)$$

when terms of order $\beta^3 f^3$ and higher are neglected.

Equating separately the first- and second-order terms in (2.10) to zero results in

$$\sum_{mn} A_{mn}^{(1)} \; E(m,n,o) = 0 \qquad\qquad (2.11a)$$

$$2i \exp(-ia\nu x) \; \beta\gamma f + \sum_{mn} B_{mn}^{(1)} \; E(m,n,o) = 0 \qquad (2.11b)$$

and

$$\sum_{mn} \left[A_{mn}^{(2)} + f_x C_{mn}^{(1)} - ib(m,n) \; f \; A_{mn}^{(1)} \right] E(m,n,o) = 0 \qquad (2.11c)$$

$$\sum_{mn} \left[B_{mn}^{(2)} + f_y C_{mn}^{(1)} - ib(m,n) \; f \; B_{mn}^{(1)} \right] E(m,n,o) = 0 \qquad (2.11d)$$

Expression (2.11a) specifies that $A_{mn}^{(1)} = 0$, thereby leaving three equations and four unknown coefficients, $A_{mn}^{(2)}$, $B_{mn}^{(1)}$, $B_{mn}^{(2)}$, and $C_{mn}^{(1)}$.

The additional equation required for the solution of these unknown coefficients develops from the divergence theorem $\nabla \cdot \overline{E} = 0$ which, when applied to (2.3), provides

$$am\, A_{mn}^{(i)} + an\, B_{mn}^{(i)} + b(m,n)\, C_{mn}^{(i)} = 0$$

to each order i. Detailed solutions to these equations have been derived by Rice (1951).

The coefficient solutions applied to the field equations (2.3), with the incident field $E_y(\text{incident}) = \exp[-i\beta(\alpha x - \gamma z)]$ removed, determine the scattered fields at any point above the surface in terms of the random-surface coefficients $P(m,n)$. For horizontally polarized incident waves,

$$E_x = -2\beta\gamma \sum_{mn} E(m,n,z) \sum_{k\ell} a^2(m - k)\,\ell\, Q(m,n,k,\ell)$$

$$E_y = -\exp[-i\beta(\alpha x + \gamma z)] - 2\beta\gamma \sum_{mn} E(m,n,z)\left\{ iP(m - \nu,n) \right.$$

$$\left. + \sum_{k\ell} \left[a^2(n - \ell)\,\ell - b^2(k,\ell) \right] Q(m,n,k,\ell) \right\} \qquad (2.12)$$

$$E_z = 2\beta\gamma \sum_{mn} \frac{E(m,n,z)}{b(m,n)} \left\{ ianP(m - \nu,n) \right.$$

$$\left. + \sum_{k\ell} \left[a^3\ell(m^2 + n^2 - mk - n\ell) - anb^2(k,\ell) \right] Q(m,n,k,\ell) \right\}$$

where $Q(m,n,k,\ell) = P(k - \nu,\ell)\, P(m - k,n - \ell)/b(k,\ell)$, and summations are again from $-\infty$ to ∞.

A similar perturbation procedure applied to vertically polarized incident waves yields

$$E_x = -\gamma \exp[-i\beta(\alpha x + \gamma z)] + 2 \sum_{mn} E(m,n,z) \Big\{ i(\alpha am - \beta) P(m - \nu, n)$$

$$+ \sum_{k\ell} \Big[a^2(m - k)(\nu - k) \beta + (\beta - \alpha am) b^2(k,\ell) \Big] Q(m,n,k,\ell) \Big\}$$

$$E_y = 2a \sum_{mn} E(m,n,z) \Big\{ i\alpha n P(m - \nu, n)$$

$$+ \sum_{k\ell} \Big[a(n - \ell)(\nu - k) \beta - \alpha n b^2(k,\ell) \Big] Q(m,n,k,\ell) \Big\} \tag{2.13}$$

$$E_z = \alpha \exp[-i\beta(\alpha x + \gamma z)] + 2 \sum_{mn} \frac{E(m,n,z)}{b(m,n)}$$

$$\cdot \Big\{ i \Big[a(m - \nu)\beta + \alpha b^2(m,n) \Big] P(m - \nu, n) + \sum_{k\ell} \Big[a^3(k - \nu)(m^2 + n^2 - mk - n\ell)\beta$$

$$+ a \Big[\alpha a(m^2 + n^2) - m\beta \Big] b^2(k,\ell) \Big] Q(m,n,k,\ell) \Big\}$$

Expressions (2.12) and (2.13) represent the scattered fields above a slightly rough surface in terms of the surface parameters and are the desired results from Rice's theory. The price paid for these expressions is the restriction to <u>slightly</u> rough surfaces (βf, βf_x, βf_y must be small compared to unity). An analysis carried to order $(\beta f)^3$ is required to estimate the error in these second-order results; however, such an analysis will not be undertaken here. Instead, measured and predicted radar-received powers will be compared in Chapter V to determine the validity of the second-order theory.

B. Stratton-Chu Integral

The previously derived expressions for scattered fields, (2.12) and
(2.13), assume a surface of infinite extent with plane waves incident on
the entire surface. Most practical radars, however, have limited cover-
age and only portions of the total target surface may fall within this
coverage. It is convenient, therefore, to describe the scattering prop-
erties of such large surfaces in terms of a radar cross section per unit
area. The fields scattered from a finite surface area must be known.
however, to determine this incremental radar cross section. The trans-
formation from infinite to finite surface-scattered vector fields was
first derived by Stratton and Chu [Stratton, 1941, pp. 464-470] and,
henceforth, will be called the Stratton-Chu integral.

The starting point for this integral is a vector form of Green's
second identity. Let V be a closed volume (Fig. 8) bounded by a sur-
face S, and let $\overline{P}$ and $\overline{Q}$ be two vector functions of position which,
along with their first and second derivatives, are continuous throughout
V and on S. Applying the divergence theorem to the vector $P \times \nabla \times \overline{Q}$
and expanding the volume integral yields the vector form of Green's first
identity,

$$\int_V \nabla \cdot (\overline{P} \times \nabla \times \overline{Q}) \, dv = \int_V (\nabla \times \overline{P} \cdot \nabla \times \overline{Q} - \overline{P} \cdot \nabla \times \nabla \times \overline{Q}) \, dv$$

$$= \int_S (P \times \nabla \times Q) \cdot \overline{n} \, da \qquad (2.14)$$

where $\overline{n}$ is the unit normal to the surface S. Interchanging the roles
of $\overline{P}$ and $\overline{Q}$ and subtracting the resultant integral from (2.14) leads
to the vector form of Green's second identity,

$$\int_V (\overline{Q} \cdot \nabla \times \nabla \times \overline{P} - \overline{P} \cdot \nabla \times \nabla \times \overline{Q}) \, dv = \int_S (\overline{P} \times \nabla \times \overline{Q} - \overline{Q} \times \nabla \times \overline{P}) \cdot \overline{n} \, da$$

$$(2.15)$$
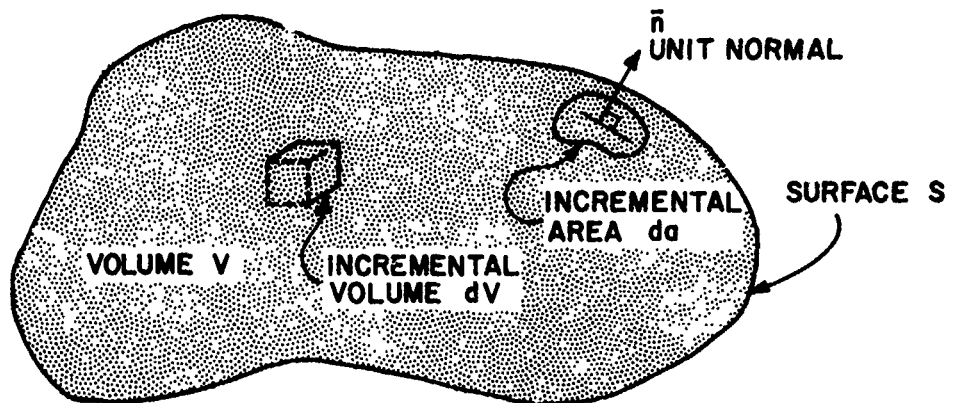
Fig. 8. VOLUME V BOUNDED BY SURFACE S.

Let $\bar{P} = \bar{E}$ and $\bar{Q} = \Phi\hat{a}$, with $\hat{a}$ an arbitrary unit vector and Φ a scalar function. Require $\bar{Q}$ to satisfy the wave equation,

$$\nabla^2\bar{Q} + \omega^2\mu\epsilon\bar{Q} = 0$$

and $\bar{E}$ to satisfy Maxwell's equations,

$$\nabla \times \bar{E} = -i\omega\mu\bar{H}$$

$$\nabla \times \bar{H} = i\omega\epsilon\bar{E} + \bar{J}$$

$$\nabla \cdot \bar{H} = 0$$

$$\nabla \cdot \bar{E} = \rho/\epsilon$$

where

μ,ϵ = permeability and permittivity of the volume material

$\bar{J}$ = current density

ρ = charge density

ω = radian frequency

Under these conditions, Green's second identity becomes

22

$$\int_V -i\omega\mu\bar{J}\Phi + \frac{\rho\nabla\Phi}{\epsilon}\, dv = \int_S [-i\omega\mu(\bar{n} \times \bar{H})\,\Phi + (n \times \bar{E}) \times \nabla\Phi + (\bar{n} \cdot \bar{E})\,\nabla\Phi]\, da$$

$$(2.16)$$

Now consider a source-free volume enclosing a small sphere about the point (x',y',z') as illustrated in Fig. 9, where the sphere has a surface S_1 with a unit normal $\bar{n}_1$. Equation (2.16) then becomes

$$\int_S [-i\omega\mu(\bar{n} \times \bar{H})\,\Phi + (\bar{n} \times \bar{E}) \times \nabla\Phi + (\bar{n} \cdot \bar{E})\,\nabla\Phi]\, da$$

$$+ \int_{S_1} \left[-i\omega\mu(\bar{n}_1 \times \bar{H})\Phi + (\bar{n}_1 \times \bar{E}) \times \nabla\Phi + (\bar{n}_1 \cdot \bar{E})\nabla\Phi\right] da_1 = 0$$

When the radius of the sphere tends to zero with $\Phi = e^{-i\beta r}/r$, where $r^2 = (x - x')^2 + (y - y')^2 + (z - z')^2$ and $\beta = 2\pi/\lambda$, Stratton has shown that the surface integral over S_1 is $-4\pi\bar{E}(x',y',z')$. Because the point (x',y',z') can be anywhere within V, the E-field at any point in V can be written as an integral over the surface fields,

$$\bar{E}(x',y',z') = \frac{1}{4\pi} \int_S [-i\omega\mu(\bar{n} \times \bar{H})\,\Phi + (\bar{n} \times \bar{E}) \times \nabla\Phi + (\bar{n} \cdot \bar{E})\,\nabla\Phi]\, da$$

$$(2.17)$$
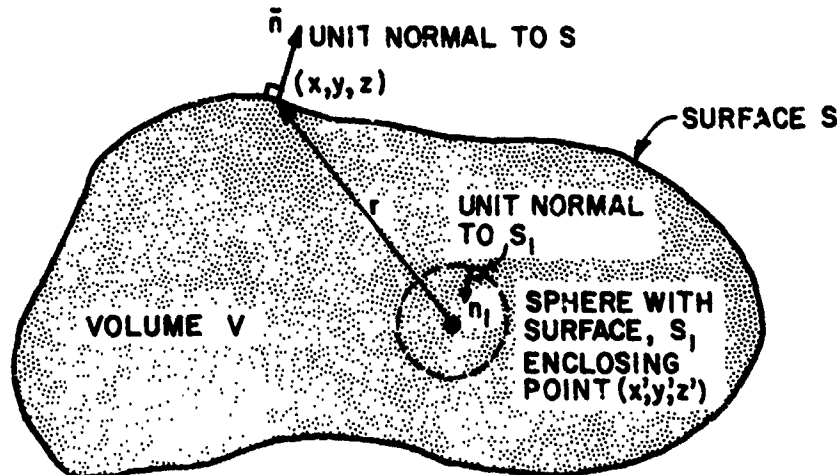
Fig. 9. EXTERNAL POINT ENCLOSED BY VOLUME V.

Now, let V be the hemisphere enclosed by $S + S_1$ (Fig. 10) and let the radius of the hemisphere extend to infinity. From Eq. (2.17), fields at any point above the x,y-planes can be calculated if they are known on S_1 and S. For convenience, $\bar{n}$ is directed into the volume with no effect on (2.17).
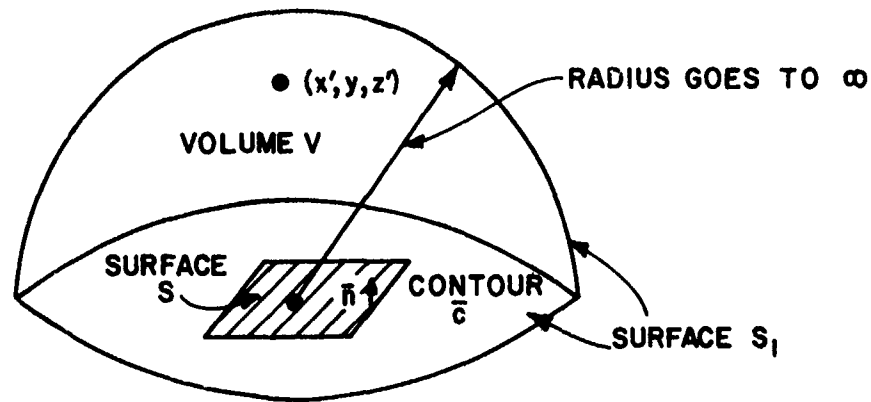
Fig. 10. HEMISPHERICAL VOLUME WITH TWO-PART SURFACE. The surface enclosing V is composed of a finite S and an infinite S_1. Nonzero fields are assumed only on S. Fields at point (x',y',z') are the result solely of fields on S and charges on contour C arising from discontinuities in the fields between S and S_1.

Simply assuming that the fields on S_1 are zero and performing the integration of (2.17) over the finite area S violates Green's theorem condition that the fields must be continuous over the entire surface. Discontinuities in the tangential fields result in surface current densities at the points of discontinuity. Only by accounting for these discontinuities can the fields above a finite surface be made to conform to Maxwell's equations. Stratton shows that the integral

$$ -\frac{1}{4\pi i\omega\epsilon} \oint_C \nabla\Phi \; \bar{H} \cdot d\bar{c} $$

over the contour C enclosing the surface S is the term that must be included in (2.17) to make the interior fields consistent with Maxwell's

24

equations and to account for the field discontinuities along C. Including the contour integral in (2.17) produces the result obtained by Stratton,

$$\bar{E}(x',y',z') = \frac{1}{4\pi} \int_S [-i\omega\mu(\bar{n} \times \bar{H}) \Phi + (\bar{n} \times \bar{E}) \times \nabla\Phi + (\bar{n} \cdot \bar{E}) \nabla\Phi] \, da$$

$$- \frac{1}{4\pi i \omega \epsilon} \oint_C \nabla\Phi \, \bar{H} \cdot d\bar{c} \qquad (2.18)$$

Two modifications render (2.18) more convenient for the calculation of $\bar{E}(x',y',z')$. The first changes the contour integral to a surface integral through Stokes's theorem; the second changes the mixed-field expression to one in terms of $\bar{E}$ alone.

Consider the contour-integral portion of (2.18) in component form,

$$\frac{1}{4\pi i \omega \epsilon} \left[\hat{a}_x \oint_C \frac{\partial\Phi}{\partial x} \bar{H} \cdot d\bar{c} + \hat{a}_y \oint_C \frac{\partial\Phi}{\partial y} \bar{H} \cdot d\bar{c} + \hat{a}_z \oint_C \frac{\partial\Phi}{\partial z} \bar{H} \cdot d\bar{c} \right] \qquad (2.19)$$

where $\hat{a}_j$ are unit vectors along the jth Cartesian axis. In this form, Stokes's theorem,

$$\oint_C \bar{V} \cdot d\bar{c} = \int_S (\nabla \times \bar{V}) \cdot d\bar{s} = \int_S (\nabla \times \bar{V}) \cdot \bar{n} \, ds$$

can be applied to the vectors $\partial\Phi/\partial x \, \bar{H}$, $\partial\Phi/\partial y \, \bar{H}$, and $\partial\Phi/\partial z \, \bar{H}$, where $\bar{V}$ is any vector and $\bar{n}$ is the unit normal to the surface element ds.

The partial differentiation of Φ is simplified when r is expressed in the geometry of Fig. 11; then,

$$\Phi = \frac{\exp(-i\beta r)}{r} = \frac{\exp[-i\beta(R - \bar{\beta}/\beta \cdot \bar{\rho})]}{r} \qquad (2.20)$$

where

$$\bar{\beta} = \beta(\sin\theta \cos\emptyset \, \hat{a}_x + \sin\theta \sin\emptyset \, \hat{a}_y + \cos\theta \, \hat{a}_z)$$
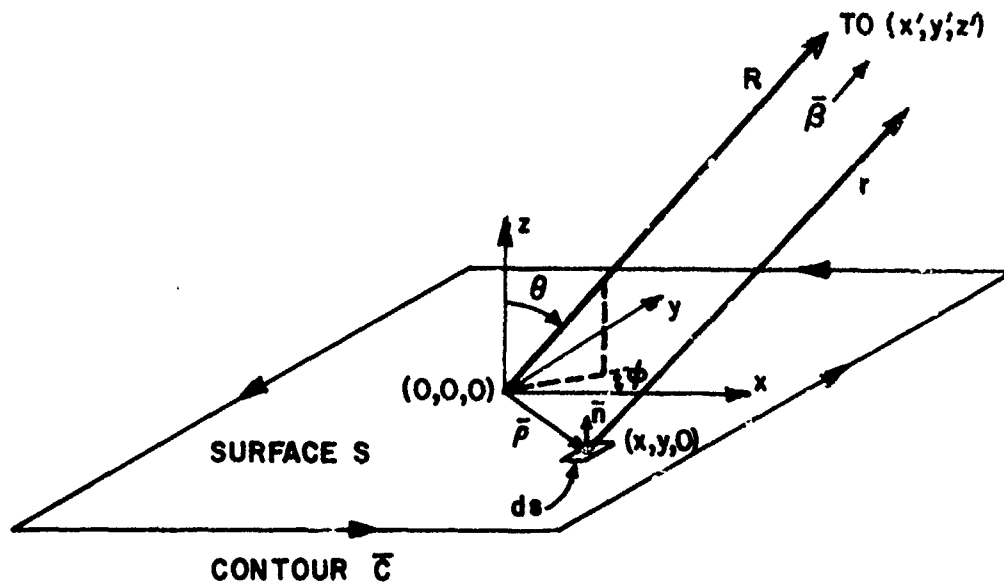
Fig. 11. GEOMETRY FOR CONTOUR INTEGRAL.

$$\beta = |\vec{\beta}| = 2\pi/\lambda$$

$$R^2 = x'^2 + y'^2 + z'^2$$

The vector $\vec{\rho}$ is the radial vector describing the position of the elemental surface area ds on the surface S,

$$\vec{\rho} = x\hat{a}_x + y\hat{a}_y + z\hat{a}_z \qquad (2.21)$$

Combining Eqs. (2.20) and (2.21) yields

$$\Phi = \frac{\exp(-i\beta R)}{R} \exp[i\beta(x \sin \theta \cos \phi + y \sin \theta \sin \phi + z \cos \theta)] \qquad (2.22)$$

where, for large r, letting $R = r$ in the amplitude of Φ has a negligible effect. From (2.22) the partials of Φ can be obtained as

$$\frac{\partial \Phi}{\partial x} = i\beta \sin \theta \cos \phi \, \Phi = i\beta_x \Phi$$

26

$$\frac{\partial \Phi}{\partial y} = i\beta \sin \theta \sin \emptyset \; \Phi = i\beta_y \Phi$$

$$\frac{\partial \Phi}{\partial z} = i\beta \cos \theta \; \Phi = i\beta_z \Phi$$

Applying Stokes's theorem to the x-component of the contour integral gives

$$\frac{1}{4\pi i \omega \epsilon} \oint_C \frac{\partial \Phi}{\partial x} \overline{H} \cdot d\overline{c} = \frac{1}{4\pi i \omega \epsilon} \int_S \left[\nabla \times \left(\frac{\partial \Phi}{\partial x} \overline{H} \right) \right] \cdot \overline{n} \; ds$$

$$= \frac{\beta_x}{4\pi \omega \epsilon} \int_S [\nabla \times (\Phi\overline{H})] \cdot \overline{n} \; ds$$

$$= \frac{\beta_x}{4\pi \omega \epsilon} \left[\int_S (\nabla\Phi \times \overline{H}) \cdot \overline{n} \; ds + \int_S \Phi(\nabla \times \overline{H}) \cdot \overline{n} \; ds \right]$$

(2.23)

Similar expressions exist for the y- and z-components of the contour integral and combine with (2.23) to produce the total-vector contour integral,

$$\frac{1}{4\pi i \omega \epsilon} \oint_C \nabla\Phi \; \overline{H} \cdot d\overline{c} = \frac{\beta}{4\pi \omega \epsilon} \int_S [(\nabla\Phi \times \overline{H}) \cdot \overline{n} + i\omega\epsilon\Phi\overline{E} \cdot \overline{n}] \; ds$$ (2.24)

where $\nabla \times \overline{H} = i\omega\epsilon\overline{E}$ (one of Maxwell's equations in time-harmonic source-free form) replaces $\nabla \times \overline{H}$ in (2.23).

With the following auxiliary relationships,

$$(\nabla\Phi \times \overline{H}) \cdot n = -(\overline{n} \times \overline{H}) \cdot \nabla\Phi$$

$$\nabla\Phi = i\overline{\beta}\Phi$$

$$\beta = \omega\sqrt{\mu\epsilon}$$

$$\hat{\beta} = \frac{\overline{\beta}}{\beta}$$

(2.25)

Eq. (2.24) can be incorporated into the total-field expression (2.18) to yield

$$\overline{E}(x',y',z') = \frac{i\omega\mu e^{-i\beta R}}{4\pi R} \int_S \left[-(\overline{n} \times \overline{H}) + \sqrt{\frac{\epsilon}{\mu}} \, (\overline{n} \times \overline{E}) \times \hat{\beta} + \hat{\beta} \cdot (\overline{n} \times \overline{H}) \, \hat{\beta} \right]$$

$$\cdot \, e^{i\overline{\beta}\cdot\overline{\rho}} \, ds \qquad\qquad (2.26)$$

which is the Stratton-Chu integral rewritten as a single-surface integral. It expresses the field, at any point (x',y',z'), caused by the fields on a given surface S, where S may be only a portion of a larger surface. Rice has conveniently provided expressions (2.12) and (2.13) for the scattered fields everywhere above a slightly rough surface. These fields, when evaluated at the scattering surface, can be used in the Stratton-Chu integral to obtain the field $\overline{E}(x',y',z')$ scattered from a finite portion of the surface.

A subtle but important point concerning the Stratton-Chu integral is that the scattering surface need not be the surface over which the integration is performed. For example, the fields derived from Rice's theory can be evaluated at any surface; however, no matter where evaluated, they remain the fields caused by the scattering surface. As a result, a surface convenient for the integration of (2.26) can be chosen, the fields scattered by the slightly rough surface can be evaluated at this new surface, and the Stratton-Chu integral then applied.

A convenient surface in evaluating (2.26) is one contained in the $z = 0$ plane; then, $\overline{n} = \hat{a}_z$ and

$$\overline{n} \times \overline{H} = -H_y \hat{a}_x + H_x \hat{a}_y$$

$$\overline{n} \times \overline{E} = -E_y \hat{a}_x + E_x \hat{a}_y$$

Using Maxwell's curl equation for electric field

$$\nabla \times \overline{E} = -i\omega\mu\overline{H}$$

28

$\overline{H}$ can be expressed as partial derivatives of $\overline{E}$,

$$H_y = -\frac{1}{i\omega\mu}\left(\frac{\partial E_x}{\partial z} - \frac{\partial E_z}{\partial x}\right)$$

$$H_x = -\frac{1}{i\omega\mu}\left(\frac{\partial E_z}{\partial y} - \frac{\partial E_y}{\partial z}\right)$$

Substituting these components of $\overline{H}$ in (2.26) results in an integral expression to which the E-fields derived by Rice can be applied directly,

$$
\begin{aligned}
\overline{E}(x',y',z') = \frac{e^{-i\beta R}}{4\pi R}\int_S & \left\{\left[\left(\frac{\partial E_z}{\partial x} - \frac{\partial E_x}{\partial z}\right)\hat{a}_x + \left(\frac{\partial \overline{E}_z}{\partial y} - \frac{\partial E_y}{\partial z}\right)\hat{a}_y\right]_{z=0}\right. \\
& + i\beta\left[E_x \cos\theta\,\hat{a}_x + E_y\cos\theta\,\hat{a}_y\right. \\
& \left.- (E_x\sin\theta\cos\emptyset + E_y\sin\theta\sin\emptyset)\,\hat{a}_z\right]_{z=0} \\
& - \left[\left(\frac{\partial E_z}{\partial x} - \frac{\partial E_y}{\partial z}\right)\sin\theta\cos\emptyset + \left(\frac{\partial E_z}{\partial y} - \frac{\partial E_y}{\partial z}\right)\sin\theta\sin\emptyset\right]_{z=0} \\
& \left.\cdot\left[\sin\theta\cos\emptyset\,\hat{a}_x + \sin\theta\sin\emptyset\,\hat{a}_y + \cos\theta\,\hat{a}_z\right]\right\}e^{i\overline{\beta}\cdot\overline{\rho}}\,ds
\end{aligned}
$$

$$(2.27)$$

This equation plus (2.12) and (2.13) are the tools to be used in determining per unit area radar cross sections for slightly rough random surfaces.

C.   First- and Second-Order Radar Cross Sections

The following discussion is the first of three in which the radar cross section per unit area for a slightly rough surface is derived. At this point, the surface is still perfectly conducting and motionless. Later (in D and E), the time-varying and finite-conductivity aspects of the rough surface will be described.

1.   Radar Cross Section as Power-Density Ratios

Radar cross section has been defined as that area σ where, when multiplied by the incident power density S_i, provides a power σS_i that, if reradiated isotropically $(\sigma S_i/4\pi R^2)$ would produce the actual power density S_s at the receiver a distance R from the target. As an equation,

$$S_s = \frac{\sigma S_i}{4\pi R^2} \tag{2.28}$$

For time-harmonic electromagnetic waves, time-average power density $\overline{S}$ is used;

$$\overline{S} = \frac{1}{2} \, \mathrm{Re}(\overline{E} \times \overline{H}^*)$$

when electromagnetic fields are expressed in complex form. For waves propagating in homogeneous media with permittivity ϵ and permeability μ, $\overline{E}$ and $\overline{H}$ are in space quadrature with $E = \sqrt{\mu/\epsilon} \, H$; therefore,

$$\overline{S} = \frac{1}{2} \, \mathrm{Re}(EH^*) = \frac{|E|^2}{2\sqrt{\mu/\epsilon}}$$

From (2.28), the radar cross section becomes

$$\sigma = 4\pi R^2 \frac{|E_s|^2}{|E_i|^2}$$

30

If the scatterer is a surface of size $L \times L$, the radar cross section per unit area becomes

$$\frac{\sigma}{L^2} = 4\pi R^2 \frac{|E_s|^2/L^2}{|E_i|^2}$$

Because only cross sections per unit area are considered henceforth, σ can be used to represent them without confusion.

To be consistent with Rice's work, the incident-field magnitude is taken to be one; then, σ becomes

$$\sigma = 4\pi R^2 \frac{|E_s|^2}{L^2}$$

A field scattered from the slightly rough surface described in Section B is a random variable, and an average radar cross section $\bar{\sigma}$ can be defined, where the average is taken over all possible rough surfaces of the same class. Later, when time-varying surfaces are introduced, E_s is generated by an ergodic random process in which the time-average power is equated to the statistical average power, and the notation returns to σ rather than $\bar{\sigma}$. In either case, the quantity $\langle E_s E_s^* \rangle$ must be calculated. For a time-invariant or static surface, the average radar cross section is

$$\bar{\sigma} = 4\pi R^2 \frac{\langle E_s E_s^* \rangle}{L^2} \qquad (2.29)$$

2. Scattered Fields from Rough Surfaces of Finite Extent

The fields to be used in the radar cross-section equations presented above are found by performing the Stratton-Chu integration of Rice's field expressions over a planar surface of size $L \times L$, where L is allowed to be the same as the period of the rough surface defined by Eq. (2.1). As a specific example, consider a vertically polarized

31

incident wave (Fig. 12). The Stratton-Chu integral (2.27) requires that the infinite-surface scattered fields [Eqs. (2.13)] and their partial derivatives must be evaluated at the surface over which the integration is performed. Applying (2.27) to the x-component of the scattered field, evaluated at $z = 0$, yields

$$
\begin{aligned}
E_x(x',y',z') = \frac{2ie^{-i\beta R}}{4\pi R} \int\!\!\!\int_{-L/2}^{L/2} & \left\{ -\frac{\beta}{2}(1 - \alpha^2 \sin^2\theta \cos^2\phi + \gamma \cos\theta)\, e^{-i\beta\alpha x} \right. \\
& + \sum_{mn} \left[b(m,n)(1 - \sin^2\phi \cos^2\theta) + \beta\cos\theta \right] E(m,n,o) \\
& \qquad \cdot \left[i(\alpha am - \beta)\, P(m - \nu,n) \right. \\
& \qquad + \sum_{k\ell} \left\{ a^2(m - k)(\nu - k)\,\beta + (\beta - \alpha am)\,b^2(k,\ell) \right\} Q(m,n,k,\ell) \bigg] \\
& + a\sum_{mn} - b(m,n)\, E(m,n,o) \left[i\alpha n P(m - \nu,n) \right. \\
& \qquad + \sum_{k\ell} \left\{ a(n - \ell)(\nu - k)\,\beta - \alpha n b^2(k,\ell) \right\} Q(m,n,k,\ell) \bigg] \\
& + \sum_{mn} \left[am(\sin^2\theta\cos^2\phi - 1) + an\sin^2\theta\sin\phi\cos\phi \right]\left[\frac{E(m,n,o)}{b(m,n)} \right] \\
& \qquad \cdot \left[i\left\{ a(m - \nu)\,\beta + \alpha b^2(m,n) \right\} P(m - \nu,n) \right. \\
& \qquad + \sum_{k\ell} \left\{ a^3(k - \nu)(m^2 + n^2 - mk - n\ell)\,\beta \right. \\
& \qquad \left. + a\left[\alpha a(m^2 + n^2) - m\beta \right] b^2(k,\ell) \right\} Q(m,n,k,\ell) \bigg] \bigg\}\, e^{i\overline{\beta}\cdot\overline{\rho}}\, dxdy
\end{aligned}
$$

(2.30)
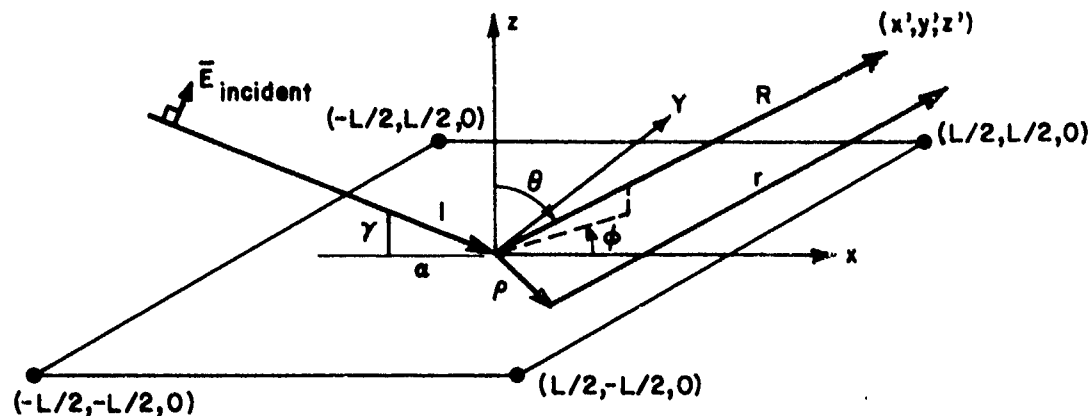
Fig. 12. SCATTERING GEOMETRY--VERTICALLY POLARIZED INCIDENT PLANE WAVE.

The integration of this equation can be readily performed because the only terms involving the variables of integration (x and y) are exponential, $\exp(-i\beta\alpha x)$, $\exp(i\bar{\beta}\cdot\bar{\rho})$, and

$$E(m,n,o) = \exp[-ia(mx + ny)]$$

where these variables are separable. The integrals to be evaluated are

$$\int\int_{-L/2}^{L/2} \exp[-ia(mx + ny)] \exp[\beta(\sin\theta\cos\emptyset\,x + \sin\theta\sin\emptyset\,y)]\,dxdy$$

and

$$\int\int_{-L/2}^{L/2} \exp(-i\beta\alpha x) \exp[\beta(\sin\theta\cos\emptyset\,x + \sin\theta\sin\emptyset\,y)]\,dxdy$$

The results of integration are the familiar $\operatorname{sinc}(x) = \sin(x)/x$ functions,

$$L^2 \left[\frac{\sin \{(\beta \sin \theta \cos \phi - am) L/2\}}{(\beta \sin \theta \cos \phi - am) L/2} \right] \cdot \left[\frac{\sin \{(\beta \sin \theta \sin \phi - an) L/2\}}{(\beta \sin \theta \sin \phi - an)} \right]$$

$$\underbrace{\qquad\qquad}_{\text{sinc(XR)}} \qquad\qquad \underbrace{\qquad\qquad}_{\text{sinc(YR)}}$$

(2.31a)

and

$$L^2 \left[\frac{\sin \{(\beta \sin \theta \cos \phi - \beta\alpha) L/2\}}{(\beta \sin \theta \cos \phi - \beta\alpha) L/2} \right] \cdot \left[\frac{\sin \{(\beta \sin \theta \sin \phi) L/2\}}{(\beta \sin \theta \sin \phi) L/2} \right]$$

$$\underbrace{\qquad\qquad}_{\text{sinc(XI)}} \qquad\qquad \underbrace{\qquad\qquad}_{\text{sinc(YI)}}$$

(2.31b)

The definitions XI, YI, XR, and YR allow the x-component of the scattered field to be written in compact form,

$$E_x(x',y',z') = \frac{2ie^{-i\beta R}}{4\pi R}$$

$$\cdot L^2 \Bigg\{ -\frac{\beta}{2} (1 - \alpha^2 \sin^2 \theta \cos^2 \phi + \gamma \cos \theta) \, \text{sinc(XI)} \, \text{sinc(YI)}$$

$$+ \sum_{mn} \left[b(m,n)(1 - \sin^2 \phi \cos^2 \phi) + \beta \cos \theta \right]$$

$$\cdot \text{sinc(XR)} \, \text{sinc(YR)} \qquad [E_x \text{ terms}]$$

$$+ \sum_{mn} - ab(m,n) \sin^2 \theta \sin \phi \cos \phi$$

$$\cdot \text{sinc(XR)} \, \text{sinc(YR)} \qquad [E_y \text{ terms}]$$

$$+ \sum_{mn} \left[am(\sin^2 \theta \cos^2 \phi - 1) + an \sin^2 \theta \sin \phi \cos \phi \right]$$

$$\cdot \frac{\text{sinc(XR)} \, \text{sinc(YR)}}{b(m,n)} \qquad [E_z \text{ terms}] \Bigg\} \qquad (2.32a)$$

34

where the $[E_x \text{ terms}]$, $[E_y \text{ terms}]$, and $[E_z \text{ terms}]$ are the coefficients of $E(m,n,z)$ in the x-, y-, and z-components of the scattered fields in (2.13), respectively. The $[E_z \text{ terms}]$ are actually the coefficients of $E(m,n\ z)/b(m,n)$. From (2.13), they are

$$[E_x \text{ terms}] = i(\alpha am - \beta) P(m - \nu, n) + \sum_{k\ell} \left[a^2(m - k)(\nu - k) \beta \right.$$

$$\left. + (\beta - \alpha am) b^2(k,\ell) \right] Q(m,n,k,\ell)$$

$$[E_y \text{ terms}] = i\alpha n P(m - \nu, n) + \sum_{k\ell} \left[a(n - \ell)(\nu - k) \beta - \alpha n b^2(k,\ell) \right] Q(m,n,k,\ell)$$

$$[E_z \text{ terms}] = i\left[a(m - \nu) \beta + \alpha b^2(m,n) \right] P(m - \nu, n) + \sum_{k\ell} \left\{ a^3(k - \nu) \right.$$

$$\cdot (m^2 + n^2 - mk - n\ell) \beta + a\left[\alpha a(m^2 + n^2) - m\beta \right] b^2(k,\ell) \right\} Q(m,n,k,\ell)$$

The y- and z-components of the scattered field for vertically polarized plane-wave incidence are obtained in the same manner. They are

$$E_y(x',y',z') = \frac{2i e^{(-i\beta R)} L^2}{4\pi R} \left\{ \frac{\beta}{2} \alpha^2 \sin^2 \theta \sin \emptyset \cos \emptyset \ \text{sinc}(XI) \ \text{sinc}(YI) \right.$$

$$+ \sum_{mn} -b(m,n) \sin^2 \theta \sin \emptyset \cos \theta \ \text{sinc}(XR) \ \text{inc}(YR) \ [E_x \text{ terms}]$$

$$+ a \sum_{mn} \left[b(m,n)(1 - \sin^2 \theta \sin^2 \emptyset) + \beta \cos \theta \right]$$

$$\cdot \text{sinc}(XR) \ \text{sinc}(YR) \quad [E_y \text{ terms}] \tag{2.32b}$$

35

$$+ \sum_{mn} \left[an(\sin^2 \theta \sin^2 \emptyset - 1) + am \sin^2 \theta \sin \emptyset \cos \emptyset \right]$$

$$\cdot \frac{\text{sinc(XR) sinc(YR)}}{b(m,n)} \quad [E_z \text{ terms}] \Bigg\} \qquad \text{(2.32b)}$$
Cont.

and

$$E_z(x',y',z') = \frac{2ie^{(-i\beta R)} L^2}{4\pi R} \Bigg\{ \frac{\beta}{2} \left[\gamma \sin \theta \cos \emptyset + \alpha^2 \sin \theta \cos \emptyset \cos \theta \right]$$

$$\cdot \text{sinc(XI) sinc(YI)}$$

$$- \sum_{mn} \sin \theta \cos \emptyset \left[\beta + b(m,n) \cos \theta \right]$$

$$\cdot \text{sinc(XR) sinc(YR)} \quad [E_x \text{ terms}]$$

$$- a \sum_{mn} \sin \theta \sin \emptyset \left[\beta + b(m,n) \cos \theta \right]$$

$$\cdot \text{sinc(XR) sinc(YR)} \quad [E_y \text{ terms}]$$

$$+ \sum_{mn} \sin \theta \cos \theta \left[am \cos \emptyset + an \sin \emptyset \right]$$

$$\cdot \frac{\text{sinc(XR) sinc(YR)}}{b(m,n)} \quad [E_z \text{ terms}] \Bigg\} \qquad \text{(2.32c)}$$

Similar expressions result when the incident wave is horizontally polarized.

3. Polarized Components of Scattered Fields

Because power received from a scattered field generally will
depend on the polarization of the receive antenna and of the wave

incident on the scatterer, it is convenient to express the scattered field in terms of polarized components. Incident waves have been described as either horizontally or vertically polarized; likewise, scattered fields can also be expressed in terms of horizontally and vertically polarized components. In the spherical coordinates shown in Fig. 13, the direction $\hat{a}_\emptyset$ is perpendicular to the direction of propagation $\hat{a}_r$ and to the plane defined by $\hat{a}_r$ and the z-axis. Scattered-field components in the $\hat{a}_\emptyset$ direction are horizontally polarized according to the definitions used for the incident waves; similarly, field components in the $\hat{a}_\theta$ direction are vertically polarized.
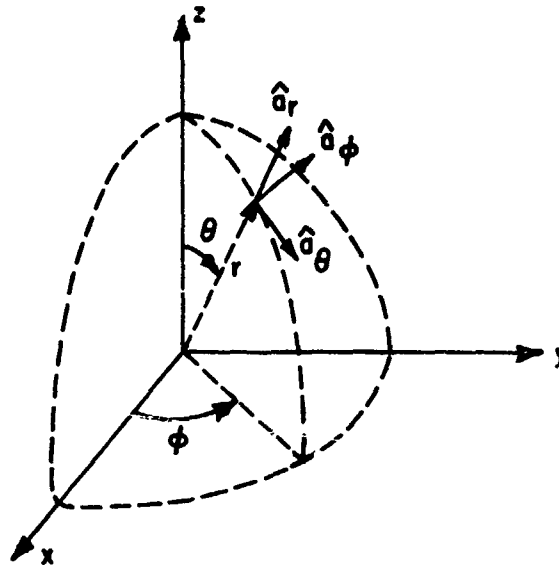
Fig. 13. SPHERICAL COORDINATE SYSTEM.

In terms of the Cartesian components of the scattered field $(E_x, E_y, \text{ and } E_z)$, the vertically and horizontally polarized components $(E_\theta \text{ and } E_\emptyset)$ are

$$E_\theta = E_x \cos \emptyset \cos \theta + E_y \sin \emptyset \cos \theta - E_z \sin \theta \qquad (2.33a)$$

and

$$E_\emptyset = -E_x \sin \emptyset + E_y \cos \emptyset \qquad (2.33b)$$

37

where E_x, E_y, and E_z may be the result of either vertically or horizontally polarized incident waves.

Considering only these two orthogonal polarizations results in four possible combinations for radar cross section,

σ_{VV} = vertical incident, vertical reflected

σ_{VH} = vertical incident, horizontal reflected

σ_{HH} = horizontal incident, horizontal reflected

σ_{HV} = horizontal incident, vertical reflected

Only σ_{VV} will be calculated here (results for σ_{HH} will be presented at the end of this section), but the same procedure used to obtain σ_{VV} and σ_{HH} applies to the cross-polarized σ_{VH} and σ_{HV} as well.

4. Calculation of $\bar{\sigma}_{VV}$

The average radar cross section $\bar{\sigma}_{VV}$ is derived in two steps, using Eq. (2.29). First, the average $\langle E_\theta E_\theta^* \rangle$ is found, and then the limit of $\langle E_\theta E_\theta^* \rangle / L^2$ as L goes to infinity is taken, thereby converting sums to integrals.

From the field components in (2.32), the vertical field E_θ according to (2.33a) is

$$E_\theta = \frac{2ie^{(i\beta R)}L^2}{4\pi R} \left\{ -\underbrace{\frac{\beta}{2}(\gamma + \cos\theta)\cos\emptyset\ \text{sinc}(XI)\ \text{sinc}(YI)}_{A} \right.$$

$$+ \underbrace{\sum_{mn}{}' \cos\emptyset\ (\beta + b(m,n)\cos\theta)\ \text{sinc}(XR)\ \text{sinc}(YR)}_{B} \quad [E_x\ \text{terms}]$$

$$\text{(2.34)}$$

$$+ \varepsilon\underbrace{\sum_{mn}{}' \sin\emptyset\ (\beta + b(m,n)\cos\theta)\ \text{sinc}(XR)\ \text{sinc}(YR)}_{C} \quad [E_y\ \text{terms}]$$

$$\left. + \underbrace{\sum_{mn}{}' -\cos\theta\ (am\cos\emptyset + an\sin\emptyset)\frac{\text{sinc}(XR)\ \text{sinc}(YR)}{b(m,n)}}_{D} \quad [E_z\ \text{terms}] \right\}$$

38

With the abbreviated notation,

$$E_\rho E_\theta^* = \frac{L^4}{4\pi^2 R^2} [AA^* + BB^* + CC^* + DD^* + (A^*B + B^*A) + (A^*C + C^*A)$$

$$+ (A^*D + D^*A) + (B^*C + C^*B) + (B^*D + D^*B) + (C^*D + D^*C)]$$

$$(2.35)$$

a.   Zero and First Order

Zero-order terms are those products in Eq. (2.35) that involve no random variables $P(m,n)$; first-order terms have products of two random variables. Because $P(m,n)$ are zero mean and gaussian, the product of three random variables averages to zero [Thomas, 1969, p. 64].

Only one representative term from each of the above combinations will be examined here. The AA^* term involves no random variables and its average is

$$\langle AA^* \rangle = \frac{\beta^2}{4} (\gamma + \cos\theta)^2 \cos^2\phi \ \text{sinc}^2(XI) \ \text{sinc}^2(YI) \qquad (2.36)$$

The A^*B term is obtained from Eq. (2.34) and from the definition of the $[E_x \text{ terms}]$ in Section C.2. When products involving a single random variable are omitted (these average to zero), A^*B becomes

$$A^*B = -\frac{\beta}{2} (\gamma + \cos\theta) \cos\phi \ \text{sinc}(XI) \ \text{sinc}(YI) \sum_{mn} \cos\phi \ [\beta + b(m,n) \cos\theta]$$

$$\cdot \ \text{sinc}(XR) \ \text{sinc}(YR) \sum_{k\ell} \left[a^2(m-k)(v-k) \ \beta + (\beta - \alpha_{am}) \ b^2(k,\ell) \right]$$

$$\cdot \ Q(m,n,k,\ell) \qquad (2.37)$$

Recall that

$$Q(m,n,k,\ell) = \frac{P(k-v,\ell) \ P(m-k, \ n-\ell)}{b(k,\ell)}$$

and, by Eqs. (2.2), the relations $k - \nu = -(m - k)$ and $\ell = -(n - \ell)$ must hold for a nonzero average; therefore, $m = \nu$ and $n = 0$. Under these conditions,

$$\langle Q(m,n,k,\ell) \rangle = \frac{\pi^2 W(ak - a\nu, a\ell)}{L^2 b(k,\ell)}$$

which leaves only the double sum over k and ℓ. The terms in the sum over m and n are evaluated only at $m = \nu$ and $n = 0$ with the result,

$$b(m,n) \rightarrow b(\nu,o) = \beta\gamma$$

$$\mathrm{sinc}(XR) \rightarrow \mathrm{sinc}(XI)$$

$$\mathrm{sinc}(YR) \rightarrow \mathrm{sinc}(YI)$$

Relabeling the summation indices k and ℓ as m and n, the average of A^*B can be written as

$$\langle A^*B \rangle = -\frac{\beta^2}{2} (\gamma + \cos\theta) \cos^2 \phi \, \mathrm{sinc}^2(XI) \, \mathrm{sinc}^2(YI)(1 + \gamma \cos\theta)$$

$$\cdot \sum_{mn} \left[a^2 (\nu - m)^2 \beta + (\beta - \alpha a\nu) b^2(m,n) \right] \frac{\pi^2 W(am - a\nu, an)}{L^2 b(m,n)} \quad (2.38)$$

If $b(m,n)$ is real, then $\langle A^*B \rangle = \langle AB^* \rangle$; if $b(m,n)$ is imaginary, then $\langle A^*B \rangle = -\langle AB^* \rangle$ and the AB cross terms cancel. All of the cross terms involving A have this property.

The average of other terms involving A are similar. The remaining self and cross terms take on another form and can be represented by a single example. Consider BC^*, omitting factors involving more than two random variables. Under these conditions,

$$BC^* = \sum_{mn} \cos \emptyset \ [\beta + b(m,n) \cos \theta] \ \text{sinc}(XR) \ \text{sinc}(YR)[i(\alpha am - \beta) \ P(m - \nu,n)]$$

$$\cdot \ a \sum_{m'n'} \sin \emptyset \ [\beta + b^*(m',n') \cos \theta]$$

$$\cdot \ \text{sinc}(XR') \ \text{sinc}(YR')[-i\alpha n'P^*(m' - \nu,n')]$$

The random terms are

$$P(m - \nu,n) \ \cdot \ P^*(m' - \nu,n')$$

For a nonzero average, the conditions $m = m'$ and $n = n'$ must hold. After averaging, the result is

$$\langle BC^* \rangle = a \sum_{mn} \cos \emptyset \sin \emptyset \ [\beta + b(m,n) \cos \theta]$$

$$\cdot \ [\beta + b^*(m,n) \cos \theta] \ \text{sinc}^2(XR) \ \text{sinc}^2(YR)$$

$$\cdot \ [\alpha n(\alpha am - \beta)] \ \frac{\pi^2 W(am - a\nu,an)}{L^2} \tag{2.39}$$

In this case, $\langle BC^* \rangle = \langle B^*C \rangle$.

To obtain the radar cross section per unit area, $\langle E_\theta E_\theta^* \rangle/L^2$ is evaluated in the limit as L tends to infinity. From (2.35),

$$\frac{\langle E_\theta E_\theta^* \rangle}{L^2} = \frac{L^2}{4\pi^2 R^2} \ \langle AA^* + BB^* + \ldots \rangle$$

and the term-by-term evaluation is in the form of $\lim_{L \to \infty} L^2 \langle XY^* \rangle$.

41

When evaluated in the limit, each of the three examples considered provides results that can be interpreted physically and are in agreement with intuition. The $\langle AA^* \rangle$ term in (2.36) can be rewritten as

$$\lim_{L \to \infty} L^2 \langle AA^* \rangle = \lim_{L \to \infty} \frac{\beta^2}{4} (\gamma + \cos \theta)^2 \cos^2 \phi \ L \left[\frac{\sin \ \{(\beta \sin \theta \cos \phi - \beta\alpha)L/2\}}{(\beta \sin \theta \cos \phi - \beta\alpha)L/2} \right]^2$$

$$\cdot \ L \left[\frac{\sin \ \{(\beta \sin \theta \sin \phi)L/2\}}{(\beta \sin \theta \sin \phi)L/2} \right]^2$$

where $\text{sinc}^2(XI)$ and $\text{sinc}^2(YI)$ are given in complete form.

In taking the limit, the following [Thomas, 1969, p. 587] can be used:

$$\lim_{L \to \infty} L \left[\frac{\sin(XL/2)}{XL/2} \right]^2 = 2\pi \ \delta(X) \tag{2.40}$$

where $\delta(X)$ is the Dirac delta function. Although this equation is not proven here, $L \cdot \text{sinc}^2$ has all the properties associated with the more common functions whose limiting value defines the delta function. As L tends to infinity, the limit in (2.40) tends to zero everywhere, except at $X = 0$ where it tends to infinity. The integral of $L \cdot \text{sinc}^2$ from $-\infty$ to ∞ is finite and has the value of 2π, independent of L.

Applying (2.40) to $L^2 \langle AA^* \rangle$ yields

$$\lim_{L \to \infty} L^2 \langle AA^* \rangle = \pi^2 \beta^2 (\gamma + \cos \theta)^2 \cos^2 \phi \ \delta(\beta \sin \theta \cos \phi - \beta\alpha) \ \delta(\beta \sin \theta \sin \phi)$$

$$\tag{2.41}$$

By the sampling property of the delta function, this limit has a nonzero value only under the conditions that

$$\beta \sin \theta \cos \phi - \beta\alpha = 0$$

$$\beta \sin \theta \sin \phi = 0$$

42

Because $\sin \theta$ is nonzero by the first condition, $\sin \emptyset$ must be zero by the second; hence, $\cos \emptyset = \pm 1$. From Fig. 12, both $\sin \theta$ and α are positive, thereby limiting $\cos \emptyset$ to $+1$. The conditions for non-zero $\langle AA^* \rangle$ can be rewritten as

$$\sin \theta = \alpha$$

$$\sin \emptyset = 0$$

$$\cos \emptyset = 1$$

According to Fig. 12, the above conditions specify the specular direction. This is not surprising because $\langle AA^* \rangle$ comes from that portion of the field scattered by a plane reflector.

The second example (2.38) contains a double summation that becomes a double integral in the limit. Using the delta-function definition of (2.40),

$$\lim_{L \to \infty} L^2 \langle A^* B \rangle = -4\pi^2 \gamma \beta^2 (1 + \gamma^2)\ \delta(\beta \sin \theta \cos \emptyset - \beta\alpha)\ \delta(\beta \sin \theta \sin \emptyset)$$

$$\cdot \frac{\beta}{4} \iint_{-\infty}^{\infty} \left[(\beta\alpha - p)^2 + \gamma^2 b^2(p,q) \right] \frac{W(p - \beta\alpha, q)}{b(p,q)}\ dpdq \tag{2.42}$$

where the limiting conditions

$$am \to p$$

$$an \to q$$

$$a\nu \to \beta\alpha$$

were used, and

$$\iint_{-\infty}^{\infty} \frac{\pi^2}{L^2}\ W(am - a\nu, an)\ dmdn \to \iint_{-\infty}^{\infty} \frac{1}{4}\ W(p - \beta\alpha, q)\ dpdq$$

as $L \to \infty$. Again, the contribution to the radar cross section is in the specular direction only, but this time it is weighted by an integral of the surface-roughness spectrum over all wave numbers, p and q.

43

There is no entirely specular constraint in the third example, $\langle BC^* \rangle$. Equation (2.39) shows that, in the limit of large L, there will be delta functions within the integrals; therefore, analytical integration is possible, using the sampling property of the delta function. First, formally taking the limit,

$$\lim_{L \to \infty} L^2 \langle BC^* \rangle = \iint_{-\infty}^{\infty} \pi^2 \cos \emptyset \sin \emptyset \, [\beta + b(p,q) \cos \theta][\beta + b^+(p,q) \cos \theta]$$

$$\times \delta(\beta \sin \theta \cos \emptyset - p) \, \delta(\beta \sin \theta \sin \emptyset - q)[\alpha q(\alpha p - \beta)]$$

$$\cdot W(p - \beta\alpha, q) \, dpdq$$

and, then integrating,

$$\lim_{L \to \infty} L^2 \langle BC^* \rangle = \alpha \pi^2 \beta^4 \sin^2 \emptyset \cos \emptyset \, (1 + \cos^2 \theta)^2 \sin \theta \, (\alpha \sin \theta \cos \emptyset - 1)$$

$$\cdot W(\beta \sin \theta \cos \emptyset - \beta\alpha, \, \beta \sin \theta \sin \emptyset) \qquad (2.43)$$

This example indicates that, generally, there will be scattered power at any observation angles θ and $\emptyset$ (that is, a nonzero radar cross section). For a given set of incidence and observation angles, however, only a particular portion of the surface-roughness spectrum contributes to this nonspecular power. Later, it will be shown that the components of the surface spectrum causing the scattering in a given direction are those that meet the conditions for Bragg scattering.

The average radar cross sections to zero and first orders are found by applying Eq. (2.29) to all the average terms. For specular reflection, the result is

$$\bar{\sigma}_{VV} = 4\pi\beta^2\gamma^2 \, \delta(\beta \sin \theta \cos \emptyset - \beta\alpha) \, \delta(\beta \sin \theta \sin \emptyset)$$

$$(2.44)$$

$$\cdot \, 1 - \frac{\beta}{2} \iint_{-\infty}^{\infty} \left[\frac{(p - \beta\gamma)^2}{\gamma} + b^2(p,q)\gamma \right]\left[\frac{1}{b(p,q)} + \frac{1}{b^*(p,q)} \right] W(p - \beta\alpha, q) \, dpdq$$

and, for nonspecular scattering,

$$\overline{\sigma}_{VV} = 4\pi\beta^4 (\alpha \sin \theta - \cos \varnothing)^2 \, W(\beta \sin \theta \cos \varnothing - \beta\alpha, \, \beta \sin \theta \sin \varnothing)$$

$$(2.45)$$

These equations represent the average radar cross section per unit area (to first order) of a perfectly conducting slightly rough time-invariant surface of infinite extent. Note that the roughness contribution to the specular cross section goes to zero when the radio-wave propagation constant in the z-direction $b(p,q)$ becomes imaginary. Physically, this phenomenon corresponds to surfaces whose roughness scale is small compared to the incident radio wavelength; in other words, the surface appears smooth to radio wavelengths longer than a certain value.

b. Second Order

The second-order terms are of considerable interest because they account, in part, for the sideband structure observed in radar echoes from ocean surfaces.

To determine the second-order contribution to radar cross section, the average $\langle Q(m,n,k,\ell) \times Q^*(m',n',k',\ell') \rangle$ must be evaluated for the various products in (2.35). In terms of the random variables $P(m,n)$,

$$\langle Q(m,n,k,\ell) \, Q^*(m',n',k',\ell') \rangle$$

$$= \left\langle \frac{P(k - \nu, \ell) \, P(m - k, \, n - \ell) \, P^*(k' - \nu, \ell') \, P^*(m'-k', \, n' - \ell')}{b(k,\ell) \, b^*(k',\ell')} \right\rangle$$

For gaussian random variables, the average can be expanded [Thomas, 1969, p. 64] as follows:

$$\langle P_1 P_2 P_3 P_4 \rangle = \langle P_1 P_2 \rangle \langle P_3 P_4 \rangle + \langle P_1 P_3 \rangle \langle P_2 P_4 \rangle + \langle P_1 P_4 \rangle \langle P_2 P_3 \rangle$$
$$-2 \langle P_1 \rangle \langle P_2 \rangle \langle P_3 \rangle \langle P_4 \rangle$$

where the P_i need not be independent. When expanded, the average $\langle QQ^* \rangle$ becomes

$$\frac{\langle P(k - \nu, \ell) \; P(m - k, \; n - \ell) \rangle \langle P(\nu - k', -\ell') \; P(k' - m', \; \ell' - n') \rangle}{b(k, \ell) \; b^*(k', \ell')}$$

$$+ \; \frac{\langle P(k - \nu, \ell) \; P(k' - m', \; \ell' - n') \rangle \langle P(m - k, \; n - \ell) \; P(\nu - k', -\ell') \rangle}{b(k, \ell) \; b^*(k', \ell')}$$

$$+ \; \frac{\langle P(k - \nu, \ell) \; P(\nu - k', -\ell') \rangle \langle P(m - k, \; n - \ell) \; P(k' - m', \; \ell' - n') \rangle}{b(k, \ell) \; b^*(k', \ell')}$$

$$(2.46)$$

where $P^*(m, n) = P(-m, -n)$ replaces the conjugate terms.

It is not difficult to see why calculation of radar cross section is limited to second order; the number of averages increases six-fold in going from first to second order. The averaging process becomes mechanical after the first or second term, however, so that consideration of a representative term in (2.35) will suffice in demonstrating the techniques involved.

Consider, for example, the BB^* term in (2.35) and omit the first-order contributions; the result is

$$BB^* = \left\{ \sum_{mn} \cos \emptyset \; [\beta + b(m, n) \cos \theta] \; \text{sinc}(XR) \; \text{sinc}(YR) \right.$$

$$\cdot \sum_{k\ell} \left[a^2(m - k)(\nu - k) \; \beta + (\beta - \alpha am) \; b^2(k, \ell) \right] Q(m, n, k, \ell) \Big\}$$

$$\cdot \left\{ \sum_{m'n'} \cos \emptyset \; [\beta + b^*(m', n') \cos \theta] \; \text{sinc}(XR') \; \text{sinc}(YR') \right.$$

$$\cdot \sum_{k'\ell'} \left[a^2(m' - k')(\nu - k') \; \beta + (\beta - \alpha am') \; b^2(k', \ell') \right] Q(m', n', k', \ell') \Big\}$$

$$(2.47)$$

This eightfold summation can be reduced to something less formidable by using the condition,

$$\langle P(m,n)\ P(u,v) \rangle = 0$$

unless $m = -u$ and $n = -v$. Applying this condition to the first term in (2.46),

$$\frac{\langle P(k - v,\ell)\ P(m - k,\ n - \ell) \rangle \langle P(v - k',-\ell')\ P(k' - m',\ \ell' - n') \rangle}{b(k,\ell)\ b^*(k',\ell')}$$

imposes the following constraints on the summation indices. For the first average,

$$k - v = k - m$$
$$\ell = \ell - n$$

and, for the second average,

$$v - k' = m' - k$$
$$-\ell' = n' - \ell'$$

When combined, these conditions become

$$m = m' = v$$
$$n = n' = 0$$

$$(2.48a)$$

while k, ℓ, k', and ℓ' are unconstrained indices. These conditions provide a nonzero result for the first term of (2.46). Index constraints for the second and third terms are

$$m = m'$$
$$n = n'$$
$$k' = m - k + v$$
$$\ell' = n - \ell$$

$$(2.48b)$$

47

and

$$k = k'$$

$$\ell = \ell'$$

$$m = m'$$ (2.48c)

$$n = n'$$

The average of BB^* is now performed in three steps by evaluating the three terms in (2.46) under the above conditions, respectively. For convenience, these separate averages will be denoted by $\langle BB^* \rangle_1$, $\langle BB^* \rangle_2$, and $\langle BB^* \rangle_3$.

When (2.48a) is applied to BB^* as defined by (2.47), the summations over m, n, m', and n' reduce to a single term, leaving a fourfold summation over k, ℓ, k', and ℓ'. The result is

$$\langle BB^* \rangle_1 = \cos^2 \phi \; (\beta + \beta\gamma \cos \theta)^2 \; \mathrm{sinc}^2(XI) \; \mathrm{sinc}^2(YI)$$

$$\cdot \sum_{k,\ell} \left[a^2(\nu - k)^2 \beta + (\beta - \alpha a\nu) \, b^2(k,\ell) \right] \frac{\pi^2 W(ak - a\nu, a\ell)}{L^2 b(k,\ell)}$$

$$\cdot \sum_{k',\ell'} \left[a^2(\nu - k')^2 \beta + (\beta - \alpha a\nu) \, b^2(k',\ell') \right] \frac{\pi^2 W(ak' - a\nu, a\ell')}{L^2 b^*(k',\ell')}$$

The limit of $L^2 \langle BB^* \rangle_1$ as L goes to infinity is evaluated by the same method used for first-order limits. The result is a second-order contribution to the specular-direction radar cross section,

$$\lim_{L \to \infty} L^2 \langle BB^* \rangle_1 = \frac{\pi^2 \beta^4}{4} (1 + \gamma^2)^2 \; \delta(\beta \sin \theta \cos \phi - \beta\alpha) \; \delta(\beta \sin \theta \sin \phi)$$

$$\times \iiint_{-\infty}^{\infty} \left[(\beta\alpha - p)^2 + \gamma^2 b^2(p,q) \right]\left[(\beta\alpha - p')^2 + \gamma^2 b^2(p',q') \right]$$

$$\cdot \frac{W(p - \beta\alpha, q) \; W(p' - \beta\alpha, q')}{b(p,q) \; b^*(p',q')} \; dp \, dq \, dp' dq' \qquad (2.49a)$$

48

When (2.48b) is applied,

$$\langle \ \rangle_2 = \sum_{mn} \cos^2 \emptyset \ [\beta + b(m,n) \cos \theta][\beta + b^*(m,n) \cos \theta] \ \text{sinc}^2(XR) \ \text{sinc}^2(YR)$$

$$\cdot \sum_{k\ell} \left[a^2(m-k)(\nu-k) \ \beta + (\beta - \alpha am) \ b^2(k,\ell)\right] \pi^2 \frac{W(ak - a\nu, a\ell)}{L^2 b(k,\ell)}$$

$$\cdot \left[a^2(k-\nu)(k-m) \ \beta + (\beta - \alpha am) \ b^2(m-k+\nu, n-\ell)\right]$$

$$\cdot \pi^2 \frac{W(am - ak, an - a\ell)}{L^2 b^*(m-k+\nu, n-\ell)}$$

and taking the limit of $L^2 \langle BB^* \rangle_2$ as L goes to infinity results in

$$\lim_{L \to \infty} L^2 \langle BB^* \rangle_2 = \iint_{-\infty}^{\infty} \left\{ \cos^2 \emptyset \ [\beta + b(p,q) \cos \theta][\beta + b^*(p,q) \cos \theta] \ 4\pi^2 \right.$$

$$\cdot \ \delta(\beta \sin \theta \cos \emptyset - p) \ \delta(\beta \sin \theta \sin \emptyset - q)$$

$$\cdot \iint_{-\infty}^{\infty} \left[(p-u)(\beta\alpha - u) \ \beta + (\beta\alpha - p) \ b^2(u,v)\right] \left[(u - \beta\alpha)(u-p) \ \beta \right.$$

$$\left. + (\beta - \alpha p) \ b^2(p-u+\nu, q-v)\right]$$

$$\left. \cdot \frac{W(\upsilon - \beta\alpha, v) \ W(p-u, q-v)}{16 \ b(u,v) \ b^*(p-u+\nu, q-v)} \ dudv \right\} \ dpdq$$

The delta functions in this expression allow analytical integration over p and q. After integration, the variables u and v are relabeled as p and q for consistency of notation with previous results.

$$\lim_{L\to\infty} L^2 \langle BB^* \rangle_2 = \frac{\pi^2 \beta^4}{4} (1 + \cos^2\theta) \cos^2\phi \iint_{-\infty}^{\infty} \Big[(\beta \sin\theta \cos\phi - p)$$

$$+ (1 - \alpha \sin\theta \cos\phi)\, b^2(p,q) \Big] \Big[(\beta \sin\theta \cos\phi - p)(\beta\alpha - p)$$

$$+ (1 - \alpha \sin\theta \cos\phi) b^2(\beta \sin\theta \cos\phi - p + \beta\alpha, \beta \sin\theta \sin\phi - q) \Big]$$

$$\cdot \frac{W(p - \beta\alpha, q)\, W(\beta \sin\theta \cos\phi - p, \beta \sin\theta \sin\phi - q)}{b(p,q)\, b^*(\beta \sin\theta \cos\phi - p + \beta\alpha, \beta \sin\theta \sin\phi - q)}\, dp\, dq$$

$$(2.49b)$$

This expression represents a second-order contribution to the nonspecular radar cross section. In Chapter IV, it will be shown that the roughness-spectrum arguments in (2.49b) meet the conditions for double Bragg scatter; that is, an electromagnetic wave incident at an angle $\sin^{-1}(\alpha)$ is Bragg scattered by those surface spectral components having wave numbers $p - \beta\alpha$ in the x-direction and q in the y-direction. These scattered fields are, in turn, Bragg scattered in the (θ, ϕ) direction by the surface spectral components of wave numbers $\beta \sin\theta \cos\phi - p$ in the x-direction and $\beta \sin\theta \sin\phi - q$ in the y-direction (Fig. 12). Expression (2.49b) is an integral over all surface spectral components that meet the Bragg-scattering conditions for the specified angles of incidence and observation.

When (2.48c) is applied, the third-term average of (2.46) becomes

$$\lim_{L\to\infty} L^2 \langle BB^* \rangle_3 = \frac{\pi^2 \beta^4}{4} \cos^2\phi\, (1 + \cos^2\theta)^2 \iint_{-\infty}^{\infty} \Big[(\beta \sin\theta \cos\phi - p)(\beta\alpha - p)$$

$$+ (1 - \alpha \sin\theta \cos\phi)\, b^2(p,q) \Big]^2 \qquad (2.49c)$$

$$\cdot \frac{W(p - \beta\alpha, q)\, W(\beta \sin\theta \cos\phi - p, \beta \sin\theta \sin\phi - q)}{b(p,q)\, b^*(p,q)}\, dp\, dq$$

The total average of the BB^* term in the limit of large L is then

$$\lim_{L \to \infty} L^2 \langle BB^* \rangle = \lim_{L \to \infty} L^2 \langle BB^* \rangle_1 + \lim_{L \to \infty} L^2 \langle BB^* \rangle_2 + \lim_{L \to \infty} L^2 \langle BB^* \rangle_3$$

When these averaging and limiting procedures are performed on the remaining terms and cross terms in (2.35) and the results are collected, the total field average $\lim_{L \to \infty} \langle E_\theta E_\theta^* \rangle / L^2$ required to calculate the second-order radar cross section by (2.29) is obtained. The final result to second order, including the zero and first-order terms in (2.44) and (2.45), is as follows.

For specular reflection:

$$\bar{\sigma}_{VV} = 4\pi\beta^2\gamma^2 \ \delta(\beta \sin \theta \cos \phi - \beta\alpha) \ \delta(\beta \sin \theta \sin \phi)$$

$$\cdot \left\{ 1 - \frac{\beta}{2} \iint_{-\infty}^{\infty} \left[\frac{(p - \beta\alpha)^2}{\gamma} + b^2(p,q) \ \gamma \right] \left[\frac{1}{b(p,q)} + \frac{1}{b^*(p,q)} \right] W(p - \beta\alpha, q) \ dpdq \right.$$

$$\left. + \frac{\beta^2}{4} \iiint_{-\infty}^{\infty} \left[\frac{(p - \beta\alpha)^2}{\gamma} + b^2(p,q) \ \gamma \right] \left[\frac{(p' - \beta\alpha)^2}{\gamma} + b^2(p',q') \ \gamma \right] \frac{W(p - \beta\alpha, q) \ W(p' - \beta\alpha, q')}{b(p,q) \ b^*(p',q')} \ dpdq \ dp'dq' \right\}$$

$$(2.50)$$

For nonspecular scattering:

$$\bar{\sigma}_{VV} = 4\pi\beta^4(\alpha \sin \theta - \cos \phi)^2 \ W(\beta \sin \theta \cos \phi - \beta\alpha, \ \beta \sin \theta \sin \phi)$$

$$+ \pi\beta^4 \iint_{-\infty}^{\infty} \left\{ \frac{[(\beta \sin \theta - p \cos \phi - q \sin \phi)(\beta\alpha - p) - (\alpha \sin \theta - \cos \phi) \ b^2(p,q)]^2}{b(p,q) \ b^*(p,q)} \right.$$

$$+ \left[\frac{(\beta \sin \theta - p \cos \phi - q \sin \phi)(\beta\alpha - p) - (\alpha \sin \theta - \cos \phi) \ b^3(p,q)}{b(p,q)} \right]$$

$$\left. \cdot \left[\frac{(\beta \sin \theta \cos \phi - p)[\cos \phi \ (\beta\alpha - p) - q \sin \phi] - (\alpha \sin \theta - \cos \phi) \ b^2(\beta \sin \theta \cos \phi - p + \beta\alpha, \ \beta \sin \theta \sin \phi - q)}{b^*(\beta \sin \theta \cos \phi - p + \beta\alpha, \ \beta \sin \theta \sin \phi - q)} \right] \right\}$$

$$\cdot W(p - \beta\alpha, q) \ W(\beta \sin \theta \cos \phi - p, \ \beta \sin \theta \sin \phi - q) \ dpdq \qquad (2.51)$$

51

The same techniques employed to determine $\bar{\sigma}_{VV}$ can be used to derive $\bar{\sigma}_{HH}$ by evaluating $\lim\limits_{L \to \infty} \langle E_\phi E_\phi^* \rangle / L^2$ for incident horizontal polarization. The results are as follows.

For specular reflection:

$$\bar{\sigma}_{HH} = 4\pi\beta^2\gamma^2\,\delta(\beta\sin\theta\cos\phi - \beta\alpha)\,\delta(\beta\sin\theta\sin\phi)$$

$$\cdot\left\{1 - \frac{1}{2}\beta\gamma \iint\limits_{-\infty}^{\infty} \left[q^2 + b^2(p,q)\right]\left[\frac{1}{b(p,q)} + \frac{1}{b^*(p,q)}\right] W(p - \beta\alpha, q)\,dpdq\right.$$

$$\left. + \frac{1}{4}\beta^2\gamma^2 \iiiint\limits_{-\infty}^{\infty} \left[q^2 + b^2(p,q)\right]\left[q'^2 + b^2(p',q')\right]\frac{W(p - \beta\alpha, q)\,W(p' - \beta\alpha, q')}{b(p,q)\,b^*(p',q')}\,dpdq\,dp'dq'\right\}$$

(2.52)

For nonspecular scattering:

$$\bar{\sigma}_{HH} = 4\pi\beta^4\gamma^2\cos^2\theta\cos^2\phi\,W(\beta\sin\theta\cos\phi - \beta\alpha,\,\beta\sin\theta\sin\phi)$$

$$+ \pi\beta^4\gamma^2\cos^2\theta \iint\limits_{-\infty}^{\infty}\left\{\frac{[\sin\phi\,(\beta\sin\theta\cos\phi - p)\,q - q\cos\phi\,(\beta\sin\theta\sin\phi - q) + \cos\phi\,b^2(p,q)]^2}{b(p,q)\,b^*(p,q)}\right.$$

$$+ \left[\frac{\sin\phi\,(\beta\sin\theta\cos\phi - p)\,q - q\cos\phi\,(\beta\sin\theta\sin\phi - q) + \cos\phi\,b^2(p,q)}{b(p,q)}\right]$$

$$\cdot\left[\frac{\sin\phi\,(p - \beta\alpha)(\beta\sin\theta\sin\phi - q) - q\cos\phi\,(\beta\sin\theta\sin\phi - q) + \cos\phi\,b^2(\beta\sin\theta\cos\phi - p + \beta\alpha,\,\beta\sin\theta\sin\phi - q)}{b^*(\beta\sin\theta\cos\phi - p + \beta\alpha,\,\beta\sin\theta\sin\phi - q)}\right]\right\}$$

$$\cdot W(p - \beta\alpha,\,q)\,W(\beta\sin\theta\cos\phi - p,\,\beta\sin\theta - q)\,dpdq$$

(2.53)

The above four expressions represent per unit area radar cross sections to second order averaged over the range of random slightly rough surfaces defined by Eq. (2.1). They are valid for arbitrary angles of incidence and observation but are restricted to static infinitely conducting surfaces; furthermore, they represent only the expected value of the radar

cross section and would not necessarily correspond to the cross section measured for a particular sample surface.

D. Radar Cross Sections for Time-Varying Surfaces

A characteristic of radar echoes from ocean surfaces is the doppler shift imparted to the incident radio wave by the motion of the ocean waves. The scattering theory developed above for static random surfaces is inadequate for predicting this feature and must be expanded to include time-varying rough surfaces.

1. Time-Varying Surfaces and Scattered Fields

A natural extension to Rice's theory provides a model for random time-varying surfaces. The surface is again a Fourier expansion with random coefficients, but the expansion is now in time as well as in space. With the time factor included, the surface determined by (2.1) becomes

$$f(x,y,t) = \sum_{mnI} P(m,n,I) \exp[-ia(mx + ny) - iwIt]$$

where $T = 2\pi/w$ is the time period of the Fourier expansion and corresponds to the spatial period L. The field expansions corresponding to those in Section A are in the form of

$$E = \sum_{mnI} A_{mnI} E(m,n,z,I)$$

where

$$E(m,n,z,I) = \exp[-ia(mx + ny) - ib(m,n) z - iwIt]$$

The statistics of the time-varying surface Fourier coefficients are

$$\langle P(m,n,I) \rangle = 0 \qquad\qquad (2.54a)$$

53

$$\langle P(m,n,I) \ P(u,v,J) \rangle = 0 \qquad (u,v,J) \neq (-m,-n,-I) \tag{2.54b}$$

$$\langle P(m,n,I) \ P^*(m,n,I) \rangle = \langle P(m,n,I) \ P(-m,-n,-I) \rangle = \frac{2\pi^3}{L^2 T} W(p,q,wI) \tag{2.54c}$$

where the factor of 2 in (2.54c) is retained from the Fourier transform over the time domain (see Section A.1). Although this does not follow Rice's convention, it allows the Fourier transformation of the autocorrelation functions, following the normal convention.

The procedure for matching boundary conditions and solving for the coefficients of the field expansions in terms of the surface coefficients is exactly the same as that for static surfaces. The resulting field expressions are those previously obtained, (2.12) and (2.13), except that $P(m,n,I)$ replaces $P(m,n)$, $Q(m,n,I,k,\ell,J)$ replaces $Q(m,n,k,\ell)$, and $E(m,n,z,I)$ replaces $E(m,n,z)$.

When the Stratton-Chu integral (2.27) is applied to the time-varying version of the scattered field for vertically polarized incidence (2.13), the θ-component of the field scattered by a finite surface becomes

$$
E_\theta = \frac{2ie^{(-i\beta R)}L^2}{4\pi R} \left\{ \underbrace{-\beta \cos\phi \cos\theta \ \mathrm{sinc}(XI) \ \mathrm{sinc}(YI) \ e^{i\omega_o t}}_{A} \right.
$$

$$
+ \underbrace{\sum_{mnI} \cos\phi \ [\beta + b(m,n)\cos\theta] \ \mathrm{sinc}(XR) \ \mathrm{sinc}(YR) \ [E_x \text{ terms}] \ e^{-i(wI-\omega_o)t} e^{ik_I R}}_{B}
$$

$$
+ a\underbrace{\sum_{mnI} \sin\phi \ [\beta + b(m,n)\cos\theta] \ \mathrm{sinc}(XR) \ \mathrm{sinc}(YR) \ [E_y \text{ terms}] \ e^{-i(wI-\omega_o)t} e^{ik_I R}}_{C}
$$

$$
\left. + \underbrace{\sum_{mnI} -\cos\theta \ (am\cos\phi + an\sin\phi) \frac{\mathrm{sinc}(XR)\ \mathrm{sinc}(YR)}{b(m,n)} [E_z \text{ terms}] \ e^{-i(wI-\omega_o)t} e^{ik_I R}}_{D} \right\}
$$

$$\tag{2.55}$$

54

where $k_I = Iw \sqrt{\mu\epsilon}$ and ω_o is the incident radian frequency. Implicit here is the assumption of a slowly varying surface, as can be seen by considering the exponential term,

$$E(m,n,z,I) \, e^{i\omega_o t} = \exp\left[-ia(mx + ny) - ib(m,n) \, z - i(wI - \omega_o) \, t\right]$$

To be exact, the factors $b(m,n)$ and β should also be functions of I because the electromagnetic propagation constant $\beta = \omega/c$ is really $\beta = (\omega_o - Iw)/c$, where $c = 1/\sqrt{\mu\epsilon}$ is the velocity of electromagnetic-wave propagation. Radar observations of ocean surfaces, however, indicate doppler shifts on the order of hertz for incident frequencies in the megahertz region. As a result, $(\omega_o - Iw) = \omega_o$ is allowed in the amplitude factors while the exact formulation for the phase terms (the exponential terms) is retained. Fortunately, because the surface of integration is taken in the $z = 0$ plane, the factor $b(m,n,I)$ never appears as a phase term.

2. $\sigma(\omega)$ Defined

Before proceeding further, the derivation of a useful expression from (2.55) for radar cross section must be considered. Because the effects of surface motion appear as doppler shifts in the frequency of the radar received power, it is convenient to express the per unit area radar cross section as a distribution over frequency (a per unit area radar cross section per unit frequency). The time-averaged scattered power per unit area is replaced, therefore, by a power spectral density per unit area $\Phi(\omega)$ in expressions for incremental radar cross section. Hence,

$$\sigma(\omega) \equiv \frac{4\pi R^2 \Phi(\omega)}{|E_i|^2} \tag{2.56}$$

where ω is radio-wave radian frequency.

55

For a given function of time $E(t)$, the power spectral density $\Phi(\omega)$ is the Fourier transform of the time autocorrelation function $\mathcal{R}(\tau)$ [Thomas, 1969, Ch. 3], where

$$\mathcal{R}(\tau) \equiv \lim_{T \to \infty} \frac{1}{2T} \int_{-\infty}^{\infty} E(t) \, E^*(t + \tau) \, dt$$

At $\tau = 0$, $\mathcal{R}(\tau) = \mathcal{R}(0) = \overline{|E(t)|^2}$ where the bar indicates the time average.

By definition,

$$\Phi(\omega) = \mathscr{F}[\mathcal{R}(\tau)] = \frac{1}{2\pi} \int_{-\infty}^{\infty} \mathcal{R}(\tau) \, e^{-i\omega\tau} \, d\tau$$

As a check on consistency of definitions, consider the per unit area radar cross section[†] σ^o, where

$$\sigma^o = \int_{-\infty}^{\infty} \sigma(\omega) \, d\omega$$

From (2.5$\supset$) and the definition of $\Phi(\omega)$,

$$\sigma^o = \frac{4\pi R^2}{|E_1|^2} \int_{-\infty}^{\infty} \frac{1}{2\pi} \int_{-\infty}^{\infty} \mathcal{R}(\tau) \, e^{-i\omega\tau} \, d\tau d\omega$$

When the order of integration is interchanged, the integral over ω defines the Dirac delta function given in Section A.1. Therefore,

---

[†] σ^o denotes the per unit area radar cross section of a time-varying surface while σ designates static surfaces. Both are defined in terms of time-average scattered power; however, the power scattered from a static surface is monochromatic; the power scattered from a time-varying surface is not.

$$\sigma^0 = \frac{4\pi R^2}{|E_i|^2} \int_{-\infty}^{\infty} \Re(\tau) \, \delta(\tau) \, d\tau = 4\pi R^2 \, \frac{\overline{|E(t)|^2}}{|E_i|^2}$$

where $\overline{|E(t)|^2}$ represents the per unit area time-average power in the scattered field. This expression for σ^0 is consistent with those for σ, the static-surface incremental radar cross section, defined in Section C.1; however, time dependence is stated explicitly because the scattered fields are no longer simple time-harmonic functions.

Equation (2.55), from which $\Phi(\omega)$ must be obtained, represents a stochastic process. If the time averages of all orders are equal to the corresponding statistical averages, the process is called ergodic. In particular, if the process is ergodic,

$$\Re(\tau) = R(\tau)$$

where $R(\tau)$ is the statistical autocorrelation function from which $\Phi(\omega)$ can be calculated. For Eq. (2.55), $R(\tau) = R(t_1 - t_2) = \langle E_\theta(t_1) \cdot E_\theta^*(t_2) \rangle / L^2$.

Although ergodicity is generally impossible to prove for a given process, there are times when it can be reasonably assumed from the physical mechanism generating the process. For a homogeneous ocean surface where the wind has been blowing steadily for a long time and the wave-height statistics are independent of time, ergodicity is often assumed for the random process describing surface height. The process represented by (2.55) is taken to be ergodic by the argument that the scattered-field statistics are generated by the scattering surface.

Assuming ergodicity, the radar cross-section expression (2.56) becomes

$$\sigma(\omega) = 4\pi R^2 \, \frac{\mathfrak{F}[\langle E_\theta(t_1) \, E_\theta^*(t_2) \rangle]}{L^2} \tag{2.57}$$

where $|E_i|^2 = 1$ as before, and $\langle E_\theta(t_1) \, E_\theta^*(t_2) \rangle / L^2 = R(t_1 - t_2)$.

57

3. Calculation of $\sigma_{VV}(\omega)$

The derivation of $\sigma_{VV}(\omega)$, the radar cross section per unit area per unit frequency, follows that of $\overline{\sigma}_{VV}$ in Section C.4. The average $\langle E_\theta(t_1) E_\theta^*(t_2) \rangle / L^2$ is found, the limit is taken as L and T go to infinity, and a Fourier transform places the result in the frequency domain.

For time-varying surfaces and using the abbreviated notation in (2.55), Eq. (2.35) becomes

$$E_\theta(t_1) E_\theta^*(t_2) = \frac{L^4}{4\pi^2 R^2} \left\{ A(t_1) A^*(t_2) + B(t_1) B^*(t_2) + C(t_1) C^*(t_2) \right.$$

$$\left. + D(t_1) D^*(t_2) + \left[A(t_1) B^*(t_2) + B(t_1) A^*(t_2) \right] + \ldots \right\}$$

$$(2.58)$$

The averages of the various terms are calculated to zero, first and second order as before.

a. Zero and First Order

The AA^* term contains no random variables (zero order) and is

$$\langle A(t_1) A^*(t_2) \rangle = \frac{\beta^2}{4} (\gamma + \cos\theta)^2 \cos^2\phi \ \text{sinc}^2(XI) \ \text{sinc}^2(YI) \ e^{i\omega_o(t_1 - t_2)}$$

Taking the limit of $L^2 \langle A(t_1) A^*(t_2) \rangle$ as L goes to infinity produces

$$\lim_{L \to \infty} L^2 \langle A(t_1) A^*(t_2) \rangle = 4\pi^2 \frac{\beta^2}{4} (\gamma + \cos\theta)^2 \cos^2\phi \ \delta(\beta \sin\theta \cos\phi - \beta\alpha)$$

$$\cdot \delta(\beta \sin\theta \sin\phi) \ e^{i\omega_o \tau} \qquad (2.59)$$

where $\tau = t_1 - t_2$ and, from Eq. (2.40),

$$\lim_{L \to \infty} L \, \text{sinc}^2 \frac{xL}{2} = 2\pi\delta(x)$$

The Fourier transform,

$$\mathcal{F}[\cdot] = \frac{1}{2\pi} \int_{-\infty}^{\infty} [\cdot] \, e^{-i(\omega-\omega_o)\tau} \, d\tau$$

provides the power spectral density from the autocorrelation function (2.59),

$$\mathcal{F}[R_{AA}] = 4\pi^2 \beta^2 \gamma^2 \, \delta(\beta \sin \theta \cos \emptyset - \rho\alpha) \, \delta(\beta \sin \theta \sin \emptyset)$$

$$\cdot \frac{1}{2\pi} \int_{-\infty}^{\infty} e^{-i(\omega-\omega_o)\tau} \, d\tau \qquad (2.60)$$

where

$$R_{AA} = \lim_{L \to \infty} L^2 \langle A(t_1) \, A^*(t_2) \rangle$$

$$\cos^2 \emptyset = 1$$
$$\cos^2 \theta = \gamma^2$$

from the delta functions. The integral

$$\frac{1}{2\pi} \int_{-\infty}^{\infty} e^{-i(\omega-\omega_o)\tau} \, d\tau$$

is the Fourier transform of a constant (unity in this case) and is $\delta(\omega - \omega_o)$ from the previous definition of the Dirac delta function. The AA contribution to the power spectral density per unit scattering area is then

$$\Phi_{AA}(\omega) = \mathcal{F}[R_{AA}] = 4\pi^2 \beta^2 \gamma^2 \; \delta(\beta \sin \theta \cos \emptyset - \beta\alpha) \; \delta(\beta \sin \theta \sin \emptyset) \; \delta(\omega - \omega_o)$$

$$(2.61)$$

and represents power scattered in the specular direction at the incident radian frequency ω_o.

The addition of time variation to the slightly rough surface does not affect the zero-order scattered power (power reflected from a planar surface) except to specify its frequency. The total average reflected power is the same for both time-varying and static surfaces; for the time-varying surface, it is [except for the multiplicative factor of $(4\pi^2 R^2)^{-1}$]

$$\int_{-\infty}^{\infty} \Phi_{AA}(\omega) \; d\omega$$

or, equivalently,

$$R_{AA}(\tau) \Big|_{\tau=0}$$

Performing the indicated integration eliminates $\delta(\omega - \omega_o)$ from (2.61) which then becomes identical to the average power term (2.41) for the static surface.

First-order terms contributing to power scattered in the specular direction are derived from the cross terms involving A in (2.58). As an example, consider the cross term

$$A(t_1) B^*(t_2) = -\frac{\beta}{2} (\gamma + \cos \theta) \cos \emptyset \; \text{sinc(XI) sinc(YI)} \; e^{i\omega_o t_1}$$

$$\cdot \sum_{mnI} \cos \emptyset \; [\beta + b^*(m,n) \cos \theta] \; \text{sinc(XR) sinc(YR)}$$

$$\cdot e^{i(wI-\omega_o)t_2} e^{-ik_I R}$$

$$\cdot \sum_{k\ell J} \left[a^2(m-k)(\nu-k)\beta + (\beta-\alpha m) \; b^2(k,\ell) \right] Q^*(m,n,I,k,\ell,J)$$

$$(2.62)$$

60

where only those parts that produce first-order terms (product of two random variables) have been included. The average of (2.62) is nonzero only if

$$\langle Q^*(m,n,I,k,\ell,J) \rangle \neq 0$$

where

$$Q^*(m,n,I,k,\ell,J) = \frac{P^*(k - \nu, \ell, J) \; P^*(m - k, \; n - \ell, \; I - J)}{b^*(k,\ell)}$$

Under the restrictions on m,n,I, the first summation reduces to a single term where, again,

$$b(m,n) \rightarrow b(\nu,0) = \beta\gamma$$

$$\mathrm{sinc}(XR) \rightarrow \mathrm{sinc}(XI)$$

$$\mathrm{sinc}(YR) \rightarrow \mathrm{sinc}(YI)$$

The average becomes

$$\langle AB^* \rangle = -\frac{\beta}{2}(\gamma + \cos\theta)\cos^2\phi \; \mathrm{sinc}^2(XI) \; \mathrm{sinc}^2(YI)(\beta + \beta\gamma\cos\theta)$$

$$\cdot \; e^{i\omega_o(t_1 - t_2)} \sum_{k\ell J} \left[a^2(\nu - k)^2 \beta + (\beta - \alpha a\nu) b^2(k,\ell) \right]$$

$$\cdot \; \frac{2\pi^3}{L^2 T} \frac{W(ak - a\nu, a\ell, wJ)}{b^*(k,\ell)}$$

When the limit of $L^2\langle AB^* \rangle$ is taken as L and T go to infinity,

$$ak \rightarrow p$$

$$a\ell \rightarrow q$$

$$wJ \rightarrow \Omega$$

and the summations become integrals over k, ℓ, and J. The variables of integration are then changed to p, q, and Ω with the result that

$$\lim_{L,T \to \infty} \langle AB^* \rangle = -4\pi^2 \beta^3 \gamma \, (1 + \gamma^2) \, \delta(\beta \sin \theta \cos \emptyset - \beta\alpha) \, \delta(\beta \sin \theta \sin \emptyset)$$

$$\cdot \; e^{i\omega_o \tau} \iiint_{-\infty}^{\infty} \left[(\beta\alpha - p)^2 + \gamma^2 b^2(p,q) \right] \frac{W(p - \beta\alpha, q, \Omega)}{4b^*(p,q)} \, dp \, dq \, d\Omega$$

$$= R_{AB}$$

The Fourier transform of R_{AB} yields another delta function in frequency,

$$\Phi_{AB}(\omega) = \mathcal{F}[R_{AB}] = -\pi^2 \beta^3 \gamma (1 + \gamma^2) \, \delta(\beta \sin \theta \cos \emptyset - \beta\alpha) \, \delta(\beta \sin \theta \sin \emptyset) \, \delta(\omega - \omega_o)$$

$$\cdot \iiint_{-\infty}^{\infty} \left[(\beta\alpha - p)^2 + \gamma^2 b^2(p,q) \right] \frac{W(p - \beta\alpha, q, \Omega)}{b^*(p,q)} \, dp \, dq \, d\Omega$$

$$\tag{2.63}$$

Again power is scattered in the specular direction but, surprisingly, only at the incident wave frequency although this power depends on a rough, rather than planar, time-varying surface.

The remainder of the cross terms in (2.58) involving $A(t)$ are similar to (2.63) and, when combined as

$$\sigma_{VV}(\omega) = 4\pi R^2 \left(\frac{1}{4\pi^2 R^2} \right) \left[\Phi_{AA}(\omega) + \Phi_{AB}(\omega) + \Phi_{BA}(\omega) + \Phi_{AC}(\omega) + \ldots \right]$$

determine the specular radar cross section per unit area per unit frequency to first order,

$$\sigma_{VV}(\omega) = 4\pi\beta^2\gamma^2 \, \delta(\beta \sin \theta \cos \emptyset - \beta\alpha) \, \delta(\beta \sin \theta \sin \emptyset) \, \delta(\omega - \omega_o)$$

$$\cdot \left\{ 1 - \frac{\beta}{2} \iiint\limits_{-\infty}^{\infty} \left[\frac{(p - \beta\alpha)^2}{\gamma} + \gamma b^2(p,q) \right] \right.$$

$$\left. \cdot \left[\frac{1}{b(p,q)} + \frac{1}{b^*(p,q)} \right] W(p - \beta\alpha, q, \Omega) \, dpdqd\Omega \right\} \qquad (2.64)$$

The nonspecular radar cross section to first order involves the terms in (2.58) that do not contain $A(t)$. For example,

$$B(t_1, \, C^*(t_2) = \sum_{mnI} \cos \emptyset \, [\beta + b(m,n) \cos \theta] \, \text{sinc}(XR) \, \text{sinc}(YR)$$

$$\cdot \, i(\alpha am - \beta) \, P(m - \nu, n, I) \, e^{-i(wI - \omega_o)t_1} \, e^{ik_I R}$$

$$\cdot \sum_{m'n'I'} -\sin \emptyset \, [\beta + b^*(m',n') \cos \theta] \, \text{sinc}(XR') \, \text{sinc}(YR')$$

$$\cdot \, i\alpha an' P^*(m' - \nu, n', I') \, e^{i(wI' - \omega_o)t_2} \, e^{-ik_{I'} R} \qquad (2.65)$$

where only the first-order terms are retained.

From condition (2.54c), a nonzero average requires $m = m'$, $n = n'$, and $I = I'$, thereby reducing the average of (2.65) to

$$\langle BC^* \rangle = \sum_{mnI} \sin \emptyset \cos \emptyset \, [\beta + b(m,n) \cos \theta][\beta + b^*(m,n) \cos \theta] \, \text{sinc}^2(XR) \, \text{sinc}^2(YR)$$

$$\cdot \, c \, (\alpha am - \beta) \exp\left[-i(wI - \omega_o)(t_1 - t_2) \right]$$

$$\cdot \, \frac{2\pi^3}{TL^2} \, W(am - a\nu, an, wI)$$

Taking the limit of large L and T and changing the variables of integration as in the previous example gives

$$\lim_{L,T \to \infty} L^2 \langle BC^* \rangle = 4\pi^2 \iiint_{-\infty}^{\infty} \cos \emptyset \sin \emptyset \; [\beta + b(p,q) \cos \theta][\beta + b^*(p,q) \cos \theta]$$

$$\cdot \; \delta(\beta \sin \theta \cos \emptyset - p) \; \delta(\beta \sin \theta \sin \emptyset - q)$$

$$\cdot \; \alpha q (\alpha p - \beta) \; e^{-i(\Omega - \omega_o)\tau} \; \frac{W(p - \beta\alpha, q, \Omega)}{4} \; dp\,dq\,d\Omega$$

The delta functions are used to integrate analytically over p and q,

$$\lim_{L,T \to \infty} L^2 \langle BC^* \rangle = \pi^2 \cos \emptyset \sin \emptyset \; \beta^4 (1 + \cos^2 \theta)^2 \; [\alpha \sin \theta \sin \emptyset (\alpha \sin \theta \sin \emptyset - 1)]$$

$$\cdot \int_{-\infty}^{\infty} W(\beta \sin \theta \cos \emptyset - \beta\alpha, \; \beta \sin \theta \sin \emptyset, \Omega) \; e^{-i(\Omega - \omega_o)\tau} \; d\Omega$$

$$= R_{BC}$$

In Fourier transforming the above, the order of integration is exchanged. For the integral alone,

$$\int_{-\infty}^{\infty} d\Omega \left[\frac{1}{2\pi} \int_{-\infty}^{\infty} W(\beta \sin \theta \cos \emptyset - \beta\alpha, \; \beta \sin \theta \sin \emptyset, \Omega) \; e^{-i(\Omega - \omega_o + \omega)\tau} \; d\tau \right]$$

$$= \int_{-\infty}^{\infty} \delta(\Omega - \omega_o + \omega) \; W(\beta \sin \theta \cos \emptyset - \beta\alpha, \; \beta \sin \theta \sin \emptyset, \Omega) \; d\Omega$$

$$= W(\beta \sin \theta \cos \emptyset - \beta\alpha, \; \beta \sin \theta \sin \emptyset, \; \omega_o - \omega)$$

The spectral density for the BC^* term is then

$$\Phi_{BC}(\omega) = \pi^2 \cos \emptyset \sin \emptyset \, \beta^4 (1 + \cos^2 \theta)^2 [\alpha \sin \theta \sin \emptyset \, (\alpha \sin \theta \sin \emptyset - 1)]$$

$$\cdot \, W(\beta \sin \theta \cos \emptyset - \beta\alpha, \, \beta \sin \theta \sin \emptyset, \, \omega_o - \omega)$$

Again, the remainder of the first-order products in (2.58) have similar spectral densities and combine to determine the first-order nonspecular radar cross section per unit area per unit frequency,

$$\sigma_{VV}(\omega) = 4\pi\beta^4(\alpha \sin \theta - \cos \emptyset)^2 \, W(\beta \sin \theta \cos \emptyset - \beta\alpha, \, \beta \sin \theta \sin \emptyset, \, \omega_o - \omega)$$

$$(2.66)$$

Unlike the specular cross section, the nonspecular cross section provides for returned powers at other than the incident-wave frequency. Because specular power contains a single frequency, specular scattering in this case is also coherent scattering; the nonspecular power containing a spread of frequencies is referred to as incoherent scattered power.

b. Second Order

Second-order terms for time-varying surfaces are derived in the same manner as those for static surfaces except that the statistical averages must be Fourier transformed. Recall that the second-order terms are those containing the product of four random variables in the form of $Q(m,n,I,k,\ell,J) \, Q^*(m',n',I',k',\ell',J')$. The average of QQ^* is expanded into three terms as before,

$$\langle Q(m,n,I,k,\ell,J) \, Q^*(m',n',I',k',\ell',J') \rangle$$

$$= \frac{\langle P(k-v,\ell,J) \, P(m-k, \, n-\ell, \, I-J) \rangle \langle P(v-k', \, -\ell, -J') \, P(k'-m', \, \ell'-n', \, J'-I') \rangle}{b(k,\ell) \, b^*(k',\ell')}$$

$$+ \frac{\langle P(k-v,\ell,J) \, P(k'-m', \, \ell'-n', \, J'-I') \rangle \langle P(m-k, \, n-\ell, \, I-J) \, P(v-k',-\ell',-J') \rangle}{b(k,\ell) \, b^*(k',\ell')}$$

$$+ \frac{\langle P(k-v,\ell,J) \, P(v-k', \, -\ell'-J') \rangle \langle P(m-k, \, n-\ell, \, I-J) \, P(k'-m', \, \ell'-n', \, J'-I') \rangle}{b(k,\ell) \, b^*(k',\ell')}$$

$$(2.67)$$

65

For nonzero averages in the first term, the index constraints are

$$m' = m = \nu$$
$$n' = n = 0 \qquad (2.68a)$$
$$I' = I = 0$$

and are analogous to those of (2.48a) for the static surface. The conditions for nonzero averages for the second and third terms are

$$m = m' \qquad k' = m - k + \nu$$
$$n = n' \qquad \ell' = n - \ell \qquad (2.68b)$$
$$I = I' \qquad J' = I - J$$

and

$$m = m' \qquad k = k'$$
$$n = n' \qquad \ell = \ell' \qquad (2.68c)$$
$$I = I' \qquad J = J'$$

A typical term in (2.58) is evaluated t illustrate the technique used to find the second-order time-varying radar cross section. All second-order terms are similar, and their averages are computed by means of the three-term expansion (2.67). As in the static-surface second-order example, the typical term is

$$B(t_1)\, B^*(t_2) = \sum_{mnI} \cos \phi \, [\beta + b(m,n) \cos \theta] \operatorname{sinc}(XR) \operatorname{sinc}(YR)\; e^{-i(wI - \omega_o)t_1}$$

$$\cdot\; e^{ik_I R} \sum_{k\ell J} \left[a^2 (m - k)(\nu - k)\, \beta + (\beta - \alpha am)\, b^2(k,\ell) \right]$$

$$\cdot\; Q(m,n,I,k,\ell J) \qquad (2.69)$$

$$\cdot \sum_{m'n'I'} \cos \emptyset \; [\beta + b^*(m',n') \cos \theta] \; \mathrm{sinc}(XR') \; \mathrm{sinc}(YR')$$

$$\cdot \; e^{i(wI'-\omega_o)t_2} \; e^{-ik_{I'}\cdot R}$$

$$\cdot \sum_{k'\ell'J'} \left[a^2(m'-k')(\nu-k') \beta + (\beta - \alpha am') \, b^2(k',\ell') \right]$$

$$\cdot \; Q^*(m',n',I',k',\ell',J') \qquad\qquad (2.69)$$
$$\text{Cont.}$$

The three averages corresponding to the three terms in (2.67) are denoted as $\langle BB^* \rangle_1$, $\langle BB^* \rangle_2$, and $\langle BB^* \rangle_3$ and are evaluated by using the conditions stated in (2.68).

Applying condition (2.68a) to the average in (2.69) yields

$$\langle BB^* \rangle_1 = \cos^2 \emptyset \; \beta^2 (1 + \gamma \cos \theta)^2 \; \mathrm{sinc}^2(XI) \; \mathrm{sinc}^2(YI) \; e^{i\omega_o\tau}$$

$$\cdot \sum_{k\ell Jk'\ell'J'} \left[a^2(\nu-k)^2 \beta + (\beta - \alpha\nu) \, b^2(k,\ell) \right]$$

$$\cdot \left[a^2(\nu-k')^2 \beta + (\beta - \alpha a\nu) \, b^2(k',\ell') \right]$$

$$\cdot \; \frac{W(ak - a\nu, a\ell, wJ) \; W(ak' - a\nu, a\ell', wJ')}{b(k,\ell) \; b^*(k',\ell')} \left(\frac{2\pi^3}{TL^2} \right)^2$$

The limit of $L^2 \langle BB^* \rangle_1$ as T and L go to infinity is taken as before. Fourier transformation provides a delta function in frequency because of the $e^{i\omega_o\tau}$ term, and the result

$$\Phi_{BB1}(\omega) = \frac{\pi^2}{4} \beta^4 (1 + \gamma^2)^2 \, \delta(\beta \sin \theta \cos \emptyset - \beta\alpha) \, \delta(\beta \sin \theta \sin \emptyset) \, \delta(\omega - \omega_o)$$

$$\cdot \iiiint_{-\infty}^{\infty} \left[(\beta\alpha - p)^2 + \gamma^2 b^2(p,q) \right] \left[(\beta\alpha - p')^2 + \gamma^2 b^2(p',q') \right]$$

$$\cdot \frac{W(p - \beta\alpha, q, \Omega) \, W(p' - \beta\alpha, q', \Omega')}{b(p,q) \, b^*(p,q)} \, dp \, dq \, d\Omega \, dp' \, dq' \, d\Omega' \qquad (2.70a)$$

is a second-order contribution to the specular radar cross section.

Applying condition (2.68b) to (2.69) and averaging provides

$$\langle BB^* \rangle_2 = \sum_{mnI} \cos^2 \emptyset \, [\beta + b(m,n) \cos \theta][\` + b^*(m,n) \cos \theta]$$

$$\cdot \text{sinc}^2(XR) \, \text{sinc}^2(YR) \, e^{-i(wI - \omega_o)\tau}$$

$$\cdot \sum_{k \ell J} \left[a^2(m - k)(\nu - k) \, \beta + (\beta - \alpha am) \, b^2(k,\ell) \right]$$

$$\cdot \left[a^2(k - \nu)(k - m) \, \beta + (\beta - \alpha am) \, b^2(m - k + \nu, \, n - \ell) \right]$$

$$\cdot \frac{W(ak - a\nu, a\ell, wJ) \, W(am - ak, \, an - a\ell, \, wI - wJ)}{b(k,\ell) \, b^*(m - k + \nu, \, n - \ell)} \left(\frac{2\pi^3}{TL^2} \right)^2$$

In the limit of large L and T, a sixfold integral is encountered; however, the sinc functions become delta functions and two of the integrations can be performed by inspection,

$$\lim_{L, T \to \infty} L^2 \langle BB^* \rangle_2 = \frac{\pi^2}{4} \cos^2 \emptyset \, \beta^4 (1 + \cos^2 \theta)^2 \int_{-\infty}^{\infty} e^{-i(\Omega' - \omega_o)\tau}$$

$$\cdot \left\{ \iiint_{-\infty}^{\infty} \left[(\beta \sin\theta \cos\phi - p)(\beta\alpha - p) + (1 - \alpha \sin\theta \cos\phi)\, b^2(p,q) \right] \right.$$

$$\cdot \left[(p - \beta\alpha)(p - \beta \sin\theta \cos\phi) + (1 - \alpha \sin\theta \cos\phi) \right.$$

$$\left. \cdot\ b^2(\beta \sin\theta \cos\phi - p + \beta\alpha,\ \beta \sin\theta \sin\phi - q) \right]$$

$$\left. \cdot\ \frac{W(p - \beta\alpha, q, \Omega)\ W(\beta \sin\theta \cos\phi - p,\ \beta \sin\theta \sin\phi - q,\ \Omega' - \Omega)}{b(p,q)\ b^*(\sin\theta \cos\phi - p + \beta\alpha,\ \beta \sin\theta \sin\phi - q)}\ dp\,dq\,d\Omega \right\}\ d\Omega'$$

Fourier transformation yields the delta function $\delta(\Omega' - \omega_o + \omega)$ which allows analytical integration over Ω'. The result is

$$\Phi_{BB2}(\omega) = \frac{\pi^2}{4} \cos^2\phi\ \beta^4 (1 + \cos^2\theta)^2$$

$$\cdot \iiint_{-\infty}^{\infty} \left[(\beta \sin\theta \cos\phi - p)(\beta\alpha - p) + (1 - \alpha \sin\theta \cos\phi)\, b^2(p,q) \right]$$

$$\cdot \left[(p - \beta\alpha)(p - \beta \sin\theta \cos\phi) + (1 - \alpha \sin\theta \cos\phi) \right.$$

$$\left. \cdot\ b^2(\beta \sin\theta \cos\phi - p + \beta\alpha,\ \beta \sin\theta \sin\phi - q) \right]$$

$$\cdot\ \frac{W(p - \beta\alpha, q, \Omega)\ W(\beta \sin\theta \cos\phi -\ \ \beta \sin\theta \sin\phi - q,\ \omega_o - \omega - \Omega)}{b(p,q)\ b^*(\beta \sin\theta \cos\phi - p + \beta\alpha,\ \beta \sin\theta \sin\phi - q)}$$

$$\cdot\ dp\,dq\,d\Omega \tag{2.70b}$$

To find the third-term average (2.68c), the procedure is the same as for the second-term average. After averaging, limiting, and transforming,

$$\Phi_{BB3}(\omega) = \frac{\pi^2}{4} \cos^2 \emptyset \; \beta^4 (1 + \cos^2 \theta)^2$$

$$\cdot \iiint_{-\infty}^{\infty} \left[(\beta \sin \theta \cos \emptyset - p)(\beta\alpha - p) + (1 - \alpha \sin \theta \cos \emptyset) \; b^2(p,q) \right]^2$$

$$\cdot \frac{W(p - \beta\alpha, q, \Omega) \; W(\beta \sin \theta \cos \emptyset - p, \; \beta \sin \theta \sin \emptyset - q, \; \omega_o - \omega - \Omega)}{b(p,q) \; b^*(p,q)}$$

$$\cdot \; dp \, dq \, d\Omega \tag{2.70c}$$

As in the static-surface case, $\langle BB^* \rangle_1$ contributes to the specular cross section, and $\langle BB^* \rangle_2$ and $\langle BB^* \rangle_3$ contribute to the nonspecular cross section.

When all terms in (2.58) have been evaluated to second order in the manner described for $B(t_1) \, B^*(t_2)$, they are combined and used in (2.57) to arrive at the second-order radar cross section per unit area per unit frequency. The radar cross sections to second order (including zero- and first-order terms) are as follows.

Coherent:

$$\sigma_{VV}(\omega) = 4\pi\beta^2 \gamma^2 \quad (\beta \sin \theta \cos \emptyset - \beta\alpha) \; \delta(\beta \sin \theta \sin \emptyset) \; \delta(\omega_o - \omega)$$

$$\cdot \left\{ 1 - \frac{\beta}{2} \iiint_{-\infty}^{\infty} \left[\frac{(p - \beta\alpha)^2}{\gamma} + \gamma b^2(p,q) \right] \left[\frac{1}{b(p,q)} + \frac{1}{b^*(p,q)} \right] W(p - \beta\alpha, q, \Omega) \; dp \, dq \, d\Omega \right.$$

$$\cdot \frac{\beta^2}{4} \iiiint_{-\infty}^{\infty} \left[\frac{(p - \beta\alpha)^2}{\gamma} + \gamma b^2(p,q) \right] \left[\frac{(p' - \beta\alpha)^2}{\gamma} + \gamma b^2(p',q') \right]$$

$$\left. \cdot \frac{W(p - \beta\alpha, q, \Omega) \; W(p' - \beta\alpha, q', \Omega')}{b(p,q) \; b^*(p',q')} \; dp \, dq \, d\Omega \; dp' \, dq' \, d\Omega' \right\} \tag{2.71}$$

Incoherent:

$$\sigma_{VV}(\omega) = 4\pi\beta^4 (\alpha \sin\theta - \cos\emptyset)^2 \; W(\beta \sin\theta \cos\emptyset - \beta\alpha, \; \beta \sin\theta \sin\emptyset, \; \omega_0 - \omega)$$

$$+ \pi\beta^4 \iiint_{-\infty}^{\infty} \left\{ \frac{[(\beta \sin\theta - p\cos\emptyset - q\sin\emptyset)(\beta\alpha - p) - (\alpha \sin\theta - \cos\emptyset)\, b^2(p,q)]^2}{b(p,q)\, b^*(p,q)} \right.$$

$$+ \left[\frac{(\beta \sin\theta - p\cos\emptyset - q\sin\emptyset)(\beta\alpha - p) - (\alpha \sin\theta - \cos\emptyset)\, b^2(p,q)}{b(p,q)} \right]$$

$$\left. \cdot \left[\frac{(\beta \sin\theta \cos\emptyset - p)[\cos\emptyset(\beta\alpha - p) - q\sin\emptyset] - (\alpha \sin\theta - \cos\emptyset)\, b^2(\beta \sin\theta \cos\emptyset - p + \beta\alpha, \; \beta \sin\theta \sin\emptyset - q)}{b^*(\beta \sin\theta \cos\emptyset - p + \beta\alpha, \; \beta \sin\theta \sin\emptyset - q)} \right] \right\}$$

$$\cdot W(p - \beta\alpha, q, \Omega)\; W(\beta \sin\theta \cos\emptyset - p, \; \beta \sin\theta \sin\emptyset - q, \; \omega_0 - \omega - \Omega)\; dp\,dq\,d\Omega \qquad (2.72)$$

The derivation of $\sigma_{HH}(\omega)$ is similar to that for $\sigma_{VV}(\omega)$, and the results are as follows.

Coherent:

$$\sigma_{HH}(\omega) = 4\pi\beta^2\gamma^2 \; \delta(\beta \sin\theta \cos\emptyset - \beta\alpha)\; \delta(\beta \sin\theta \sin\emptyset)\; \delta(\omega_0 - \omega)$$

$$\cdot \left\{ 1 - \frac{\beta\gamma}{2} \iiint_{-\infty}^{\infty} \left[q^2 + b^2(p,q) \right]\left[\frac{1}{b(p,q)} + \frac{1}{b^*(p,q)} \right] W(p - \beta\alpha, q, \Omega)\; dp\,dq\,d\Omega \right.$$

$$+ \frac{\beta^2\gamma^2}{4} \iiiint_{-\infty}^{\infty} \left[q^2 + b^3(p,q) \right]\left[q'^2 + b^2(p',q') \right] \frac{W(p - \beta\alpha, q, \Omega)\; W(p' - \beta\alpha, q', \Omega')}{b(p,q)\, b^*(p',q')}\; dp\,dq\,d\Omega\; dp'\,dq'\,d\Omega' \left. \right\}$$

$$(2.73)$$

Incoherent:

$$\sigma_{HH}(\omega) = 4\pi\beta^4\gamma^2 \cos^2\theta \left\{ \cos^2\phi \, W(\beta\sin\theta\cos\phi - \beta\alpha, \, \beta\sin\theta\sin\phi, \, \omega_o - \omega) \right.$$

$$+ \frac{1}{4} \iiint \left\{ \frac{[q\sin\phi \, (\beta\sin\theta\cos\phi - p) - q\cos\phi \, (\beta\sin\theta\sin\phi - q) + \cos\phi \, b^2(p,q)]^2}{b(p,q) \, b^*(p,q)} \right.$$

$$+ \left[\frac{q\sin\phi \, (\beta\sin\theta\cos\phi - p) - q\cos\phi \, (\beta\sin\theta\sin\phi - q) + \cos\phi \, b^2(p,q)}{b(p,q)} \right]$$

$$\cdot \left[\frac{\sin\phi \, (p-\beta\alpha)(\beta\sin\theta\sin\phi - q) - q\cos\phi \, (\beta\sin\theta\sin\phi - q) + \cos\phi \, b^2(\beta\sin\theta\cos\phi - p + \beta\alpha, \, \beta\sin\theta\sin\phi - q)}{b^*(\beta\sin\theta\cos\phi - p + \beta\alpha, \, \beta\sin\theta\sin\phi - q)} \right] \right\}$$

$$\cdot \, W(p - \beta\alpha, \, q, \, \Omega) \, W(\beta\sin\theta\cos\phi - p, \, \beta\sin\theta\sin\phi - q, \, \omega_o - \omega - \Omega) \, dp\,dq\,d\Omega \right\} \qquad (2.74)$$

Expressions (2.71) through (2.74) for the second-order bistatic-radar cross sections per unit area per unit frequency for a slightly rough time-varying surface are the major results obtained in this chapter. They represent radar cross sections in terms of the surface-height directional spectrum and will be used in Chapters IV and V to analyze ocean surfaces.

E. Effects of Finitely Conducting Surfaces

For smooth surfaces, the difference between fields reflected by a perfect conductor and those reflected by a good conductor are small, except at vertically polarized grazing incidence; Jordan (1950, pp. 621-623) provides examples of these differences in the form of dipole far-field radiation patterns. Vertically polarized waves propagating along a finite conductor are continuously attenuated by ohmic losses until, at large distances from the source, they are no longer detectable. No such attenuation occurs along perfect conductors. On the other hand, tangential boundary conditions cause horizontally polarized fields to vanish at grazing incidence for both perfectly and finitely conducting surfaces.

For the slightly rough surfaces considered here, the assumption of perfect conductivity causes a singularity in the expressions for the scattered field. As might be expected, this singularity is associated with radio waves propagating along the surface; however, both σ_{VV} and

72

σ_{HH} exhibit singularities because of depolarization caused by surface roughness.

When $b(p,q) = 0$, (2.71) through (2.74) become singular, surprisingly, at all angles of incidence and observation. By the definition in (2.5), $b(p,q)$ represents the z-component of the radio-wave propagation constant for a wave in which p and q denote the x- and y-components of propagation, respectively; therefore, when $b(p,q) = 0$, propagation occurs entirely along the x,y-plane or mean scattering surface. For finitely conducting surfaces, however, there is always a component of propagation directed into the surface to provide for ohmic losses (Fig. 14) and, as a result, the z-component of propagation cannot be represented entirely by $b(p,q)$. In Chapter IV, the radio wave defined by p,q, and $b(p,q)$ is identified as the intermediate scattered wave associated with double Bragg scattering; consequently, it can assume grazing propagation independent of the incidence and observation angles.

Including the effects of finite conductivity in (2.71) through (2.74) not only allows evaluation of σ_{VV} and c_{HH}, but also provides a more realistic scattering model. For good conductors such as sea water and only slightly rough scattering surfaces, the effects of finite
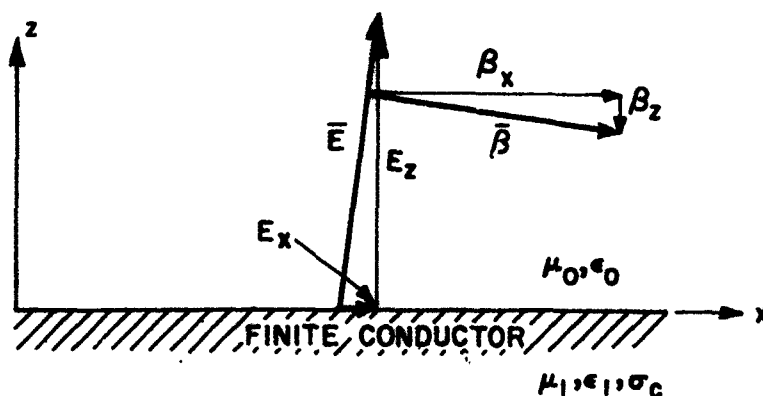

Fig. 14. PROPAGATION ALONG A FINITE CONDUCTOR. Vertically polarized waves propagating along a surface of finite conductivity are tilted slightly toward the surface, thereby providing a component of propagation into the surface. Power flow into the surface accounts for ohmic losses arising from field-induced currents flowing in the finite conductor.

conductivity are most apparent at vertically polarized grazing propagation. Under these conditions, deviation from perfect-conductor theory is explained by the small component of wave propagation directed into the surface. The equations for σ_{VV} and σ_{HH} are modified by replacing $b(p,q)$ with

$$b(p,q) + \delta\beta_z$$

where $\delta\beta_z$ represents the z-component of the propagation constant for grazing conditions $[b(p,q) = 0]$. The substitution is justified only if $\delta\beta_z$ is small compared to $b(p,q)$, except near grazing propagation.

The procedure used here to determine $\delta\beta_z$ follows that of Jordan (1965, pp. 204-207). A vertically polarized plane wave propagating along the interface between air and a finitely conducting smooth surface is assumed (Fig. 14). There are no variations in the y-direction; variations in the x-direction are designated by $e^{-\gamma_o x}$ in the air and by $e^{-\gamma_1 x}$ in the conductor. Variations in the z-direction are to be determined.

The following are Maxwell's equations in source-free time-harmonic form.

In air:

$$\frac{\partial E_x}{\partial z} + \gamma_o E_z = -i\omega\mu_o H_y$$

$$- \gamma_o H_y = i\omega\epsilon_o E_z$$

$$- \frac{\partial H_y}{\partial z} = i\omega\epsilon_o E_x \tag{2.75a}$$

Within the conductor:

$$\frac{\partial E_x}{\partial z} + \gamma_1 E_z = -i\omega\mu_1 H_y$$

$$- \gamma H_y = (\sigma_c + i\omega\epsilon_1) E_z$$

$$- \frac{\partial H_y}{\partial z} = (\sigma_c + i\omega\epsilon_1) E_x \tag{2.75b}$$

74

where ϵ and μ represent the permittivity and permeability of the media. Subscripts o and 1 refer to the air and conductor regions, respectively. Conductivity in region 1 is σ_c. Combining these expressions produces the following results.

In air:

$$\frac{\partial^2 H_y}{\partial z^2} = -\underbrace{\left(\gamma_o^2 + \omega^2 \mu_o \epsilon_o\right)}_{h_o^2} H_y \qquad (2.76a)$$

Within the conductor:

$$\frac{\partial^2 H_y}{\partial z^2} = \underbrace{\left[i\omega\mu_1(\sigma_c + i\omega\epsilon_1) - \gamma_1^2\right]}_{h_1^2} H_y \qquad (2.76b)$$

The solutions to these are as follows.

In air:

$$H_y = c_1 e^{h_o z} + c_2 e^{-h_o z}$$

Within the conductor:

$$H_y = c_3 e^{h_1 z} + c_4 e^{-h_1 z}$$

Taking the positive square root for h^2 requires c_1 and c_4 to be zero for finite fields to exist at $z = \infty$ in air and at $z = -\infty$ in the conductor.

Including the x-variation in the expressions for H_y yields the following results.

In air:

$$H_y = c_2 e^{-h_o z} e^{-\gamma_o x}$$

Within the conductor:

$$H_y = c_3 e^{h_1 z} e^{-\gamma_1 x}$$

These expressions must be equal at the interface $z = 0$ to maintain the continuity of H_y; therefore, $c_2 = c_3$ and $\gamma_o = \gamma_1$.

From Maxwell's equations and the expressions for H_y,

In air:

$$E_x = \frac{h_o c_2}{i\omega\epsilon_o} e^{-h_o z} e^{-\gamma_o x}$$

In the conductor:

$$E_x = \frac{-h_1 c_2}{\sigma_c + i\omega\epsilon_1} e^{h_1 z} e^{-\gamma_o x}$$

Again, for continuity of fields, the two expressions for E_x must be equal at the interface; therefore,

$$h_o^2 = \frac{-\omega^2 \epsilon_o^2 h_1^2}{(\sigma_c + i\omega\epsilon_1)^2} = (i\delta\beta_z)^2$$

For sea water with conductivity $\sigma_c \approx 4.0$ mhos/m and permittivity $\epsilon_1 \approx 0.72 \times 10^{-9}$ F/m,

$$\sigma_c \gg \omega\epsilon_1$$

at the radio frequencies of interest (less than 30 MHz); then,

76

$$h_o = i\delta\beta_z \approx i\beta(1 + i)\sqrt{\frac{\omega\epsilon_o}{2\sigma_c}}$$

where $\beta = \omega\sqrt{\mu_o\epsilon_o}$ is the radio-wave propagation constant in air, and $\mu_o \approx \mu_1$ is assumed.

Using the expression

$$Z_s = (1 + i)\sqrt{\frac{\omega\mu}{2\sigma_c}}$$

[Ramo and Whinnery, 1953, p. 239] for the conductor surface impedance results in the simple form,

$$\delta\beta_z = \beta\frac{Z_s}{\eta} = \beta\Delta \tag{2.77}$$

where $\eta = \sqrt{\mu_o/\epsilon_o}$ is the characteristic impedance of free space, and Δ represents the normalized surface impedance of the conductor. At 30 MHz, the normalized impedance for a smooth ocean surface is $\Delta = 0.0144$ $(1 + i)$. For a smooth perfectly conducting surface, the z-component of the propagation constant can be written as

$$b(p,q) = \beta \cos\theta$$

The angle θ at which $\beta \cos\theta = |\delta\beta_z|$ is 88.8°; consequently, $\delta\beta_z$ is small compared to $b(p,q)$, except near grazing propagation ($\theta = 90°$). Barrick (1971) has calculated the increase in ocean-surface impedance caused by roughness and indicates that the total normalized surface impedance is still small compared to $b(p,q)$. Although the modifications to (2.71) through (2.74) are slight in this case, they are sufficient to allow evaluation of σ_{VV} and σ_{HH}.

Chapter III

HYDRODYNAMIC THEORY

A theory was developed in Chapter II for electromagnetic wave scat-
tering from a slightly rough surface, resulting in expressions relating
incremental radar cross section per unit frequency to the scattering
surface-height spectrum. In this chapter, the ocean surface is examined
to determine the salient features of its surface- or wave-height spec-
trum.

In Section A, the equations of motion and boundary conditions re-
quired to describe the ocean surface are developed and found to be non-
linear. Because of the boundary-condition nonlinearities, perturbation
techniques are employed to solve the equations of motion, again only to
second order. The result is a surface-height spectrum composed of first-
and second-order terms. The first-order spectrum is the superposition
of sinusoidal waves, each of which obeys a wave equation and a first-or-
der dispersion relationship. The second-order spectrum is a result of
the nonlinear interactions of the waves in the first-order spectrum.

In Section B, Tick's perturbation method [Kinsman, 1965, p. 588]
is expanded to three dimensions, and a second-order wave-height spectrum
is derived in terms of a general first-order spectrum. Section C pre-
sents some of the first-order wave-height directional spectra that have
been postulated for ocean surfaces. A model for ocean swell is proposed
in Section D.

A.   Equations of Motion and Boundary Conditions

The development of the equations of motion and boundary conditions
presented here follows that of Kinsman (1965, Ch. 2).

1.   Equation of Motion, Continuity Equation, and Velocity Potential

The development of the equation of motion begins with Newton's
second law of motion,

$$\frac{d\bar{u}}{dt} = \bar{f}_p + \bar{f}_g \qquad\qquad (3.1)$$

where $\bar{u}$ is the velocity and $\bar{f}_p$ and $\bar{f}_g$ are pressure and gravity forces per unit mass (Fig. 15). Other forces associated with fluids (such as friction, surface tension, and Coriolis) are neglected because they have little effect on the 2 to 400 m ocean wavelengths of interest here [Kinsman, p. 23].
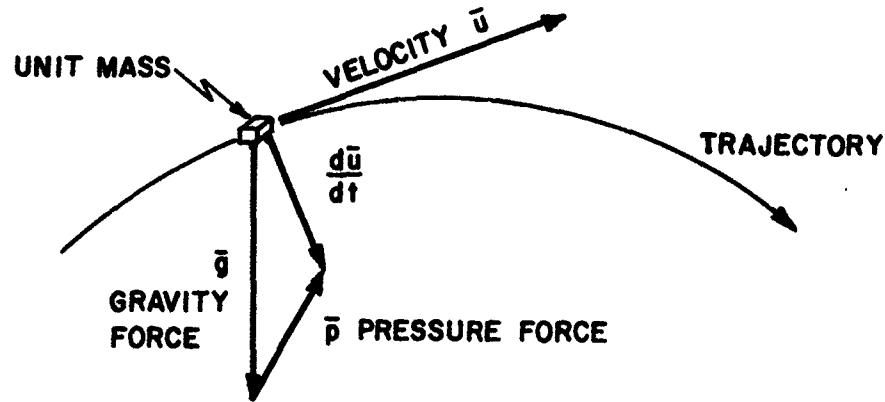

Fig. 15.   FORCES ON A UNIT MASS.

The total time derivative of a component of $\bar{u}$ is written as

$$\frac{du_x}{dt} = \frac{\partial u_x}{\partial t} + \frac{\partial u_x}{\partial x}\frac{dx}{dt} + \frac{\partial u_x}{\partial y}\frac{dy}{dt} + \frac{\partial u_x}{\partial z}\frac{dz}{dt}$$

or

$$\frac{du_x}{dt} = \frac{\partial u_x}{\partial t} + u_x\frac{\partial u_x}{\partial x} + u_y\frac{\partial u_x}{\partial y} + u_z\frac{\partial u_x}{\partial z}$$

The time derivatives of the y- and z-components are similar and, when these three components are combined, the total derivative can be written in vector form as

$$\frac{d\bar{u}}{dt} = \frac{\partial\bar{u}}{\partial t} + \frac{1}{2}\nabla(\bar{u}\cdot\bar{u}) + (\nabla\times\bar{u})\times\bar{u}$$

80

where ∇ is the gradient operator and $\nabla \times$ is the curl operator.

The pressure force in (3.1) is obtained by considering a small volume of fluid δx, δy, δz with pressure p at its center (Fig. 16).
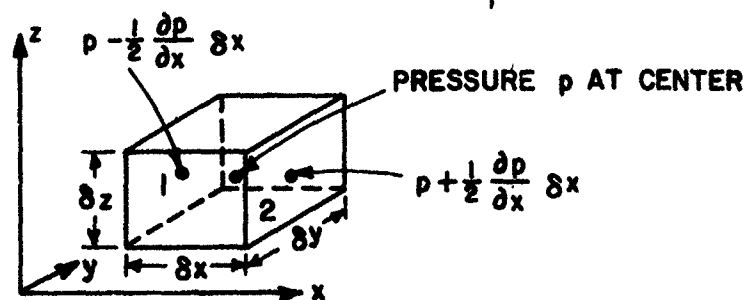

Fig. 16. PRESSURE ON A SMALL VOLUME OF FLUID.

The force in the x-direction is the difference between the force at the face with x-coordinate $-\frac{1}{2} \delta x$ and at the face with the coordinate $\frac{1}{2} \delta x$ with respect to the center of the volume. The pressure at the first face is

$$p - \frac{1}{2} \frac{\partial p}{\partial x} \delta x$$

and, at the second face, is

$$p + \frac{1}{2} \frac{\partial p}{\partial x} \delta x$$

The force is pressure times the area of the face; therefore, the total force in the x-direction is

$$\left(p - \frac{1}{2} \frac{\partial p}{\partial x} \delta x \right) \delta y \delta z - \left(p + \frac{1}{2} \frac{\partial p}{\partial x} \delta x \right) \delta y \delta z = - \frac{\partial p}{\partial x} \delta x \delta y \delta z$$

Force per unit mass is simply force divided by the total mass $\rho \delta x \delta y \delta z$,

$$f_{px} = - \frac{1}{\rho} \frac{\partial p}{\partial x}$$

81

where ρ is the fluid density. The total force per unit mass is then

$$\overline{f}_p = -\frac{1}{\rho} \nabla p$$

If the z-axis is aligned with gravity, then $\overline{f}_g = -g\hat{a}_z$, where $\hat{a}_z$ is a unit vector in the z-direction.

For fluid motion, Newton's second law becomes

$$\frac{\partial \overline{u}}{\partial t} + \frac{1}{2} \nabla(\overline{u} \cdot \overline{u}) + (\nabla \times \overline{u}) \times \overline{u} = -\frac{1}{\rho} \nabla p - g\hat{a}_z \qquad (3.2)$$

If the vorticity $\nabla \times \overline{u}$ is zero, the fluid is irrotational. Generally, fluid motion is irrotational if it results from conservative forces. In deep water with small surface viscosity, the effect of vorticity on over-all wave dynamics is negligible [Phillips, 1966, p. 36]; therefore, irrotational fluid motion will be assumed.

In addition to the equation of motion, there is the continuity equation

$$\frac{\partial \rho}{\partial t} + \frac{\partial(\rho u_x)}{\partial x} + \frac{\partial(\rho u_y)}{\partial y} + \frac{\partial(\rho u_z)}{\partial z} = 0$$

Because the total derivative $d\rho/dt$ is

$$\frac{d\rho}{dt} = \frac{\partial \rho}{\partial t} + \frac{\partial \rho}{\partial x}\frac{dx}{dt} + \frac{\partial \rho}{\partial y}\frac{dy}{dt} + \frac{\partial \rho}{\partial z}\frac{dz}{dt}$$

the continuity equation in vector form becomes

$$\frac{1}{\rho}\frac{d\rho}{dt} + \nabla \cdot \overline{u} = 0 \qquad (3.3)$$

which can be derived by applying the law of conservation of mass to a small fluid volume similar to that in Fig. 16.

From the continuity equation, $\nabla \cdot \overline{u} = 0$ if the fluid is in-compressible ($d\rho/dt = 0$). Sea water is nearly incompressible and can

be so assumed with insignificant effect on the surface-wave dynamics of interest. These incompressible and irrotational properties will permit the use of scalar functions rather than the velocity vector in the derivation of second-order wave-height spectra.

From the irrotational condition $\nabla \times \bar{u} = 0$, $\bar{u}$ can be written as the gradient of a scalar because

$$\nabla \times (\nabla \varphi) \equiv 0$$

In fluid dynamics, φ is the velocity potential and is related to $\bar{u}$ by

$$-\nabla \varphi = \bar{u} \tag{3.4}$$

The minus sign originates from an alternate method for deriving φ; namely,

$$\varphi_b - \varphi_a = \int_a^b \bar{u} \cdot d\bar{s}$$

where $\bar{s}$ defines a path from a to b. When $\varphi_a - \varphi_b$ is path independent, both the irrotational condition and (3.4) will result.

If the fluid is incompressible, then from (3.3),

$$\nabla \cdot \bar{u} = 0$$

and φ obeys Laplace's equation

$$\nabla^2 \varphi = 0 \tag{3.5}$$

The velocity potential and (3.5) will be used to derive the second-order wave-height spectrum.

2. Wave Equation

If the second-order terms and the effect of pressure force are neglected in the equation of motion (3.2), the result, in conjunction

83

with the continuity equation, will require that the ocean-surface profile must obey a wave equation

$$\nabla^2 \eta(x,y,t) = \frac{1}{C^2} \frac{\partial^2 \eta(x,y,t)}{\partial t^2} \tag{3.6}$$

where $\eta(x,y,t)$ is surface displacement from some reference (Fig. 17), and C is the phase velocity of the propagating wave. The general solution to the wave equation is a sinusoid traveling at phase velocity C. As a result, ocean-surface wave-height spectra will contain sinusoidal components, each obeying the wave equation. A complete solution requires the imposition of boundary conditions. These constraints, written in terms of the velocity potential, will be combined with Laplace's equation to obtain a second-order wave-height directional spectrum as a function of first-order spectra whose components obey a first-order dispersion relationship.
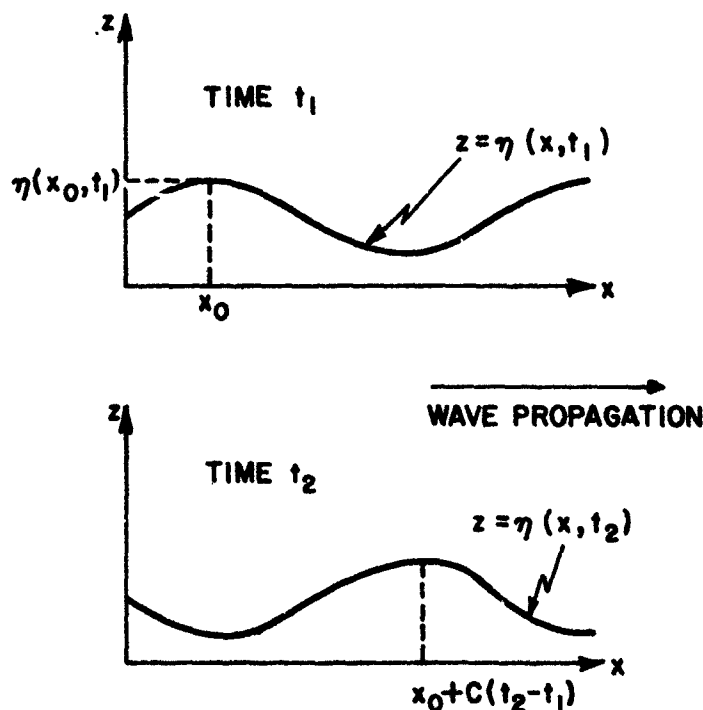

Fig. 17. WAVE PROFILE IN ONE DIMENSION. As time passes, the wave profile appears to be rigid and to move with velocity C.

3.   Boundary Conditions

The boundary conditions for ocean surfaces are of two types--fixed and free (Fig. 18). A fixed boundary, such as the ocean bottom, has no component of velocity perpendicular to the boundary. In terms of velocity potential, this condition is

$$\frac{\partial \varphi}{\partial z}\bigg|_{z=-h} = 0 \tag{3.7}$$

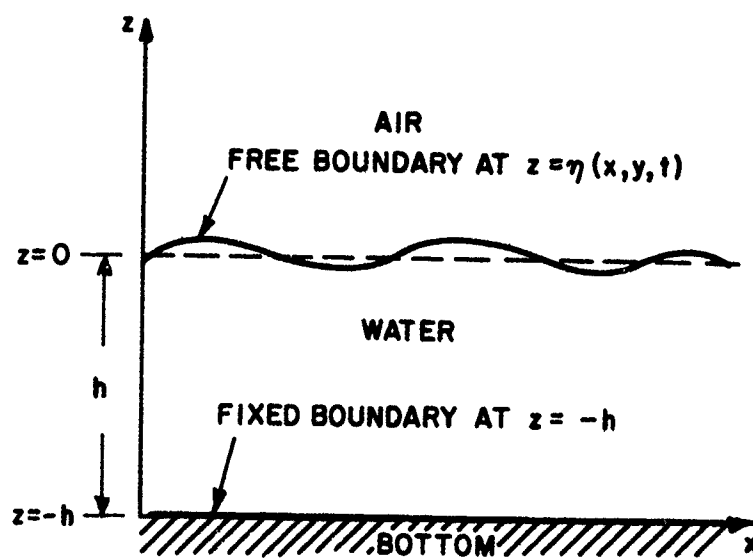where the rigid boundary is a plane perpendicular to the z-axis at a depth h.

Fig. 18. FLUID BOUNDARIES.

There are two free-surface boundary conditions--kinematic and dynamic. The kinematic condition requires surface fluid particles to remain at the surface. If points on the surface are represented by $\eta(x,y,t)$ and if z is the position of a particle, then

$$\frac{d}{dt}\left[z - \eta(x,y,t)\right]\bigg|_{z=\eta} = 0$$

which states that the position of a fluid particle relative to the surface profile or height must remain constant for all time if the particle is on the surface $(z = \eta)$. When expanded, this expression becomes

$$\left(u_z - \frac{\partial \eta}{\partial t} - u_x \frac{\partial \eta}{\partial x} - u_y \frac{\partial \eta}{\partial y} \right)\Bigg|_{z=\eta} = 0$$

In terms of velocity potential,

$$u_x = -\frac{\partial \varphi}{\partial x}$$

$$u_y = -\frac{\partial \varphi}{\partial y}$$

$$u_z = -\frac{\partial \varphi}{\partial z}$$

and the kinematic boundary condition becomes

$$\frac{\partial \eta}{\partial t} = -\frac{\partial \varphi}{\partial z} + \frac{\partial \varphi}{\partial x} \frac{\partial \eta}{\partial x} + \frac{\partial \varphi}{\partial y} \frac{\partial \eta}{\partial y} \Bigg|_{z=\eta} \tag{3.8}$$

The dynamic free-surface boundary condition requires that fluid at the surface must also conform to the equation of motion (3.2). Under the condition of irrotational motion, (3.2) becomes

$$\frac{\partial \bar{u}}{\partial t} + \frac{1}{2} \nabla (\bar{u} \cdot \bar{u}) = -\frac{1}{\rho} \nabla p - g \hat{a}_z \tag{3.9}$$

which, in component form, is

$$-\frac{\partial^2 \varphi}{\partial x \partial t} + \frac{1}{2} \frac{\partial}{\partial x} (\bar{u} \cdot \bar{u}) = -\frac{1}{\rho} \frac{\partial p}{\partial x}$$

$$-\frac{\partial^2 \varphi}{\partial y \partial t} + \frac{1}{2} \frac{\partial}{\partial y} (\bar{u} \cdot \bar{u}) = -\frac{1}{\rho} \frac{\partial p}{\partial y}$$

$$- \frac{\partial^2 \varphi}{\partial z \partial t} + \frac{1}{2} \frac{\partial}{\partial z} (\bar{u} \cdot \bar{u}) = - \frac{1}{\rho} \frac{\partial p}{\partial z} - g$$

where $\bar{u}$ has been replaced by $-\nabla \varphi$ in the time derivative. Multiplying the first expression by dx, the second by dy, and the third by dz and summing the results produces

$$d \left[- \frac{\partial \varphi}{\partial t} + \frac{1}{2} (\bar{u} \cdot \bar{u}) \right] + g dz = - \frac{dp}{\rho} \qquad (3.10)$$

where

$$d = \left(\frac{\partial}{\partial a} da + \frac{\partial}{\partial b} db + \frac{\partial}{\partial c} dc + \dots \right)$$

is the total differential operator. Assuming a constant density ρ and integrating (3.10) yields

$$- \frac{\partial \varphi}{\partial t} + \frac{1}{2} (\bar{u} \cdot \bar{u}) + g z + F(t) = - \frac{p}{\rho} \qquad (3.11)$$

where $F(t)$ is a constant of integration that can be absorbed in $\varphi(x, y, z, t)$.

The dynamic boundary condition can be obtained by evaluating (3.11) at the surface $z = \eta$,

$$g \eta = \frac{\partial \varphi}{\partial t} - \frac{1}{2} \left[\left(\frac{\partial \varphi}{\partial x} \right)^2 + \left(\frac{\partial \varphi}{\partial y} \right)^2 + \left(\frac{\partial \varphi}{\partial z} \right)^2 \right]\Bigg|_{z=\eta} \qquad (3.12)$$

where $\bar{u}$ is written in terms of the velocity potential φ. Overlying atmospheric pressure is assumed to be zero because interest is not in wind-generated waves but in wave-generated or second-order ocean waves.

The boundary conditions (3.8) and (3.12) are expressed as scalar functions, a nice feature; they are also nonlinear which is troublesome in that it requires resorting to perturbation techniques to find an approximate $\varphi(x,y,z,t)$ to satisfy the conditions in (3.7), (3.8), and (3.12).

B. Second-Order Wave-Height Directional Spectrum

The results obtained above will now be combined to determine the effects of nonlinearities (wave-wave interaction) on ocean-surface wave-height spectra. The analysis is carried to second-order and results in a spectrum that is a nonlinear function of first-order spectra. As a consequence, the rough-surface radar cross-section equations in Chapter II can be rewritten as functions of first-order wave-height directional spectra and still contain the effects of ocean-wave nonlinearities to second order.

1. Tick's Method

The following analysis is based on Tick's second-order double-perturbation method [Kinsman, 1965, p. 588] expanded to three dimensions. To be consistent with Tick's formulation, the velocity potential is defined by $\bar{u} = \nabla\varphi$. Changing the sign of φ and using subscripts to indicate partial differentiation reduces the boundary conditions (3.7), (3.8), and (3.12) to (where subscripts denote partial differentiation)

$$\varphi_z \rightarrow 0 \quad \text{as} \quad z \rightarrow -\infty \tag{3.13a}$$

$$\eta_t + \varphi_x \eta_x + \varphi_y \eta_y = \varphi_z \Big|_{z=\eta} \tag{3.13b}$$

$$g\eta + \varphi_t + \frac{1}{2}\left(\varphi_x^2 + \varphi_y^2 + \varphi_z^2\right)\Big|_{z=\eta} = 0 \tag{3.13c}$$

Deep water is assumed by allowing the rigid boundary to recede to $-\infty$.

The first perturbation in Tick's method results from expanding $\varphi(x,y,z,t)$ in a Taylor series about the point $z = 0$,

$$\varphi(x,y,z,t) = \varphi(x,y,z,t)\Big|_{z=0}$$

$$+ \frac{\partial\varphi(x,y,z,t)}{\partial z}\Big|_{z=0} z + \frac{1}{2}\frac{\partial^2 \varphi(x,y,z,t)}{\partial z^2}\Big|_{z=0} z^2 + \ldots \tag{3.14}$$

Substituting this expansion into the kinematic and dynamic boundary conditions (3.13b) and (3.13c) and retaining only terms to second order in φ and η provides

$$\eta_t + \eta_x\varphi_x + \eta_y\varphi_y = \varphi_z + \eta\varphi_{zz}\Big|_{z=0} \qquad (3.15a)$$

$$g\eta + \varphi_t + \varphi_{zt}\eta + \frac{1}{2}\left(\varphi_x^2 + \varphi_y^2 + \varphi_z^2\right)\Big|_{z=0} = 0 \qquad (3.15b)$$

from which η can be obtained to second order by noting that, to maintain the expression to second order, the third term in (3.15b) requires knowing η to first order. Condition (3.15b) defines η to first order as

$$\eta^{(1)} = -\frac{1}{g}\varphi_t^{(1)}\Big|_{z=0}$$

where the superscripts denote the order. Consequently, η to second order is

$$\eta = -\frac{1}{g}\left[\varphi_t - \frac{1}{g}\varphi_{zt}\varphi_t + \frac{1}{2}\left(\varphi_x^2 + \varphi_y^2 + \varphi_z^2\right)\right]\Big|_{z=0} \qquad (3.16)$$

This expression can now be differentiated with respect to x, y, and t, separately, and the results can be substituted into the kinematic boundary condition (3.15a) for η_x, η_y, and η_t. To second order,

$$\varphi_{tt} + g\varphi_z = \frac{1}{g}\left(\varphi_{zt}\varphi_{tt} + \varphi_{ztt}\varphi_t\right) - 2\varphi_x\varphi_{xt} - 2\varphi_y\varphi_{yt} - \varphi_z\varphi_{zt} + \varphi_t\varphi_{zz}\Big|_{z=0}$$

$$\qquad (3.17)$$

This partial differential equation contains both the kinematic and dynamic boundary conditions and is written completely in terms of the velocity potential function. It is to be solved under the constraints of Laplace's equation (3.5) and the condition stated in (3.13a). When φ

89

is found from (3.17), the surface displacement η follows directly from (3.16). The Fourier transform of the autocorrelation function of η will provide the desired surface wave-height spectrum to second order.

The second perturbation in Tick's double-perturbation method results from solving (3.17) to first order in φ and then using the first-order solution to obtain a second-order solution. To first order, (3.17) is

$$\varphi_{tt} + g\varphi_z \Big|_{z=0} = 0 \qquad (3.18)$$

Normally, when solving differential equations, a general form for the solution is assumed and the original differential equation plus any auxiliary equations are used to determine the complete solution. The first-order term in (3.16),

$$\eta = -\frac{\varphi_t}{g}\Big|_{z=0} \qquad (3.19)$$

suggests a general form for φ. Because η was represented by a Fourier series in Chapter II, a series solution in the following form is sought,

$$\varphi(x,y,z,t) = \sum_{mnI} A(m,n,I,z) \exp[-ia(mx + ny) - iIwt]$$

Applying Laplace's equation $\nabla^2\varphi = 0$ to this series yields

$$\sum_{mnI} \left[A_{zz}(m,n,I,z) - (a^2m^2 + a^2n^2)\, A(m,n,I,z) \right] \exp[-ia(mx + ny) - iIwt] = 0$$

If this differential equation is to be zero for all x, y, and t, then,

$$A_{zz}(m,n,I,z) - k_{mn}^2 A(m,n,I,z) = 0$$

90

for each term, where $k_{mn}^2 = a^2 m^2 + a^2 n^2$, and the solution takes the form of

$$A(m,n,I,z) = B_1(m,n,I) \exp(k_{mn}z) + B_2(m,n,I) \exp(-k_{mn}z)$$

The rigid-surface boundary condition

$$\frac{\partial \varphi}{\partial z} \to 0 \quad \text{as} \quad z \to -\infty$$

requires that $B_2(m,n,I) = 0$ for all m,n,I; therefore, with the subscript on B_1 omitted,

$$\varphi(x,y,z,t) = \sum_{mnI} B(m,n,I) \exp(k_{mn}z) \exp[-ia(mx + ny) - iIwt] \tag{3.20}$$

When this expression is applied to (3.19), the first-order wave height becomes

$$\eta^{(1)} = -\frac{1}{g} \sum_{mnI} (-iIw) B^{(1)}(m,n,I) \exp[-ia(mx + ny) - iIwt]$$

where the superscripts explicitly indicate the order. The $B^{(1)}(m,n,I)$ are obtained by equating the coefficients in this expression for $\eta^{(1)}$ with those in the random-surface representation

$$\eta^{(1)} = \sum_{mnI} P(m,n,I) \exp[-ia(mx + ny) - iIwt]$$

assumed in Chapter II. Combining the results with (3.20) provides the first-order solution,

$$\varphi^{(1)} = \sum_{mnI}{}' - ig \frac{F(m,n,I)}{Iw} \exp(k_{mn}z) \exp[-ia(mx + ny) - iIwt] \tag{3.21}$$

91

which, when substituted into the original differential equation (3.18), yields

$$gk_{mn} = (Iw)^2 \tag{3.22}$$

and this becomes

$$gk = \Omega^2 \qquad (k^2 = p^2 + q^2) \tag{3.23}$$

in the limit of large L and T, where

$$am \rightarrow p$$

$$an \rightarrow q$$

$$Iw \rightarrow \Omega$$

The above expression is a dispersion relationship for first-order ocean waves that obey the wave equation and, from it, the phase velocity of ocean waves can be determined,

$$C \equiv \frac{\Omega}{k} = \frac{g}{\Omega} = \pm \sqrt{\frac{g}{k}} \tag{3.24}$$

which is a function of the wave frequency Ω.

Returning to the search for η to second order, it can be seen by rewriting (3.16) with the order explicitly denoted that a first-order solution for φ is not sufficient to determine η to second order,

$$\eta^{(2)} = -\frac{1}{g} \left\{ \varphi_t^{(2)} - \frac{1}{g} \varphi_{zt}^{(1)} \varphi_t^{(1)} + \frac{1}{2} \left[\left(\varphi_x^{(1)} \right)^2 + \left(\varphi_y^{(1)} \right)^2 + \left(\varphi_z^{(1)} \right)^2 \right] \right\} \bigg|_{z=0} \tag{3.25}$$

where $\eta^{(1)}$ has been replaced by $-\varphi_t/g$ from (3.19). The term $\varphi_t^{(2)}$ requires that η be known to second order. Substituting the first-order solution for φ back into the original differential equation (3.17)

92

provides $\varphi_{tt}^{(1)} = -g\varphi_z^{(1)}$ and $\varphi_{ztt}^{(1)} = -g\varphi_{zz}^{(1)}$; therefore, the equation to be solved for second-order φ is

$$\varphi_{tt}^{(1)} + g\varphi_z^{(2)} = -2\left(\varphi_x^{(1)}\varphi_{xt}^{(1)} + \varphi_y^{(1)}\varphi_{yt}^{(1)} + \varphi_z^{(1)}\varphi_{zt}^{(1)}\right)\Bigg|_{z=0} \qquad (3.26)$$

A general solution in the form of (3.20) is again assumed for $\varphi^{(2)}$,

$$\varphi^{(2)}(x,y,z,t) = \sum_{mnI} B^{(2)}(m,n,I)\, \exp(k_{mn}z)\, \exp[-ia(mx + ny) - iIwt]$$

Substituting this solution into the left side of the differential equation (3.26) and the first-order solution (3.21) into the right side yields

$$\sum_{mnI} B^{(2)}(m,n,I)(gk_{mn} - I^2w^2)\, e^u$$

$$= 2 \sum_{m'n'I'} am'g\, \frac{P(m',n',I')}{I'w}\, e^{u'} \cdot \sum_{m''n''I''} iam''gP(m'',n'',I'')\, e^{u''}$$

$$+ 2 \sum_{m'n'I'} an'g\, \frac{P(m',n',I')}{I'w}\, e^{u'} \cdot \sum_{m''n''I''} ian''gP(m'',n'',I'')\, e^{u''}$$

$$- 2 \sum_{m'n'I'} gk_{m'n'}\, \frac{P(m',n',I')}{I'w}\, e^{u'} \cdot \sum_{m''n''I''} igk_{m''n''}P(m'',n'',I'')\, e^{u''}$$

$$(3.27)$$

where $u = -ia(mx + ny) - iIwt$, $u' = -ia(m'x + n'y) - iI'wt$, etc. The coefficients $B^{(2)}(m,n,I)$ can be determined by noting that the left side of (3.27) is a Fourier series, and taking its Fourier transform results in

$$\frac{1}{(2\pi)^3} \iiint_{-\infty}^{\infty} \sum_{mnI} B(m,n,I)(gk_{mn} - I^2 w^2)$$

$$\cdot \exp\left[-ia(m_o + m)\,x - ia(n_o + n)\,y - iw(I_o + I)\,t\right]\,dx\,dy\,dt$$

$$= \sum_{mnI} B^{(2)}(m,n,I)(gk_{mn} - I^2 w^2)\,\delta(m_o + m)\,\delta(n_o + n)\,\delta(I_o + I)$$

$$= B^{(2)*}(m_o,n_o,I_o)\left(gk_{m_o n_o} - I_o^2 w^2\right)$$

The Fourier transform of the right side requires the use of the convolution theorem where, if $\mathcal{F}[x(t)] = X(\omega)$ and $\mathcal{F}[y(t)] = Y(\omega)$, then

$$\mathcal{F}[x \cdot y] = \int_{-\infty}^{\infty} X(\omega_o - \omega)\,Y(\omega)\,d\omega$$

For discrete variables,

$$\int_{-\infty}^{\infty} X(\omega_o - \omega)\,Y(\omega)\,d\omega \rightarrow \sum_{m} X(m_o - m)\,Y(m)$$

The convolution theorem on the right side of (3.27) provides

$$B^{(2)*}(m_o,n_o,I_o)\left(gk_{m_o n_o} - I_o^2 w^2\right)$$

$$= -2 \sum_{m'n'I'} am'g\,\frac{P^*(m',n',I')}{I'w}\,ia(m_o - m')gP^*(m_o - m', n_o - n', I_o - I')$$

$$-2 \sum_{m'n'I'} an'g\,\frac{P^*(m',n',I')}{I'w}\,ia(n_o - n')gP^*(m_o - m', n_o - n', I_o - I')$$

$$+2 \sum_{m'n'I'} gk_{m'n'}\,\frac{P^*(m',n',I')}{I'w}\,igk_{m_o - m', n_o - n'}P^*(m_o - m', n_o - n', I_o - I')$$

Dividing through by $(gk_{m_o n_o} - I^2 w^2)$, taking the conjugate of both sides, and dropping the subscript o determines the $B^{(2)}(m,n,I)$ which are the coefficients in the series expansion for $\varphi^{(2)}$. To second-order, then,

$$\varphi^{(2)}(x,y,z,t) = 2ig^2 \sum_{mnI} \frac{e^{k_{mn} z} e^u}{(gk_{mn} - I^2 w^2)}$$

$$\cdot \sum_{m'n'I'} \left[a^2 m'(m - m') + a^2 n'(n - n') - k_{m'n'} k_{m-m',n-n'} \right]$$

$$\cdot \frac{P(m',n',I') \, P(m - m', \, n - n', \, I - I')}{I'w} \qquad (3.28)$$

This series can be verified as a second-order solution by substituting $\varphi^{(2)}$ and $\varphi^{(1)}$ back into the original equation (3.26). Replacing $\varphi^{(1)}$ and $\varphi^{(2)}$ with (3.21) and (3.28) in the equation for $\eta^{(2)}$, performing the indicated differentiations, and evaluating the result at $z = 0$ derives a second-order surface height in terms of the random coefficients of the first-order Fourier series,

$$\eta^{(2)}(x,y,t) = - 2g \sum_{mnI} \frac{Iw \, e^u}{gk_{mn} - I^2 w^2}$$

$$\cdot \sum_{m'n'I'} \left[a^2 m'(m - m') + a^2 (n - n') - k_{m'n'} k_{m-m',n-n'} \right]$$

$$\cdot \frac{P(m',n',I') \, P(m - m', \, n - n', \, I - I')}{I'w}$$

$$+ \sum_{mnI} P(m,n,I) \, e^u \cdot \sum_{m'n'I'} k_{m'n'} P(m',n',I') \, e^{u'} \qquad (3.29)$$

$$- \frac{g}{2} \sum_{mnI} am \, \frac{P(m,n,I)}{Iw} \, e^u \cdot \sum_{m'n'I'} am' \, \frac{P(m',n',I')}{i'w} \, e^{u'}$$

$$- \frac{g}{2} \sum_{mnI} an \, \frac{P(m,n,I)}{Iw} \, e^u \cdot \sum_{m'n'I'} an' \, \frac{P(m',n',I')}{I'w} \, e^{u'}$$

$$+ \frac{g}{2} \sum_{mnI} k_{mn} \, \frac{P(m,n,I)}{Iw} \, e^u \cdot \sum_{m'n'I'} k_{m'n'} \, \frac{P(m',n',I')}{I'w} \, e^{u'}$$

$$(3.29)$$
Cont.

2. Second-Order Wave-Height Spectrum from $\eta^{(2)}$

The second-order wave-height spectrum can be obtained from (3.29) by evaluating the autocorrelation function

$$R(x_1 - x_2, \; y_1 - y_2, \; t_1 - t_2) = \langle \eta(x_1,y_1,t_1) \, \eta^*(x_2,y_2,t_2) \rangle = R(x,y,t)$$

$$(3.30)$$

and taking a three-dimensional Fourier transform. The transform over x and y places the spectrum in k-space; the transform over t places it in the frequency domain.

Again, as in Chapter II, only a single-term example from (3.29) is required to illustrate the techniques for calculating the second-order spectrum. All product terms resulting from (3.30) will contain the product of four random variables. Averaging over this fourfold product requires the three-term expansions in Chapter II.C.4.b. When the first term of (3.29) is used in (3.30), the fourfold average to be evaluated is

$$\langle P(m',n',I') \, P(m - m', \, n - n', \, I - I') \, P^*(m'',n'',I'')$$

$$\cdot \, P^*(m'' - m''', \, n'' - n''', \, I'' - I''') \rangle \qquad (3.31)$$

$$= \langle P(m',n',I') \, P(m - m', \, n - n', \, I - I') \rangle$$

$$\cdot \; \langle P^*(m''',n''',I''') \, P^*(m'' - m''', \, n'' - n''', \, I'' - I''') \rangle$$

$$+ \; \langle P(m',n',I') \, P^*(m''',n''',I''') \rangle$$

$$\cdot \; \langle P(m - m', \, n - n', \, I - I') \, P^*(m'' - m''', \, n'' - n''', \, I'' - I''') \rangle$$

$$+ \; \langle P(m',n',I') \, P^*(m'' - m''', \, n'' - n''', \, I'' - I''') \rangle$$

$$\cdot \; \langle P(m - m', \, n - n', \, I - I') \, P^*(m''',n''',I''') \rangle \tag{3.31}$$

<div align="right">Cont.</div>

where the first term requires

$$m,n,I,m'',n'',I'' = 0 \tag{3.32a}$$

for a nonzero average. The second and third terms have the following index constraints:

$$
\begin{array}{ll}
m' = m''' & m = m'' \\
n' = n''' & n = n'' \\
I' = I''' & I = I''
\end{array}
\tag{3.32b}
$$

and

$$
\begin{array}{ll}
m = m'' & m''' = m - m' \\
n = n'' & n''' = n - n' \\
I = I'' & I''' = I - I'
\end{array}
\tag{3.32c}
$$

Examination of (3.29) with (3.32a) applied reveals that the first-term average in (3.31) is a constant; therefore, the corresponding spectrum is concentrated at zero frequency. This term denotes a perfectly smooth surface and is consistent with the corresponding terms in the scattering theory that represent scattering from a planar surface. All averages of $\eta\eta^*$ with (3.32a) applied have the same form and will

<div align="center">97</div>

contribute to the specular radar cross section. These terms will not be considered further because the incoherent radar cross section is the primary concern here.

Applying (3.32b) to (3.30), again for the first term in the expression for $\eta^{(2)}$ yields

$$R_{11}(\tau) = 4g^2 \sum_{mnI} \frac{(Iw)^2 \, e^{-i\tau}}{\left(gk_{mn} - I^2w^2\right)^2}$$

$$\cdot \sum_{m'n'I'} \left[a^2 m'(m - m') + a^2 n'(n - n') - k_{m'n'}k_{m-m',n-n'}\right]^2$$

$$\cdot \left(\frac{2\pi^3}{L^2 T}\right)^2 \frac{W(am', an', I'w) \; W(am - am', \; an - an', \; Iw - I'w)}{(I'w)^2}$$

where the subscripts on R indicate which terms in (3.29) are averaged, and

$$\tau = \left[m(x_1 - x_2) \, a + n(y_1 - y_2) \, a + Iw(t_1 - t_2)\right]$$

Taking the limit of large L and T and changing the variables of integration from m, n, I to p, q, Ω results in

$$R_{11}(\tau) = 4g^2 \iiint_{-\infty}^{\infty} \frac{\Omega^2 \, e^{-i\tau}}{\left(gk_{pq} - \Omega^2\right)^2}$$

$$\cdot \iiint_{-\infty}^{\infty} \left[p'(p - p') + q'(q - q') - k_{p',q'}k_{p-p',q-q'}\right]^2$$

$$\cdot \frac{W(p',q',\Omega') \; W(p - p', \; q - q', \; \Omega - \Omega')}{(4)^2 \Omega'^2} \, dp'dq'd\Omega' \; dpdqd\Omega$$

The first-order spectra in (3.33) indicate that two ocean waves contribute to the second-order spectrum for a given set p, q, p', and q'. The propagation constants of these waves are

$$\overline{k}_1 = p'\hat{a}_x + q'\hat{a}_y$$

$$\overline{k}_2 = (p - p')\,\hat{a}_x + (q - q')\,\hat{a}_y$$

from which

$$\left[p'(p - p') + q'(q - q') - k_{p'q'}k_{p-p',q-q'} \right]$$

in (3.33) can be rewritten as

$$(\overline{k}_1 \cdot \overline{k}_2 - k_1 k_2)$$

where $k_1 = |\overline{k}_1|$ and $k_2 = |\overline{k}_2|$.

When all terms resulting from the Fourier transform of (3.30) are combined, the second-order ocean-surface wave-height spectrum becomes

$$W^{(2)}(p,q,\Omega) = \frac{1}{2} \iiint_{-\infty}^{\infty} \left[k_1 + k_2 + (k_1 k_2 - \overline{k}_1 \cdot \overline{k}_2)\left(1 - \frac{2\Omega^2}{\Omega^2 - gk_{pq}}\right)\left(\frac{g}{\Omega'(\Omega - \Omega')}\right) \right]^2$$

$$\cdot\ W(p',q',\Omega')\ W(p - p',\ q - q',\ \Omega - \Omega')\ dp'dq'd\Omega'$$

$$(3.34)$$

where $k_{pq} = \sqrt{p^2 + q^2}$. This expression can be simplified by enforcing the dispersion relationship (3.24),

$$\Omega = \pm \sqrt{gk}$$

Under this condition, the first-order spectra can be written as

100

$$W(p', q', \Omega') = W(p', q') \, \delta(\Omega' \pm \sqrt{gk_1})$$

$$W(p - p', q - q', \Omega - \Omega') = W(p - p', q - q') \, \delta(\Omega - \Omega' \pm \sqrt{gk_2})$$

which, when substituted into (3.34), allows integration over Ω' because of the delta functions,

$$W^{(2)}(p,q,\Omega) = \frac{1}{2} \iint\limits_{-\infty}^{\infty} \left[k_1 + k_2 + \text{sgn}(k_1 k_2 - \bar{k}_1 \cdot \bar{k}_2) \left(1 - \frac{2\Omega^2}{\Omega^2 - \omega_B^2}\right)\left(\frac{g}{\omega_1 \omega_2}\right) \right]^2$$

$$\cdot \, \delta(\Omega \pm \omega_1 \pm \omega_2) \, W(p',q') \, W(p - p', q - q') \, dp' dq'$$

(3.35)

where $\omega_1 = \sqrt{gk_1}$, $\omega_2 = \sqrt{gk_2}$, $\omega_B = \sqrt{gk_{pq}}$, and sgn $= 1$ if the signs within the delta function are the same and sgn $= -1$ if they are different. The second-order spectrum is seen to be composed of waves that result from the nonlinear interaction between pairs of first-order waves obeying the dispersion relationship.

In Chapter IV, Eq. (3.35) will be combined with the results obtained in Chapter II to derive an expression for ocean-surface radar cross section that includes both electromagnetic and hydrodynamic effects to second order. First, however, some possible models for first-order ocean-surface wave-height spectra will be considered.

C. First-Order Directional Spectrum Models

First-order spectra comprise the freely propagating ocean waves that obey the dispersion relationship (3.23). They appear in the second-order expressions for the radar cross section and directional spectrum derived previously and must be represented either empirically or analytically if those expressions are to be evaluated. In the following discussion, some of the proposed analytical models for first-order directional spectra are described.

For the spectra to be considered here, their directional and amplitude aspects are assumed separable. For example, for waves traveling at an angle Θ with respect to some reference axis (usually along the wind direction), the wave-height directional spectrum can be written as

$$S(\omega,\Theta) = \Phi(\omega) \; G(\Theta)$$

where $\Phi(\omega)$ is a nondirectional amplitude spectrum (ω is the radian wave frequency) and $G(\Theta)$ is a directional factor such that

$$\int_0^{2\pi} S(\omega,\Theta) \; d\Theta = \Phi(\omega)$$

1.   The Amplitude Spectrum

S. A. Kitaigorodskii [Pierson and Moskowitz, 1964] has postulated that the dominant part of the amplitude spectrum $\Phi(\omega)$ is a function of only four variables—wave frequency, gravity, wind speed, and fetch (the distance over which the wind–ocean interaction takes place). If an unlimited fetch and a saturated[†] sea exist, the amplitude spectrum becomes a function of gravity and frequency only,

$$\Phi(\omega) = f(\omega,g)$$

In the MKS system, the units of $\Phi(\omega)$ are meters squared per radian per second or meters squared seconds; therefore, the dimensions are length squared time. To obtain these dimensions from ω and g only requires that

$$\Phi(\omega) \propto \frac{g^2}{\omega^5}$$

[†] A sea is saturated at some wave frequency if the height of the waves at that frequency no longer increases with an increase in wind speed. At saturation, these ocean waves cannot support additional wind energy, and the excess energy transfers to the longer waves that are not yet saturated.

Adding a constant of proportionality results in

$$\Phi(\omega) = \frac{\beta_e g^2}{\omega^5} \tag{3.36}$$

which is the Phillips saturation spectrum [Phillips, 1958]. Observed values of the equilibrium range constant β_e vary between 0.8×10^{-2} and 1.48×10^{-2} [Phillips, 1966, p. 114]. For a given wind speed, waves with frequencies below a certain cutoff value no longer develop. An often used cutoff for (3.36) is derived from the point where wind and wave speeds are the same. If it is assumed that waves cannot travel faster than the wind driving them, then, from the dispersion relationship (3.24),

$$\Phi(\omega) = \begin{cases} \dfrac{\beta_e g^2}{\omega^5} & \text{for} \quad \omega \geq g/u \\ 0 & \text{for} \quad \omega < g/u \end{cases} \tag{3.37}$$

where u is the wind speed.

With observed spectra as a basis, Pierson and Moskowitz (1964) proposed the following form for the amplitude spectrum:

$$\Phi(\omega) = \frac{\beta_e g^2}{\omega^5} \exp\left[-\nu(\omega_c/\omega)^4\right] \tag{3.38}$$

where the Phillips saturation spectrum has been modified by an exponential term whose value is a function of wind speed through $\omega_c = g/u$. Figure 19 illustrates both the Phillips saturation and the Pierson-Moskowitz spectra for 20 and 40 knot winds when $\beta_e = 0.81 \times 10^{-2}$ and $\nu = 0.74$. In the Pierson-Moskowitz spectra, considerable energy can be observed in waves traveling faster than the wind that generates them; however, no known mechanism exists for the direct transfer of wind energy to these faster waves, and it is assumed that they result from the
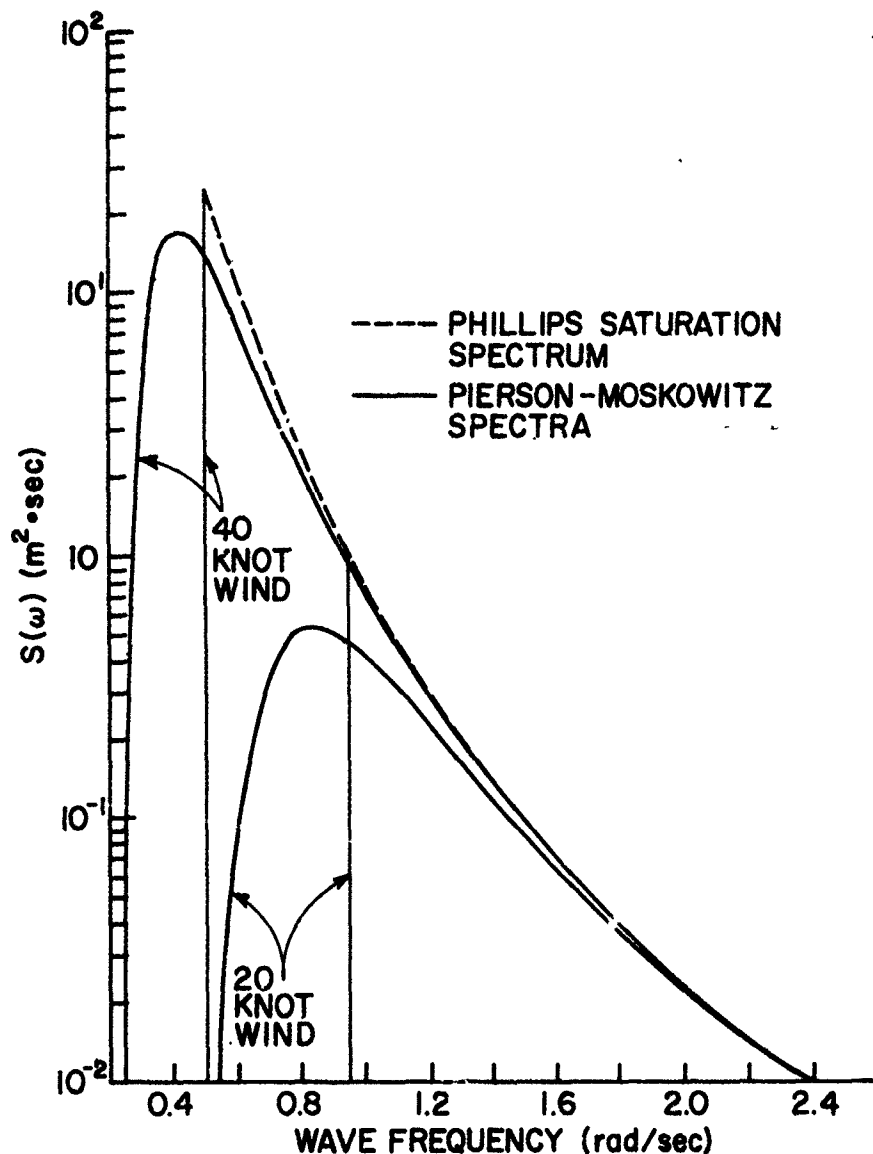
103

Fig. 19. PHILLIPS SATURATION AND PIERSON-MOSKOWITZ AMPLI-
TUDE SPECTRA. The cutoff frequencies for the Phillips
spectrum correspond to waves traveling at the indicated
wind speed.

nonlinear interactions among slower waves. Although second-order waves
cannot propagate freely, third- and higher order solutions to the equa-
tion of motion predict resonant waves that grow with time and that obey
the first-order dispersion relationship [Kinsman, 1965, Ch. 13]. Conse-
quently, first-order wave-height spectra contain all waves, wind driven

104

or the result of wave-wave interactions, that obey this dispersion relationship.

There are other forms for amplitude spectra [Kinsman, 1965], but (3.37) and (3.38) serve as adequate examples.

2. Directional Aspects

Just as $\Phi(\omega)$ is associated with wind speed, the directional aspects of the spectrum are often associated with wind direction. In one of the examples to be considered, however, these properties are a function of wind and wave speeds in addition to wind direction.

One of the simplest directional forms is semi-isotropic (Fig. 20), where

$$
G(\Theta) = \begin{cases} \dfrac{1}{\pi} & \text{for} \quad \varphi - \pi/2 < \Theta \leq \varphi + \pi/2 \\[3mm] 0 & \text{otherwise} \end{cases}
$$

and φ is the wind direction with respect to some reference. Combining this $G(\Theta)$ with (3.37) provides the Phillips semi-isotropic directional spectrum

$$
S(\omega,\Theta) = \begin{cases} \dfrac{\beta_e g^2}{\pi \omega^5} & \text{for} \quad \omega \geq g/u \quad \text{and} \quad \varphi - \pi/2 < \Theta \leq \varphi + \pi/2 \\[3mm] 0 & \text{otherwise} \end{cases} \tag{3.39}
$$

A similar expression is obtained when the Pierson-Moskowitz amplitude spectrum is combined with the semi-isotropic assumption,

$$
S(\omega,\Theta) = \begin{cases} \dfrac{\beta_e g^2}{\pi \omega^5} \exp\left[-\nu(\omega_c/\omega)^4\right] & \text{for} \quad \varphi \quad \pi/2 < \Theta \leq \varphi + \pi/2 \\[3mm] 0 & \text{otherwise} \end{cases} \tag{3.40}
$$

105
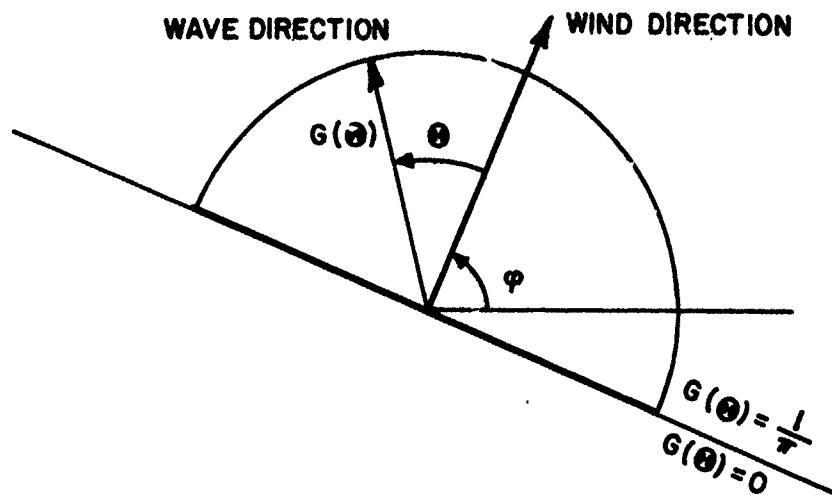
Fig. 20. SEMI-ISOTROPIC DIRECTIONAL DISTRIBUTION.

Another class of directional functions that allows $S(\omega,\Theta)$ to decrease gradually as Θ moves from the wind direction is represented by

$$G(\Theta) = \frac{\cos^s (a\Theta)}{N} \qquad (3.41)$$

where $\Theta = 0$ specifies the wind direction and N is a normalization constant such that

$$\int_0^{2\pi} G(\Theta) \, d\Theta = 1$$

In one form of (3.41), $s = 2$, $a = 0.5$, and $-\pi \leq \Theta \leq \pi$; therefore,

$$G(\Theta) = \frac{1}{\pi} \cos^2 \left(\frac{\Theta}{2}\right) \quad \text{for} \quad -\pi \leq \Theta \leq \pi \qquad (3.42)$$

This expression represents a cardioid distribution (Fig. 21) which allows wave propagation in all directions except the one against the wind. There is little evidence to indicate that this or any other function

106

WIND DIRECTION

PROPAGATION DIRECTION

$$G(\Theta) = \frac{1}{\pi} \cos^2(\Theta/2)$$

Θ

$G(\Theta)$
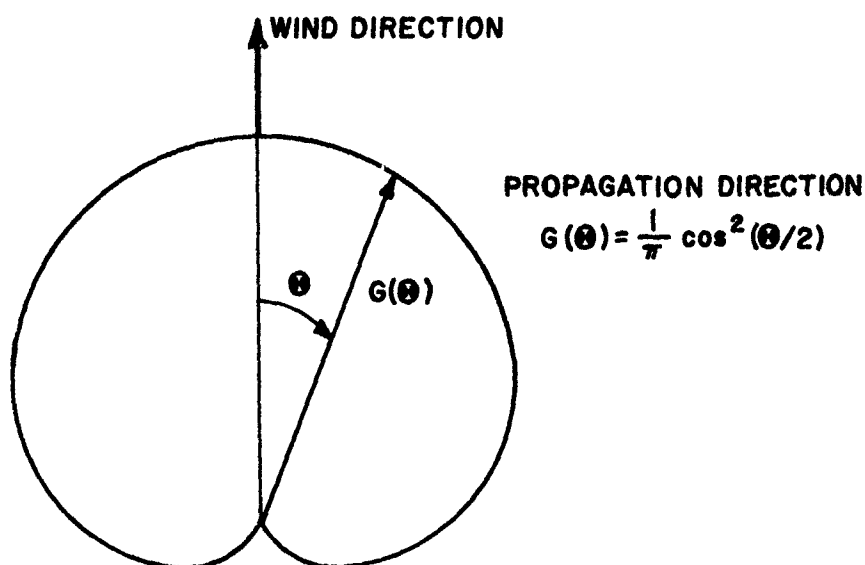
Fig. 21. CARDIOID DIRECTIONAL DISTRIBUTION.

adequately describes the directional propagation of wind-driven ocean waves. It has been observed [Tyler et al, 1974] that waves do propagate at angles greater than 90° with respect to the wind and, for this reason, (3.42) is expected to be a better model than semi-isotropic propagation. The exponent 2 in the cosine distribution has been used by others [Barrick et al, 1974] and is chosen here simply for convenience. Equation (3.42) will be combined with the Pierson-Moskowitz amplitude spectrum in Chapter IV to illustrate the dependence of radar cross section on directional ocean-wave propagation.

In a summary of the evolution of the cosine form of $G(\Theta)$, Munk [Tyler et al, 1974] introduced another form of the cosine type. His version is a modification of one introduced by Longuet-Higgins, Cartwright, and Smith [Tyler, 1974] where

$$G(\Theta) = \frac{\cos^s(\Theta/2)}{N(s)} \qquad -\pi \leq \Theta \leq \pi \qquad (3.43)$$

and s is a function of ocean-wave frequency and wind speed. The argument is that lower frequency waves traveling at speeds approaching that

107

of the wind should be confined to a narrow region about the wind direction, indicating large values for s. Higher frequency waves traveling substantially slower than the wind are allowed a wider range, indicating values of s ≈ 1 (Fig. 22).
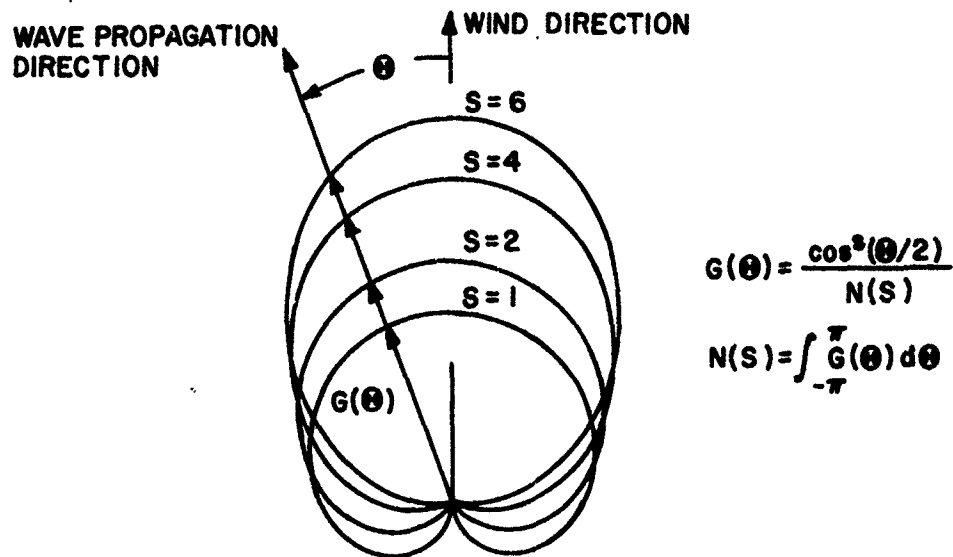

Fig. 22. COSINE DIRECTIONAL DISTRIBUTION.

Munk expanded (3.43) to allow for a small amount of energy traveling opposite to the wind and proposed a relationship between wind speed, wave speed, and s. This modified directional function is

$$G(\Theta) = \frac{[\epsilon + (1 - \epsilon) \cos^s (\Theta/2)]}{N(s)} \qquad -\pi \leq \Theta < \pi \qquad (3.44)$$

where ϵ is assumed small compared to 1. The normalization factor N is

$$N(s) = \int_{-\pi}^{\pi} G(\Theta) \, d\Theta = 2\pi\epsilon + (1 - \epsilon) L(s)$$

108

where

$$L(s) = 2\pi^{1/2} \frac{\Gamma(\frac{1}{2}s + 1/2)}{\Gamma(\frac{1}{2}s + 1)}$$

and Γ is the gamma function.

In seeking a spread factor s as a function of wind speed u, Munk accounts for variations in measured wind speed with anemometer height by assuming a logarithmic wind profile such that

$$u(z) = \frac{u_*}{\kappa} \ln\left(\frac{z}{z_o}\right) \qquad (3.45)$$

where

z = height at which wind speed is measured

κ = Karman's constant (≈ 0.41)

u_* = Prandtl's shear-stress (or friction) velocity

and z_o is defined as

$$z_o = \frac{\Lambda}{\kappa^2} \frac{u_*^2}{g} \qquad (3.46)$$

where Λ/κ^2 is Charnock's constant (≈ 0.0156) and g is the acceleration caused by gravity. Kinsman (1965, p. 560) provides a detailed description of the log profile and associated constants.

A given wind-speed profile can be characterized by the single parameter u_* if the logarithmic assumption is valid and if measurements of $u(z)$ are within the region of validity. Figure 23 plots $u(z)$ as a function of u_* for wind-speed measurement heights of 2 and 12 m.

The next assumption relating s to wind speed is that, at some height z_r, a resonance condition exists where the component of wind speed in the direction of wave propagation is equal to the velocity of propagation for that wave,

$$u(z_r) \cdot \cos \Theta_r = C \qquad (3.47)$$

where C is the wave phase velocity and Θ_r is the resonance angle (Fig. 24). Some motivation and justification for this assumption can be found in Phillips (1966, pp. 128-129). Combining (3.45), (3.46), and (3.47) yields the resonance condition in terms of the friction velocity u_*,

$$\frac{u_*}{\kappa} \ln \left(\frac{z_r g \kappa^2}{\Lambda u_*^2} \right) \cos \Theta_r = C$$
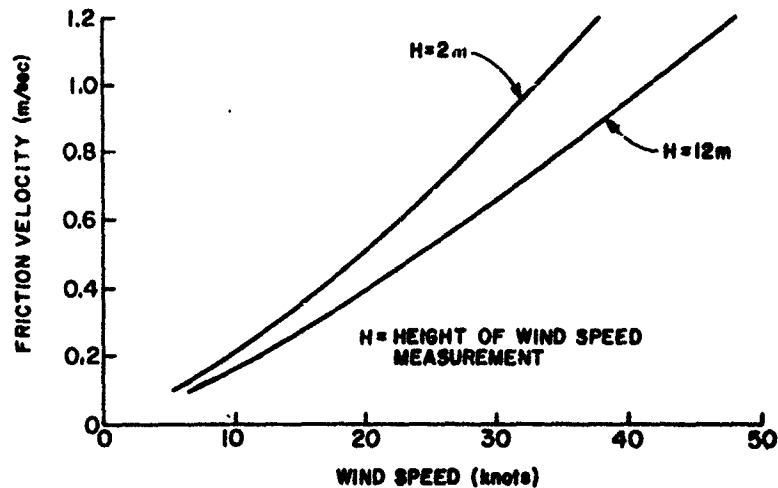

Fig. 23. WIND SPEED VS FRICTION VELOCITY FOR A LOGARITHMIC WIND-SPEED PROFILE.

Munk assumed a resonance height z_r proportional to the wavelength λ of the wave with velocity C; that is,

$$z_r = \frac{A}{k}$$

where $k = 2\pi/\lambda$ and A is a constant. The resonance condition then becomes

$$\sec \Theta_r = \mu \ln (A \Lambda^{-1} \mu^{-2}) \qquad (3.48)$$

110
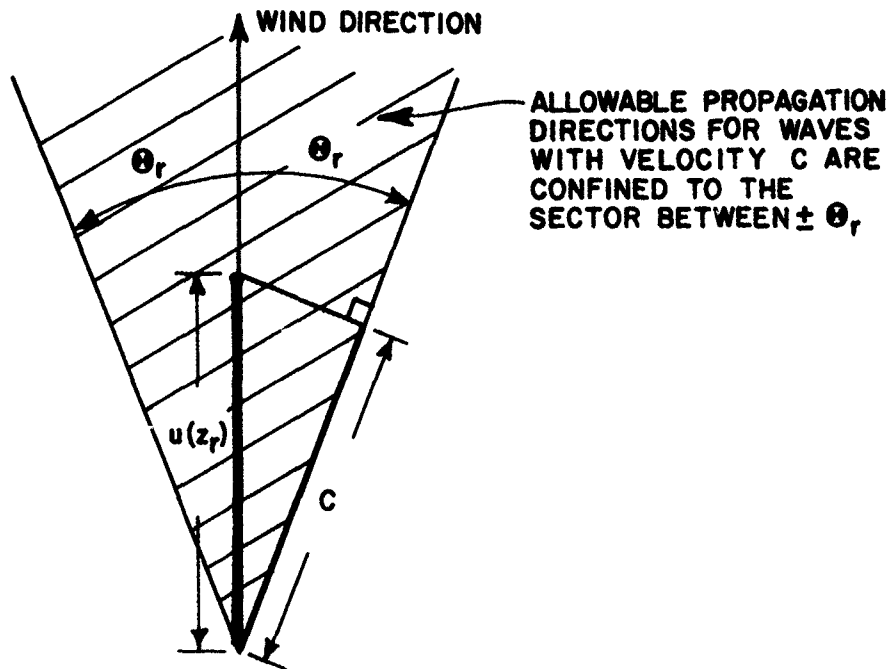
Fig. 24. ALLOWABLE PROPAGATION DIRECTIONS FOR RESONANT WAVES.
The resonance condition states that wind speed $u(z_r)$ at
some height z_r is related to wave speed C by $C = \cos(\Theta_r)$
$\cdot u(z_r)$, where Θ_r defines the limiting direction in which
waves with velocity C can propagate.

where $\mu \equiv u_*/(CK)$ and $C = \sqrt{g/k}$ from the dispersion relationship
(3.24).

When $\Theta_r = 0$, the allowable propagation region in Fig. 24
reduces to a single line that corresponds to the cutoff condition for
waves traveling faster than the wind. Under this constraint,

$$1 = \mu_o \; \ell n \left(A \Lambda^{-1} \mu_o^{-2} \right) \qquad (3.49)$$

and the selection of a value for A determines μ_o which is the cut-
off value for μ (Munk chose $\mu_o = 0.1$, admittedly rather arbitrar-
ily). To obtain the single line corresponding to $\Theta_r = 0$ in Fig. 24,
s must go to infinity in Eq. (3.43). For any Θ_r, it is assumed that
$\cos^s(\Theta_r/2)$ will have some finite and constant value. In particular,
as μ tends to infinity, Θ_r tends to $90°$ and $\cos^s(\Theta_r/2) = \sqrt{2}/2$ for
the lower limit of $s = 1$ chosen by Munk.

111

From (3.43), (3.48), and the condition that $N(s)G(\Theta_r) = \sqrt{2}/2$,

$$s = \frac{\ell n \ (1/2)}{\ell n \left\{ \dfrac{1}{2} + \dfrac{1}{2} \ \dfrac{1}{\mu \ \ell n \ (A\Lambda^{-1}\mu^{-2})} \right\}} \qquad \begin{array}{l} 1 < s < \infty \\[2mm] \infty > \mu > \mu_o \end{array} \qquad (3.50a)$$

or, including (3.49),

$$s = \frac{\ell n \ (1/2)}{\ell n \left\{ \dfrac{1}{2} + \dfrac{1}{2} \ \dfrac{\mu_o/\mu}{[1 + 2\mu_o \ \ell n \ (\mu_o/\mu)]} \right\}} \qquad \begin{array}{l} 1 < s < \infty \\[2mm] \infty > \mu > \mu_o \end{array} \qquad (3.50b)$$

From the definition of μ, $\mu_o/\mu = C/C_o$ where C_o is the cutoff velocity corresponding to μ_o, and s becomes

$$s = \frac{\ell n \ (1/2)}{\ell n \left\{ \dfrac{1}{2} + \dfrac{1}{2} \ \dfrac{C/C_o}{[1 + 2\mu_o \ \ell n \ (C/C_o)]} \right\}} \qquad \begin{array}{l} 1 < s < \infty \\[2mm] 0 < C < C_o \end{array} \qquad (3.50c)$$

The spread factor s presented here is seen to be a function of both wind speed (as represented by the friction velocity u_*) and wave speed C. The μ-parameter conveniently combines both C and u_*, making s a function of a single variable. Figure 25 plots the relationship between μ and s when $\mu_o = 0.1$ and $N(s) \ G(\Theta_r) = \sqrt{2}/2$.

When Eq. (3.44) is combined with the Phillips saturation amplitude spectrum (3.36), the result, attributed to Munk, is

$$S(\omega,\Theta) = \frac{\beta_e g^2}{\omega^5} \ \frac{\epsilon + (1 - \epsilon) \cos^s (\Theta/2)}{N(s)} \qquad (3.51)$$

where s is defined by Eqs. (3.50).

The low-frequency cutoff condition for the Munk spectrum is contained in s and is essentially the same as that contained in (3.37) where wave speeds must be less than the wind speed. For example, when
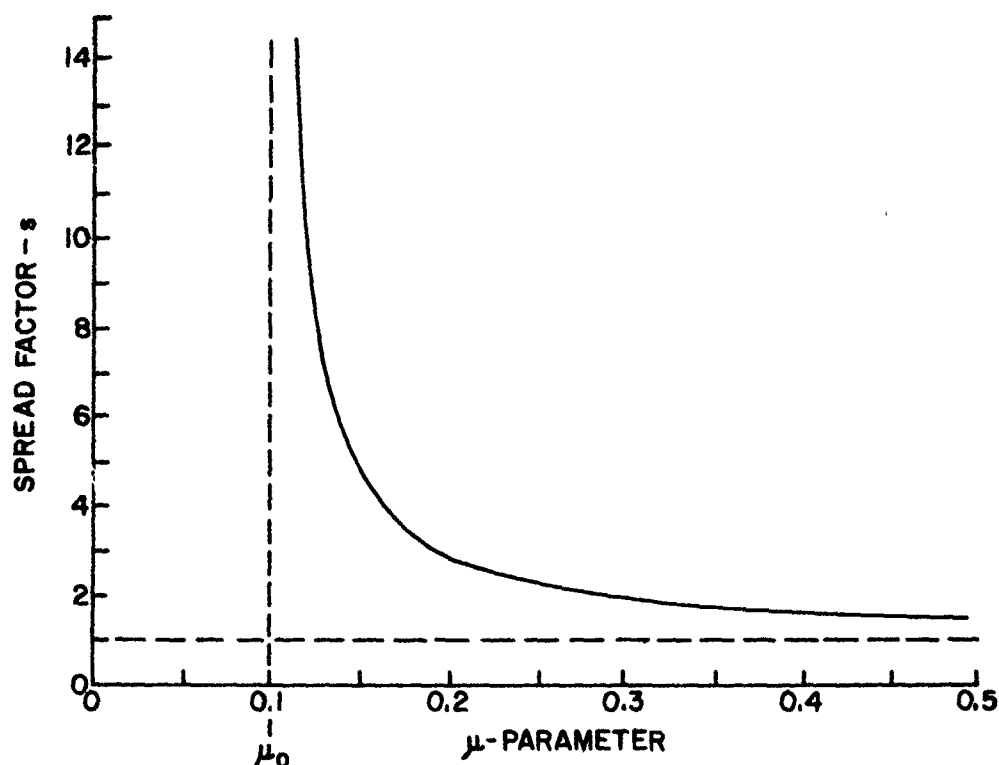
112

Fig. 25. SPREAD FACTOR s AS A FUNCTION OF THE μ-PARAMETER.

$\mu_o = 0.1$, the low-frequency cutoff occurs at 0.98 rad/sec for a 20 knot wind measured at a height of 12 m (Fig. 23); the corresponding value for the flat wind profile in (3.37) is 0.95 rad/sec. Figure 19 shows the difference of 0.03 rad/sec to be negligible in view of the overall spectrum scale. Changing the value chosen for μ_o changes the value of the low-frequency cutoff proportionately and, hence, the agreement between the cutoff obtained from the spread factor and that obtained from the condition in (3.37).

3.   Special Considerations for Second-Order Calculations

Not all first-order spectra models are adequate for calculations of radar cross section to second order although they may provide excellent predictions of first-order cross sections. The reason is that second-order cross section is a function of the entire ocean-wave

113

spectrum while first-order cross sections involve only a portion of the spectrum. For example, consider the first-order term for incoherent radar cross section in (2.72),

$$\sigma_{VV}(\omega) \propto W(\beta \sin \theta \cos \emptyset - \beta\alpha, \ \beta \sin \theta \sin \emptyset, \ \omega_o - \omega)$$

where $\beta \sin \theta \cos \emptyset - \beta\alpha = k_x$ and $\beta \sin \theta \sin \emptyset = k_y$ are the ocean-wave propagation constants in the x- and y-directions (Fig. 26). The
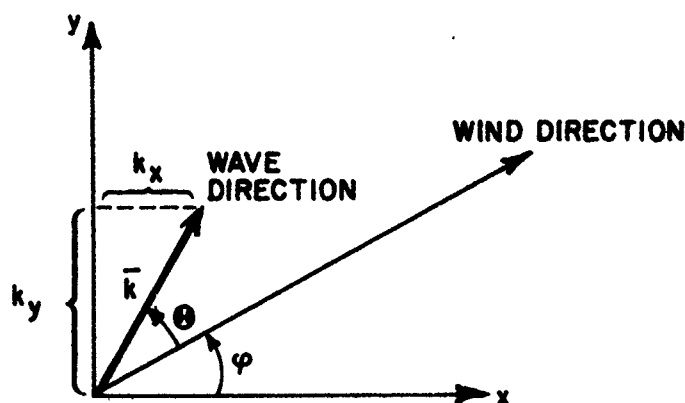
Fig. 26. RELATIONSHIP BETWEEN OCEAN-WAVE AND WIND DIRECTIONS.

frequency $\omega_o - \omega$ is the ocean-wave radian frequency in terms of the incident radio-wave radian frequency ω_o and the observed scattered radio-wave radian frequency ω. Relationship (3.24) requires that

$$\omega_o - \omega = \pm \sqrt{gk}$$

where $k = \sqrt{k_x^2 + k_y^2} = \beta \sqrt{(\sin \theta \cos \emptyset - \alpha)^2 + (\sin \theta \sin \emptyset)^2}$; therefore, the spectrum W can be written as

$$W(k_x, k_y, \omega_o - \omega) = W(k_x, k_y) \ \delta\left(\omega_o - \omega \pm \sqrt{g\beta \left[(\sin \theta \cos \emptyset - \alpha)^2 + (\sin \theta \sin \emptyset)^2\right]^{1/2}}\right)$$

$$(3.52)$$

114

because $\omega_o - \omega$ is fixed by the values of k_x and k_y.

With the ocean-wave frequency set by k_x and k_y which, in turn, are completely specified by the incident radio-wave frequency through β and the incident and observation directions given by θ, $\emptyset$, and α, there can be only a single ocean-wave frequency contributing to the radar cross section for fixed radar geometry and transmitted radio frequency; consequently, only a portion of the ocean-wave spectrum can be observed. In particular, if the observations are confined to ocean waves that are saturated, the Phillip's saturation spectrum (3.36) and the Pierson-Moskowitz spectrum (3.38) will serve as good first-order amplitude spectra models (Fig. 19).

On the other hand, second-order radar cross sections for fixed radar geometry and frequency involve the entire spectrum through the integral over all ocean-wave frequencies [see Eq. (2.72)]; therefore, the ocean-wave model chosen for second-order calculation should represent the ocean surface under both saturated and nonsaturated conditions. Consequently, a model of the Pierson-Moskowitz form is preferable to the Phillip's saturation model for nondirectional amplitude spectra, at least for these calculations.

All of the directional functions $G(\Theta)$ can be combined with the Pierson-Moskowitz amplitude spectrum (3.38) to provide directional spectra models suitable for second-order cross-section calculations.

4. First-Order Models in Terms of Wave Number

Thus far, ocean-wave directional spectra have been considered only in terms of wave frequency and angle from the wind direction; however, the spectra in the expressions for radar cross section in Chapter II are written as functions of ocean-wave propagation constants in the x- and y-directions. The transformation from the first form to the second is obtained from the spectrum property,

$$\langle h^2 \rangle = \int_{-0}^{\infty} \int_{0}^{2\pi} S_{\omega,\Theta}(\omega,\Theta)\ d\omega d\Theta = \int_{-\infty}^{\infty}\int_{-\infty}^{\infty} S_{k_x,k_y}(k_x,k_y)\ dk_x dk_y \tag{3.53}$$

115

where $\langle h^2 \rangle$ is the mean square ocean-wave height.

The Jacobian J, as defined by the determinant in

$$dk_x dk_y = \begin{vmatrix} \dfrac{\partial k_x}{\partial \omega} & \dfrac{\partial k_x}{\partial \Theta} \\[2mm] \dfrac{\partial k_y}{\partial \omega} & \dfrac{\partial k_y}{\partial \Theta} \end{vmatrix} d\omega d\Theta \qquad (3.54)$$

can be made exact with the aid of (3.24) and Fig. 26. The result is

$$k_x = k \cos (\Theta + \varphi) = \frac{\omega^2}{g} \cos (\Theta + \varphi)$$

$$k_y = \frac{\omega^2}{g} \sin (\Theta + \varphi)$$

Performing the partial differentiation indicated by (3.54) and evaluating the determinant yields

$$J = \frac{2\omega^3}{g^2}$$

From the expression defining $\langle h^2 \rangle$,

$$S_{k_x, k_y} (k_x, k_y) = \frac{g^2}{2\omega^3} S_{\omega, \Theta} (\omega, \Theta) \qquad (3.55a)$$

or

$$S_{k_x, k_y} (k_x, k_y) = \frac{g}{2 \left[g \sqrt{k_x^2 + k_y^2} \right]^{3/2}} S_{\omega, \Theta} \left[\sqrt{g \left(k_x^2 + k_y^2 \right)^{1/2}}, \tan^{-1} \left(\frac{k_y}{k_x} \right) - \varphi \right]$$

$$(3.55b)$$

In Chapter II.A, the surface-height spectrum W defined by Rice is four times that defined by (3.53); hence,

116

$$4S(k_x, k_y) = W(k_x, k_y)$$

Table 1 summarizes both forms of the first-order directional spectra presented here ($\varphi = 0$ in the table).

D. A Model for Sw

The first-order spectra models considered above describe only those ocean waves created by local winds. Waves also may be present that were generated by a distant wind system (or storm) and then have propagated to the local region; such waves are called "swell" [Kinsman, 1965, Ch. 1].

Swell generally consists of higher energy low-frequency waves that have survived the damping effects of turbulence and viscosity. In swell originating in very distant storms, only the lowest frequency waves exist and these propagate in a single direction through the local region (Fig. 27).

A wave-height model for swell could be

$$S_s(k_x, k_y) = \langle h^2 \rangle \, \delta(k_x - k_{xo}) \, \delta(k_y - k_{yo}) \qquad (3.56)$$

where $\langle h^2 \rangle$ is the mean-square height of swell, consisting of a single frequency

$$\omega = \sqrt{g \left(k_{xo}^2 + k_{yo}^2 \right)^{1/2}}$$

and traveling in the direction given by $\tan^{-1}(k_{yo}/k_{xo})$.

Because there are no ocean wave-wave interactions to first-order, the total first-order wave-height spectrum of a given ocean region can be written as the superposition of a local wind-generated spectrum $S_w(k_x, k_y)$ and the swell spectrum $S_s(k_x, k_y)$; that is,

$$S(k_x, k_y) = S_w(k_x, k_y) + S_s(k_x, k_y) \qquad (3.57)$$

117

Table 1

SUMMARY OF FIRST-ORDER MODELS FOR OCEAN WAVE-HEIGHT DIRECTIONAL SPECTRA
(See text for ranges of validity)

Spectrum	$S(\omega,\Theta)$	$S(k_x,k_y)$
Phillips Semi-Isotropic Saturation	$\dfrac{\beta_e g^2}{\pi\omega^5}$	$\dfrac{\beta_e}{2\pi k^4}$
Pierson-Moskowitz Semi-Isotropic	$\dfrac{\beta_e g^2}{\pi\omega^5}\cdot\exp\left[-\nu(\omega_c/\omega)^4\right]$	$\dfrac{\beta_e}{2\pi k^4}\exp\left[-\nu(k_c/k)^2\right]$
Pierson-Moskowitz $\cos^2(\Theta/2)$	$\dfrac{\beta_e g^2}{\pi\omega^5}\exp\left[-\nu(\omega_c/\omega)^4\right]\cos^2(\Theta/2)$	$\dfrac{\beta_e}{2\pi k^4}\exp\left[-\nu(k_c/k)^2\right]\cos^2\left[\tfrac{1}{2}\tan^{-1}(k_y/k_x)\right]$
Munk	$\dfrac{\beta_e g^2}{\omega^5}\dfrac{\left[\epsilon+(1-\epsilon)\cos^s\left(\tfrac{1}{2}\Theta\right)\right]}{\left[2\pi\epsilon+(1-\epsilon)2\sqrt{\pi}\cdot\dfrac{\Gamma(\tfrac{1}{2}s+\tfrac{1}{2})}{\Gamma(\tfrac{1}{2}s+1)}\right]}$	$\dfrac{\beta_e\left\{\epsilon+(1-\epsilon)\cos^s\left[\tfrac{1}{2}\tan^{-1}(k_y/k_x)\right]\right\}}{2k^4\left[2\pi\epsilon+(1-\epsilon)2\sqrt{\pi}\dfrac{\Gamma(\tfrac{1}{2}s+\tfrac{1}{2})}{\Gamma(\tfrac{1}{2}s+1)}\right]}$

$k = \sqrt{k_x^2 + k_y^2}$

$k_c = g/u^2$

u = wind speed
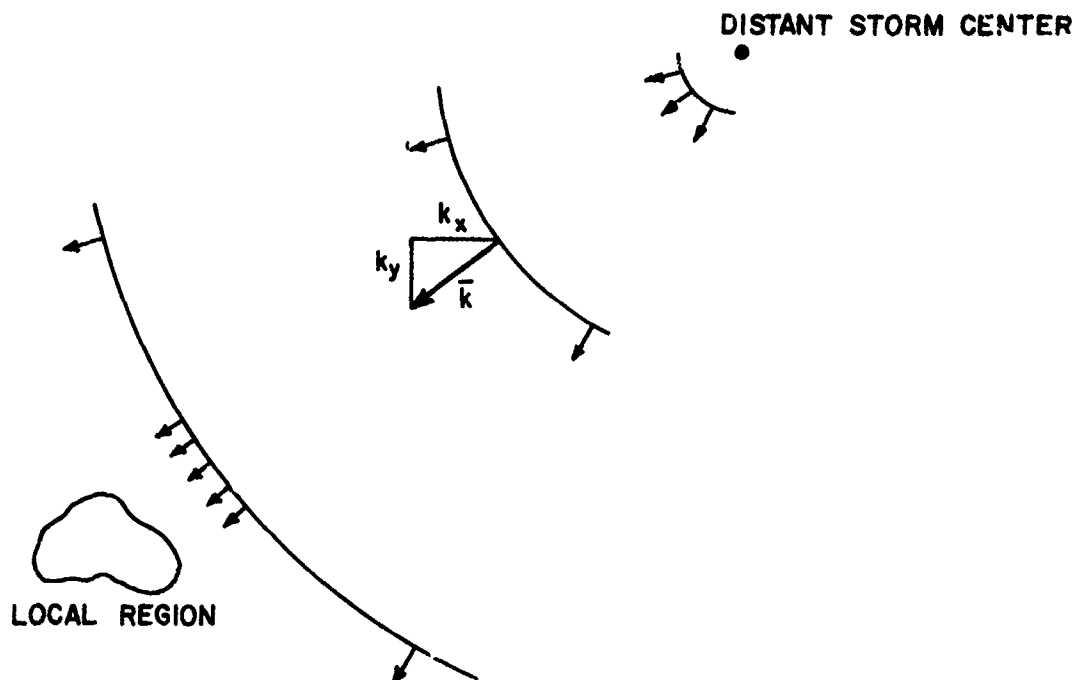
Fig. 27. PROPAGATION OF SWELL. To a local observer, swell from a
distant storm appears to be traveling in a single direction.

If local swell originates from more than one storm or wind system, its
spectrum can be represented by a superposition of the individual swell
spectra from each storm. Only a single source is considered here and
in the remaining chapters.

To be realistic, a model for swell should allow for a small spread
in wave frequency and, possibly, for deviations in the local propagation
direction. Such a model is obtained from (3.56) by replacing the delta
functions with gaussian functions,

$$S_s(k_x, k_y) = \frac{\langle h^2 \rangle}{2\pi \sigma_{kx} \sigma_{ky}} \exp\left[-\frac{1}{2}\left(\frac{k_x - k_{xm}}{\sigma_{kx}}\right)^2\right] \exp\left[-\frac{1}{2}\left(\frac{k_y - k_{ym}}{\sigma_{ky}}\right)^2\right] \quad (3.58)$$

The σ_{kx} and σ_{ky} are standard deviations of the x- and y-components
of the ocean-wave propagation constant about the means k_{xm} and k_{ym},
respectively. As these deviations tend to zero, the gaussian functions

119

become delta functions [Thomas, 1969, p. 587] and (3.58) reverts to (3.56).

The use of gaussian functions in (3.58) is not meant to imply that the actual distribution of swell-propagation constants is necessarily gaussian. The intent is to provide a model that allows for a small but finite band of wave frequencies and a small angular distribution of propagation directions. As the origin of swell becomes further removed from the local region, any model is expected to approach that of (3.56); therefore, if σ_{kx} and σ_{ky} are kept small, the difference between the gaussian and other possible models will be minimal.

To relate σ_{kx} and σ_{ky} to variations in the swell-propagation constant and propagation direction, consider the geometry in Fig. 28, where k_m is the mean value of the propagation constant and θ_m specifies the mean propagation direction. Let Δk and $\Delta\theta$ represent the maximum deviations of the ocean-wave propagation constant and direction from their mean values, respectively. The maximum positive deviation of the x-component k_x from its mean value k_{xm} is

$$\Delta k_x = (k_m + \Delta k) \cos (\theta_m - \theta) - k_m \cos \theta_m \qquad (3.59)$$

where $k_m \cos \theta_m = k_{xm}$.
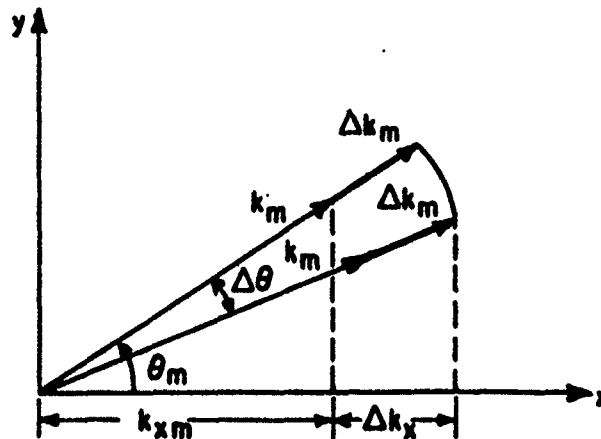
Fig. 28. DEVIATION OF A COMPONENT OF THE SWELL PROPAGATION CONSTANT.

For small directional deviations, $\Delta\theta \ll 1$, $\cos(\Delta\theta) \approx 1$, and $\sin(\Delta\theta) \approx \Delta\theta$. When terms of order Δ^2 are neglected, (3.59) can be approximated by

$$\Delta k_x = k_m \Delta\theta \sin\theta_m + \Delta k \cos\theta_m \qquad (3.60)$$

A maximum negative deviation $-\Delta k_x$ occurs when Δk is negative and $\Delta\theta$ is positive; therefore, the x-component k_x has a value in the range of $k_{xm} \pm \Delta k_x$, where Δk_x is defined in (3.60). A similar analysis shows the maximum deviation of the y-component k_y to be

$$\Delta k_y = k_m \Delta\theta \cos\theta_m + \Delta k \sin\theta_m \qquad (3.61)$$

Either of two arguments can be employed to relate the maximum deviations Δk_x and Δk_y to the standard deviations σ_{kx} and σ_{ky}. The first assumes that the gaussian function can be truncated for values of the variables greater than a few standard deviations from the mean. For example, at three standard deviations from the mean, the gaussian function has a value of 1.1 percent of its peak; values at greater than three can be considered negligible. The maximum deviation could be written as

$$\Delta k = 3\sigma_k$$

Alternately, rather than using maximum deviations for k and θ in (3.60) and (3.61), standard deviations σ_k and σ_θ could be assumed, such that

$$\sigma_{kx} = k_m \sigma_\theta \sin\theta_m + \sigma_k \cos\theta \qquad (3.62a)$$

$$\sigma_{ky} = k_m \sigma_\theta \cos\theta_m + \sigma_k \sin\theta_m \qquad (3.62b)$$

The σ_k and σ_θ are not derived from the distributions of k and θ obtained by transforming (3.58) from Cartesian to polar coordinates; they are simply a measure of the spread of k and θ about their means.

Because either method of selecting values for σ_{kx} and σ_{ky} is based on approximations and assumptions, the form expressed in (3.62a) and (3.62b) is chosen for simplicity.

In Chapter IV, calculations of radar cross section based on the swell model (3.58) indicate that the mean values of k_x and k_y are all that are required to produce the effects of swell and that the delta-function model (3.56) would suffice if it were amenable to numerical analysis.

Chapter IV

INTERPRETATION AND EVALUATION OF OCEAN-
SURFACE RADAR CROSS-SECTION INTEGRALS

The second-order results obtained in the previous two chapters will
be combined in this chapter to derive an integral expression for ocean-
surface incremental radar cross section per unit frequency that contains
both electromagnetic and hydrodynamic terms to second order. Section A
describes the transition from general time-varying surfaces to ocean sur-
faces. The concept of multiple Bragg scattering is introduced in Section
B and is shown to provide a physical interpretation of the cross-section
equations. Section C discusses the analytical techniques that will re-
duce these expressions to a form suitable for numerical analysis, and the
results of this evaluation are presented in Section D.

A.   Radar Cross Section for Ocean Surfaces

Expressions for the radar cross section of ocean surfaces can be
obtained from the general incoherent time-varying rough-surface cross-
section equations (2.72) and (2.74). Consider, for example,

$$\sigma_{VV}(\omega) = 4\pi\beta^4 (\alpha \sin\theta - \cos\emptyset)^2 \ W(k_x, k_y, \omega_o - \omega)$$

$$+ \pi\beta^4 \iiint_{-\infty}^{\infty} \Gamma^2 W(k_{1x}, k_{1y}, \Omega) \ W(k_{2x}, k_{2y}, \omega_o - \omega - \Omega) \ dpdqd\Omega \tag{4.1}$$

where Γ^2 represents the bracketed terms in (2.72). This expression
applies to ocean surfaces when hydrodynamic effects are introduced
through the spectra terms. In Chapter III, the ocean-surface spectrum
was represented by first-order and higher terms of which the second-or-
der terms were derived as a function of the first-order terms (3.35).
This spectrum can be written as

$$W(k_x, k_y, \Omega) = W^{(1)}(k_x, k_y, \Omega) + W^{(2)}(k_x, k_y, \Omega) + \text{higher order terms} \tag{4.2}$$

Substituting (4.2) into (4.1) and retaining only terms to second order leads to an equation that contains both electromagnetic and hydrodynamic effects to second order,

$$\sigma_{VV}(\omega) = 4\pi\beta^4 (\alpha \sin\theta - \cos\emptyset)^2 \left[W^{(1)}(k_x, k_y, \Omega) + W^{(2)}(k_x, k_y, \Omega) \right]$$

$$+ \pi\beta^4 \iiint_{-\infty}^{\infty} \Gamma^2 W^{(1)}(k_{1x}, k_{1y}, \Omega) \ W^{(1)}(k_{2x}, k_{2y}, \omega_o - \omega - \Omega) \ dpdqd\Omega$$

$$(4.3)$$

For the first-order spectral terms, the relationship between ocean-wave frequency and propagation constants k_x and k_y is determined by (3.24); therefore, the spectrum can be written as

$$W^{(1)}(k_x, k_y, \Omega) = W^{(1)}(k_x, k_y) \ \delta\left(\Omega \pm \sqrt{g\left[k_x^2 + k_y^2\right]^{1/2}}\right) \qquad (4.4)$$

as previously indicated in (3.52).

Either delta function that develops when (4.4) is substituted into the integral portion of (4.3) allows integration over Ω with the result that

$$\sigma_{VV}(\omega) = 4\pi\beta^4 (\alpha \sin\theta - \cos\emptyset)^2 \Bigg\{ W^{(1)}(\beta \sin\theta \cos\emptyset - \beta\alpha, \ \beta \sin\theta \sin\emptyset)$$

$$\cdot \ \delta\left(\omega_o - \omega \pm \sqrt{g\left[(\beta \sin\theta \cos\emptyset - \beta\alpha)^2 + (\beta \sin\theta \sin\emptyset)^2\right]^{1/2}}\right)$$

$$+ W^{(2)}(\beta \sin\theta \cos\emptyset - \beta\alpha, \ \beta \sin\theta \sin\emptyset, \ \omega_o - \omega) \Bigg\}$$

$$+ \pi\beta^4 \iint_{-\infty}^{\infty} \Gamma_{EM}^2 W^{(1)}(p - \beta\alpha, q) \ W^{(1)}(\beta \sin\theta \cos\emptyset - p, \ \beta \sin\theta \sin\emptyset - q)$$

$$\cdot \ \delta(\omega_o - \omega \pm \sqrt{gk_1} \pm \sqrt{gk_2}) \ dpdq \qquad (4.5)$$

124

where the actual spectra arguments from (2.72) have been incorporated. The subscript EM indicates that Γ results entirely from electromagnetic effects, and k_1, k_2 represent

$$\sqrt{(p - \beta\alpha)^2 + q^2} \quad \text{and} \quad \sqrt{(\beta \sin \theta \cos \phi - p)^2 + (\beta \sin \theta \sin \phi - q)^2}$$

respectively. The choice of signs in the delta functions in (4.5) is not arbitrary, and considerable care will be taken in Section C.5 to determine the regions of integration where each sign is valid.

The second-order spectrum in (4.5) has been expressed as an integral over first-order spectra in (3.35); therefore,

$$W^{(2)}(\beta \sin \theta \cos \phi - \beta\alpha, \beta \sin \theta \sin \phi, \omega_o - \omega)$$

$$= \frac{1}{2} \iint_{-\infty}^{\infty} \Gamma_H^2 W^{(1)}(p', q') \, W^{(1)}(\beta \sin \theta \cos \phi - \beta\alpha - p', \beta \sin \theta \sin \phi - q')$$

$$\cdot \delta(\omega_o - \omega \pm \sqrt{gk_1} \pm \sqrt{gk_2}) \, dp' dq' \tag{4.6}$$

where Γ_H represents the bracketed term in (3.35) and is the result of hydrodynamic effects alone. The k_1 and k_2 in this expression do not yet correspond to the definitions in (4.5); however, with the following change of variables,

$$q' \rightarrow q$$

$$p' \rightarrow p - \beta\alpha$$

the spectral terms and propagation constants become those in (4.5).

If the second-order spectrum in (4.5) is replaced by (4.6) and the two integrals are then combined, the desired expression for incoherent second-order incremental radar cross section per unit frequency becomes

125

$$\sigma_{VV}(\omega) = 4\pi\beta^4 (\alpha \sin\theta - \cos\emptyset)^2 \, W(\beta \sin\theta \cos\emptyset - \beta\alpha, \, \beta \sin\theta \sin\emptyset) \cdot \delta(\eta \pm \omega_\beta)$$

$$+ \pi\beta^4 \iint_{-\infty}^{\infty} \left\{ \frac{[(\beta \sin\theta - p\cos\emptyset - q\sin\theta)(\beta\alpha - p) - (\alpha \sin\theta - \cos\emptyset)\, b^2(p,q)]^2}{b(p,q)\, b^*(p,q)} \right.$$

$$+ \left[\left(\frac{(\beta \sin\theta - p\cos\emptyset - q\sin\emptyset)(\beta\alpha - p) - (\alpha\sin\theta - \cos\emptyset)\, b^2(p,q)}{b(p,q)} \right) \right.$$

$$\left. \cdot \left(\frac{(\beta\sin\theta\cos\emptyset - p)(\cos\emptyset\,(\beta\alpha - p) - q\sin\emptyset) - (\alpha\sin\theta - \cos\emptyset)\, b^2(\beta\sin\theta\cos\emptyset - p + \beta\alpha,\ \beta\sin\theta\sin\emptyset - q)}{b^*(\beta\sin\theta\cos\emptyset - p + \beta\alpha,\ \beta\sin\theta\sin\emptyset - q)} \right) \right]$$

$$+ 2(\alpha\sin\theta - \cos\emptyset)^2 \left[k_1 + k_2 + \text{sgn}\,(k_1 k_2 - \bar{k}_1 \cdot \bar{k}_2) \left(1 - \frac{2\eta^2}{\eta^2 - \omega_\beta^2} \right) \frac{g}{\omega_1\omega_2} \right]^2 \right\}$$

$$\cdot \, \delta(\eta \pm \omega_1 \pm \omega_2) \, W(p - \beta\alpha, q) \, W(\beta\sin\theta\cos\emptyset - p, \, \beta\sin\theta\sin\emptyset - q) \, dp\,dq \qquad (4.7)$$

where

$$\bar{k}_1 = (p - \beta\alpha)\, \hat{a}_x + q\hat{a}_y$$

$$\bar{k}_2 = (\beta\sin\theta\cos\emptyset - p)\, \hat{a}_x + (\beta\sin\theta\sin\emptyset - q)\, \hat{a}_y$$

with $k_1 = |\bar{k}_1|$ and $k_2 = |\bar{k}_2|$. The radian ocean-wave frequencies are

$$\omega_1 = \sqrt{gk_1}$$

$$\omega_2 = \sqrt{gk_2}$$

$$\omega_B = \sqrt{g\left[(\beta\sin\theta\cos\emptyset - \beta\alpha)^2 + (\beta\sin\theta\sin\emptyset)^2 \right]^{1/2}}$$

The doppler shift of the returned signal $\omega_o - \omega$ is denoted by η. All spectral terms are now first order.

A similar expression for $\sigma_{HH}(\omega)$ can be obtained by replacing $(\alpha \sin\theta - \cos\emptyset)^2$ with $\cos^2\emptyset$ and multiplying the entire result by $(\gamma \cos\theta)^2$.

Equation (4.7) for $\sigma_{VV}(\omega)$ and its horizontal complement for $\sigma_{HH}(\omega)$ represent ocean-surface second-order __bistatic__ radar cross sections (per unit area and frequency) and are presented here for the first time. In Section C, Eq. (4.7) will be reduced to a backscatter

126

grazing-incidence geometry and shown to be equivalent to previously pub-
lished results [Barrick, 1972] except for a difference in the relative
weighting between the electromagnetic and hydrodynamic contributions.

B. Bragg Scattering

The concept of Bragg or resonant scattering from periodic structures
has been shown to be responsible for the dominant first-order doppler-
shifted radar echoes from ocean surfaces [Crombie, 1955] and for the
smaller second-order sideband structure illustrated in Fig. 1 [Barrick,
1972]. In this section, this concept is examined and is also found to
apply to the expressions for bistatic-radar cross section.

The condition for radio-wave Bragg scattering requires that energy
scattered from successive periods of a periodic structure must add in
phase [Brillouin, 1953, p. 117]. This condition can be written as

$$d_1 + d_2 = n\lambda$$

where λ is the wavelength of the incident radio wave and n is an in-
teger greater than zero (see Fig. 29). For a given periodic structure,
incident radio waves of a specific frequency and propagation direction
are reflected in a particular direction under the Bragg condition. Con-
versely, only structures of a specific period will reflect radio waves
in a specified direction for given incidence conditions. To determine
the relationship between the structure period and the incident- and re-
flected-wave directions and frequency, consider the geometry in Fig. 30
where two parallel incident rays are reflected at Cartesian coordinates
$(0,0,0)$ and $(x_0, y_0, 0)$. The distance d_1 can be written as

$$d_1 = \frac{\overline{\beta}_i}{|\overline{\beta}_i|} \cdot (x_0 \hat{a}_x + y_0 \hat{a}_y) = \frac{x_0 \beta_{ix} + y_0 \beta_{iy}}{\beta}$$

where $\hat{a}$ denotes a unit vector, and

$$|\overline{\beta}_i| = \beta = \frac{2\pi}{\lambda}$$

127
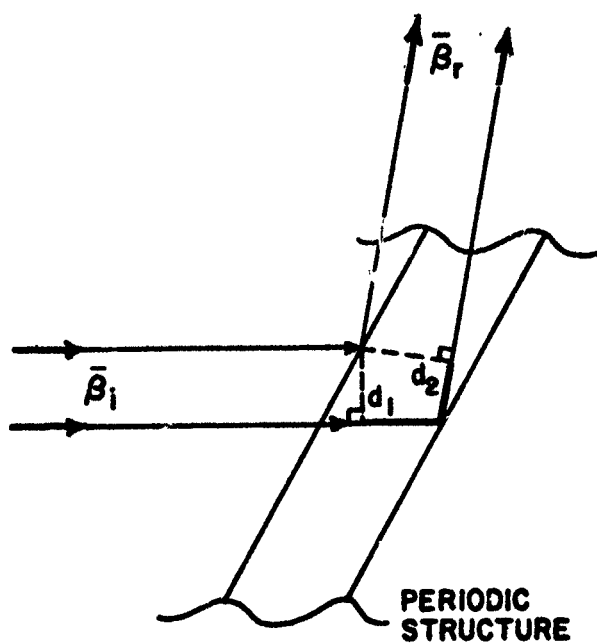
Fig. 29. REFLECTION FROM A PERIODIC
STRUCTURE. When $d_1 + d_2 = n\lambda$ (n is an
integer), reflected radio waves add in
phase and Bragg scattering occurs.
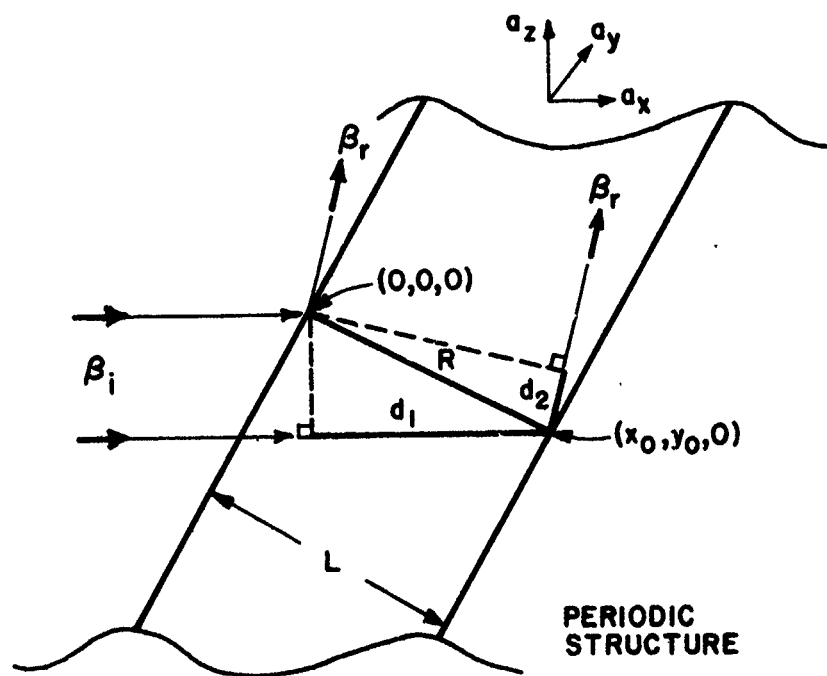
Fig. 30. BRAGG-SCATTERING GEOMETRY.

Similarly, d_2 can be written as

$$d_2 = - \frac{\bar{\beta}_r}{|\bar{\beta}_r|} \cdot (x_o \hat{a}_x + y_o \hat{a}_y) = - \frac{x_o \beta_{rx} + y_o \beta_{ry}}{\beta}$$

The Bragg condition $d_1 + d_2 = \lambda$ becomes

$$\frac{x_o (\beta_{1x} - \beta_{rx}) + y_o (\beta_{1y} - \beta_{ry})}{\beta} = \lambda$$

or

$$x_o (\beta_{1x} - \beta_{rx}) + y_o (\beta_{1y} - \beta_{ry}) = 2\pi \qquad (4.8)$$

The integer n is taken to be unity.

Equation (4.8) relates the components of the radio-wave propagation constant to point $(x_o, y_o, 0)$. A similar expression relating the orientation and period of the periodic structure to the same point can be derived and combined with (4.8) to determine the relationship between radio-wave period and direction and the structure period and orientation.

A direction can be assigned to the periodic structure by defining

$$\bar{L} \equiv L_x \hat{a}_x + L_y \hat{a}_y$$

such that $|\bar{L}| = L$, where L is the period length (Fig. 31). This direction will be associated with the propagation direction of an ocean-wave train which is a moving periodic structure. The length of the structure can be expressed as

$$\frac{\bar{L}}{L} \cdot (x_o \hat{a}_x + y_o \hat{a}_y) = L$$

or

$$L_x x_o + L_y y_o = L^2 \qquad (4.9)$$

129
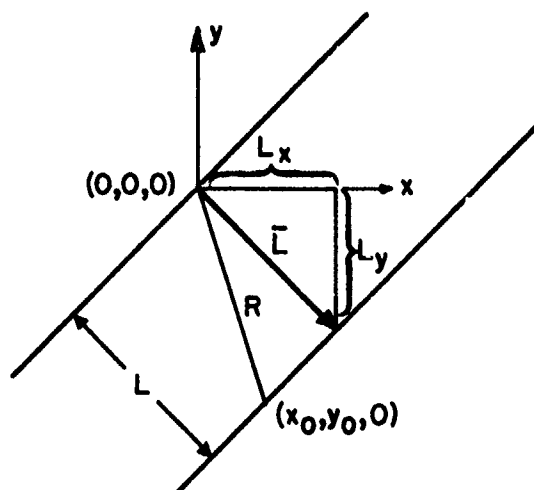
Fig. 31. A DIRECTIONAL PERIODIC
STRUCTURE.

If $\bar{k}$ is defined as

$$\bar{k} \equiv k \cos \varphi \, \hat{a}_x + k \sin \varphi \, \hat{a}_y$$

where $k = 2\pi/L$, then $p = k \cos \varphi$ and $q = k \sin \varphi$ represent the x- and y-components of the propagation constant for an ocean wave of length L.

Because $\cos \varphi = L_x/L$ and $\sin \varphi = L_y/L$, then $p = 2\pi L_x/L^2$ and $q = 2\pi L_y/L^2$, and Eq. (4.9) then becomes

$$px_o + qy_o = 2\pi \qquad (4.10)$$

which, combined with (4.8), provides a relationship between the radio-wave and ocean-wave (moving periodic structure) propagation constants,

$$\left[p - (\beta_{ix} - \beta_{rx}) \right] x_o + \left[q - (\beta_{iy} - \beta_{ry}) \right] y_o = 0 \qquad (4.11)$$

A little thought reveals that point (x_o, y_o) is not unique and that (4.11) holds for any choice of x_o and y_o; therefore,

130

$$p = \pm(\beta_{ix} - \beta_{rx})$$

$$q = \pm(\beta_{iy} - \beta_{ry})$$

<div align="right">(4.12)</div>

where the choice of signs indicates that $\overline{L}$ could have been chosen in the opposite direction. From the scattering geometry in Fig. 32,

$$\beta_{ix} = \beta\alpha \qquad\qquad \beta_{iy} = 0$$

$$\beta_{rx} = \beta \sin \theta \cos \emptyset \qquad\qquad \beta_{ry} = \beta \sin \theta \sin \emptyset$$

and (4.12) becomes

$$p = \beta \sin \theta \cos \emptyset - \beta\alpha$$

$$q = \beta \sin \theta \sin \emptyset$$

The spectrum in the first-order term in (4.7) is to be evaluated at precisely these values of p and q; as a result, a first-order contribution to the radar cross section is made by only those ocean waves (or, more correctly, by those components in Rice's model) that meet the Bragg condition for $n = 1$.
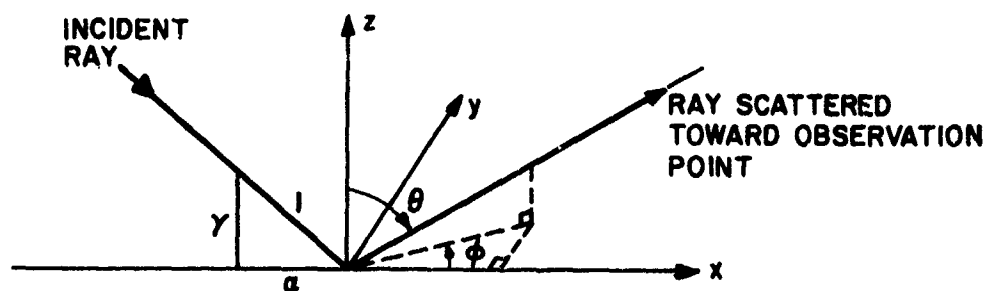
Fig. 32. INCIDENT- AND REFLECTED-RAY GEOMETRY.

To explain the second-order terms in (4.7) by means of a double Bragg-scattering process (Fig. 33), consider two ocean wave trains whose propagation constants are designated by p_1, q_1 and p_2, q_2, where p
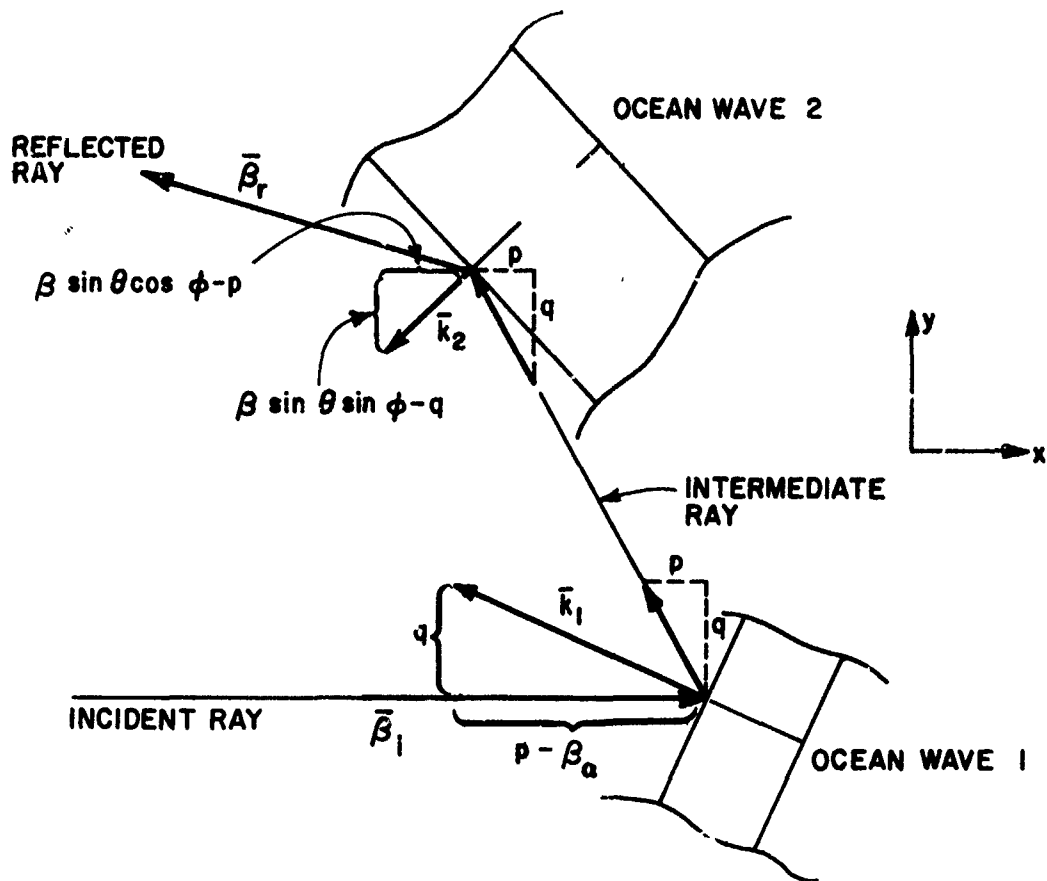
Fig. 33. DOUBLE BRAGG-SCATTERING GEOMETRY.

and q represent the x- and y-components of the propagation constants, respectively. Double Bragg scattering occurs when radio waves scattered from one wave train [according to the conditions stated in (4.12)] are, in turn, Bragg scattered by a second wave train.

Assume that the propagation constant of the intermediate radio wave (the wave scattered from the first ocean-wave train and incident on the second) is

$$\overline{\beta} = p\hat{a}_x + q\hat{a}_y + r\hat{a}_z \qquad (4.13)$$

where $|\overline{\beta}| = 2\pi/\lambda$. Conditions (4.12) applied to the first wave train require that

$$\beta_{ix} = \beta\alpha \qquad\qquad \beta_{iy} = 0$$

$$\beta_{rx} = p \qquad\qquad \beta_{ry} = q$$

and, hence,

$$p_1 = p - \beta\alpha$$

$$q_1 = q$$

(4.14)

Bragg scattering from the second wave train requires that

$$\beta_{ix} = p \qquad\qquad \beta_{rx} = \beta \sin\theta \cos\phi$$

$$\beta_{iy} = q \qquad\qquad \beta_{ry} = \sin\theta \sin\phi$$

and, therefore,

$$p_2 = \beta \sin\theta \cos\phi - p$$

$$q_2 = \beta \sin\theta \sin\phi - q$$

(4.15)

The spectra in the second-order terms in (4.7) are to be evaluated at exactly the points specified by (4.14) and (4.15) which are the conditions for double Bragg scattering. In addition, the variables of integration in (4.7) represent the x- and y-components of the intermediate radio-wave propagation constant defined in (4.13). The concept of multiple Bragg scattering adds physical significance to the expressions for radar cross section and will be helpful in evaluating them and in interpreting the results.

C.   Integration Techniques

Techniques for evaluating the second-order terms for radar cross section will be confined to a backscatter grazing-incidence geometry for the following reasons.

(a) The radar cross-section expression is algebraically much simpler; however, there is no loss in generality for the integration techniques to be developed.

(b) Results obtained from calculated second-order radar cross section for these conditions have been published [Barrick, 1972].

(c) Available measured data that can be compared to theoretical results (Chapter V) are limited to this radar geometry.

1. Reduction of σ_{VV} to Backscatter Grazing Incidence

Equation (4.7) can be reduced to a backscatter grazing-incidence geometry by imposing the following conditions on the angles of incidence and observation (Fig. 32),

$$\theta = 90° \qquad \gamma = 0$$

$$\emptyset = 180° \qquad \alpha = 1$$

As a result of these conditions, Eq. (4.7) becomes

$$\sigma_{VV}(\omega) = 16\pi\beta^4 W(-2\beta, 0) \ \delta(\eta \pm \omega_B)$$

$$+ \pi\beta^4 \iint_{-\infty}^{\infty} \left\{ \frac{2[(\beta + p)(\beta - p) - 2b^2(p,q)]^2}{b(p,q) \ b^*(p,q)} \right.$$

$$+ 8\left[k_1 + k_2 + \mathrm{sgn}(k_1 k_2 - \overline{k}_1 \cdot \overline{k}_2)\left(1 - \frac{2\eta^2}{\eta^2 - \omega_B^2}\right)\left(\frac{g}{\omega_1\omega_2}\right)\right]^2 \right\}$$

$$\cdot \ \delta(\eta \pm \omega_1 \pm \omega_2) \ W(p - \beta, q) \ W(-\beta - p, -q) \ dpdq \qquad (4.16)$$

where

$$\overline{k}_1 = (p - \beta) \ \hat{a}_x + q\hat{a}_y$$

$$\overline{k}_2 = (-p - \beta) \ \hat{a}_x - q\hat{a}_y$$

134

$$\omega_1 = \sqrt{gk_1}$$

$$\omega_2 = \sqrt{gk_2}$$

$$\omega_B = \sqrt{2\beta g}$$

$$k_1 = |\bar{k}_1|$$

$$k_2 = |\bar{k}_2|$$

When finite conductivity is assumed, $b(p,q) + \beta\Delta$ replaces $b(p,q)$ as the z-component of the intermediate wave propagation constant (Chapter II.E), where Δ is the normalized surface impedance. Because $\beta\Delta$ is small compared to $b(p,q)$, except for $b(p,q)$ near zero, this replacement can be omitted except when $b(p,q)$ appears as a denominator; omission of $\beta\Delta$ in the denominator of (4.16) causes a singularity when $b(p,q) = 0$. From Chapter II,

$$b(p,q) = \begin{cases} \sqrt{\beta^2 - p^2 - q^2} & \beta^2 \geq p^2 + q^2 \\ -i\sqrt{p^2 + q^2 - \beta^2} & \beta^2 < p^2 + q^2 \end{cases}$$

which, combined with the definitions of $\bar{k}_1$ and $\bar{k}_2$, yields

$$\left| \sqrt{\bar{k}_1 \cdot \bar{k}_2} + \beta\Delta \right|^2$$

for $b(p,q) \, b^*(p,q)$ in the denominator of (4.16). Consistency with the definition of $b(p,q)$ requires the negative solution for negative arguments of the radical.

In the numerator of (4.16), where $\beta\Delta$ can be neglected,

$$b^2(p,q) = \bar{k}_1 \cdot \bar{k}_2$$

$$\beta + p = -k_{2x}$$

$$\beta - p = -k_{1x}$$

135

and the entire integrand can be written in terms of the ocean-wave propagation constants k_1, k_2 as

$$\sigma_{VV}(\omega) = 16\pi\beta^4 W(-2\beta,0)\ \delta(\eta \pm \omega_B) \cdot \pi\beta^4 \iint\limits_{-\infty}^{\infty} \left\{ \left[\underbrace{\frac{k_{1x}k_{2x} - 2\bar{k}_1 \cdot \bar{k}_2}{|\sqrt{\bar{k}_1 \cdot \bar{k}_2} + \beta\Delta|}}_{\Gamma_{EM}} \right]^2 \right.$$

$$\left. + 4\left[\underbrace{k_1 + k_2 + \mathrm{sgn}(k_1 k_2 - k_1 \cdot k_2)\left(1 - \frac{2\eta^2}{\eta^2 - \omega_B^2}\right)\frac{g}{\omega_1\omega_2}}_{\Gamma_H} \right]^2 \right\}$$

$$\cdot\ \delta(\eta \pm \omega_1 \pm \omega_2)\ W(\bar{k}_1)\ W(\bar{k}_2)\ dpdq \qquad\qquad (4.17)$$

where Γ_{EM} and Γ_H denote the contributions to radar cross section from second-order electromagnetic and hydrodynamic theory, respectively. This equation is similar to the one presented by Barrick (1972). The difference in the two occurs in the relationship between Γ_{EM} and Γ_H. Instead of writing

$$2\Gamma_{EM}^2 + 8\Gamma_H^2$$

as in (4.17), Barrick combined Γ_{EM} and Γ_H as

$$4\left|\Gamma_{EM} - i\Gamma_H\right|^2$$

where, for Γ_{EM}, the absolute-value signs are dropped.

Except for the multiplicative constants, the difference between the two forms corresponds to the difference between incoherent and coherent addition of scattered fields. The first, representing incoherent addition, comes directly from the mathematical derivation; the second can be argued from the contention that, although individual first-order ocean-wave trains may be uncorrelated, second-order wave trains are related to the first-order waves that generate them. Consequently,

136

the first-order fields scattered by the second-order ocean waves (Γ_H) should be correlated to the second-order fields scattered by the generating first-order ocean waves (Γ_{EM}). The correct form is difficult to determine; perhaps partially coherent addition best represents the actual scattering process. Incoherent addition, however, will be retained here although either form is equally suitable for the discussion of the integration techniques to follow. In Chapter V, cross sections based on both will be compared to measured data.

The difference in the multiplicative constants or relative weighting between Γ_{EM} and Γ_H would be best determined by a detailed comparison of the derivations. A derivation of the second form is not available, however, and the comparisons in Chapter V will be relied on to help resolve this discrepancy.

Thus far, care has been taken to avoid the singularity in Γ_{EM} by introducing a finite surface impedance. There are, however, singularities in Γ_H that have not been discussed, and these occur when $\eta = \omega_B$, $\omega_1 = 0$, or $\omega_2 = 0$. Actually, when $\omega_1 = 0$,

$$\omega_2 = \omega_B = \eta$$

and when $\omega_2 = 0$,

$$\omega_1 = \omega_B = \eta$$

so that a singularity occurs only at $\eta = \omega_B$. It will be seen, however, in Section C.4 that, because of the low-frequency cutoff of first-order ocean-wave height spectra, there is no contribution to second-order cross section at the first-order Bragg frequency ω_B.

2.   Change in Variables of Integration

One of the integrations required to evaluate (4.17) can be carried out analytically with the aid of the delta function,

$$\delta\left(\eta \pm \sqrt{g\sqrt{(p-\beta)^2+q^2}} \pm \sqrt{g\sqrt{(p+\beta)^2+q^2}}\right)$$

For example, the integration over q can be eliminated by integrating over p and evaluating the integrand[†] at values of q for which

$$\eta \pm \sqrt{g\sqrt{(p - \beta)^2 + q^2}} \pm \sqrt{g\sqrt{(p + \beta)^2 + q^2}} = 0 \qquad (4.18)$$

The analytical solution to this equation, however, is not readily apparent and, if numerical techniques are employed to integrate (4.17), this expression must be solved for each value of the variable of integration. The complexity of evaluating these roots can be avoided if variables can be found that permit an analytical solution. Rewriting the delta-function argument as

$$\eta \pm \sqrt{gk_1} \pm \sqrt{gk_2} \qquad (4.19)$$

reveals that the use of k_1 and k_2 or $\sqrt{gk_1}$ and $\sqrt{gk_2}$ as variables provides a simple solution for the argument zeros. If k_1 is to be the remaining variable, integration over k_2 can be performed by evaluating the integrand of (4.17) at

$$k_2 = \frac{(\eta \pm \sqrt{gk_1})^2}{g}$$

Because the signs of p and q are formally lost in the definition of k_1 and k_2, care must be exercised in selecting the proper regions of integration; these regions are discussed in Sections 3, 4, and 5.

The formal change of variables requires a Jacobian for the transformation of p and q to k_1 and k_2, defined by

$$dp\, dq = J dk_1 dk_2$$

[†] Because of the form of the arguments in the delta function, the integrand in (4.17) must be multiplied by the inverse of the derivative of (4.18) with respect to q. This additional term is explained in more detail later in this section.

where

$$
J = \begin{vmatrix} \dfrac{\partial p}{\partial k_1} & \dfrac{\partial p}{\partial k_2} \\[2em] \dfrac{\partial q}{\partial k_1} & \dfrac{\partial q}{\partial k_2} \end{vmatrix}
$$

The inverse Jacobian J^{-1} can be determined from the definitions of k_1 and k_2 and, when it exists, the Jacobian can be found from the relationship $JJ^{-1} = 1$. In this case,

$$
J = \frac{k_1 k_2}{2 |q| \beta} \tag{4.20a}
$$

The sampling property of the delta function, expressed mathematically as

$$
\int_{-\infty}^{\infty} F(x) \, \delta(x) \, dx = F(0)
$$

provides another Jacobian. If, instead of x, the argument of the delta function is some function of x [such as $f(x)$], then

$$
\int_{-\infty}^{\infty} F(x) \, \delta[f(x)] \, dx \neq F(x_o)
$$

where $f(x_o) = 0$. By changing the variable from x to $f(x)$,

$$
\int_{-\infty}^{\infty} F(x) \, \delta[f(x)] \, dx = \int_{-\infty}^{\infty} F(x) \, \frac{\delta \, f(x)}{|f'(x)|} \, df(x) = \frac{F(x_o)}{|f'(x_o)|}
$$

where the modulus sign allows for the property $\delta(-x) = \delta(x)$. For (4.19), the delta-function Jacobian is

139

$$J_\delta = |f'(k_2)|^{-1} = 2\sqrt{\frac{k_2}{g}} \qquad (4.20b)$$

With the above Jacobians included, integration over k_2 with the aid of the delta function reduces (4.17) to the single integral

$$\sigma_{VV}^{(2)}(\eta) = \pi\beta^4 \int_{-\infty}^{\infty} \left[2\Gamma_{EM}^2(\bar{k}_1, \bar{k}_{20}) + 8\Gamma_H^2(\bar{k}_1, \bar{k}_{20}) \right]$$

$$\cdot W(\bar{k}_1)\, W(\bar{k}_{20}) \cdot \frac{k_1 k_{20}}{|q|} \frac{1}{\beta} \sqrt{\frac{k_{20}}{g}}\, dk_1 \qquad (4.21)$$

where

$$\eta \pm \sqrt{gk_1} \pm \sqrt{gk_{20}} = 0$$
$$k_{20} = (\eta \pm \sqrt{gk_1})^2/g$$

The vector $\bar{k}_{20}$ can be derived from the definitions of k_1 and k_2 evaluated at k_1 and k_{20},

$$k_1^2 = (p - \beta)^2 + q^2$$

$$k_{20}^2 = (p + \beta)^2 + q^2$$

Solving for p and q yields

$$p = \frac{k_{20}^2 - k_1^2}{4\beta}$$

and

$$q = \pm\sqrt{\frac{k_1^2 + k_{20}^2}{2} - \beta^2 - \frac{\left(k_{20}^2 - k_1^2\right)^2}{16\beta^2}}$$

Then, from the definition of $\bar{k}_2$ in (4.16),

$$\overline{k}_{20} = -(p + \beta)\,\hat{a}_x - q\hat{a}_y$$

Both positive and negative values of q must be included in the evaluation of (4.21) because the original integral spanned the region $-\infty < q < \infty$; therefore, the integration must be performed twice, once for $+q$ and once for $-q$.

3. Integration Regions

The region of integration for the untransformed expression (4.17) is the entire p,q-plane divided into regions of freely propagating and evanescent intermediate waves by the circle $b(p,q) = 0$, as illustrated in Fig. 34. When $b(p,q)$ is real, the phase factor $-ib(p,q)$ is imaginary and the intermediate wave is a freely propagating wave. When $b(p,q)$ is imaginary, the phase factor is real and the intermediate wave field attenuates exponentially away from the surface with a surface phase velocity greater than that for free-space propagation. The transition from one region to another is of considerable interest because the integrands of (4.17) and (4.21) become nearly singular along this circle.
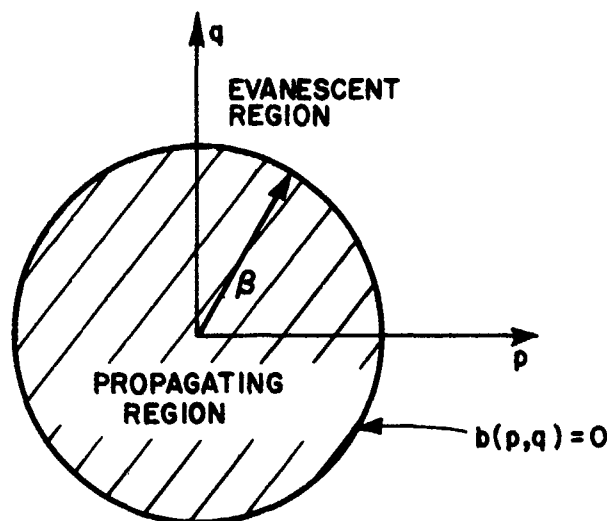
Fig. 34. PROPAGATION REGIONS FOR INTER-
MEDIATE RADIO WAVE.

In evaluating (4.21), it is helpful to view pictorially the regions of integration in both the p,q-plane and the k_1,k_2-plane. Figure 35 represents the p,q-plane with the loci of constant k_1 and k_2, defined by the circles

$$k_1 = \sqrt{(p - \beta)^2 + q^2}$$

$$k_2 = \sqrt{(p + \beta)^2 + q^2}$$

superimposed. Unless these circles intersect, no points p and q can satisfy simultaneously the definitions of k_1 and k_2. Figure 36 represents the limits of intersection from which the regions of integration in the k_1,k_2-plane can be determined. From Fig. 36a,

$$k_1 + k_2 > 2\beta \qquad (4.22a)$$
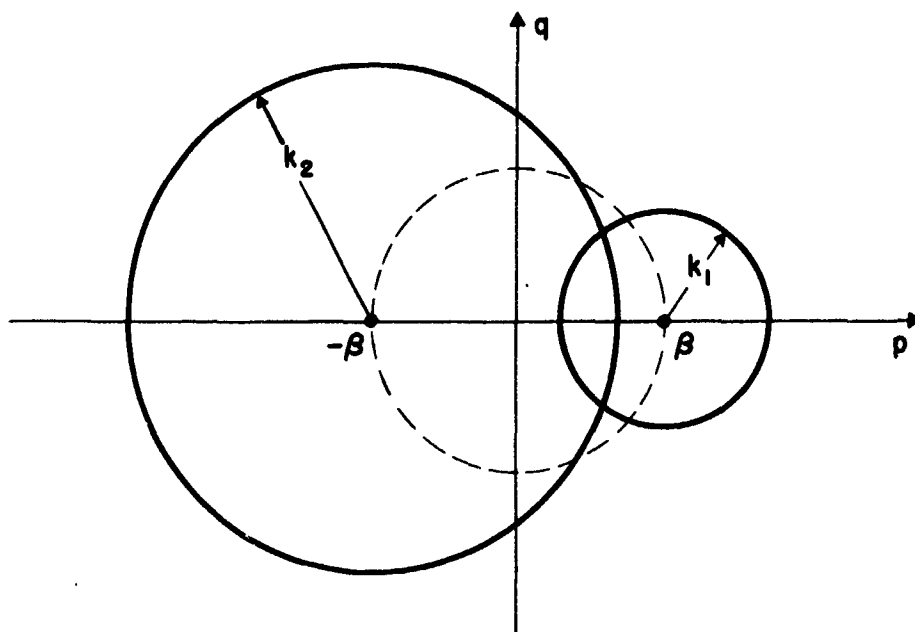
Fig. 35.   LOCI OF OCEAN-WAVE PROPAGATION CONSTANTS.
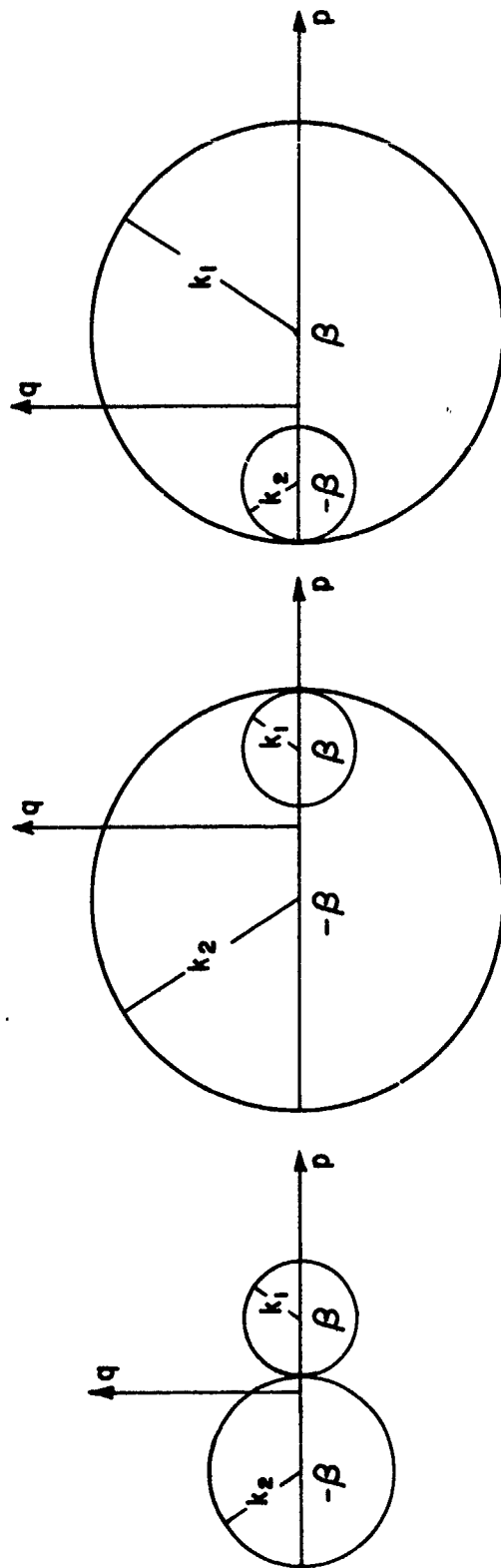
Fig. 36. LIMITS OF ALLOWABLE OCEAN-WAVE PROPAGATION CONSTANTS. Loci of constant k_1 and k_2 must intersect for there to be a contribution to second-order radar cross section. Tangent points define the limits of integration in the k_1, k_2-plane.

a. $k_1 + k_2 = 2\beta$

b. $k_2 = k_1 + 2\beta$

c. $k_1 = k_2 + 2\beta$

and from Figs. 36b and 36c,

$$k_2 < k_1 + 2\beta \qquad\qquad (4.22b)$$

$$k_1 < k_2 + 2\beta \qquad\qquad (4.22c)$$

These conditions are illustrated in Fig. 37 where the allowable region of integration in the k_1,k_2-plane is shaded. The p,q-axes indicate that this region encompasses the entire p,q-plane.
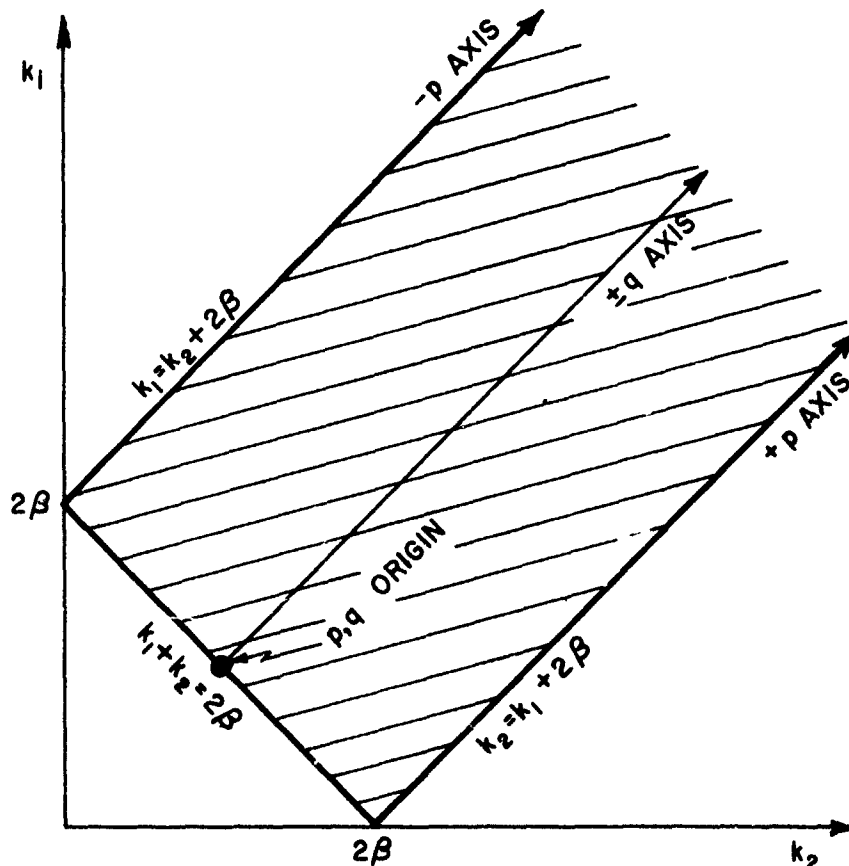
Fig. 37. INTEGRATION REGION IN THE k_1,k_2-PLANE. The shaded region contains all values of ocean-wave propagation constants that contribute to the radar cross-section integral.

The regions of propagating and evanescent waves for the inter-mediate scattered radio wave in the k_1,k_2-plane can be determined from the definitions of k_1 and k_2,

$$k_1^2 = (p^2 - 2\beta p + \beta^2) + q^2$$

$$k_2^2 = (p^2 + 2\beta p + \beta^2) + q^2$$

Adding these and using the condition

$$p^2 + q^2 = \beta$$

for the transition from one region to the other yields

$$k_1^2 + k_2^2 = 4\beta^2$$

which is the equation for a circle in the k_1,k_2-plane along which $b(p,q) = 0$ (Fig. 38).
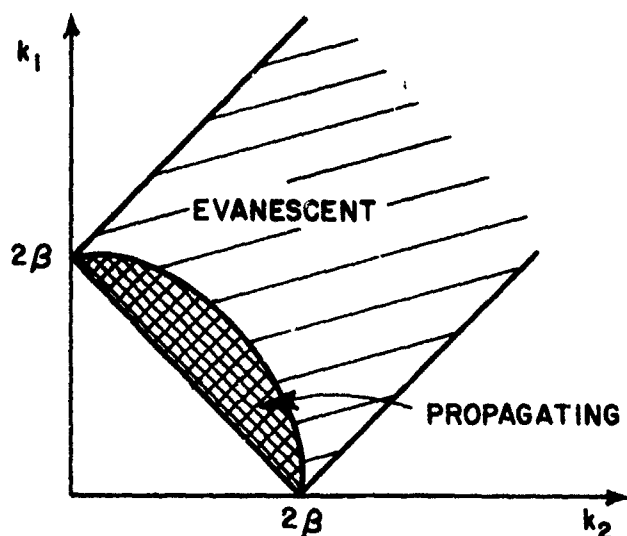
Fig. 38. PROPAGATION REGIONS FOR INTERMEDI-ATE RADIO WAVE.

4. Integration Contours

Elimination of one of the variables of integration by means of the delta function has reduced the double integral (4.17) to the contour integral (4.21), where the relationship (4.18) between k_1, k_2, and η provides the family of loci, parametric in η, along which (4.21) is to be evaluated. Much of the behavior of $\sigma_{VV}(\omega)$ as a function of η depends on how these contours traverse the regions of integration.

a. Two Modes of Integration

The choice of signs in the argument of the delta function (4.19) provides two distinct families of integration contours. According to the double Bragg-scattering concept, the doppler shift η is caused by both ocean-wave trains imparting either a positive or negative doppler shift to the radio wave (sum mode) or by one ocean-wave train imparting a positive doppler shift while the other imparts a negative doppler shift (difference mode). Figure 39 illustrates how the two modes could be visualized. If the signs are the same, the zeros of the delta function are

$$|\eta| = \left|\sqrt{gk_1} + \sqrt{gk_2}\right|$$

which is the sum mode and, if they are different, by

$$|\eta| = \left|\sqrt{gk_1} - \sqrt{gk_2}\right|$$

which is the difference mode.

In the sum mode, both $\sqrt{gk_1}$ and $\sqrt{gk_2}$ must be less than η (or equal to η if one of the radical terms is zero) for zeros of the delta function to exist. In the difference mode, however, both radical terms can be large as long as their difference is less than η.

For positive values of η, the sum-mode contours are

$$k_2 = \frac{(\eta - \sqrt{gk_1})^2}{g} \qquad \eta \geq \sqrt{gk_1}$$

146

SUM MODE   **DIFFERENCE MODE**
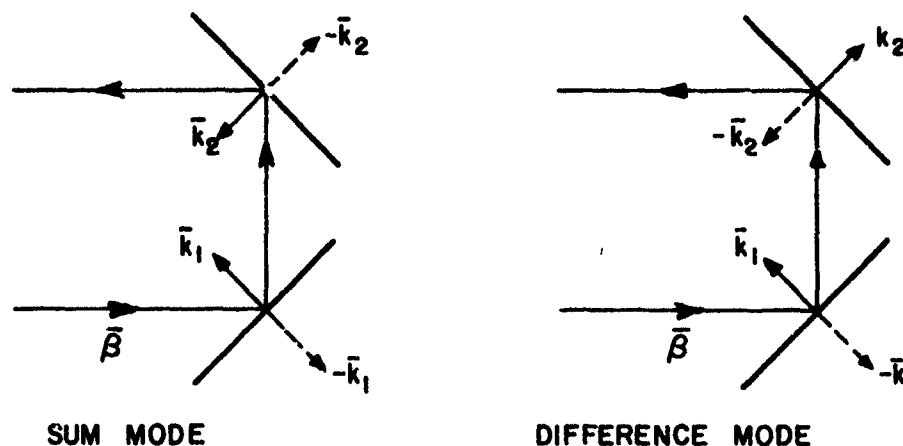
Fig. 39. DOPPLER SHIFTS FROM TWO OCEAN WAVES. Two ocean
waves can impart doppler shifts of either the same sign
(sum mode) or of different signs (difference mode). The
total shift can be positive or negative for either mode,
depending on the directions and relative magnitudes of
k_1 and k_2.

These contours, which also represent negative values of η, are plotted
in Fig. 40. Similar contours of integration for the difference mode come
from

$$k_2 = \frac{(\eta + \sqrt{gk_1})^2}{g} \qquad k_2 > k_1$$

or

$$k_1 = \frac{(\eta + \sqrt{gk_2})^2}{g} \qquad k_1 > k_2$$

The difference-mode contours (Fig. 41) are double valued.
The contour to be used in the integration for a particular value of η
depends on the relative magnitude of k_1 and k_2. For example, if η
is positive, with one ocean-wave train providing a positive doppler shift
and the other providing a negative doppler shift, then

$$\eta = \sqrt{gk_1} - \sqrt{gk_2}$$
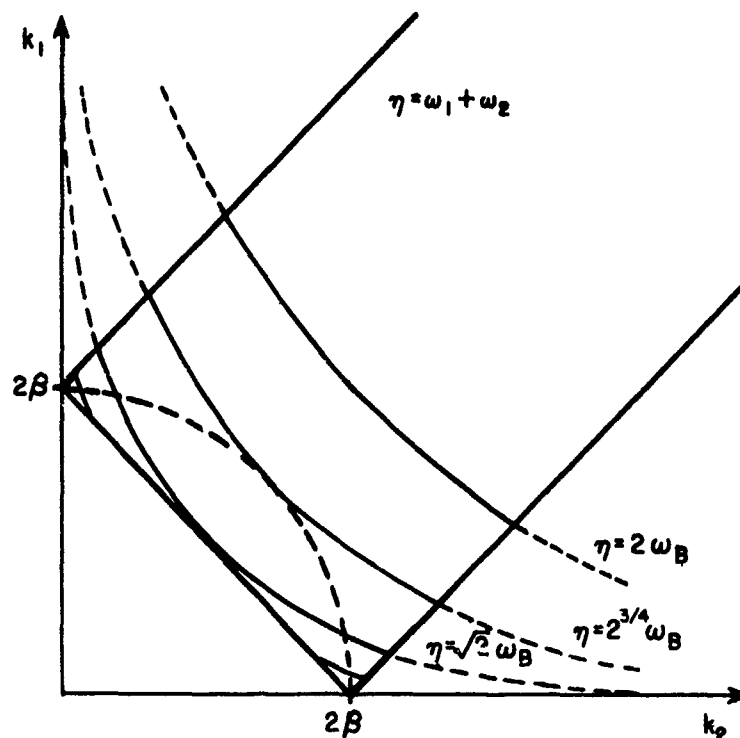
Fig. 40. SUM-MODE INTEGRATION CONTOURS.

and k_1 must always be greater than k_2. If η is negative, k_2 must be greater than k_1. If the sign of tne doppler shift from each of the wave trains is reversed, $k_2 > k_1$ implies positive η and $k_1 > k_2$ implies negative η.

A comparison of the sum- and difference-mode contours in Figs. 40 and 41 indicates that scattered radio waves with doppler shifts greater than ω_B occur in the sum mode only and that doppler shifts less than ω_B result from difference-mode scattering. This modal separation can be shown mathematically from the conditions stated in (4.22) and provides a convenient means by which to distinguish the sum- and difference-mode regions in plots of $\sigma_{VV}^{(2)}(\eta)$.[†]

[†] $\sigma_{VV}^{(2)}(\eta)$ emphasizes the dependence of radar cross section on doppler shift and replaces the notation $\sigma_{VV}^{(2)}(\omega)$. The superscript denotes second order.

148
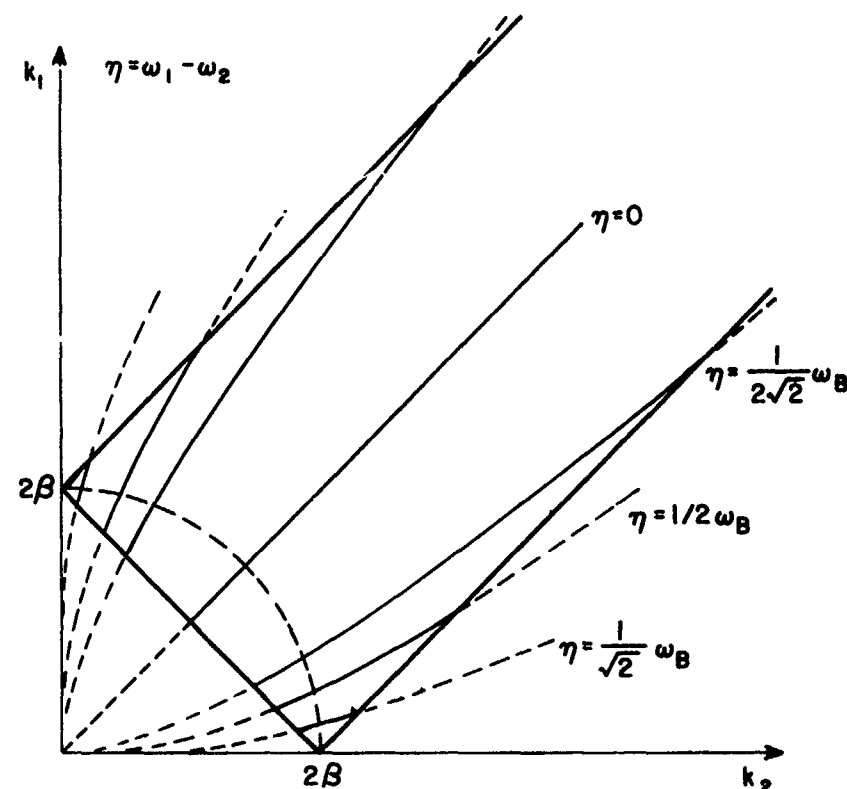
Fig. 41. DIFFERENCE-MODE INTEGRATION CONTOURS.

In either mode, the contours for $\eta = \omega_B$ cross the integration region only at points $(2\beta,0)$ or $(0,2\beta)$ in the k_1,k_2-plane. Because neither k_1 nor k_2 can be zero for real ocean waves, there is no second-order contribution to radar cross section at the first-order Bragg line; in fact, ocean-wave spectra have cutoffs well above $k = 0$ (Chapter III.C), and no second-order contribution is expected near the first-order Bragg line.

b. **Relationship between Integration Contours and** $\underline{\sigma_{VV}^{(2)}(\eta)}$

In this section, individual integration contours will be examined to determine how they are related to particular features of a typical plot of $\sigma_{VV}(\eta)$. Where applicable, these features will also be explained in terms of double Bragg scattering.

Figure 42 is a plot of $\sigma_{VV}(\eta)$ obtained by integrating (4.21) with a Munk wave-height spectrum (Table 1) at a wind speed of 30 knots (friction velocity = 0.725 m/sec). Figure 43 shows the relationship between wind direction and radio-wave propagation directions. The radar transmitter frequency is 10 MHz.
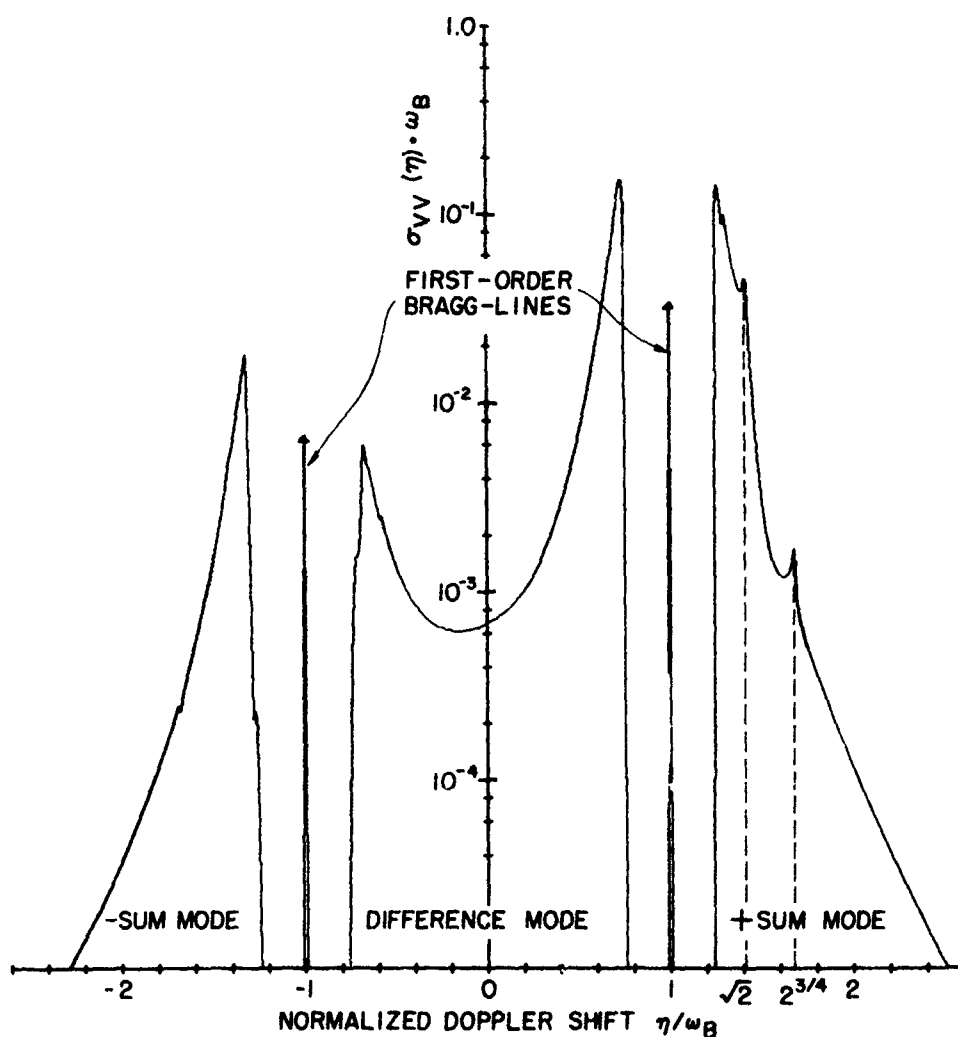
Fig. 42. TYPICAL PLOT OF INCREMENTAL RADAR CROSS SECTION FOR A MUNK WAVE-HEIGHT SPECTRUM. Wind = 30 knots at 135° with respect to the radar direction (Fig. 43). Radar frequency = 10 MHz. First-order Bragg-line height is proportional to power rather than to power spectral density.
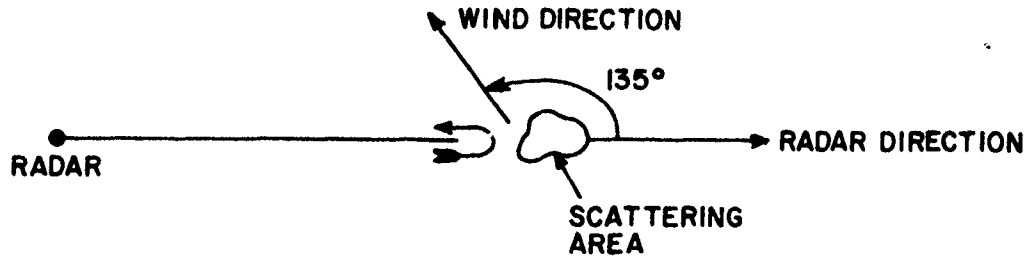
Fig. 43. RADAR-WIND GEOMETRY.

The features to be correlated with the integration contours are the spikes in Fig. 42 occurring at $\eta = \sqrt{2} \; \omega_B$ and $2^{3/4} \; \omega_B$. These peaks result when the integration contours traverse regions where the integrand becomes large or nearly singular. For example, the integrand in (4.17) is nearly singular when

$$\overline{k}_1 \cdot \overline{k}_2 = 0 \qquad\qquad (4.23)$$

if the normalized surface impedance Δ is small. Condition (4.23) defines the transition line from propagating to evanescent intermediate radio waves illustrated in Fig. 38, and integration contours approaching this line can be expected to cause high values of $\sigma_{VV}^{(2)}(\eta)$. The difference-mode contours (Fig. 41) all cross this line; however, they cross almost orthogonally so that the transition-line contribution to the integral should be small compared to the total contribution. Although the overall level of $\sigma_{VV}^{(2)}(\eta)$ in the difference region should be higher than in the regions where the contours do not approach the transition line (sum mode for $\eta > 2^{3/4} \; \omega_B$), there should be no distinguishable features for any single value of η, as indicated in Fig. 42.

In the sum mode, many of the contours do not cross the transition line (Fig. 40) but, for those that do, $\sigma_{VV}^{(2)}(\eta)$ should be higher (this is verified by Fig. 42). In particular, when $\eta = 2^{3/4} \; \omega_B$, the integration contour is tangent to the transition line and a large integrand exists over a substantial part of the contour, thereby creating a spike at this frequency.

151

In terms of multiple scattering, the transition line determined by (4.23) corresponds to ocean-wave trains traveling in orthogonal directions $(\bar{k}_1 \cdot \bar{k}_2 = 0)$ and produces a corner reflector effect (Fig. 44)[†] where radio waves incident on either wave train produce backscatter. The direction of the ocean-wave propagation vectors can be such that either the sum or difference mode exists. The lack of a definite spike at $\eta = -2^{3/4} \omega_B$ is the result of the wave-height directional spectrum and wind direction selected. Figures 43 and 44 show that one of the wave trains forming the corner reflector propagates along the line defining the wind direction. For positive doppler shifts, this wave train must have a component of propagation toward the radar (see Section C.5) and must, therefore, propagate in the wind direction; however, for negative doppler shifts, this wave train propagates directly against the wind where the Munk spectrum has zero amplitude when $\epsilon = 0$
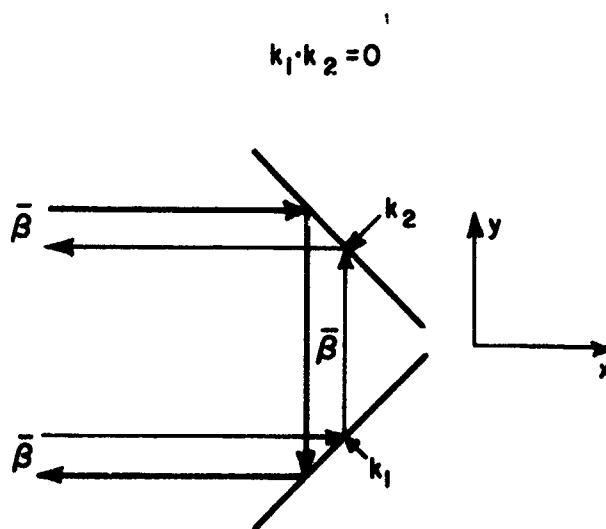
Fig. 44.   CORNER REFLECTOR.

[†]When the intermediate wave propagates on the surface with propagation constant β (this occurs on the transition line), the incident, reflected, and intermediate radio rays are coplanar for the backscatter geometry chosen and Snell's law implied by Fig. 44 is applicable. Generally, when the intermediate wave has a vertical component of propagation or is an evanescent wave, such a simple picture cannot be drawn.

and only small amplitude when ϵ is finite. At the point where the sum-mode contour is tangent to the transition line (Fig. 40), $k_1 = k_2$ and $p = 0$. As a result,

$$\eta = \pm\left[\sqrt{g\left(2\beta^2\right)^{1/2}} + \sqrt{g\left(2\beta^2\right)^{1/2}}\right] = \pm 2^{3/4}\,\omega_B$$

indicating that the tangent sum-mode contour does indeed correspond to the $2^{3/4}\,\omega_B$ spike shown in Fig. 42.

The integrand in Eq. (4.17) reveals no obvious singularities at $\eta = \sqrt{2}\omega_B$. Although the transformation Jacobian (4.20) is undefined at $q = 0$ and, hence, the transformed version (4.21) of Eq. (4.17) appears to have a singularity along the entire p-axis which bounds the region of integration in the k_1, k_2-plane, it will be shown in Appendix A that this is an integrable singularity except when $p = \beta$ and $q = 0$; in this case, the integrand is already singular because $\eta = \omega_B$.

Because no obvious singularities create the $\sqrt{2}\,\omega_B$ spike, a plot of the integrand will be examined for a clue. Figures 45a and 45b illustrate the sum- and difference-mode integrands in Eq. (4.17) with the delta function and spectral terms excluded, and Fig. 45c indicates the paths along which the integrands were calculated. The sum-mode integrand becomes quite large near the portion of the p-axis that lies on the $k_1 + k_2 = 2\beta$ line, particularly at $\eta = \sqrt{2}\,\omega_B$ where the integration contour is tangent to this segment of the p-axis. The greatest integrand contribution to this spike occurs at the p,q-origin where $k_1 = k_2 = \beta$, and $\bar{k}_1$ and $\bar{k}_2$ are aligned with the radar direction (x-axis in Fig. 32). If $\bar{k}_1$ and $\bar{k}_2$ are in the same direction, they represent a single wave train with $k = \beta$ (this is the Bragg condition for $n = 2$; see Section B). Because the phase velocity of an ocean wave is $\sqrt{g/k}$, the phase velocity of an ocean wave with $k = \beta$ is $\sqrt{2}$ times greater than that of a wave train causing first-order Bragg scattering ($k = 2\beta$).

Figure 46 illustrates what happens in terms of multiple scattering. With p and q both zero, the intermediate radio wave propagates along the z-axis and, although it propagates away from the ocean surface, the fields associated with this radio wave interact with
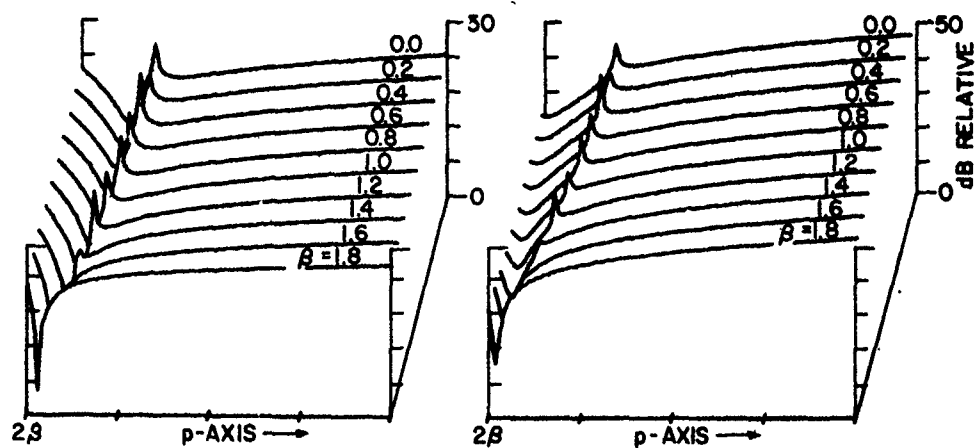
a. Sum mode   b. Difference mode
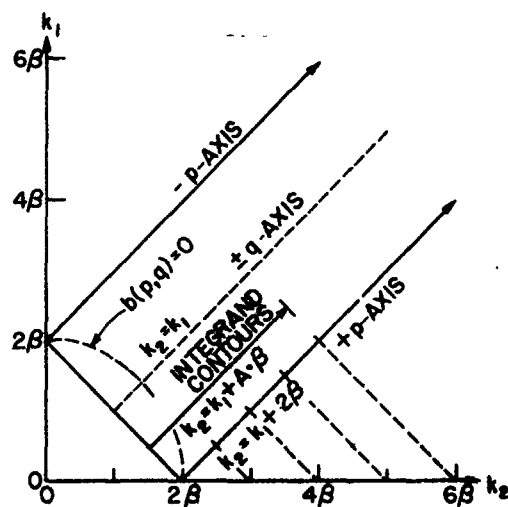
c. Integrand cuts

Fig. 45.   SECOND-ORDER RADAR CROSS-SECTION INTEGRANDS.   Sum- and difference-mode integrands are calculated along the line $k_2 = k_2 + A \cdot \beta$ in (c), where A varies from 0 to 1.8.   Integrands exclude the delta function and spectral terms in Eq.(4.17).
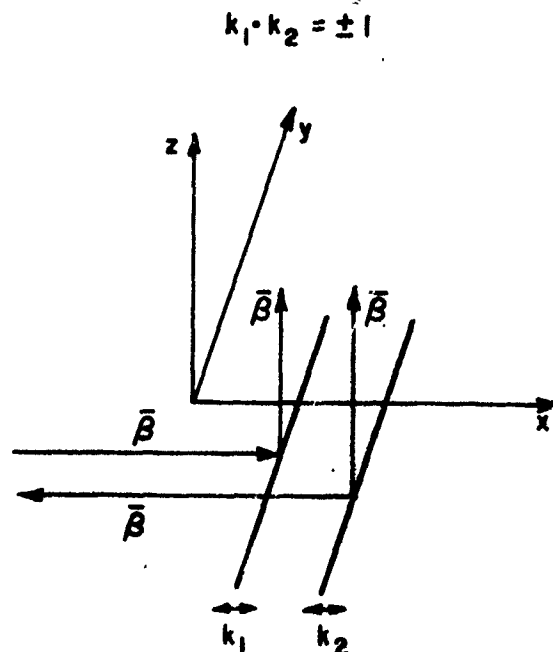
$$k_1 \cdot k_2 = \pm 1$$

Fig. 46. MULTIPLE BRAGG SCATTERING
FOR $k_1 = k_2 = \beta$. Incident radio
waves are scattered away from the
surface by wave train 1. The sec-
ond wave train scatters the inter-
mediate radio wave back along the
surface.

the second ocean-wave train in such a manner as to produce the backscat-
tered radio wave shown. Note that both the sum- and difference-mode in-
tegrands continue to increase as k_1 and k_2 increase; whereas, Fig.
42 shows that, as these constants increase, the sum-mode total integral
decreases. This is the result of the spectral terms (excluded from the
integrand calculations) decreasing at the rate of k^{-4} (see Table 1).

5. Doppler Shift as a Function of Ocean-Wave Direction

The choice of signs in the delta function in Eq. (4.17) deter-
mines which contours (sum or difference mode) are to be used in evaluat-
ing $\sigma_{VV}^{(2)}(\eta)$; however, the criterion for selecting those signs has not
been established. Whether a given wave train causes a positive or nega-
tive doppler shift in a radar signal will depend on the direction of
ocean-wave propagation.

155

The relationship between doppler shift and ocean-wave direction can be found by considering what happens when a radar signal with propagation constant $\bar{\beta}_1$ impinges on an ocean wave traveling with velocity $\bar{v}$ (Fig. 47). An observer traveling with the wave will see the radar signal doppler shifted by an amount[']

$$\omega_{d1} = -\bar{\beta}_1 \cdot \bar{v}$$

To first order,[†] a stationary observer at point 0 will see a doppler shift (relative to the frequency noted by the observer moving with the wave) of

$$\omega_{d2} = \bar{\beta}_r \cdot \bar{v}$$
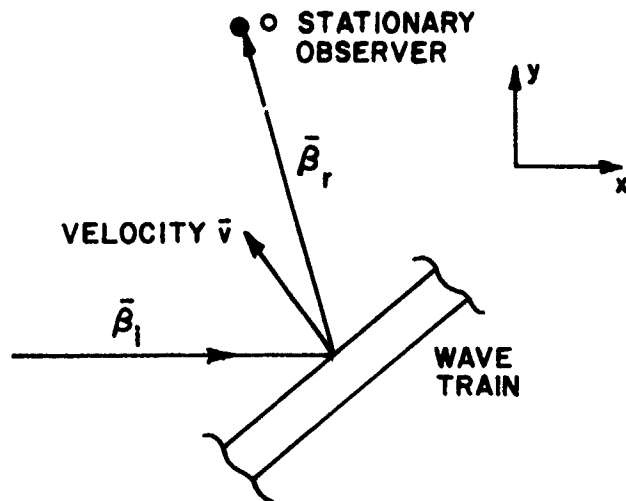
Fig. 47. SINGLE-SCATTER DOPPLER-SHIFT GEOMETRY.

[†] First order denotes that $\bar{\beta}_r$ is taken as ω_0/c rather than the more exact $(\omega_0 + \omega_{d1})/c$, where ω_0 is the transmitted frequency and c is the velocity of radio-wave propagation. This simplification was also assumed in Chapter II for the derivations that led to Eq. (4.17).

156

As a result, the total doppler shift imparted to the incident signal by the ocean wave is

$$\omega_D = \omega_{d1} + \omega_{d2} = \overline{v} \cdot (\overline{\beta}_r - \overline{\beta}_i) \qquad (4.24)$$

When the dispersion relationship (3.24) replaces $\overline{v}$ with a function of the ocean-wave propagation constant $\overline{k}$, the total doppler shift becomes

$$\omega_D = \sqrt{\frac{g}{k}} \, \frac{\overline{k}}{k} \cdot (\overline{\beta}_r - \overline{\beta}_i) \qquad (4.25)$$

The doppler shifts imparted by the two ocean-wave trains associated with (4.17) or (4.21) can now be calculated directly from (4.25). From Fig. 48, the radio- and ocean-wave propagation vectors for the first wave train are

$$\overline{\beta}_i = \beta \hat{a}_x \qquad (4.26a)$$

$$\overline{\beta}_r = p \hat{a}_x + q \hat{a}_y + r \hat{a}_z \qquad (4.26b)$$

$$\overline{k}_1 = (p - \beta) \, \hat{a}_x + q \hat{a}_y \qquad (4.26c)$$

and the doppler shift according to (4.25) is positive with a magnitude of

$$\omega_1 = \sqrt{g k_1}$$

For the second wave train,

$$\overline{\beta}_i = p \hat{a}_x + q \hat{a}_y + r \hat{a}_z \qquad (4.27a)$$

$$\overline{\beta}_r = -\beta \hat{a}_x \qquad (4.27b)$$

$$\overline{k}_2 = (-p - \beta) \, \hat{a}_x - q \hat{a}_y \qquad (4.27c)$$

157
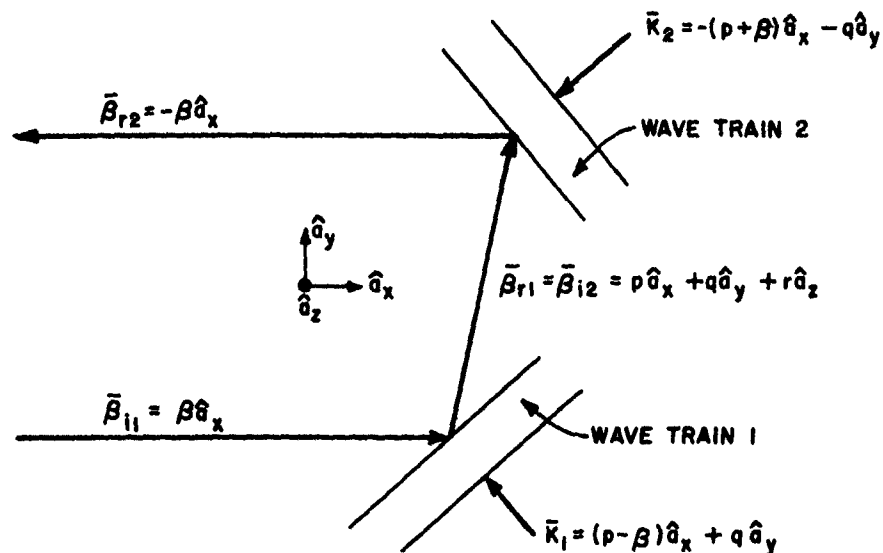
Fig. 48. RELATIONSHIP BETWEEN RADIO-WAVE AND OCEAN-WAVE PROPAGATION VECTORS.

and, again, the doppler shift is positive, but with a magnitude of

$$\omega_2 = \sqrt{gk_2}$$

The corresponding delta function in (.17) for the ocean waves defined by (4.26c) and (4.27c) is

$$\delta(\eta - \omega_1 - \omega_2)$$

To obtain delta functions representing the negative sum mode or the difference modes requires expansion of the definitions of $\bar{k}_1$ and $\bar{k}_2$ to include $\pm\bar{k}_1$ and $\pm\bar{k}_2$. The restrictions on $\bar{k}_1$ and $\bar{k}_2$ in (4.26c) and (4.27c) are a consequence of the fact that the scattering geometry (Fig. 48) is independent of wave direction. Expanding these definitions does not change the orientation of the wave trains but simply specifies their direction of propagation. The equations for radar cross section yield (4.26c) and (4.27c) rather than the negative counterparts because

158

positive directions of ocean-wave propagation were assumed in their derivation. The integral in (4.21) must be evaluated four times, once for each possible directional combination of $\overline{k}_1$ and $\overline{k}_2$ if second-order cross section is to be completely determined.

An interesting result of Eq. (4.25) is that ocean waves that appear to provide a particular sign for ω_1 or ω_2 do not. For example, an ocean wave with a velocity component in the negative x-direction (Fig. 47) could be expected to impart a positive doppler shift to a radar signal traveling in the positive x-direction. To verify that this does not necessarily occur, consider an ocean wave with the propagation vector

$$\overline{k} = -(p - \beta) \, \hat{a}_x - q\hat{a}_y$$

and a radio wave with propagation components (Fig. 48),

$$\overline{\beta}_i = \beta\hat{a}_x$$

$$\overline{\beta}_r = p\hat{a}_x + q\hat{a}_y + r\hat{a}_z$$

Equation (4.25) shows that these propagation vectors result in a negative doppler shift; however, k_x can be negative (k_x negative was expected to provide a positive doppler shift) if p is positive and larger than the radio-wave propagation constant β. Under certain conditions, then, an ocean wave with a velocity component in the direction of the radar may provide a negative doppler shift; this condition is $p > \beta$. Because

$$\beta^2 - p^2 - q^2 = b^2(p,q)$$

$b(p,q)$ is imaginary and the reflected wave is evanescent.

Because the evanescent region must be included in the integration of (4.17) or (4.21), the signs of ω_1 and ω_2 must be based on Eq. (4.25). Barrick (1972) apparently used only the sign of the x-component of the ocean-wave propagation constant as the criterion for selecting

159

these signs in the delta function, in disagreement with the conclusion here.

6.   Integration Limits

Ostensibly, the integration limits for (4.21) are from zero to infinity; however, the integration contours (Figs. 40 and 41) cross the integration region boundaries within these outer limits. Actual limits are obtained from the intersection of the contours with the region boundaries. These intersection points are shown in Fig. 49 for both sum- and difference-mode contours.
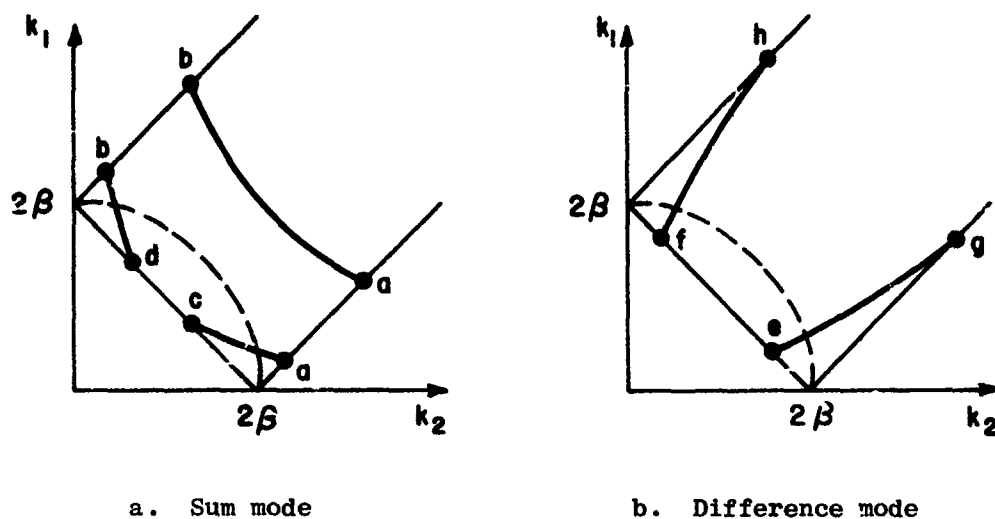

a. Sum mode   b. Difference mode

Fig. 49.   INTEGRATION LIMITS.

Point (a) for the sum mode is the intersection of the boundary

$$k_1 = k_1 + 2\beta \qquad (4.28)$$

with the contour

$$k_2 = \frac{(\eta - \sqrt{gk_1})^2}{g} \qquad (4.29)$$

160

The value of the variable of integration k_1 at this point is found by solving (4.28) and (4.29),

$$k_1(a) = \frac{\left(\omega_B^2 - \eta^2\right)^2}{4\eta^2 g} \tag{4.30}$$

Similarly, the intersection of the sum-mode contour (4.29) with the boundary

$$k_1 = k_2 + 2\beta$$

provides the value of k_1 at point (b),

$$k_1(b) = \frac{\left(\omega_B^2 + \eta^2\right)^2}{4\eta^2 g} \tag{4.31}$$

For $\eta < \sqrt{2}\,\omega_B$, this contour also intersects the boundary

$$k_1 + k_2 = 2\beta \tag{4.32}$$

Combining (4.29) and (4.32) results in a quadratic expression for k_1 whose two solutions correspond to points (c) and (d),

$$k_1(c) = \frac{\omega_B^2 - \eta\sqrt{2\omega_B^2 - \eta^2}}{2g} \tag{4.33a}$$

$$k_1(d) = \frac{\omega_B^2 + \eta\sqrt{2\omega_B^2 - \eta^2}}{2g} \tag{4.33b}$$

The difference-mode contours

$$k_2 = \frac{(\eta + \sqrt{g k_1})^2}{g}$$

161

$$k_1 = \frac{(\eta + \sqrt{gk_2})^2}{g}$$

intersecting the integration region boundaries establishes the limits

$$k_1(e) = \frac{\omega_B^2 - \eta\sqrt{2\omega_B^2 - \eta^2}}{2g} \qquad (4.34a)$$

$$k_1(f) = \frac{\omega_B^2 + \eta\sqrt{2\omega_B^2 - \eta^2}}{2g} \qquad (4.34b)$$

$$k_1(g) = \frac{\left(\omega_B^2 - \eta^2\right)^2}{4\eta^2 g} \qquad (4.34c)$$

$$k_1(h) = \frac{\left(\omega_B^2 + \eta^2\right)^2}{4\eta^2 g} \qquad (4.34d)$$

Derivation of these limits completes the prerequisites for evaluating $\sigma_{VV}^{(2)}(\eta)$ by Eq. (4.21).

D. Numerical Methods and Results

Several examples of calculated incremental radar cross section per unit frequency as a function of doppler shift are presented in this section. These examples show variations of $\sigma_{VV}(\eta)$ with wind speed and direction for the first-order wave-height spectral models described in Chapter III (Table 1). Power in the second-order sidebands is calculated and compared to first-order, or Bragg-line, power in an attempt to find methods for predicting wind speed and direction from radar measurements. Attention is restricted to $\sigma_{VV}(\eta)$ because, for grazing incidence and observation, only vertically polarized radar echoes are observed.

162

1. Integration Methods

Numerical techniques are utilized to evaluate (4.21) for $\sigma_{VV}^{(2)}(\eta)$. The integration region (Fig. 37) is subdivided into three smaller regions (Fig. 50) so as to isolate the circle $b(p,q) = 0$ where the integrand of (4.21) is nearly singular. In the annulus (region 2), the integrand is evaluated at finer increments than is required in region 1 or 3. The lengths of the radii R_1 and R_2, defining region 2, are not critical and were set at 1.8β and 2.2β for convenience. Simpson's rule for numerical integration [Herriot, 1963, pp. 25-29] was used to obtain the results presented.
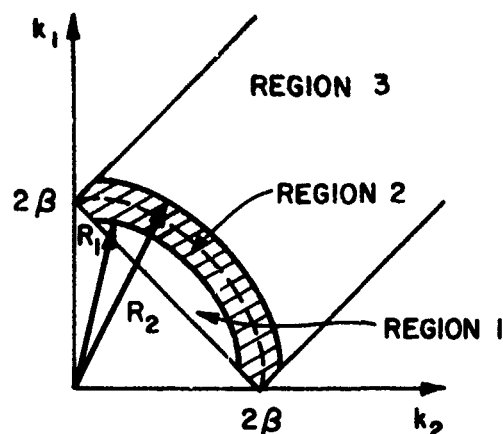
Fig. 50. SUBREGIONS OF INTEGRATION.

The number of points required by Simpson's method in region 2 depends on the steepness of the integrand slope near $b(p,q) = 0$ which, in turn, depends on the value chosen for the normalized surface impedance Δ. Barrick (1971) has calculated values of Δ as a function of wind speed for several first-order wave-height spectral models. Figure 51 presents surface impedances based on a Phillips (Table 1) isotropic spectrum. For directional spectrum models, Δ is a function of wind direction as well as wind speed for a given radio frequency [Barrick, 1971].

Except when $\eta \approx 2^{3/4}\omega_B$, the exact value selected for Δ in the evaluation of (4.21) is not critical. In the difference mode, where integration contours cross $b(p,q) = 0$ almost orthogonally (Fig. 41), the contribution to $\sigma_{VV}^{(2)}(\eta)$ from region 2 is relatively small compared to the total value of the integral. In the sum mode (Fig. 40), contributions from region 2 are again small (although not as small as those in the difference mode) except when the integration contours are nearly tangent to $b(p,q) = 0$. It can be observed in Fig. 42 that the power (area under the curve) in the received radar signal $\eta = 2^{3/4}\omega_B$ is also
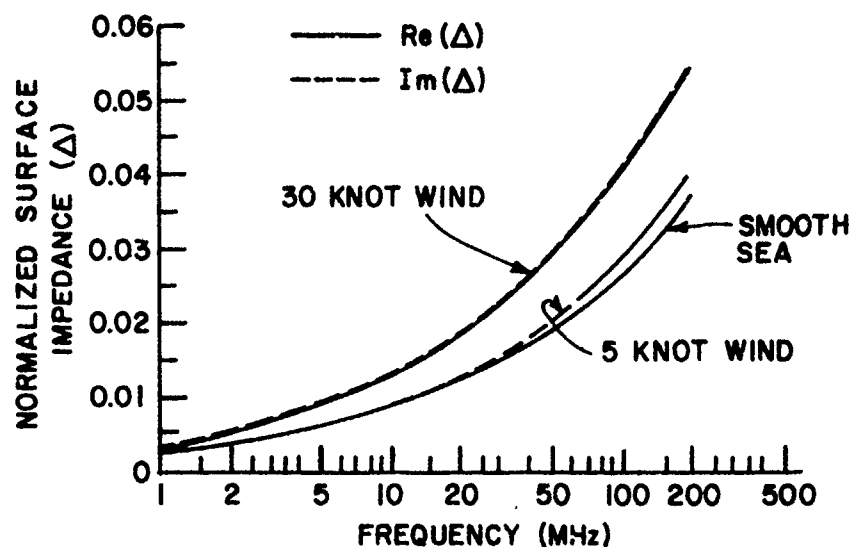
Fig. 51. EFFECTIVE SURFACE IMPEDANCE. Calculated normalized effective surface impedance Δ is based on a Phillips isotropic wave-height spectrum.

small compared to the total received power; therefore, unless a precise value of $\sigma_{VV}^{(2)}(\eta)$ is required at $\eta = 2^{3.4} \omega_B$, values of Δ larger than those indicated in Fig. 51 can be chosen with little effect on $\sigma_{VV}^{(2)}(\eta)$. To reduce the number of points at which the integrand in (4.21) must be evaluated in region 2, a value of $\Delta = 0.05 + i\, 0.05$ was set for all computations presented here.

2. Calculated Values of $\sigma_{VV}(\eta)$

Figure 52 is a plot of $\sigma_{VV}(\eta) \cdot \omega_B$ vs η/ω_B for a Phillips semi-isotropic wave-height spectrum. The wind speed is 30 knots, and the directions (Fig. 53) are crosswind and upwind, corresponding to $\theta_w = 90°$ and $\theta_w = 180°$, respectively. The value of the equilibrium range constant is $\beta_e = 0.01$ and will be maintained throughout. Swell has been neglected in the calculations leading to Fig. 52 and in most of the results presented here, except where noted. The radar frequency is 10 MHz.

The first-order contributions to incremental radar cross section per unit frequency are represented by delta functions in frequency [Eq. (4.21)]. These Bragg lines are shown in Fig. 52; however, the

164
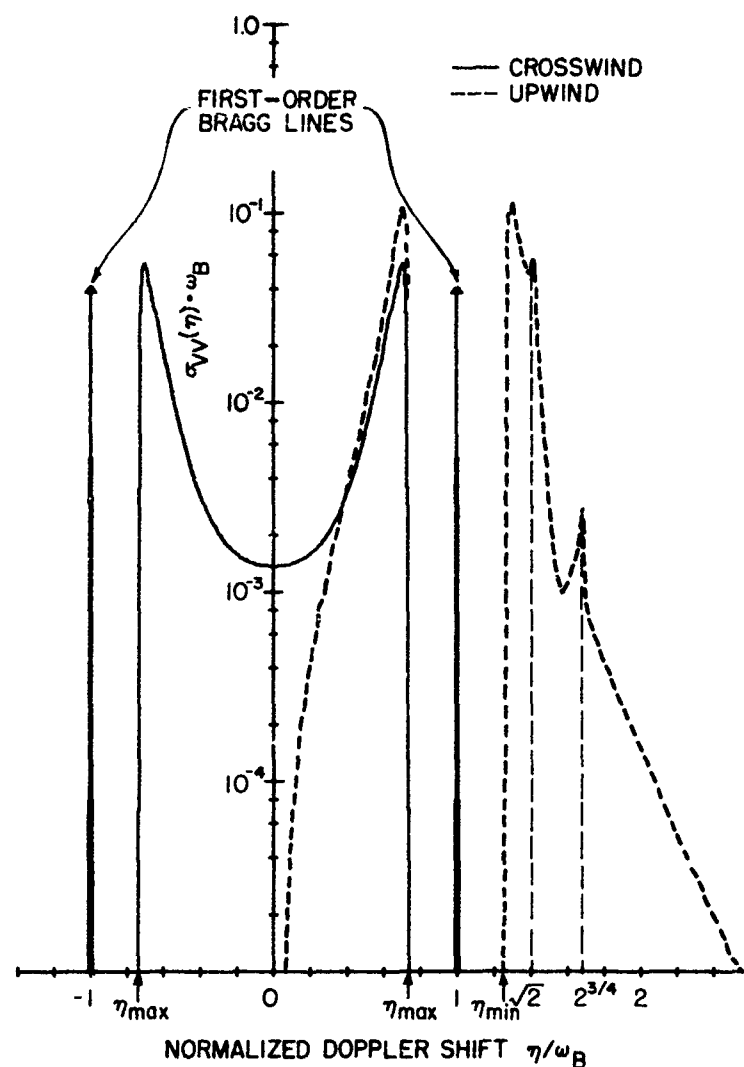
Fig. 52. RADAR CROSS SECTION FOR A PHILLIPS SEMI-
ISOTROPIC WAVE-HEIGHT SPECTRUM. Wind speed = 30
knots; radar frequency = 10 MHz.

height of the lines denotes the power in the first-order radar echo ω_B.
σ_{VV}^o, where

$$\sigma_{VV}^o = \int_0^\infty \sigma_{VV}^{(1)}(\eta)\, d\eta$$

for the positive Bragg line, and

165

$$\sigma_{VV}^{o} = \int_{-\infty}^{0} \sigma_{VV}^{(1)}(\eta) \, d\eta$$

for the negative Bragg line. The first-order contribution to (4.21) is $\sigma_{VV}^{(1)}(\eta)$ (see Appendix B).
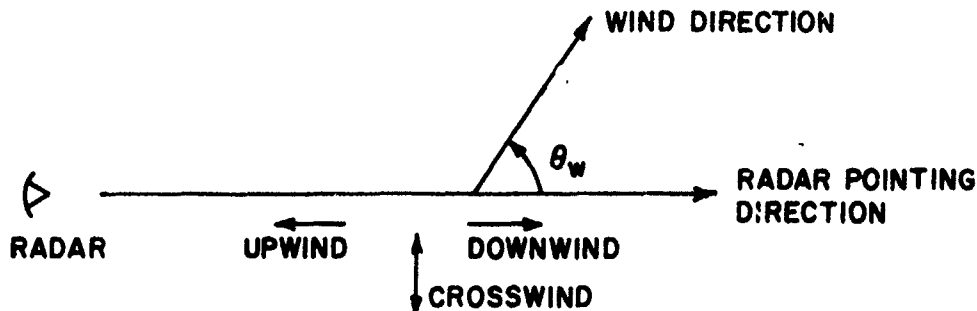
Fig. 53. WIND DIRECTIONS.

Figure 52 also exhibits the characteristic spikes at $\eta = \pm\sqrt{2}\omega_B$ and $\eta = \pm 2^{3/4}\omega_B$ that appeared in the radar cross section of the Munk spectrum (Fig. 42). These spikes were considered in some detail in Section C.4.b.

A feature characteristic of all semi-isotropic spectra is their lack of radar cross section in certain regions of doppler shift η. There is no sum-mode cross section in the crosswind direction, and scattered power has only a positive or negative doppler shift in the upwind or downwind directions, respectively. This feature can be explained by applying the double Bragg-scattering concept to a wave-height spectrum that is nonzero only on a half-plane (Fig. 20).

The sharp cutoffs in radar cross section near the Bragg lines in Fig. 52 result when the wave-height spectrum is limited to waves traveling slower than the wind. In the difference-mode region of positive doppler shift, the maximum value η_{max} at which $\sigma_{VV}^{(2)}(\eta)$ is nonzero occurs when one ocean-wave train in a double Bragg-scattering process produces the maximum possible doppler shift ω_{1max} and the second produces the minimum possible doppler shift ω_{2min}; that is,

$$\eta_{max} = \omega_{1max} - \omega_{2min}$$

or

$$\eta_{max} = \sqrt{gk_{1max}} - \sqrt{gk_{2min}}$$

Because of the wave-speed limitation, $k_{2min} = g/C_{max}^2$ where C_{max} is the wave speed equal to wind speed. From Fig. 36,

$$k_1 - k_2 \leq 2\beta$$

therefore,

$$k_{1max} = 2\beta + k_{2min} = 2\beta + \frac{g}{C_{max}^2}$$

and

$$\eta_{max} = \sqrt{2\beta g + \frac{g^2}{C_{max}^2}} - \frac{g}{C_{max}} \qquad (4.35)$$

In the sum-mode region of positive doppler shift, a similar argument leads to

$$\eta_{min} = \sqrt{2\beta g - \frac{g^2}{C_{max}^2}} + \frac{g}{C_{max}} \qquad (4.36)$$

These last two equations represent the values of doppler shift at which the second-order contribution to radar cross section near the Bragg lines becomes zero. For the examples in Fig. 52, $\eta_{max} = \pm 0.73\omega_B$ in the difference mode and $\eta_{min} = \pm 1.26\omega_B$ in the sum mode. These expressions are valid when the wave-height spectrum cutoff is determined solely by C_{max}, whatever the relationship between wind speed and maximum wave speed.

A somewhat more realistic description of incremental radar cross section is plotted in Fig. 54 where a Munk wave-height spectrum
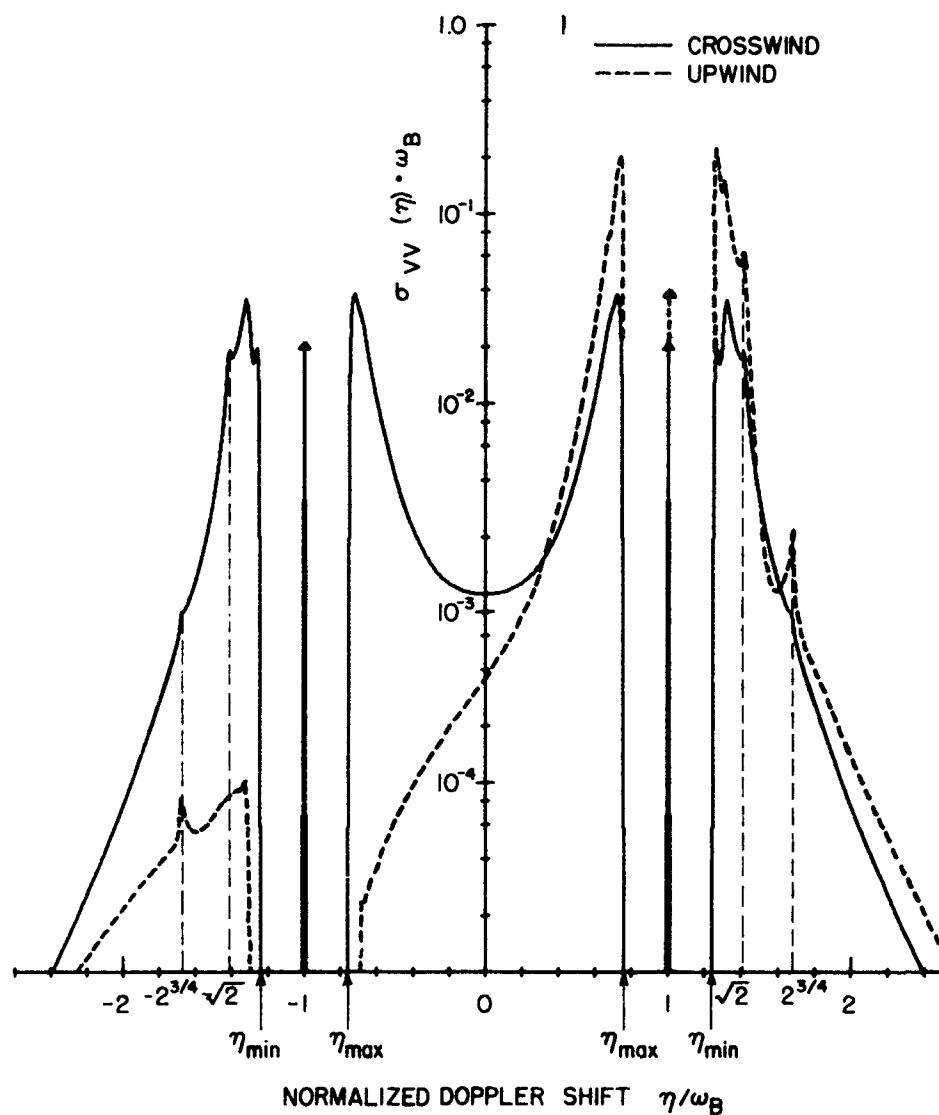
Fig. 54. RADAR CROSS SECTION FOR A MUNK WAVE-HEIGHT SPECTRUM. Wind speed = 30 knots measured at 6.4 m, radar frequency = 10 MHz, $\epsilon = 0$.

168

(Table 1) has been assumed. In this spectrum, ocean waves are allowed to propagate in all directions; as a result, there are sum- and difference-mode contributions to second-order radar cross sections at positive and negative doppler shifts for both crosswind and upwind conditions. The wind speed of 30 knots is assumed at an anemometer height of 6.4 m and corresponds to a friction velocity of 0.725 m/sec. The constant ϵ allows for ocean-wave energy propagating against the wind and is zero in this example; however, Fig. 55 illustrates the effects of finite ϵ.

The position of the near-Bragg-line cutoffs for this spectrum are determined by the μ-parameter cutoff μ_o which is related to the maximum wave velocity by

$$C_{max} = \frac{u_*}{\mu_o \kappa}$$

where κ is Karman's constant (≈ 0.41) and u_* (Chapter III.C.2) is the friction velocity defined by Eq. (3.45). For $\mu_o = 0.1$, $\eta_{max} = \pm 0.76\omega_B$ and $\eta_{min} = \pm 1.24\omega_B$ from Eqs. (4.35) and (4.36).

An example of radar cross section that does not have quite the sharp near-Bragg-line cutoffs associated with the Phillips and Munk spectra is shown in Fig. 56, where a Pierson-Moskowitz amplitude spectrum with a directional dependence of $\cos^2(\Theta/2)$ (Table 1) has been assumed. This spectrum provides an exponential wave-height decay for waves traveling faster than the wind (Fig. 19), rather than a sharp transition to zero wave height, and will be used in most of the remaining discussion of $\sigma_{VV}(\eta)$ in this chapter; however, corresponding results obtained from the Phillips and Munk spectra are presented in Appendix C.

Variations of $\sigma_{VV}(\eta)$ with wind direction are illustrated in Fig. 57 for $\theta_w = 112.5°$, $135°$, and $154.5°$ (Fig. 53). The upwind and crosswind values ($\theta_w = 180°$ and $90°$) for $\sigma_{VV}(\eta)$ are found in Fig. 56. Plots of $\sigma_{VV}(\eta)$ for θ_w between $180°$ and $90°$ also represent $\sigma_{VV}(-\eta)$ for θ_w from $0°$ to $90°$, respectively. Plots for both negative and positive values of θ_w are the same.

As the direction changes from crosswind to upwind, values of $\sigma_{VV}(\eta)$ for positive doppler shifts increase and those for negative
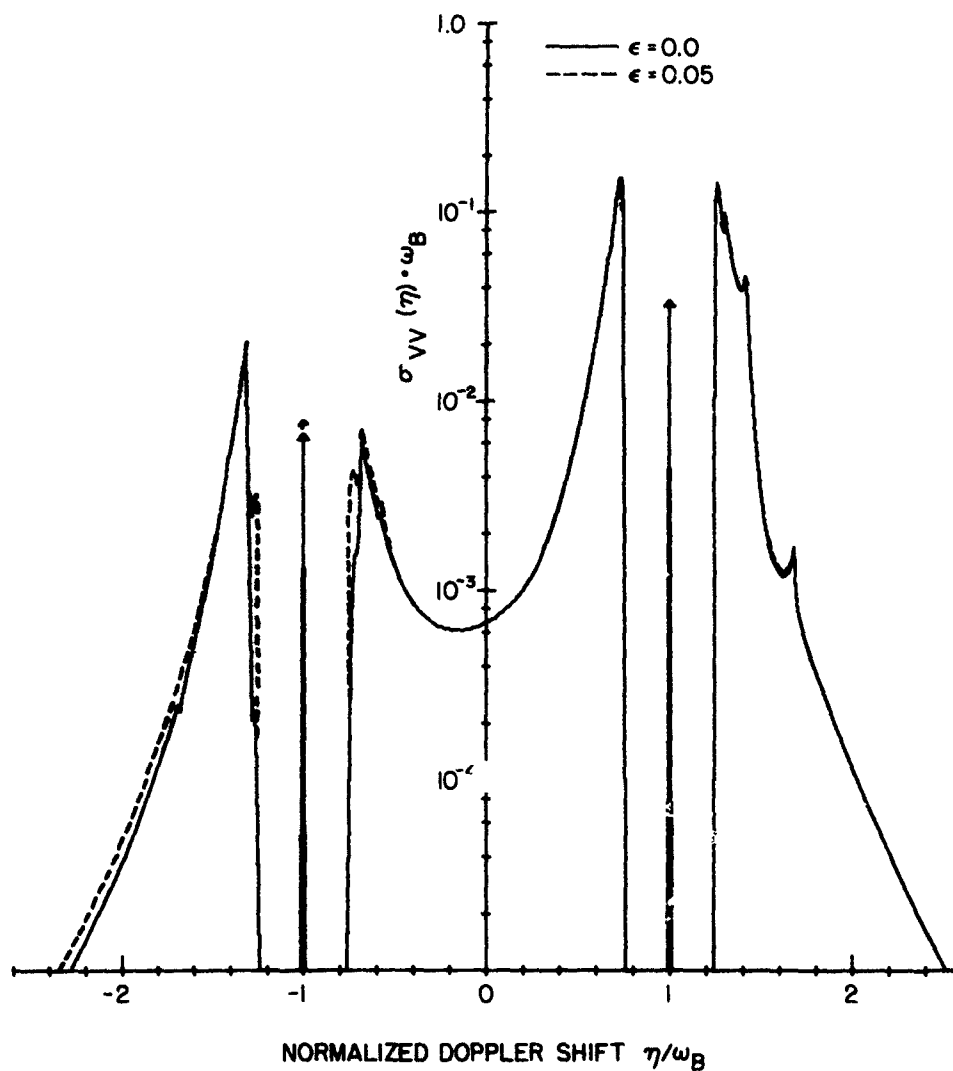
169

Fig. 55. RADAR CROSS SECTION FOR WAVES TRAVELING AGAINST THE
WIND. A Munk wave-height spectrum with wind speed = 30 knots
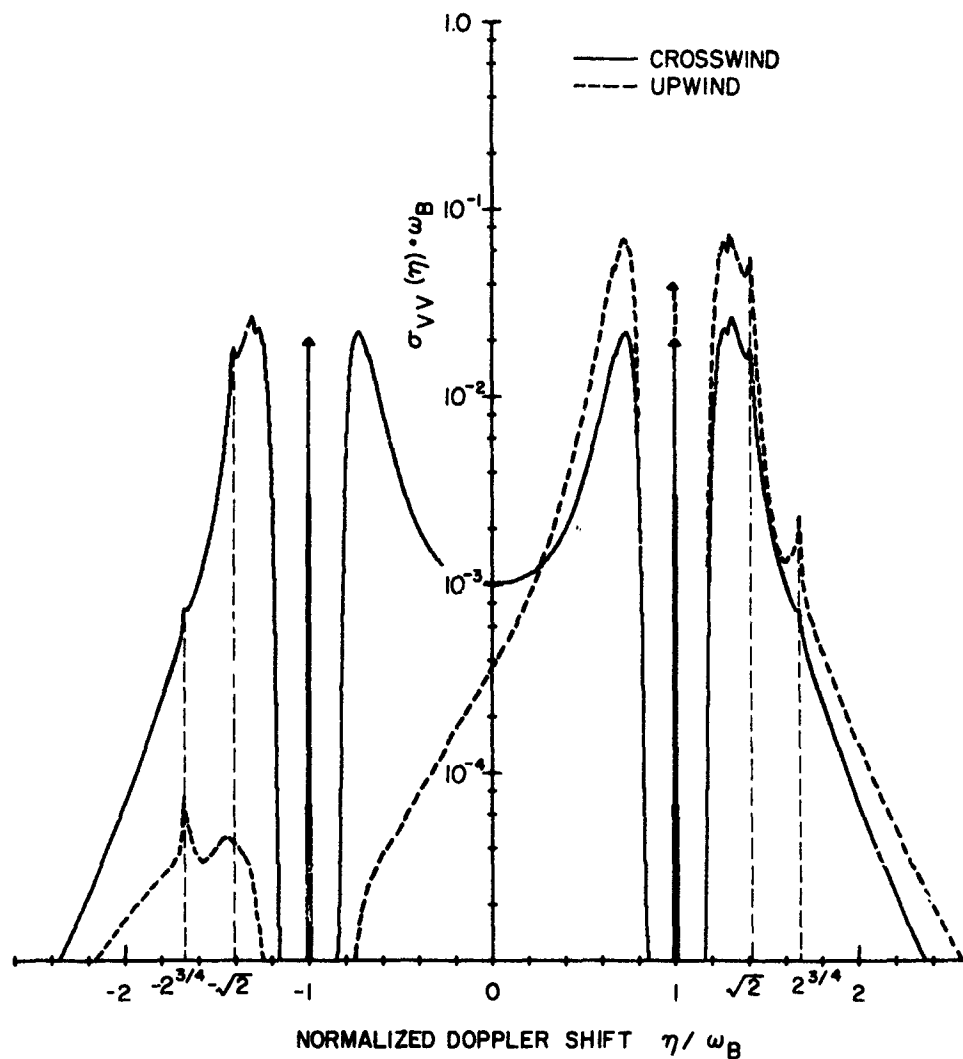and direction = 135° assumed.

170

Fig. 56. RADAR CROSS SECTION FOR A PIERSON-MOSKOWITZ COSINE-SQUARED WAVE-HEIGHT SPECTRUM. Wind speed = 30 knots; radar frequency = 10 MHz.
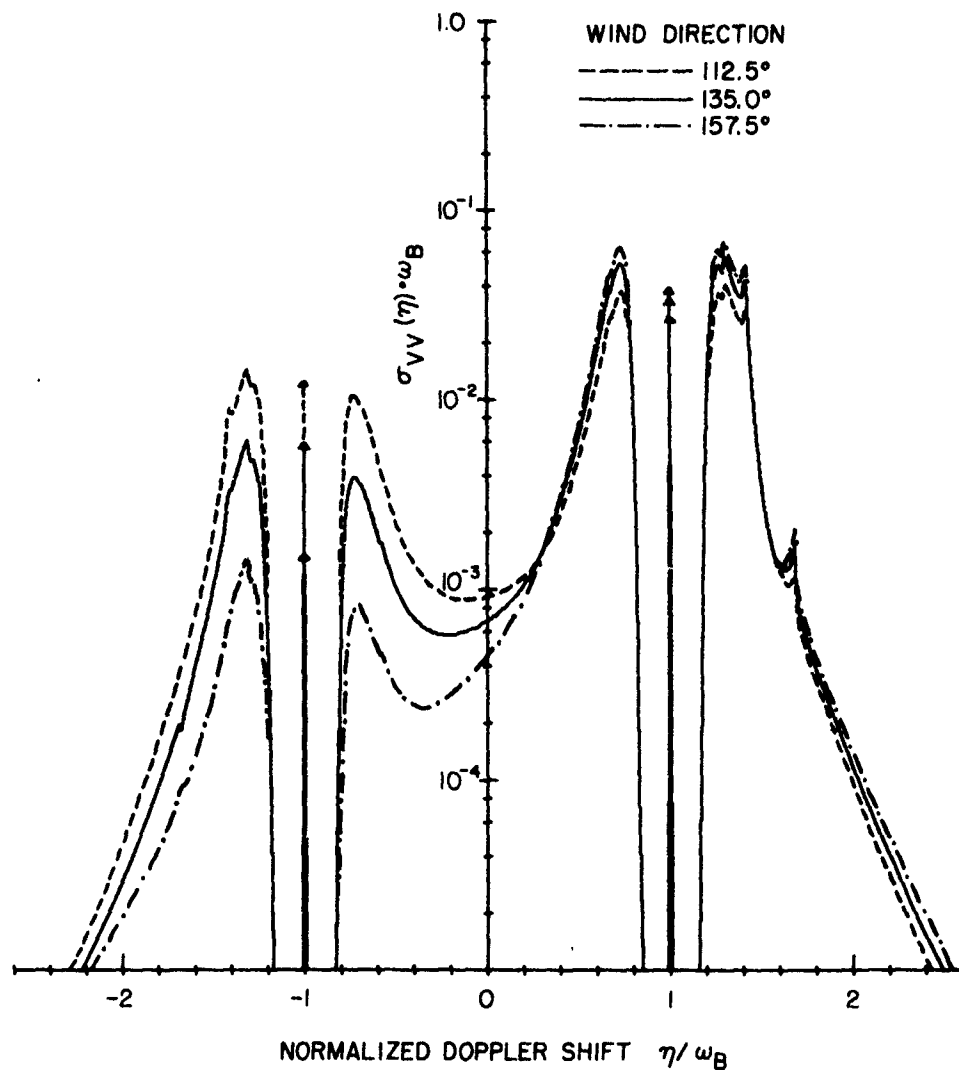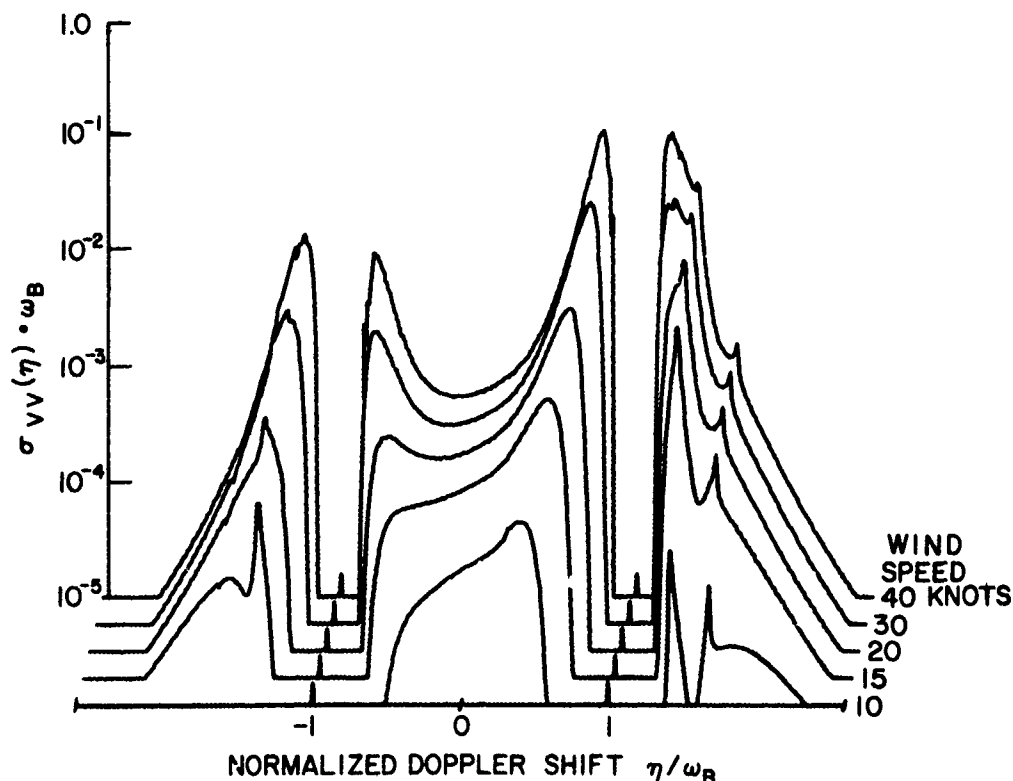
171

Fig. 57. VARIATIONS IN RADAR CROSS SECTION WITH WIND DIRECTION.
A Pierson-Moskowitz cosine-squared wave-height spectrum at wind
speed = 30 knots assumed. Radar frequency = 10 MHz.

shifts become smaller. A similar trend toward negative η occurs when the direction shifts to downwind. Both first- and second-order contributions to $\sigma_{VV}(\eta)$ exhibit this wind-direction dependence, suggesting that either could be used to determine wind direction from radar measurements. This possibility is discussed in the next section.

Variations of $\sigma_{VV}(\eta)$ with wind speed are plotted in Fig. 58, where the first-order Bragg lines have been suppressed for clarity. An increase in wind speed has little effect on ocean waves that are already saturated; however, as wind speed increases, the unsaturated lower frequency waves grow in height until equilibrium is reached (Fig. 19 illustrates the equilibrium state or wave-height spectrum for the Pierson-Moskowitz and Phillips models with wind speeds of 20 and 40 knots).

Fig. 58. VARIATIONS IN RADAR CROSS SECTION WITH WIND SPEED. A Pierson-Moskowitz cosine-squared wave-height spectrum with wind direction = 135° assumed. The first-order Bragg lines have been suppressed for clarity. Radar frequency = 10 MHz.

Increased wave height appears as an increase in the level of $\sigma_{VV}(\eta)$, whereas the addition of lower frequency waves to the wave-height spectrum causes the near-Bragg-line cutoffs to move closer to the Bragg line. The dependency of $\sigma_{VV}(\eta)$ on wind speed suggests that such speed might also be determined from radar measurements. This possibility is also discussed in the next section.

Second-order electromagnetic and hydrodynamic effects have been included in the calculations of $\sigma_{VV}(\eta)$, and Fig. 59 shows the contribution of each to the total incremental radar cross section. The hydrodynamic term Γ_H dominates, whereas the electromagnetic term Γ_{EM} influences $\sigma_{VV}(\eta)$ at $\eta = 2^{3/4} \omega_B$ and in the region near zero doppler shift. The singularity in Γ_H at $\eta = \omega_B$ causes the rather large values in $\sigma_{VV}(\eta)$ as η approaches the Bragg line. The spike at $\eta = \sqrt{2} \, \omega_B$ occurs in both Γ_{EM} and Γ_H contributions and is a result of the Bragg condition when $n = 2$ (Section C.4.b provided further details concerning this spike). The barely discernible discontinuity appearing at $\eta = -2^{3/4} \omega_B$ is a consequence of numerically evaluating (4.21) for wave-height spectra with zero amplitude for waves traveling directly against the wind. This discontinuity vanishes for finite wave amplitudes (Fig. 55, $\epsilon = 0.05$).

In Section C.1, alternate methods were suggested for combining Γ_{EM} and Γ_H in expression (4.21). There was also some controversy concerning the relative weighting of the two terms. Calculations presented here have been based on the form

$$2 \left| \Gamma_{EM} \right|^2 + 8 \left| \Gamma_H \right|^2$$

An alternate form [Barrick, 1971] suggests that fields scattered by second-order ocean waves are correlated with second-order fields scattered by first-order ocean waves and is given by

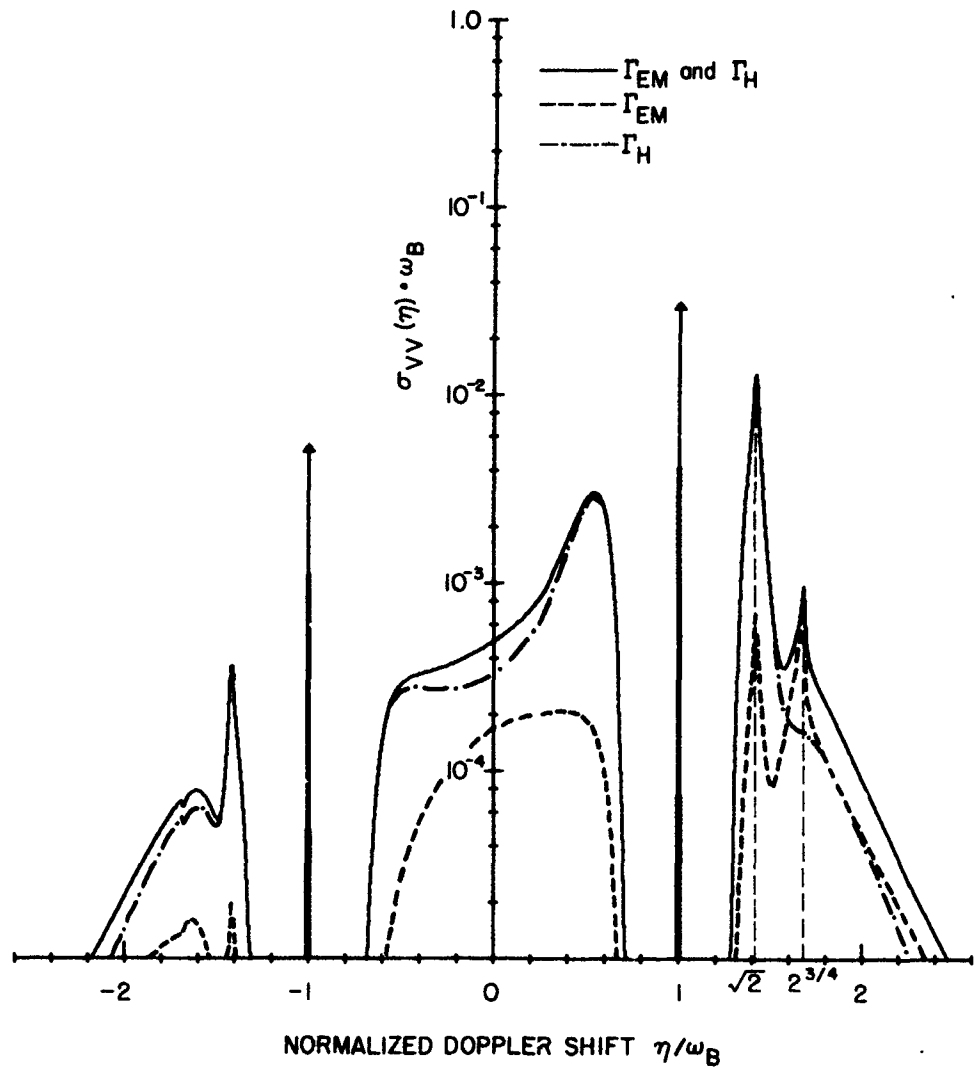$$4 \left| \Gamma_{EM} - i\Gamma_H \right|^2$$

174

Fig. 59. ELECTROMAGNETIC AND HYDRODYNAMIC CONTRIBUTIONS TO RADAR
CROSS SECTION. Equation (4.21) has been evaluated for integrand
kernels of $2\Gamma_{EM}^2 + 8\Gamma_H^2$, $2\Gamma_{EM}^2$, and $8\Gamma_H^2$. A Pierson-Moskowitz
cosine-squared wave-height spectrum with wind speed = 15 knots
and direction ≈ 135° assumed. Radar frequency = 10 MHz.

A third form results when the weighting of the first form is combined
with the coherent addition of the second,

$$|\sqrt{2}\,\Gamma_{EM} - i\sqrt{8}\,\Gamma_H|^2$$

175

Values of $\sigma_{VV}(\eta)$ based on each form are presented in Fig. 60. The difference between coherent and incoherent addition is significant only for $\eta > 2^{3/4} \omega_B$ (the sum-mode evanescent region) because, for freely propagating intermediate radio waves, Γ_{EM} is real if the surface impedance is neglected and the first and third forms are the same. Differences in the relative weighting of Γ_{EM} and Γ_H appear as differences in the magnitude of $\sigma_{VV}(\eta)$. Overall agreement among the three forms will make
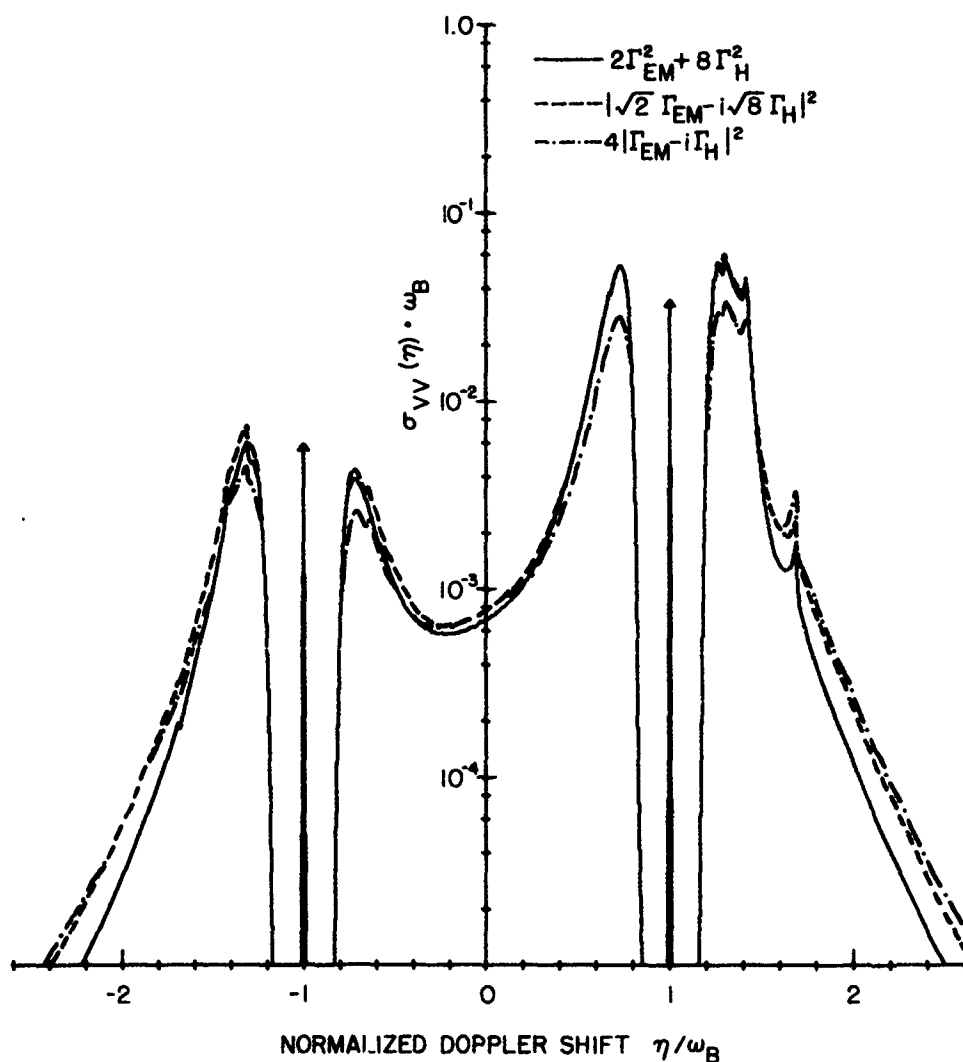
Fig. 60. RADAR CROSS SECTION FOR THREE METHODS FOR COMBINING ELECTROMAGNETIC AND HYDRODYNAMIC EFFECTS. A Pierson-Moskowitz cosine-squared wave-height spectrum with wind speed = 30 knots and direction = 135° assumed.

176

difficult a selection based on comparisons of theoretical to measured
values of $\sigma_{VV}(\eta)$.

Normalization of $\sigma_{VV}(\eta)$ and η by the Bragg frequency ω_B
allows a family of $\sigma_{VV}(\eta)$ curves to be represented by a single plot.
It is not difficult to show that values of $\sigma_{VV}(\eta/\omega_B) \cdot \omega_B$ are constant
for all wind speeds u and radar frequencies f, such that fu^2 is
constant (fu_*^2 for the Munk spectrum). The contours of fu^2 and fu_*^2
(Fig. 61) can be used to relate the curves of $\sigma_{VV}(\eta)$ presented here
and in Appendix C to various conditions of wind speed and radar frequency.

3. Estimators for Wind Speed and Direction

Plots of $\sigma_{VV}(\eta)$ in the above section varied with wind speed
and direction, suggesting that wind conditions might be obtained from
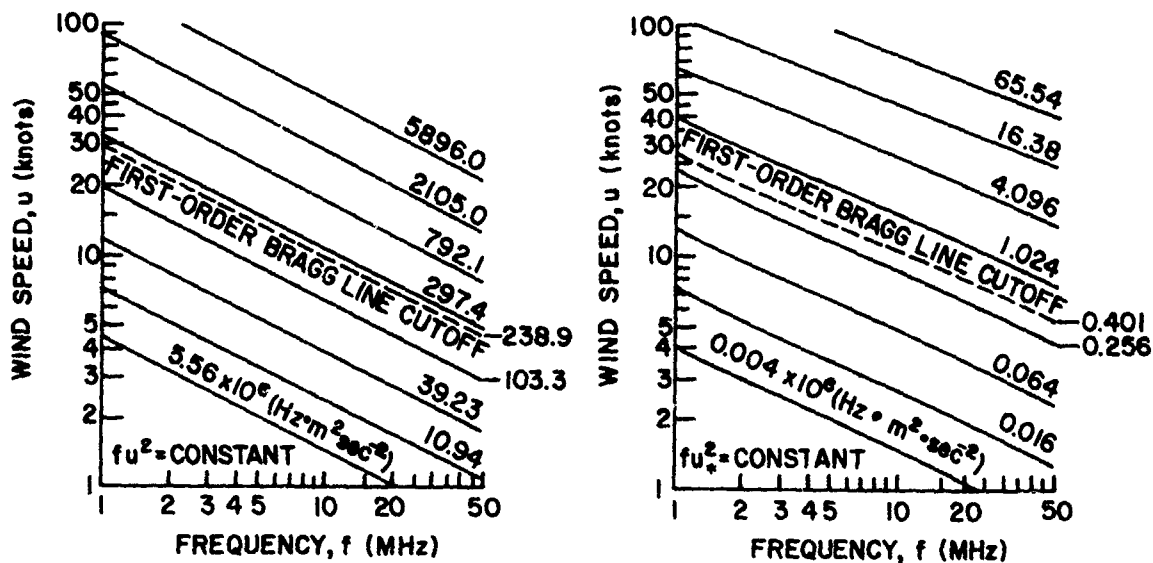
a. Phillips and Pierson-Moskow-   b. Munk spectrum
     itz spectra

Fig. 61. PARAMETERIZATION OF RADAR CROSS SECTION. A single plot of
    normalized radar cross section $\sigma(\eta) \cdot \omega_B$ vs normalized doppler shift
    η/ω_B describes all cross sections, such that fu^2 (fu_*^2 for the Munk
    spectrum) is a constant. Cross sections described by contours below
    the cutoffs contain no first-order Bragg lines. For the Munk spectrum,
    wind speed u is assumed at a height of 6.4 m.

177

radar measurements. In this section, various parameters derived from $\sigma_{vv}(\eta)$ are examined to determine which, if any, are suitable for predicting these conditions.

As a starting point, consider the ratio of positive-to-negative Bragg-line power as a function of wind direction (Fig. 62). This ratio is independent of wind speed[†] for the Pierson-Moskowitz amplitude spectrum with a $\cos^2(\Theta/2)$ directional dependence. For the Munk spectrum, however, it is a function of both wind direction and speed because, although the first-order Bragg-scattering waves are saturated, the spread factor s, which determines the directional dependence of this spectrum, is a function of wind speed [Eq. (3.50)].

Estimation of wind direction for the spectrum in Fig. 62a is straightforward because each Bragg-line ratio corresponds to a unique

a. Pierson-Moskowitz spectrum--
$\cos^2(\Theta/2)$ directional dependence

b. Munk spectrum
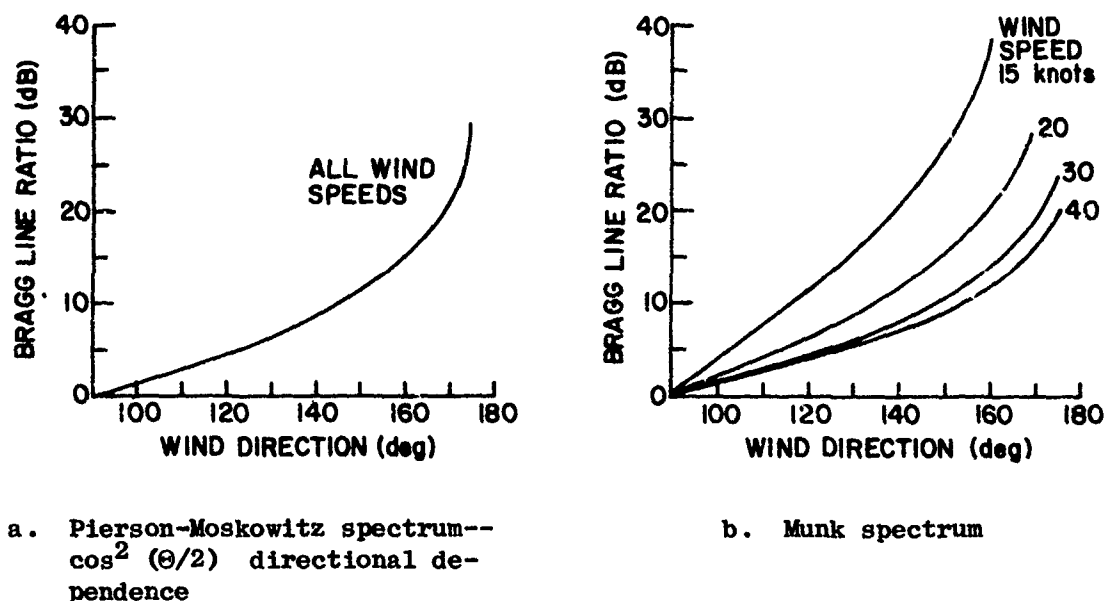
Fig. 62. BRAGG-LINE RATIO VS WIND SPEED AND DIRECTION.

[†]Waves responsible for first-order Bragg scatter are saturated for wind speeds greater than ≈ 9.5 knots when the radar frequency is 10 MHz. Only wind speeds of 10 knots or greater are considered here.

direction;[†] however, if the Munk spectrum provides a better model for
ocean-wave height, wind speed must be known so as to obtain wind direc-
tion from the Bragg-line ratios. A plot of these ratios for the Phil-
lips semi-isotropic spectrum has been omitted because both positive and
negative Bragg lines do not exist simultaneously and the amplitude of
the existing line is independent of wind direction and speed.

A possible parameter for estimating wind direction from sec-
ond-order incremental radar cross sections is illustrated in Fig. 63,
where the ratio of power with positive doppler shift to that with nega-
tive shift

$$\frac{\int_0^\infty \sigma_{VV}^{(2)}(\eta)\, d\eta}{\int_{-\infty}^0 \sigma_{VV}^{(2)}(\eta)\, d\eta}$$

is plotted as a function of wind direction. For both spectra, this ra-
tio is a function of wind speed and direction; therefore, an estimate of
wind direction requires knowledge of wind speed. This ratio is finite,
however, for all wind directions including up- and downwind—an advan-
tage over the Bragg-line ratio when only a single radar-pointing direc-
tion is available. In addition, Bragg-line power is scattered by ocean
waves of a single frequency that may not be indicative of the overall
wind-generated surface spectrum at any given time; conversely, second-
order power is derived from the entire surface-height spectrum and is
less susceptible to single-frequency anomalies.

Comparison of the plots in Fig. 63 indicates that the second-
order power ratio increases with wind speed near upwind conditions for
the Pierson-Moskowitz $\cos^2 (\Theta/2)$ spectrum but decreases for the Munk
spectrum (the same is true of the power-ratio magnitude for downwind
conditions). Such dependence of received power on a spectral model il-
lustrates the requirement for an accurate description of directional

---

[†] A mirror-image ambiguity exists about the radar line and can be r. solved
by using more than one radar-pointing direction.
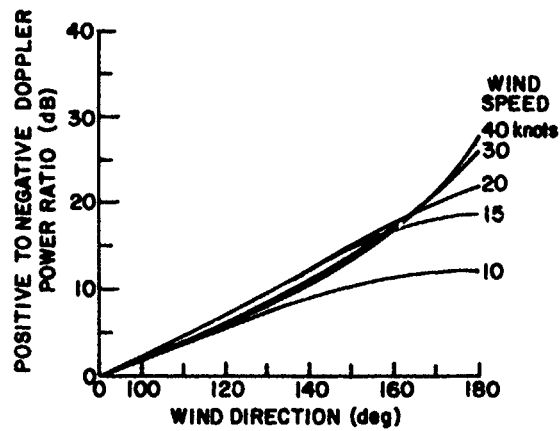
a. Pierson-Moskowitz spectrum--
   $\cos^2 (\Theta/2)$ directional depen-
   dence
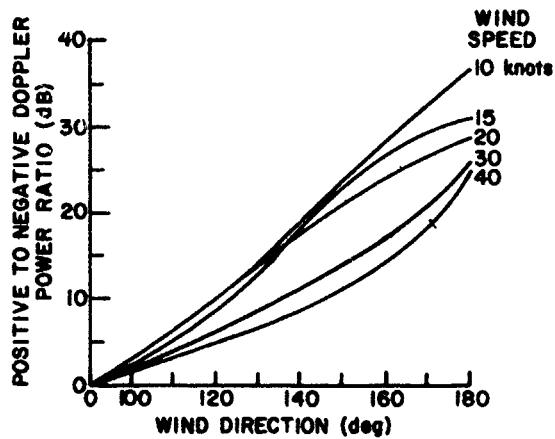
b. Munk spectrum

Fig. 63. POSITIVE-TO-NEGATIVE DOP-
PLER-SHIFTED POWER RATIO VS WIND
SPEED AND DIRECTION.

wave-height spectra before wind direction can be estimated from second-order power ratios; it also provides a means for selecting or eliminating proposed models and indicates which measurements are significant for this purpose.

A possible method for wind-speed estimation considers total second-order power compared to total Bragg-line power,

$$\frac{\int_{-\infty}^{\infty} \sigma_{VV}^{(2)}(\eta) \, d\eta}{\int_{-\infty}^{\infty} \sigma_{VV}^{(1)}(\eta) \, d\eta} \tag{4.37}$$

Ratios are used because absolute power measurements are difficult to obtain. Total Bragg-line power is nearly invariant with changes of wind speed and direction (see Appendix B) as long as ocean waves of frequency ω_B remain saturated and, therefore, provides a convenient reference for second-order power. Figure 64 presents (4.37) as a function of wind speed and direction for the Phillips semi-isotropic, Munk, and Pierson-Moskowitz $\cos^2(\Theta/2)$ spectra.

Second-order power exhibits some wind-direction dependence for each spectrum; however, variations with wind speed are large enough to be able to estimate wind speed, in most cases, without knowledge of direction. If an omnidirectional radar antenna is employed, received power is independent of wind direction and wind speed can be estimated from the average values shown.

The above ratios are only examples based on model wave-height spectra. The performance of these methods depends on how well the models describe actual first-order ocean surfaces. The examples can be extended to radar frequencies other than 10 MHz with the aid of the graphs in Fig. 61.
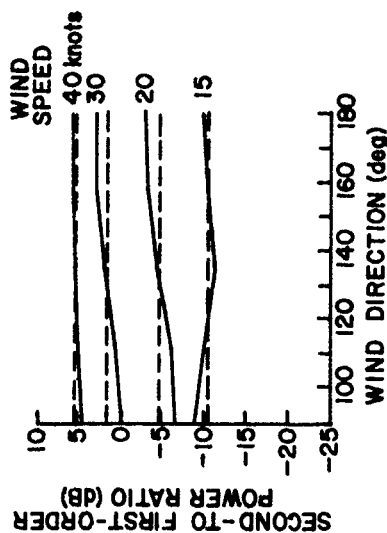
4.   Effects of Swell

Rather sharp spikes occur at discrete doppler frequencies in plots of $\sigma_{VV}(\eta)$ vs η when Eq. (4.21) is evaluated, with the model of ocean-wave swell (Chapter III.D) included. Figure 65 is an example in

181

Fig. 64. VARIATION OF SECOND-ORDER TO BRAGG-LINE POWER RATIO WITH WIND SPEED AND DIRECTION. Dashed lines represent averages over all wind directions. Radar frequency = 10 MHz.
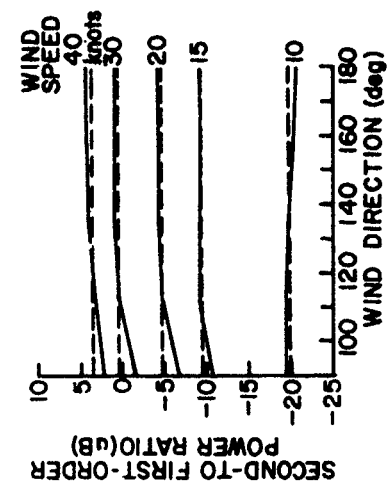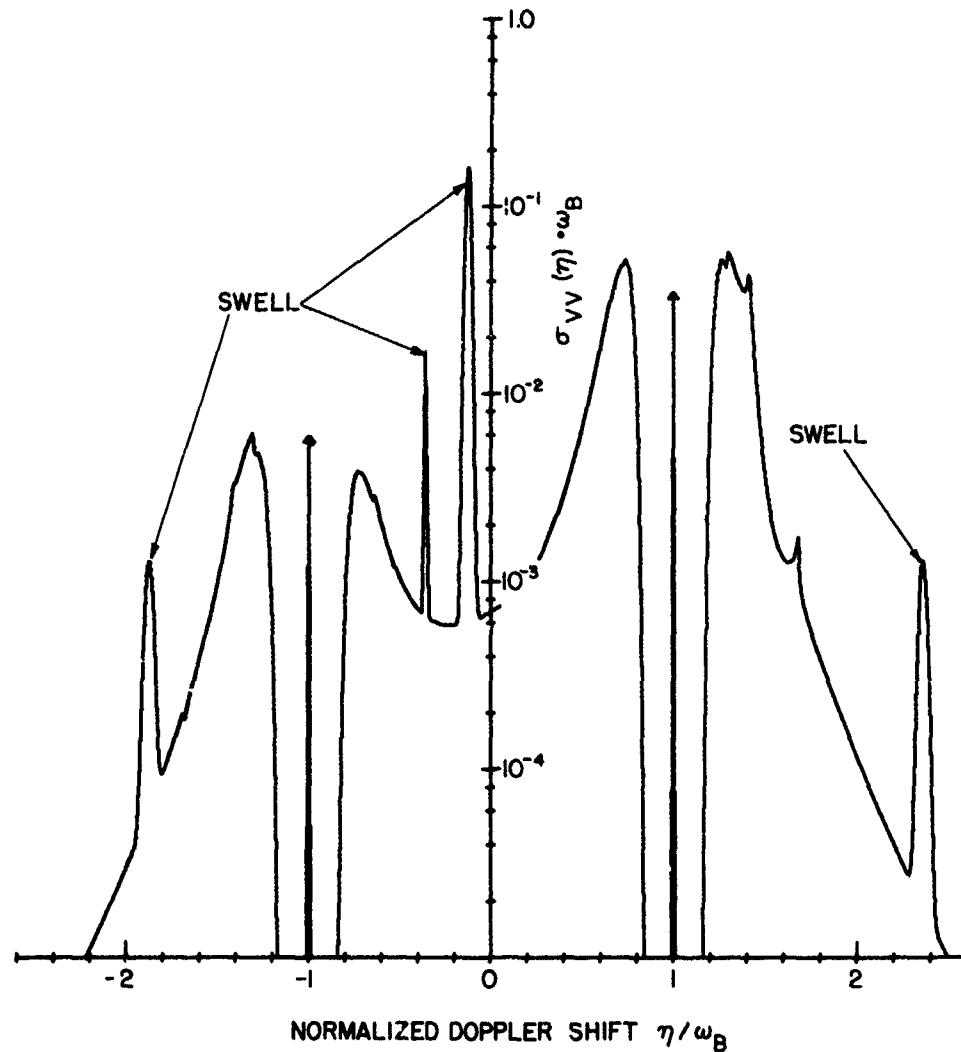
a. Phillips semi-isotropic
    spectrum
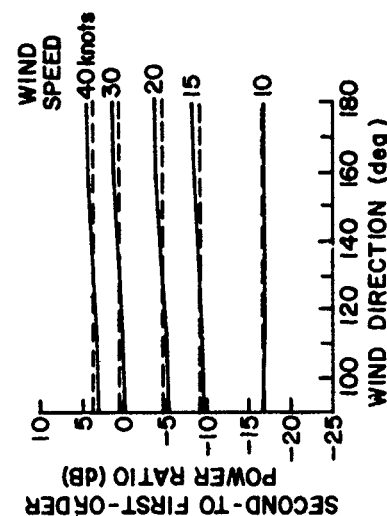
b. Pierson-Moskowitz $\cos^2 (\Theta/2)$
    spectrum

c. Munk spectrum

182

Fig. 65. RADAR CROSS SECTION WITH SWELL. The four sharp spikes
are the result of swell at a frequency ω_B and a direction of
45° (Fig. 53) interacting with local seas represented by a
Pierson-Moskowitz cosine-squared wave-height spectrum. Wind =
30 knots at 135°.

which the Pierson-Moskowitz $\cos^2 (\Theta/2)$ model represents the local wind-
generated portion of the first-order spectrum. Generally, four swell-in-
duced spikes exist at doppler frequencies that are related to the direction
of arrival and frequency of the swell; however, under special conditions,
a fifth spike may occur at $\eta = \sqrt{2}\, \omega_B$. Power contained in these spikes
is a function of swell wave height as well as speed and direction of the
local winds.

183

The relationship between swell and the resultant spikes in $\sigma_{VV}(\eta)$ can be determined by considering the spectral term $W(k_{1x},k_{1y}) \times W(k_{2x},k_{2y})$ in (4.21) with swell included,

$$W(k_{1x},k_{1y})\, W(k_{2x},k_{2y}) = \left[W_w(p - \beta, q) + W_s(p - \beta, q) \right]$$
$$\cdot \left[W_w(-p - \beta, -q) + W_s(-p - \beta, -q) \right] \quad (4.38)$$

where the subscripts w and s refer to the local wind-generated wave-height directional spectrum and the swell spectrum, respectively. The term $W_w(p - \beta, q)\, W_w(-p - \beta, -q)$ represents previously considered ocean surfaces in the absence of swell, whereas terms involving the swell spectrum represent new contributions to $\sigma_{VV}(\eta)$ and are the origin of the spikes in Fig. 65.

When arguments $-k_x$ and $-k_y$ are allowed in the spectra of (4.38), the following four possible combinations of swell and wind-generated spectra interactions exist:[†]

$$W_w(-p - \beta, -q) \cdot W_s(p - \beta, q)$$

$$W_w(-p - \beta, -q) \cdot W_s(-p + \beta, -q)$$

$$W_w(p + \beta, q) \cdot W_s(p - \beta, q) \qquad (4.39)$$

$$W_w(p + \beta, q) \cdot W_s(-p + \beta, -q)$$

From Section C.5, these combinations represent doppler shifts,

$$\eta = \omega_w + \omega_s \qquad \text{positive sum mode}$$
$$\qquad\qquad\qquad\qquad\qquad (4.40)$$
$$\eta = \omega_w - \omega_s \qquad \text{difference mode}$$

[†]An interchange of subscripts provides four additional combinations, but these create no new doppler frequencies.

$$\eta = -\omega_w + \omega_s \qquad \text{difference mode}$$

$$\eta = -\omega_w - \omega_s \qquad \text{negative sum mode}$$

<div align="right">(4.40)
Cont.</div>

The first term in (4.39) specifies that swell propagation components k_{sx} and k_{sy} (Fig. 66) must be related to the intermediate scattered radio-wave propagation components p and q, by

$$k_{sx} = p - \beta$$

$$k_{sy} = q$$

therefore,

$$k_{wx} = -k_{sx} - 2\beta$$

$$k_{wy} = -k_{sy}$$

Similar expressions relating the components of k_w to those of k_s exist for the remaining terms in (4.39). The doppler shifts in (4.40) now become

$$\eta = \sqrt{g\left[(k_{sx} + 2\beta)^2 + k_{sy}^2\right]^{1/2}} + \sqrt{gk_s}$$

$$\eta = \sqrt{g\left[(k_{sx} - 2\beta)^2 + k_{sy}^2\right]^{1/2}} - \sqrt{gk_s}$$

<div align="right">(4.41)</div>

$$\eta = -\sqrt{g\left[(k_{sx} + 2\beta)^2 + k_{sy}^2\right]^{1/2}} + \sqrt{gk_s}$$

$$\eta = -\sqrt{g\left[(k_{sx} - 2\beta)^2 + k_{sy}^2\right]^{1/2}} - \sqrt{gk_s}$$

which indicate that wind-driven waves at two frequencies interact with swell waves to produce the spikes in $\sigma_{VV}(\eta)$. These four doppler

<div align="center">185</div>
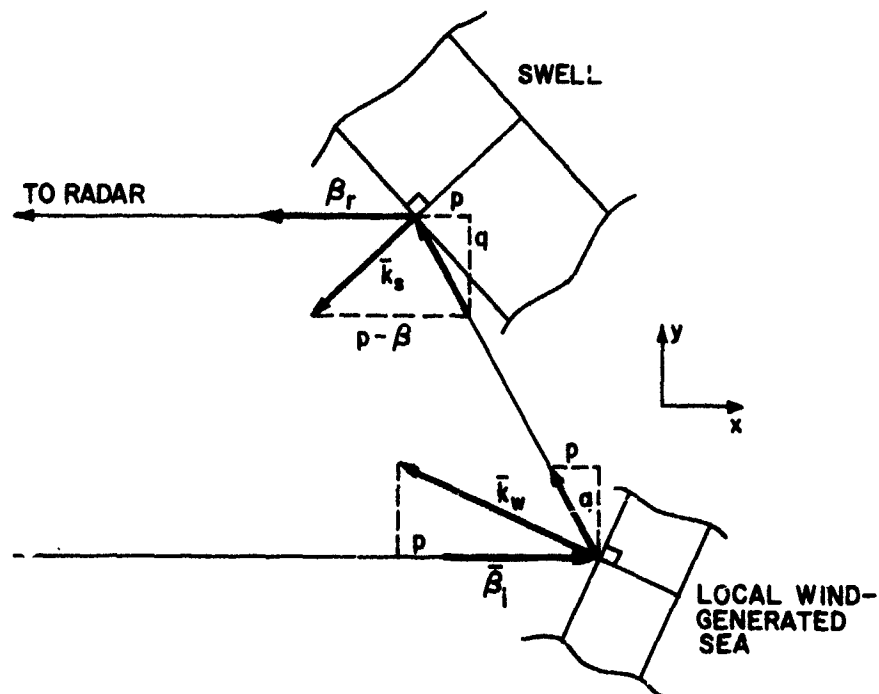
Fig. 66. RELATIONSHIPS BETWEEN RADIO-WAVE, LOCAL-SEA, AND
SWELL PROPAGATION CONSTANTS.

frequencies are a function of the swell frequency $\omega_s = \sqrt{gk_s}$ and the
swell angle of arrival $\theta_s = \tan^{-1}(k_{sy}/k_{sx})$. They also occur in pairs,
symmetric about the frequencies $\pm\sqrt{gk_s}$, thereby indicating a possible
method for determining swell conditions from radar measurements. In the
example in Fig. 65, the doppler frequencies are $\eta = 2.359\,\omega_B$, $-0.125\,\omega_B$,
$-0.359\,\omega_B$, and $-1.875\,\omega_B$ and are symmetric about ω_B (the swell fre-
quency in this example).

All four swell-induced spikes are not always present or observ-
able in plots of $\sigma_{VV}(\eta)$. If swell frequency and angle of arrival are
such that the corresponding wind-driven waves do not exist because of
wind-speed limitations, the spikes are absent in pairs. Swell conditions
may also require corresponding wind-generated waves to propagate against
the wind where the spectra models considered thus far have zero or near-
zero amplitude. In this event, only one spike of a symmetric pair is
affected because the other results from waves propagating with the wind.

186

A possible fifth spike may occur at $\eta = \sqrt{2}\,\omega_B$ but only under restricted conditions. Swell wave-wave interaction represented by $W_s(p - \beta, q)\ W_s(-p - \beta, -q)$ in (4.38) is responsible for this spike. To satisfy simultaneously the conditions

$$k_{sx} = p - \beta$$

$$k_{sx} = -p - \beta$$

requires that $p = 0$ and $k_{sx} = -\beta$; similarly, k_{sy} must be zero. Other conditions obtained by replacing the subscript w with s in (4.39) require that $\beta = 0$ for the difference modes and $k_{sx} = \beta$ and $k_{sy} = 0$ for the negative sum mode; therefore, the fifth spike occurs only when swell propagates directly toward or away from the radar, with propagation constant β ($\omega_s = \sqrt{2}\,\omega_B$). Because swell is generally associated with ocean wavelengths greater than 100 m, radar frequencies below 3 MHz are required before this fifth spike can be expected.

E.   Summary

As a result of calculating $\sigma_{VV}(\eta)$ from the rough-surface model proposed by Rice, radio-wave scattering from the sea has been interpreted as a multiple Bragg process in which pairs of ocean-wave trains are responsible for the scattered electromagnetic fields. Such an interpretation led to the concept of an intermediate scattered radio wave that could be either freely propagating or evanescent and whose Cartesian components of propagation constant were the variables of integration in Eq. (4.17) for $\sigma_{VV}(\eta)$. Subsequent transformation of these variables reduced this expression to a single integral for which contours of integration could be identified and related to particular features in curves of $\sigma_{VV}(\eta)$ vs η through the Bragg-scattering concept. Numerical evaluation of (4.17) provided a doppler continuum that is characteristic of those found in observed sea echo and also revealed the dominance of the second-order hydrodynamic effects in the scattering process. First-order Bragg-line ratios appeared to be the best estimators for wind or wave

direction, whereas total second-order power is the best indicator of wave height and, hence, wind speed; however, such estimators proved to be dependent on the directional wave-height spectral model employed. How well the second-order theory represents actual scattering from the sea is the subject of Chapter V.

Chapter V

COMPARISONS OF THEORETICAL TO EXPERIMENTAL DATA

Arguments based cn the presence of the unsymmetrical sidebands and the $\sqrt{2}\,\omega_B$ and $2^{3/4}\,\omega_B$ spikes in both measured and calculated doppler or sea-echo spectra have been offered in support of the second-order Bragg theory for radio-wave scattering from the sea [Tyler et al, 1972; Barrick, 1972; Barrick et al, 1974; Johnstone and Tyler, 1974]; however, such qualitative comparisons have neither considered the detailed structure of the doppler continuum nor have they been exact with regard to the correlation of radar observations with oceanographic and meteorological data. In this chapter, calculated doppler spectra that conform to observed wind conditions and that account for the finite beamwidth of the receive antenna are compared to grazing-incidence backscatter measurements of echo spectra that have been corroborated by in-situ tilt-buoy observations of wave height and direction. In particular, these spectra are examined for agreement in cutoff frequencies, shape, power content, and occurrence of swell.

A. The Experiment

A series of radar measurements taken at Wake Island on 12-19 November 1972 [Teague et al, 1973; Tyler et al, 1974] provides the observational data for the following comparisons. Using the LORAN-A navigation facilities on the island (Fig. 67) as a transmitting source (1.95 MHz) and a van-mounted receiver to form a synthetic aperture, Teague et al (1973) made extensive radar measurements of sea echo primarily to test the feasibility of deriving ocean-wave directional spectra from first-order Bragg-line measurements. Although doppler shifts induced by the moving receiver obscured higher order radar returns during the synthetic-aperture measurements, daily stationary observations for radar calibration did provide some good examples of second-order scattering. Not all of these observations produced useful data, however, because an attenuator placed between the antenna and the receiver to prevent clipping of the higher level first-order Bragg power scattered within approximately
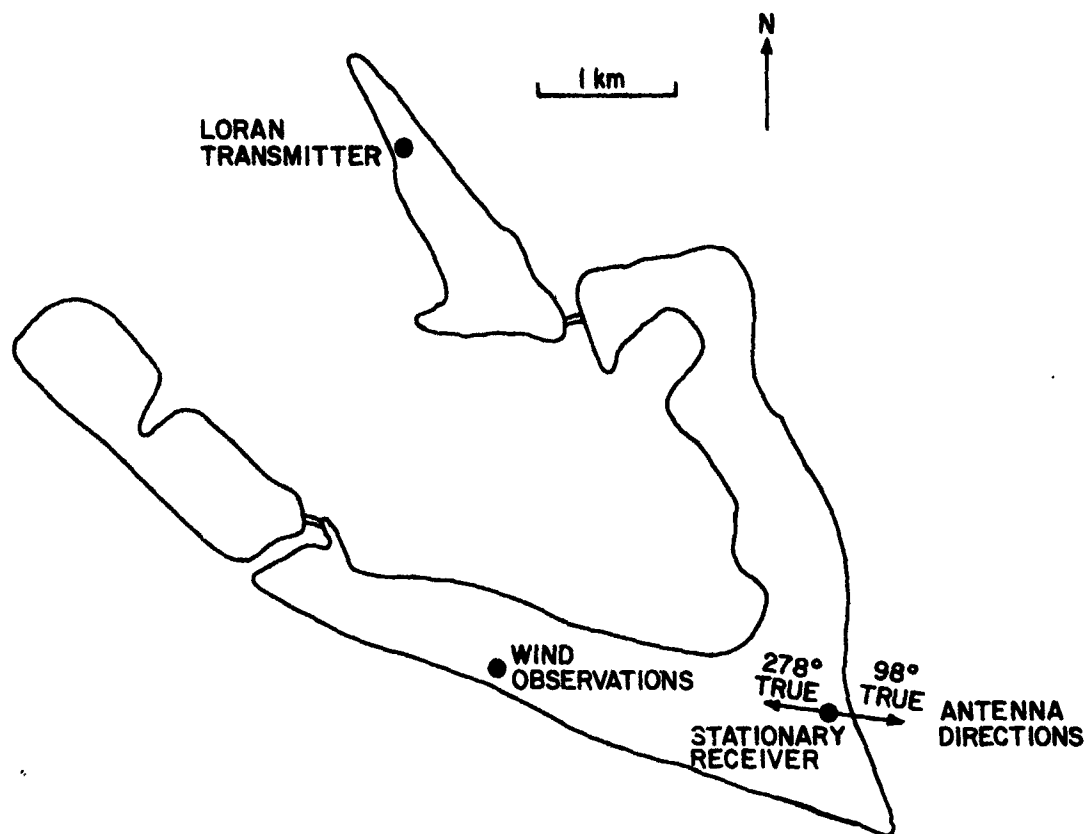
Fig. 67. MAP OF WAKE ISLAND.

20 km of the island reduced most second-order returns to the radar-system noise level. On 17, 18, and 19 November, the attenuator was removed; however, data recorded on the 17th and 18th exhibited the best second-order returns because of the higher winds on these days (Table 2).

Radar echoes were sampled at 25 μs intervals, thereby grouping data in range increments (or bins) of 3.75 km each. Direct pulses from the LORAN-A facility fall in range bin 4, and subsequent range increments determine the distances from the island to the scattering areas. Because switching transients associated with the automatic blanking of the direct pulses appear in the data from the first several bins (Fig. 68a) and

Table 2

WIND SPEED AND DIRECTION DURING THE WAKE-
ISLAND EXPERIMENT. The values represent
averages over the preceding 24 hours.
Winds are from the directions stated.

Date (Nov)	Speed		Direction (degrees true)
	m/s	knots	
12	5.0	9.7	55
13	7.8	15.2	61
14	9.8	19.1	59
15	8.2	15.9	66
16	13.0	25.3	60
17	13.0	25.3	62
18	12.2	23.7	77
19	9.1	17.7	99

because ionospheric reflections[†] (E-layer) contaminate the echoes near zero doppler shift in range bins 26 through 30 (Fig. 68c), only data in bins 15 through 25 will be considered here (Fig. 68b). These curves represent averages over the indicated range increments; however, before averaging, corrections were made for the differences in the distances between the receiver and the scattering areas by multiplying data in each range bin by the cube of the distance from the receiver to the corresponding area. This distance correction results from the assumption of free-space attenuation between the radar and a distributed scatterer [Skolnik, 1962, p. 529].

The LORAN-A antenna provided nominally omnidirectional azimuth coverage, whereas the receive antenna had an almost perfect cardioid (voltage response) radiation pattern in this same plane. The stationary

---

[†] This increase in near-zero doppler-shifted power has been identified as E-layer scattering by C. Teague. Range bin 28, corresponding to a distance of 90 km from the radar, contained most of the contaminated data.

191
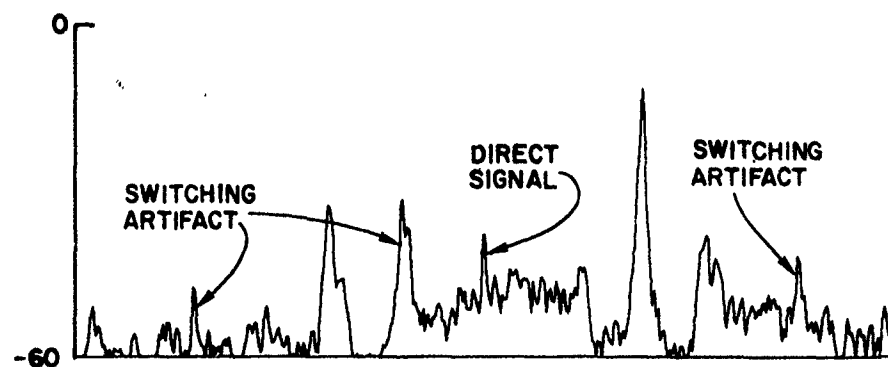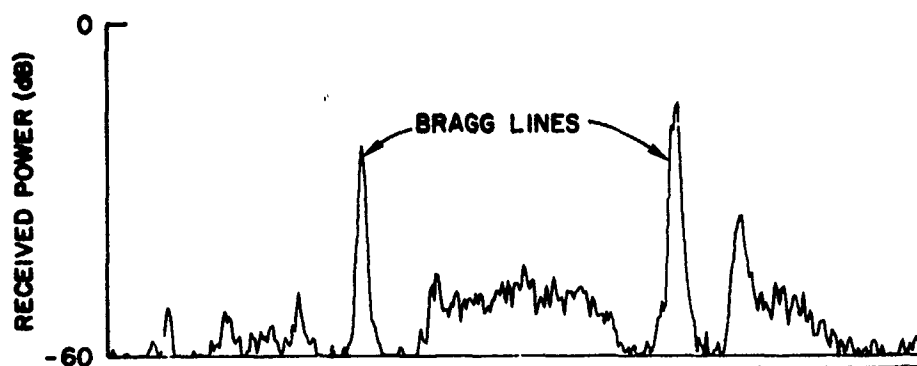
a. Range bins 1-10

b. Range bins 15-25
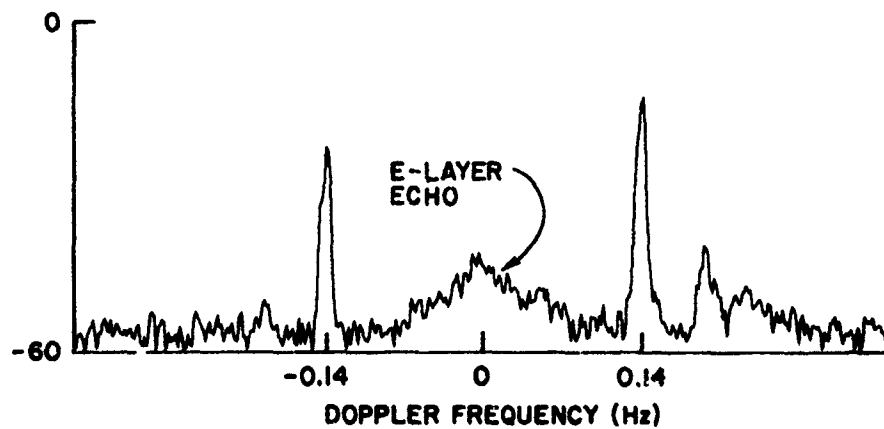
c. Range bins 26-30

Fig. 68. MEASURED DOPPLER SPECTRUM AS A FUNCTION OF DISTANCE
BETWEEN RADAR AND SCATTERING AREA. Echo power is the aver-
age over range bins indicated. Direct signal at 1.95 MHz
occurs in range bin 4. Receive antenna direction is 98°
true; wind speed and direction are 25.3 knots and 62° true.

observations were conducted with the peak of the receive-antenna beam oriented toward 98° true and repeated with the peak at 278° true (Fig. 67).

B. Comparison to Theory

Direct comparisons of power spectra derived from the expressions for incremental radar cross section per unit frequency to the Wake-Island data are inappropriate because of the broad coverage of the receive antenna. A composite of predicted spectra is formed, instead, by calculating unidirectional spectra at 10° increments of the wind direction with respect to the radar backscatter direction, and then summing the results after each has been weighted by the desired antenna response for its particular wind-direction backscatter angle (Fig. 69). Such composites, formed with an assumed cardioid antenna pattern, are to be compared to the measured spectra.

The first comparison is presented in Fig. 70 in which a Phillips semi-isotropic wave-height spectrum at a wind speed of 25 knots has been assumed. The measured spectrum was recorded on 17 November when the average wind speed and direction were 25.3 knots and 62° true (Table 2). Because absolute powers were not measured, the level of the calculated spectrum was adjusted to obtain a least-squares fit to the observed spectrum. This fit was applied to the logarithmic curves so as to provide comparisons at low- and high-power levels. The first-order Bragg lines and the calculated values that fell below 0 dB were not included in this adjustment.

The agreement in this comparison is not satisfying. The predicted cutoff frequencies, where the spectrum drops below 0 dB near the Bragg lines, are too far removed from these lines, and the spikes normally observed at $\pm\sqrt{2}\ \omega_B$ and $\pm 2^{3/4}\ \omega_B$ for higher wind speeds are absent. The only point of agreement appears to be the slight increase of power near zero doppler shift. Comparisons based on the Munk spectrum (Fig. 71) are only slightly better; the $\pm 2^{3/4}\ \omega_B$ spikes are present, but the cutoff frequencies have not changed noticeably and the spikes at $\pm\sqrt{2}\ \omega_B$ are still missing. The ratio of sum- to difference-mode power appears
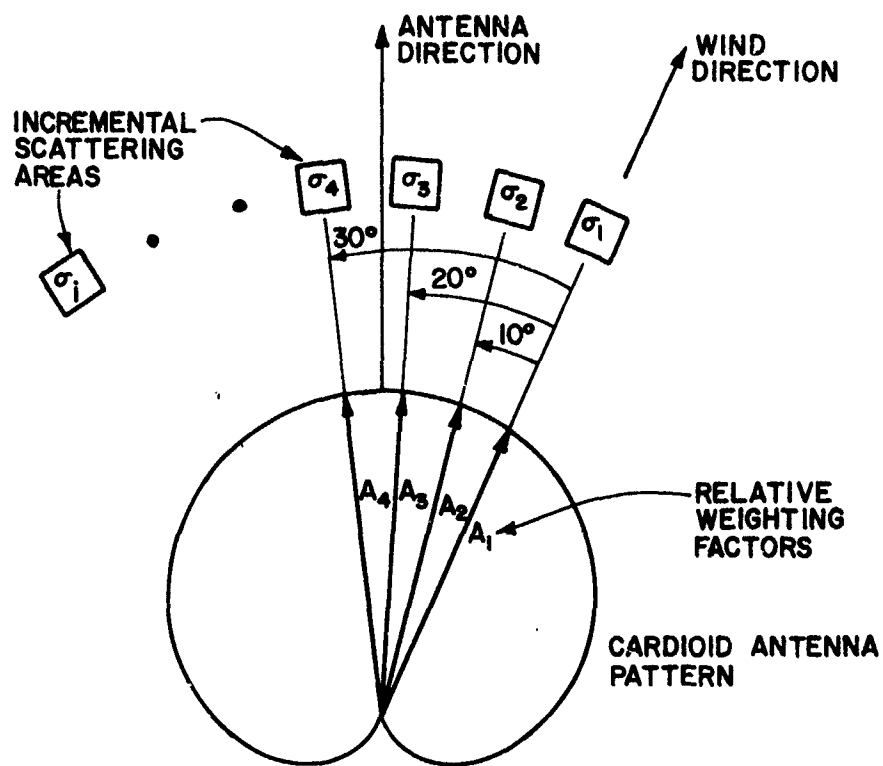
Fig. 69. FORMATION OF A COMPOSITE SPECTRUM. To account
for a finite antenna beamwidth, power backscattered
from different directions with respect to the wind is
weighted by the strength A_i of the antenna response
in the direction of the corresponding scattering area
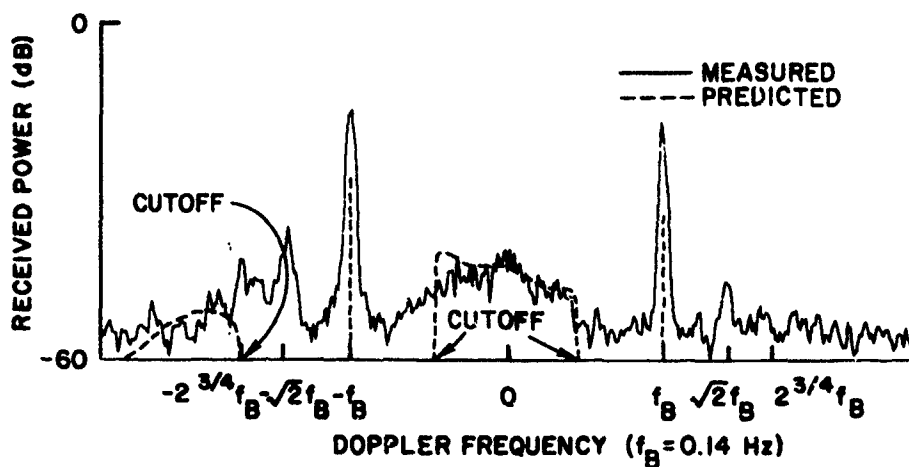and then summed.

Fig. 70. MEASURED VS PREDICTED DOPPLER SPECTRA FOR PHILLIPS
SEMI-ISOTROPIC WAVE-HEIGHT SPECTRUM. Height of the first-
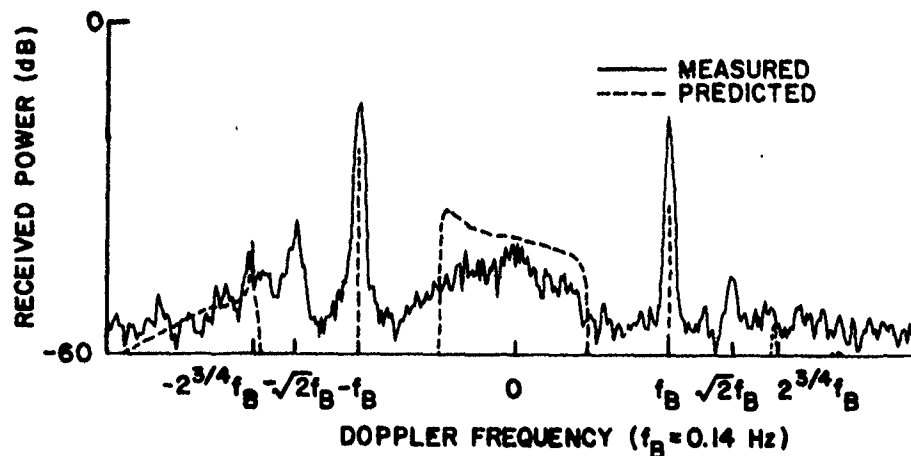order Bragg lines represents power rather than power den-
sity; power-level reference is arbitrary.

Fig. 71. MEASURED VS PREDICTED DOPPLER SPECTRA FOR MUNK WAVE-HEIGHT SPECTRUM. Power-level reference is arbitrary.

to be too low compared to that for the observations, and the near-zero doppler-shift peaking decreased from that predicted by the semi-isotropic spectrum.

The positions of the cutoff frequencies indicate that neither of these wave-height models has a sufficiently low frequency content; however, this is to be expected because they do not allow for the resonant ocean waves that travel faster than the wind. Conversely, nondirectional wave-height spectra measured by a wave-tilt buoy during 13, 15 November contain considerably lower frequencies than would be expected from wind-speed considerations (Fig. 72). To extrapolate a realistic wave-height spectrum for 17 November, the measured spectra were approximated by an analytical curve whose expression is similar to that for the Pierson-Moskowitz spectrum except that the frequency ratio in the exponent has been raised to the second, rather than to the fourth, power (Table 1). Figure 72 illustrates this curve for the wind conditions on 15 November. A comparison of predicted and measured scattered power based on this new wave-height spectrum with an assumed $\cos^2 (\Theta/2)$ direct'onal dependence is plotted in Fig. 73 in which agreement between prediction and observation is seen to have improved slightly over that based on the other models. This new wave-height spectrum appears to have too much low-frequency content, however, and, to resolve this disparity, it has been postulated that changes in wind speed between 15
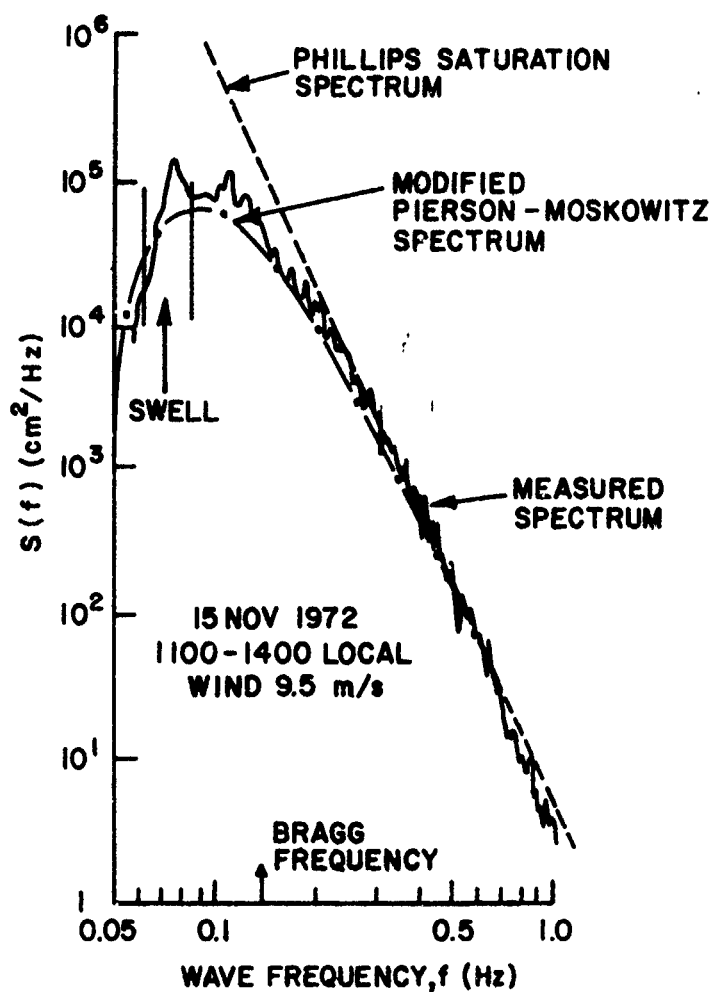
195

Fig. 72. MEASURED NONDIRECTIONAL WAVE-HEIGHT
         SPECTRUM.

and 17 November were sufficiently rapid to prevent the resonant (but not
necessarily the direct wind-driven) waves from reaching equilibrium. If
this is the case, the low-frequency cutoff for the wave-height spectrum
of 17 November would be approximately the same as that for the spectrum
measured on 15 November; therefore, the spectrum of the 17th would have
a sharper low-frequency cutoff than that predicted by the modified Pier-
son-Moskowitz approximation.

A model that exhibits this sharper cutoff and best fits the measured
data is the original Pierson-Moskowitz spectrum which provides the com-
parison illustrated in Fig. 74 when a $\cos^2 (\Theta/2)$ directional dependence

196
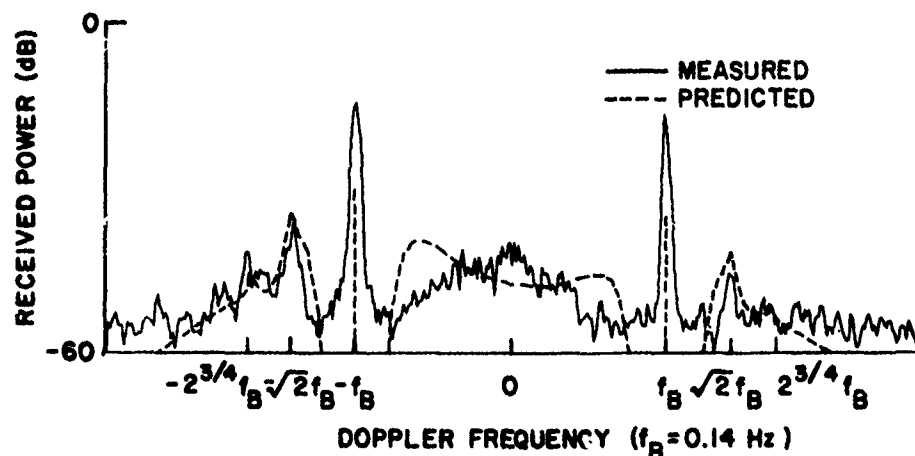
Fig. 73. MEASURED VS PREDICTED DOPPLER SPECTRA FOR MODIFIED
PIERSON-MOSKOWITZ WAVE-HEIGHT SPECTRUM. A cosine-squared
directional distribution has been assumed. Power-level
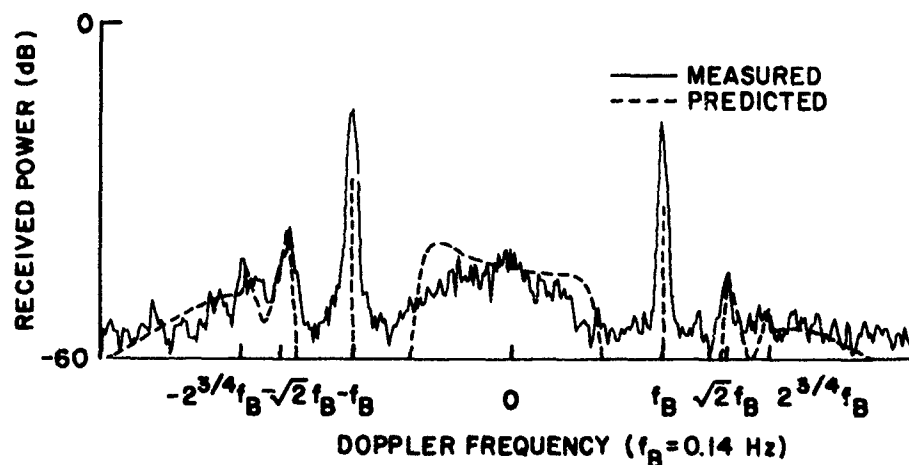reference is arbitrary.

Fig. 74. MEASURED VS PREDICTED DOPPLER SPECTRA FOR PIERSON-
MOSKOWITZ COSINE-SQUARED WAVE-HEIGHT SPECTRUM. Power-level
reference is arbitrary.

is applied. Agreement in the sum-mode sidebands is particularly good;
however, the difference-mode calculations still contain the near-Bragg-
line shoulders observed previously. Substitution of the kernel employed
by Barrick (1971) into the radar cross-section integral (4.21) results
in a slight reduction of these shoulders but at the expense of the sum-
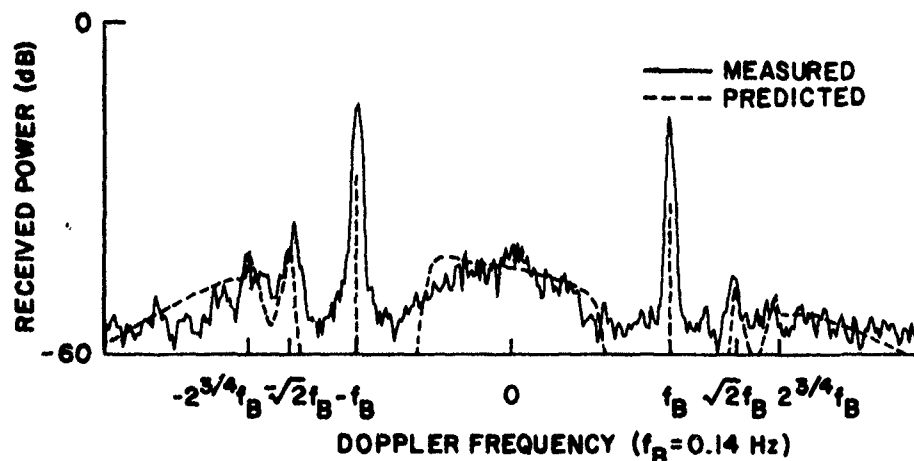mode agreement (Fig. 75). Further comparisons between predicted and

197

Fig. 75. AN ALTERNATE FORM FOR PREDICTED DOPPLER SPECTRA.
Integrand is $4\,|\Gamma_{EM} - i\Gamma_H|^2$ for the cross-section integral
producing this plot. A Pierson-Moskowitz cosine-squared
wave-height spectrum has been assumed. Power-level refer-
ence is arbitrary.

observed power spectra will be required before the differences between
the methods for combining the electromagnetic and hydrodynamic terms in
Eq. (4.21) can be resolved.

As more accurate directional wave-height spectral models become
available, the agreement between measured and predicted radar echoes
will probably improve; however, the original goals were to explain the
continuum observed in these echoes and to provide a theory that would
develop better directional models. Figures 74 and 75 illustrate that
the second-order multiple Bragg-scattering theory explains the doppler
continuum and could provide the means to better models for wave-height
spectra.

To check the quality of the wind-speed estimator introduced in
Chapter IV.D.3, the ratios of second-order power to first-order Bragg-
line power were calculated for both the predicted and observed radar
returns, and these are tabulated for various wave-height spectra in
Table 3; also included are the estimated wind speeds obtained by de-
termining the equivalent wind speeds at a radar frequency of 10 MHz
from the average ratios in Fig. 64 and then extrapolating these values
to 1.95 MHz by means of the contours in Fig. 61. Again, the Pierson-
Moskowitz $\cos^2(\theta/2)$ spectrum provides the best agreement with the

Table 3

WIND-SPEED ESTIMATION

Wave-Height Spectrum	Second- to First-Order Power	Estimated Wind Speed
Phillips Semi-Isotropic	-17.6	24.5 ± 0.5
Munk[†]	-15.9	---
Pierson-Moskowitz $\cos^2 (\Theta/2)$	-15.0	25.5 ± 0.5
Pierson-Moskowitz $\cos^2 (\Theta/2)$ (Barrick's kernel)	-16.3	23.8 ± 0.5[‡]
Approximation to Measured[*]	-11.6	---
Wake-Island Measurements[**]	-14.4	25.3

[†] First-order Bragg lines are below cutoff at 10 MHz (Fig. 61b).

[‡] This value is derived from the ratios in Fig. 61b.

[*] Power ratios as a function of wind speed were not calculated.

[**] These values obtained from data recorded on 17 November with the antenna peak at 278° true.

measured values although all wind-speed estimates are better than the spectra-shape comparisons would appear to justify. Further comparisons to observations at several wind speeds or radar frequencies will be required before the validity of this power ratio as a wind-speed estimator can be established. Because of the broad receive-antenna pattern, wind directions could not be estimated.

The received-power spectrum measured on 18 November with the antenna at 98° true exhibited some peculiar features that are now considered to be swell-induced. The nondirectional wave-height spectrum measured on 15 November (Fig. 72) indicated the presence of swell arriving from 340° true; however, when the frequency and direction of this swell were applied to the model presented in Chapter II.D, the results did not compare favorably to the measured data. It has been speculated that the faster lower frequency waves noted on the 15th had already passed through the scattering region by the 18th and that a higher frequency component was responsible for the observed characteristics. From the doppler frequency

of one of these features, the swell frequency was estimated to be closer to 0.12 than to the 0.07 Hz value measured on the 15th. Figure 76 contains plots of the measured data and a composite power spectrum based on a Pierson-Moskowitz $\cos^2 (\Theta/2)$ model for the local sea, with swell at 0.12 Hz from 340° true superimposed. This comparison cannot be considered a confirmation or a contradiction of the proposed model because the relative amplitudes of the swell components of the received-power spectrum are heavily dependent on the directional form of the local wave-height spectrum and because the actual swell conditions on the 18th are unknown. Figure 76 does indicate, however, that the swell model predicts a doppler-spectrum continuum as well as individual spikes, both of which are found in the measured data. The difference-mode shoulders, the near-zero frequency peaking, and even the outermost somewhat displaced sum-mode swell components tend to verify that swell was observed on the 18th and that the model was able to predict its occurrence, if not its frequency and direction. Particularly noticeable, in view of the comparisons in Figs. 74 and 75, is the near-zero doppler-shift peaking caused by swell. The question as to whether the similar peaking that appeared in other data was the result of swell has yet to be answered; however,
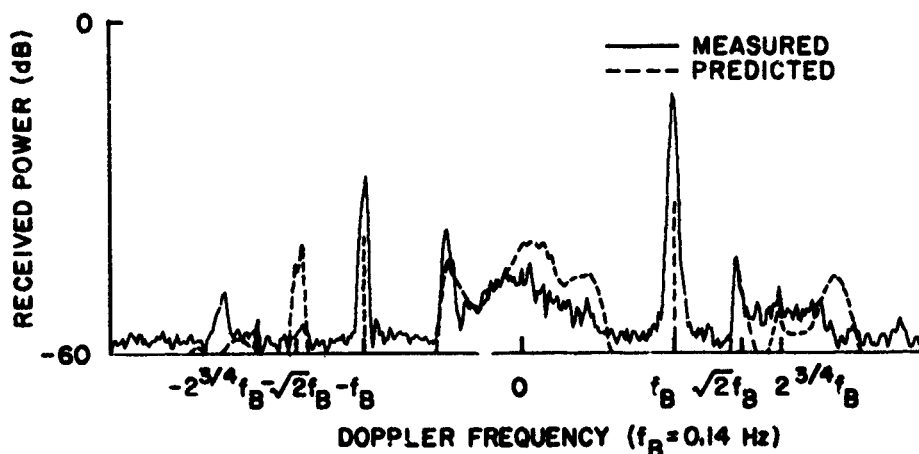

Fig. 76. DOPPLER SPECTRA WITH SWELL INCLUDED. A Pierson-Moskowitz cosine-squared wave-height spectrum has been assumed for the local wind-driven sea; swell for the predicted spectrum is from 340° true at a frequency of 0.12 Hz. Power-level reference is arbitrary.

200

this possibility must be considered if radar measurements of second-order power are to provide accurate first-order directional wave-height spectrum information.

Chapter VI

CONCLUSIONS AND RECOMMENDATIONS

The search for an explanation of the doppler-spectrum continuum observed in radar echoes from the sea led to an integral expression for the bistatic incremental radar cross section per unit frequency of ocean surfaces; electromagnetic and hydrodynamic effects were included to second order. This equation was interpreted as resulting from a double Bragg-scattering process, thereby providing physical insight into many of the prominent features observed in doppler spectra. When reduced to the special geometry for backscatter grazing incidence, this integral was found to agree with previously published results, except for two minor differences that had a negligible effect on calculated radar cross sections but, nevertheless, remain unresolved. To invert the cross-section equation so as to determine first-order wave-height spectra, the method presented for reducing this expression to a single integral without the need to solve for roots in an auxiliary transcendental equation could be of interest. Besides being numerically efficient, this approach provides easily determined finite limits of integration at all doppler frequencies except zero. The effects of swell were included in some of the calculations to determine if the doppler-spectrum features not attributable to local wind-driven seas and second-order theory were actually swell-induced.

Comparisons between predicted and observed doppler spectra revealed that second-order theory accounted for most of the continuum; however, they also indicated a need for more accurate first-order directional wave-height spectral models. Calculations, based on the presence of swell, uncovered characteristics in the doppler spectrum that had not been considered swell-related. For example, the model for swell predicted increased received power levels about zero doppler shift--a characteristic observed not only in the measured data that were expected to contain swell, but in all data examined. This particular feature could explain a major difference between predicted and observed doppler spectra.

Because the second-order expressions for radar cross section are a function of the entire first-order wave-height spectrum, a possible extension of this work would be to consider the inversion of this expression to obtain such first-order spectra from radar measurements. Although a model for swell has been introduced, the interaction of swell with local wave-height spectra and the effects of this interaction on scattered power have not been thoroughly examined. Further radar measurements at several frequencies (or under varied wind conditions), in conjunction with oceanographic observations, are also considered necessary to test completely the validity of the theories presented and to answer some of the questions.

Appendix A

INTEGRATION NEAR SINGULARITIES IN THE JACOBIAN

In Chapter IV.C, a transformation of the integral in Eq. (4.17) from the p,q-plane to the k_1,k_2-plane led to the Jacobian

$$J = \frac{k_1 k_2}{2\beta |q|}$$

which is undefined on the integration-region boundary $q = 0$ in the k_1,k_2-plane (Fig. 37). Subsequent integration of (4.17) over k_2 resulted in

$$\sigma_{VV}^{(2)}(\eta) = \pi\beta^4 \int_0^\infty \left[2\Gamma_{EM}^2(\bar{k}_1, \bar{k}_{20}) + 8\Gamma_H^2(\bar{k}_1, \bar{k}_{20}) \right]$$

$$\cdot \; W(\bar{k}_1) \, W(\bar{k}_2) \sqrt{\frac{k_{20}}{g}} \frac{k_1 k_{20}}{\beta |q|} \, dk_1 \qquad (A.1)$$

Except for the term $|q|^{-1}$, the integrand is well-behaved near $q = 0$; therefore, integration near the singularity becomes

$$\int_{\epsilon_1}^{\epsilon_2} K \, \frac{dk_1}{q}$$

where ϵ_1 and ϵ_2 correspond to $q = 0$, and $q = \delta q$ or $-\delta q$ on either the sum- or difference-mode integration contours (Figs. 40 and 41). The value of q can be made sufficiently small such that $\epsilon_2 - \epsilon_1$ is small and the remainder of the integrand K can be considered constant. From the definition

$$k_1 = \sqrt{(p - \beta)^2 + q^2}$$

it follows that

$$\frac{dk_1}{dq} = \frac{q}{k_1}$$

or

$$\frac{dk_1}{q} = \frac{dq}{k_1}$$

and, therefore,

$$K \int_{\epsilon_1}^{\epsilon_2} \frac{dk_1}{q} = K \int_0^{\delta q} \frac{dq}{\sqrt{(p - \beta)^2 + q^2}}$$

which integrates to

$$K \log \left[q + \sqrt{(p - \beta)^2 + q^2} \right] \Big|_0^{\delta q}$$

Although the integrand in (A.1) is singular at $q = 0$, the integral is not unless $p = \beta$, in which case,

$$k_1 = 0$$

$$k_2 = \sqrt{(p + \beta)^2 + q^2} = 2\beta$$

and

$$\eta = \pm \sqrt{2\beta g} = \pm \omega_B$$

In reality, however, k_1 can never be zero; therefore, no singularity can exist at $q = 0$ and no contribution to second-order radar cross section occurs at the first-order Bragg frequency.

Appendix B

EVALUATION OF FIRST-ORDER σ_{VV}^{O} FOR MONOSTATIC GRAZING INCIDENCE

First-order incremental radar cross section as defined by

$$\sigma_{VV}^{O} = \int_{-\infty}^{\infty} \sigma_{VV}^{(1)}(\eta)\, d\eta$$

represents the power contained in the first-order Bragg lines (see Fig. 42).

For a monostatic grazing-incidence radar geometry (Fig. 3), first-order incremental radar cross section per unit frequency is represented by

$$\sigma_{VV}^{(1)}(\eta) = 16\pi\beta^4\left[w(-2\beta,0)\,\delta(\eta - \omega_B) + w(2\beta,0)\,\delta(\eta + \omega_B)\right] \quad (B.1)$$

where the expanded definition of the ocean-wave propagation constant $\bar{k}$ (Chapter IV.C) has been included to explain negative doppler shifts. Arguments of the spectral terms, $w(k_x, k_y)$ in (B.1), specify that only ocean waves propagating directly toward or away from the radar with propagation constant 2β contribute to first-order Bragg lines (Fig. 77).
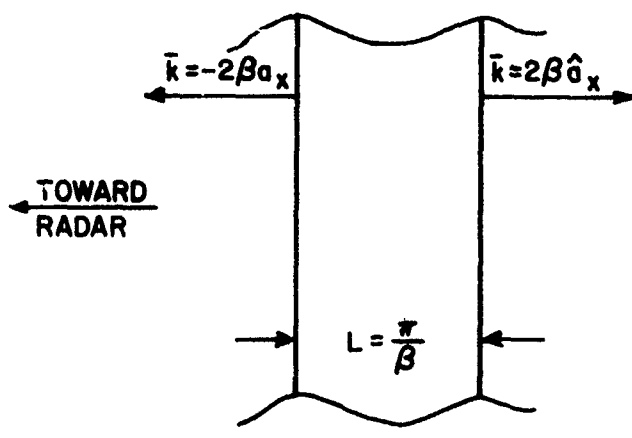
Fig. 77. OCEAN WAVE THAT PRODUCES BRAGG-LINE POWER.

For 10 MHz radar frequency, ocean waves contributing to the Bragg line have a frequency of 2.02 rad/sec. Figure 19 shows that, at this frequency, the Pierson-Moskowitz amplitude spectrum is approximated by the Phillips saturation spectrum for wind speeds greater than 20 knots; calculations of σ_{VV}^{o} (Fig. 78) verifies this approximation for wind speeds greater than 10 knots. For this reason, the Phillips saturation amplitude spectrum is considered an adequate model for sample calculations of σ_{VV}^{o}. From Table 1,

$$w(k_x, k_y) = \frac{2\beta_e}{\pi k^4}$$

where β_e is the equilibrium range constant, $k^2 = k_x^2 + k_y^2$, and the factor of 4 difference between $w(k_x, k_y)$ and $S(k_x, k_y)$ has been included.
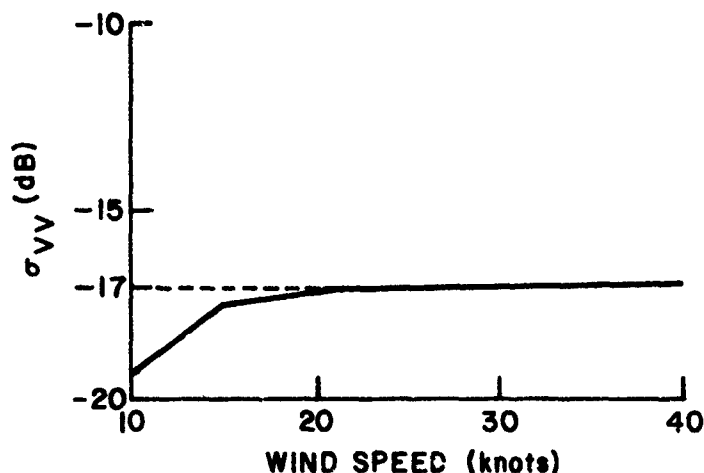
Fig. 78. FIRST-ORDER INCREMENTAL RADAR CROSS SECTION FOR A PIERSON-MOSKOWITZ WAVE-HEIGHT SPECTRUM. This plot represents either semi-isotropic or cosine-squared directional distributions.

Spectra with a semi-isotropic directional dependence (Fig. 20) can cause either positive or negative Bragg lines but not both; therefore,

$$\sigma_{VV}^{(1)}(\eta) = 16\pi\beta^4 \begin{cases} w(-2\beta,0) \; \delta(\eta - \omega_B) \\ w(2\beta,0) \; \delta(\eta + \omega_B) \end{cases}$$

For the Phillips semi-isotropic directional spectrum,

$$\sigma_{VV}^o = 16\pi\beta^4 \left[\frac{2\beta_e}{\pi k^4}\right]_{k=2\beta} = 2\beta_e = 0.02$$

and, for saturated spectra with a $\cos^2(\Theta/2)$ directional dependence (Fig. 21),

$$\sigma_{VV}^o = 16\pi\beta^4 \left[\frac{2\beta_e}{\pi k^4}\right]_{k=2\beta} \left[\cos^2\left(\frac{\Theta}{2}\right) + \cos^2\left(\frac{\Theta + \pi}{2}\right)\right] = 0.02$$

There is some question as to the validity of the value 0.02 (-17 dB) for σ_{VV}^o at grazing incidence. Derivations leading to (B.1) assume an incident field E_i for all angles of incidence. If E_i is assumed for nongrazing incidence, however, then, at grazing incidence, the total incident field above the surface is $2E_i$ and $\sigma_{VV}^o = -23$ dB. Because second-order results are based on the same fields as for first-order calculations, the absolute magnitude of $\sigma_{VV}^o(\eta)$ is affected by the change to $2E_i$ but the ratio of first- to second-order cross sections remains the same. The value of -17 dB is maintained here for consistency with the equations presented; however, the definition of incident field used in their derivation must be kept in mind when comparing theoretical and measured radar cross sections at grazing incidence.

The Phillips spectrum with either a semi-isotropic or $\cos^2(\Theta/2)$ directional dependence yields a single value (-17 dB) for σ_{VV}^o at all wind speeds (above cutoff) and directions, but the Pierson-Moskowitz spectrum yields many values as a function of wind speed (Fig. 78) for the same directional distributions. These values are nearly constant (within 3 dB), however, for wind speeds greater than $\sqrt{g/2\beta}$ (9.41 knots at a radar frequency of 10 MHz).

Values of σ_{VV}^{o} for the Munk spectrum (Fig. 79) vary with wind speed and direction because of the spread factor s. Again, these variations are small for higher wind speeds.
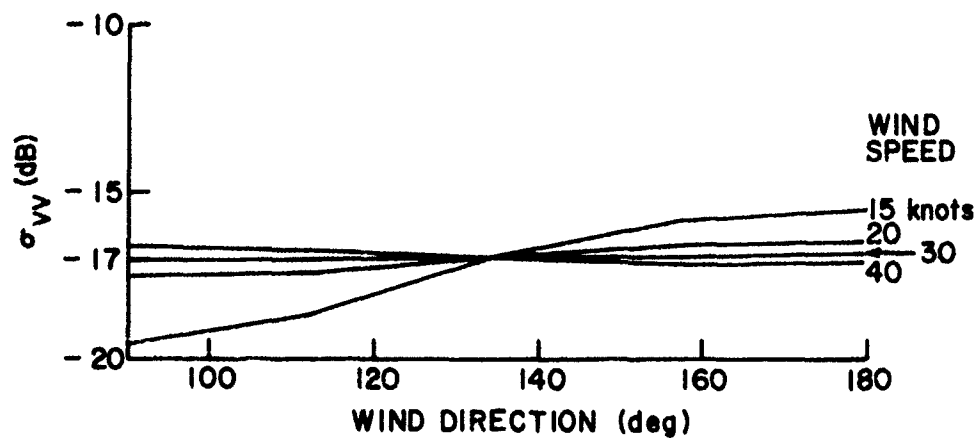

Fig. 79. FIRST-ORDER INCREMENTAL RADAR CROSS SECTION FOR A MUNK WAVE-HEIGHT SPECTRUM. Wind direction is the angle from the radar pointing direction (Fig. 53).

Appendix C

PLOTS OF INCREMENTAL RADAR CROSS SECTION FOR OCEAN SURFACES

A series of plots of $\sigma_{VV}(\eta) \cdot \omega_B$ vs η/ω_B has been generated for the Phillips semi-isotropic, Munk, and Pierson-Moskowitz $\cos^2 (\Theta/2)$ wave-height spectra. These plots were calculated for wind speeds of 40, 30, 20, 15, and 10 knots, and for wind directions (Fig. 80) of $90°$, $112.5°$, $135°$, $157.5°$, and $180°$ (Figs. 81-83). Because of symmetry, plots for the wind directions between $90°$ and $0°$ can be obtained by reversing the positive- and negative-frequency axes; those for wind directions between $0°$ and $-180°$ are the same as for $0°$ to $180°$. The radar frequency is 10 MHz; however, Fig. 61 can be used to determine other frequencies and wind speeds represented by these plots. For the Munk spectrum, $\epsilon = 0$ and the wind speed was assumed at a height of 6.4 m.
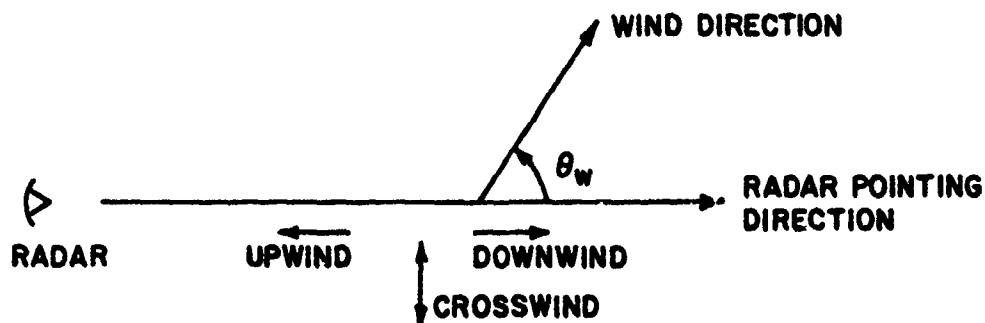
Fig. 80. WIND DIRECTIONS.

The abscissa of each plot is normalized doppler frequency between -2.6 and $+2.6$, and the ordinate is a logarithmic scale extending from 10^{-5} to 0. The height of the Bragg lines represents

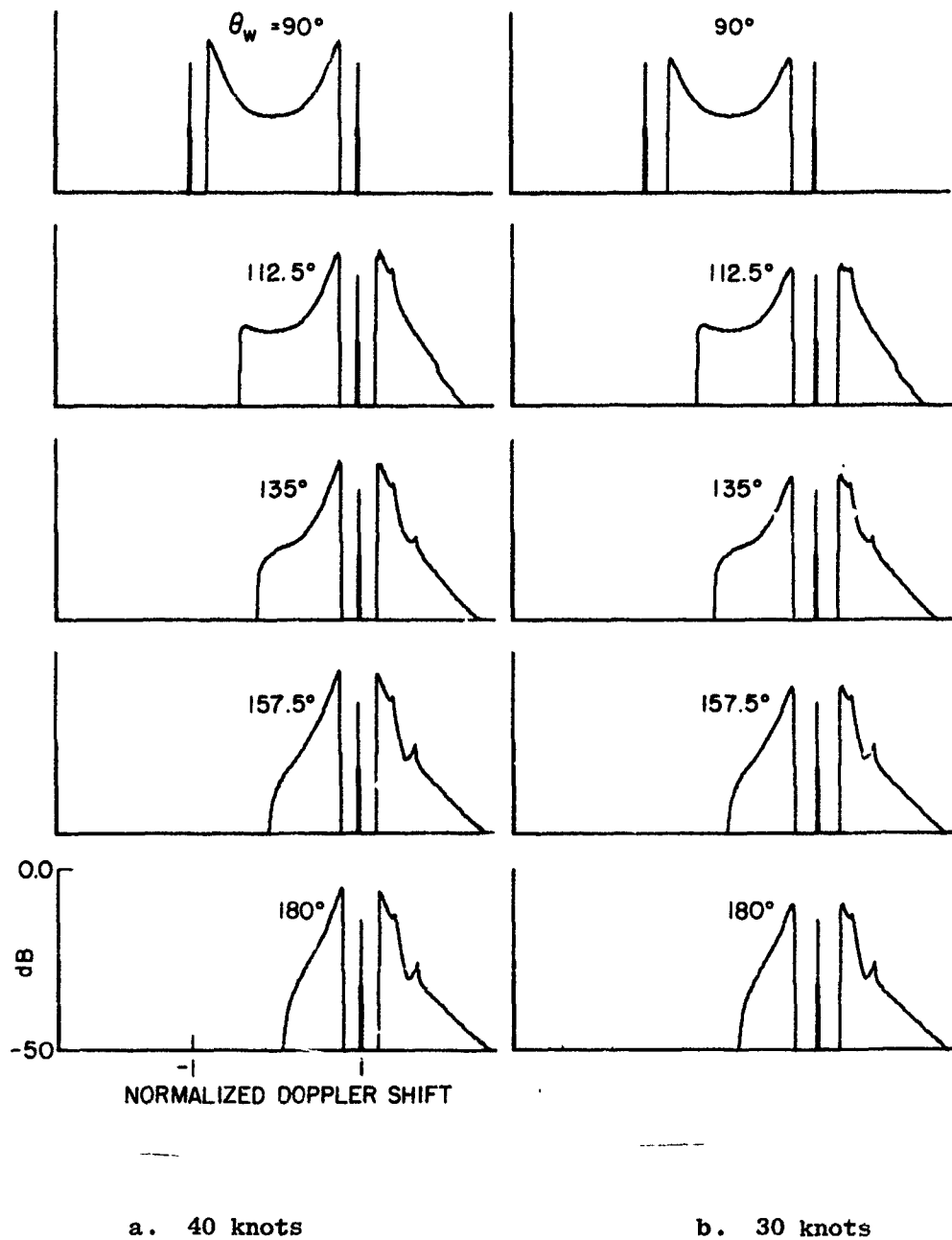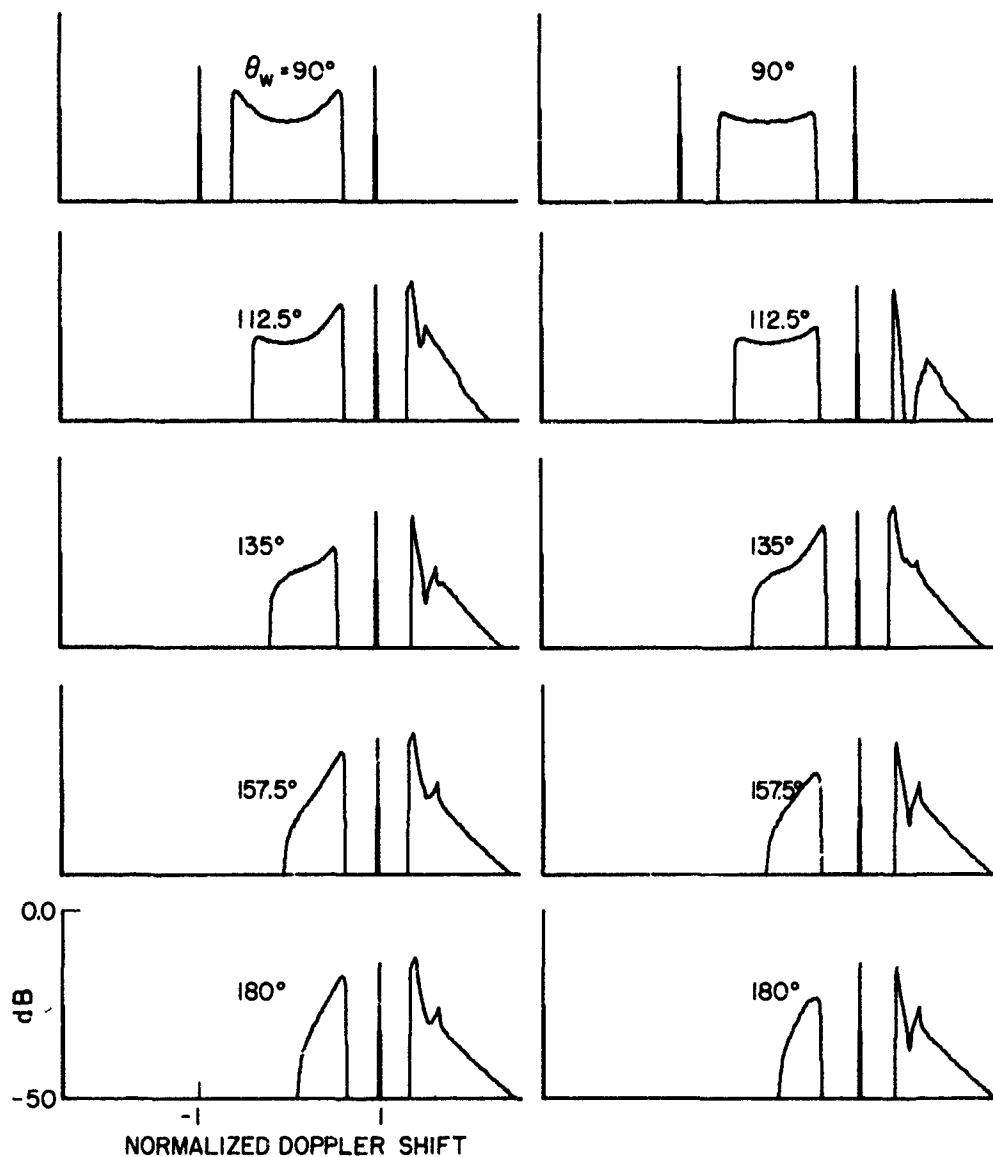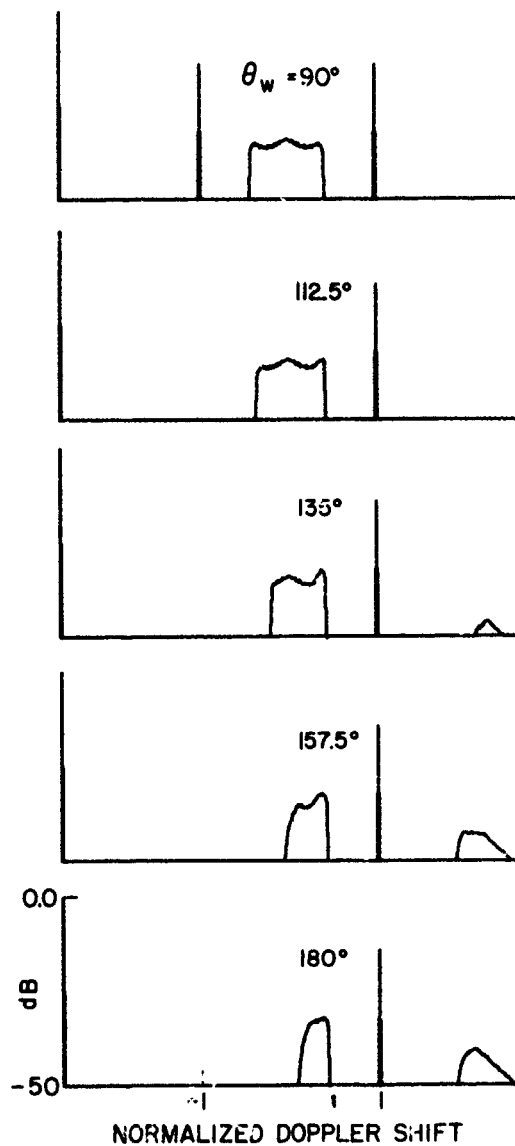$$\sigma_{VV}^{o}\omega_B \approx \omega_B \int_C^\infty \sigma_{VV}(\eta)\ \delta(\eta \pm \omega)\ d\eta$$

211

a. 40 knots   b. 30 knots

Fig. 81. INCREMENTAL RADAR CROSS SECTION FOR PHILLIPS SEMI-ISOTROPIC WAVE-HEIGHT SPECTRUM.

$\theta_w = 90°$

90°

112.5°

112.5°

135°

135°

157.5°

157.5°

0.0

dB

180°

180°

-50

-1   1

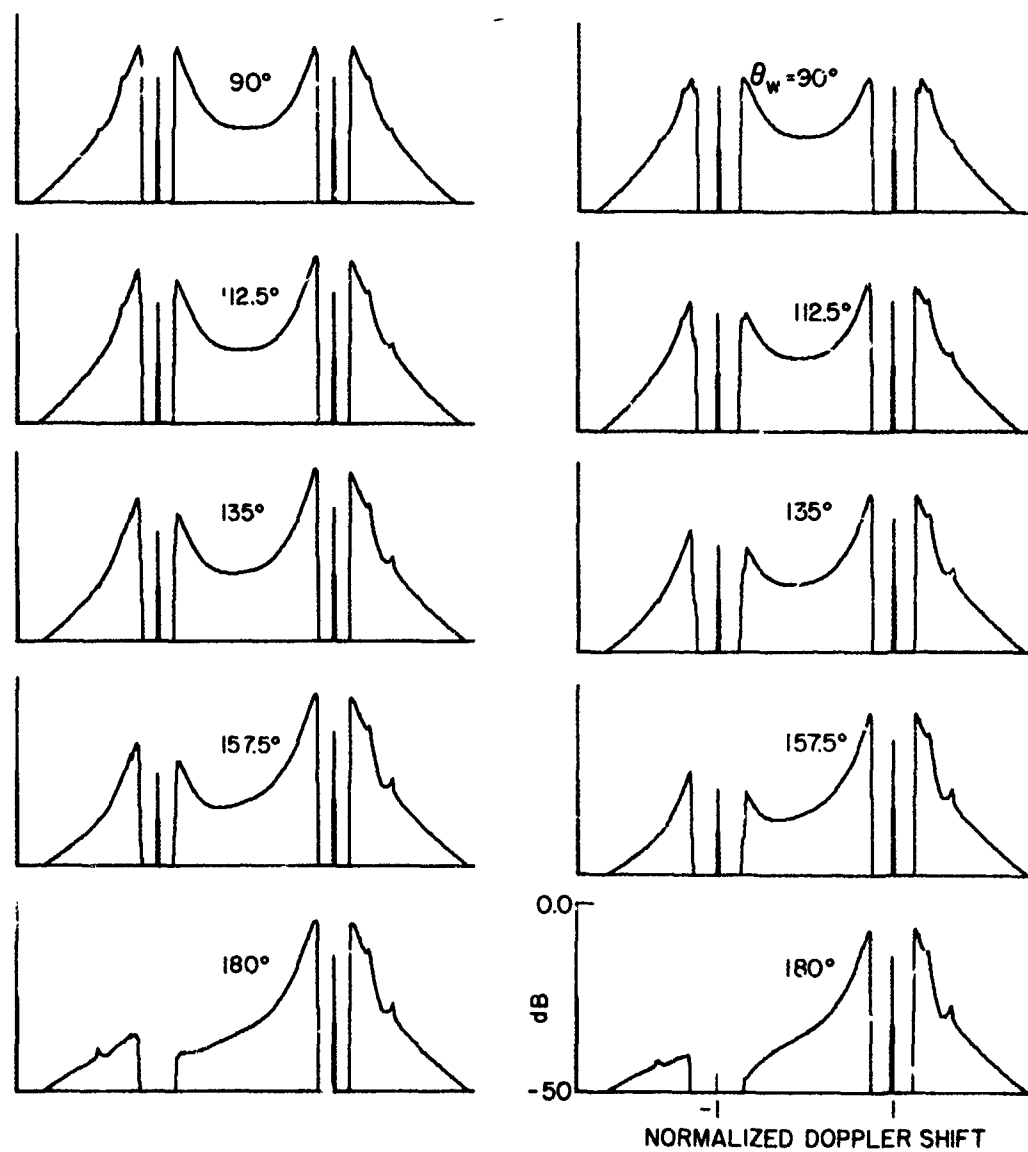NORMALIZED DOPPLER SHIFT

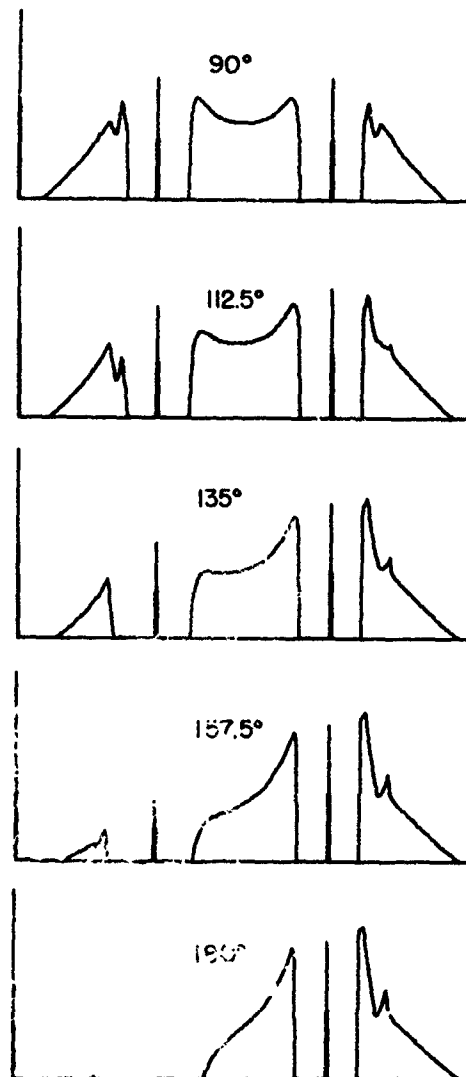c. 20 knots

d. 15 knots

Fig. 81. CONTINUED.

213

e. 10 knots

Fig. 81. CONTINUED.

214

a. 40 knots   b. 30 knots

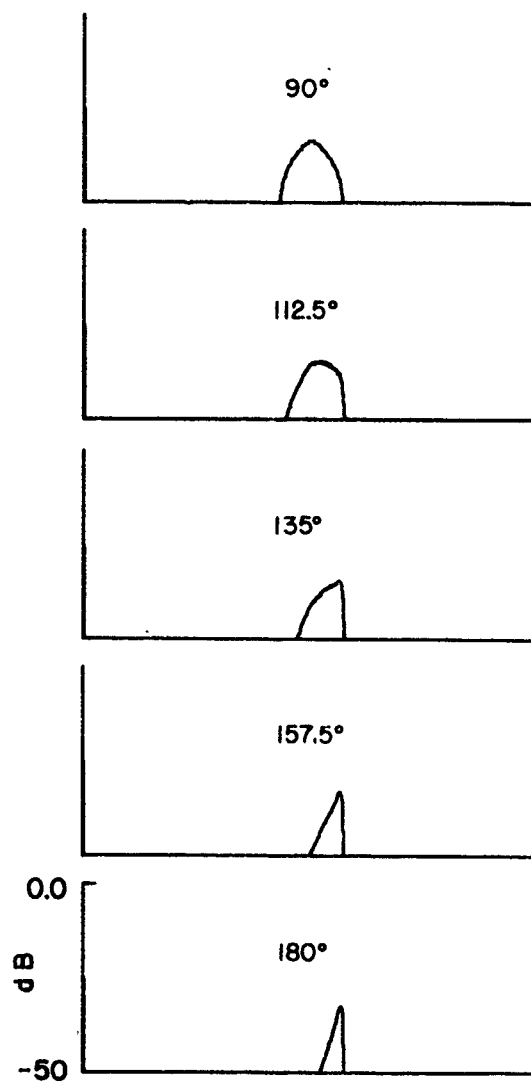Fig. 82. INCREMENTAL RADAR CROSS SECTION FOR A MUNK WAVE-HEIGHT SPECTRUM.

215

c. 20 knots   d. 15 knots

Fig. 82. CONTINUED.

90°

112.5°

135°

157.5°

0.0

dB

180°

-50

e. 10 knots

Fig. 82. CONTINUED.

217

a. 40 knots b. 30 knots
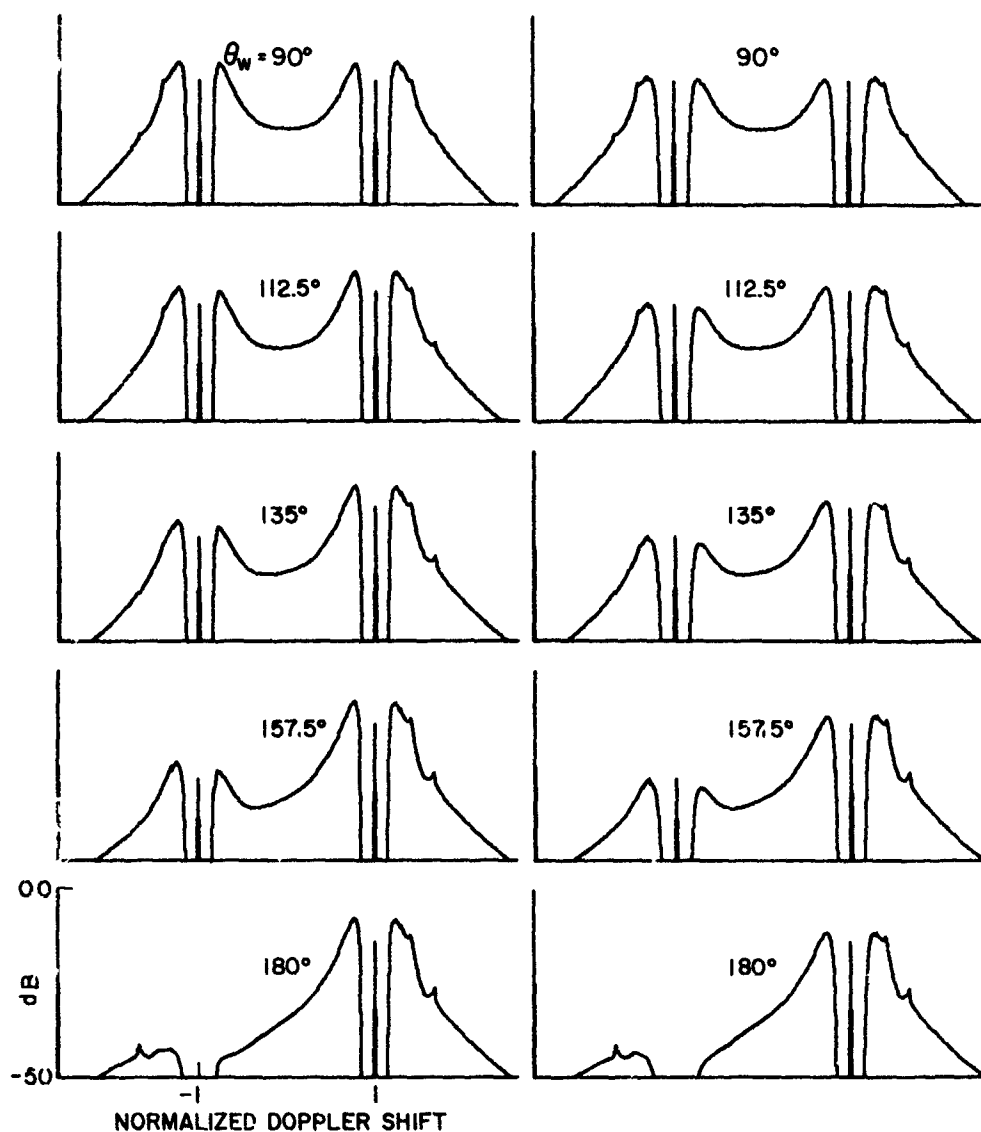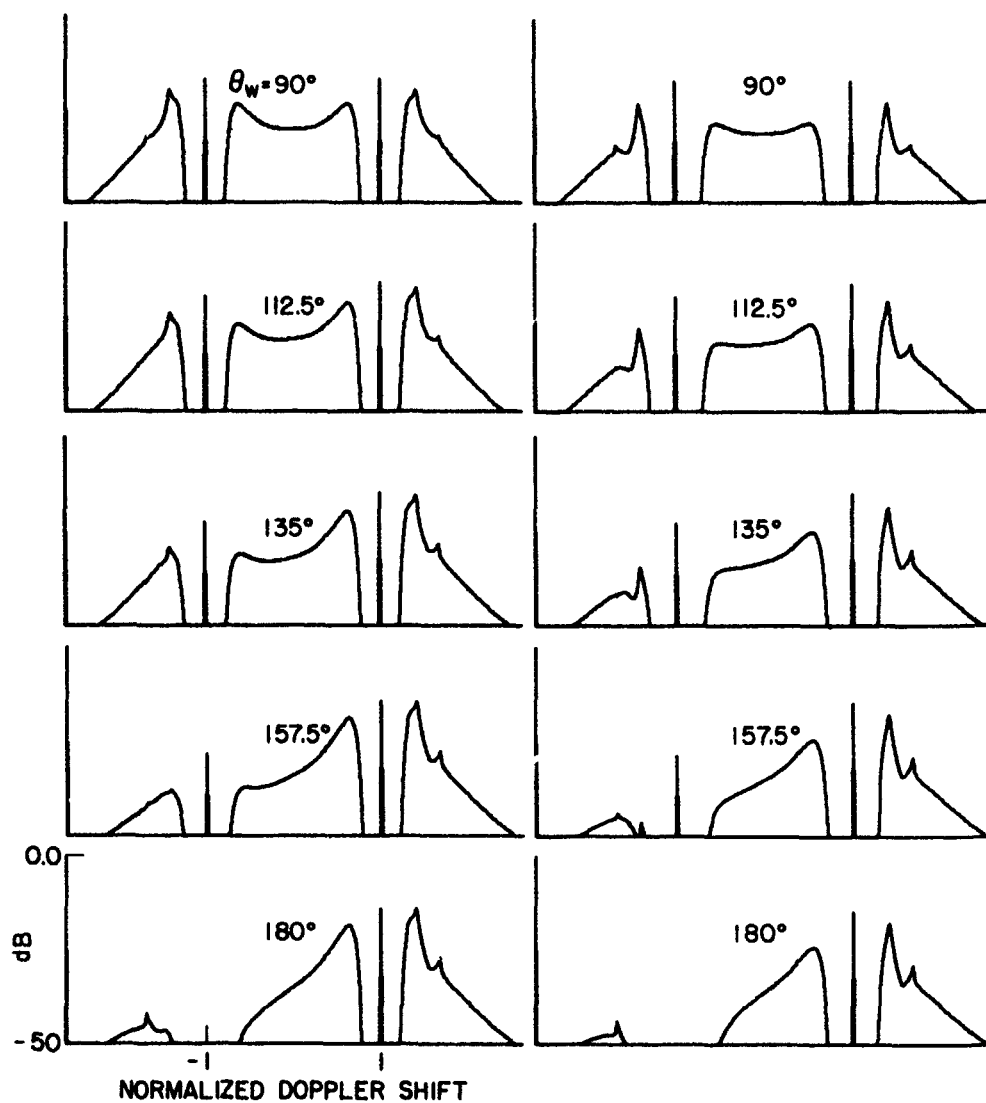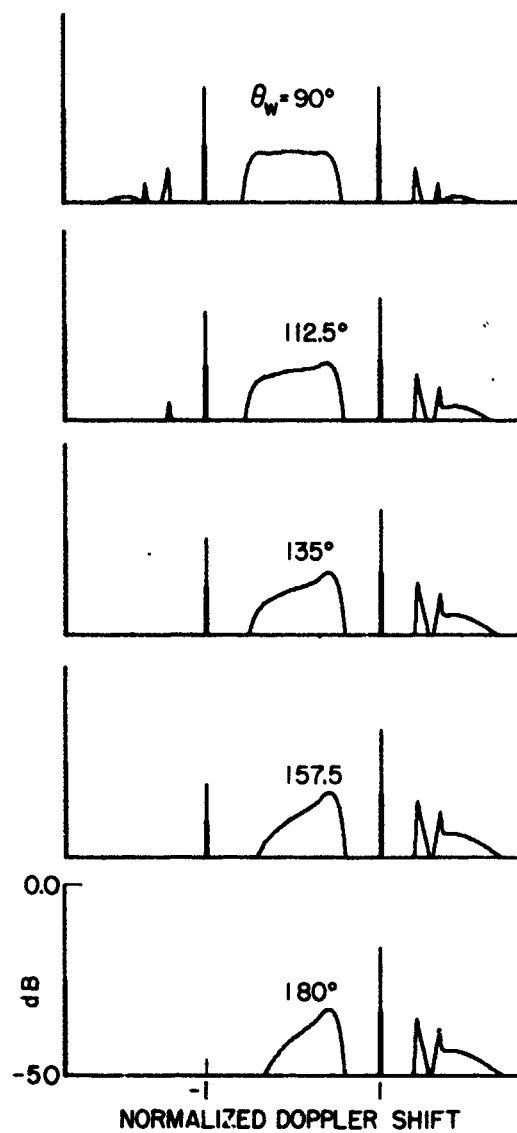
Fig. 83. INCREMENTAL RADAR CROSS SECTION FOR PIERSON-MOSKOWITZ COSINE-SQUARED WAVE-HEIGHT SPECTRUM.

c. 20 knots   d. 15 knots

Fig. 83. CONTINUED.

θ_w = 90°

112.5°

135°

157.5

180°

0.0

dB

-50

-1   1

NORMALIZED DOPPLER SHIFT

e. 10 knots

Fig. 83. CONTINUED.

BIBLIOGRAPHY

Barrick, D. E., "The Interaction of HF/VHF Radio Waves with the Sea Surface and Its Implications," paper presented at AGARD meeting, Paris, France, 22-26 Jun 1970.

Barrick, D. E., "Theory of HF and VHF Propagation across the Rough Sea," Radio Science, 6, 5, pp. 517-544, 1971.

Barrick, D. F., "Remote Sensing of Sea State by Radar," in Remote Sensing of the Troposphere (V. E. Derr, ed.), U.S. Government Printing Office, Washington, D.C., Ch. 12, 1972.

Barrick, D. E., J. M. Headrick, R. W. Bogle, and D. D. Crombie, "Sea Backscatter at HF: Interpretation and Utilization of Echo," Proc. IEEE, 62, 6, pp. 673-680, 1974.

Bracewell, Ron, The Fourier Transform and Its Applications, McGraw-Hill Book Co., New York, 1965.

Brillouin, L., Wave Propagation in Periodic Structures (2nd edition), Dover Publications, New York, 1953.

Cheng, David K., Analysis of Linear Systems, Addison-Wesley Publishing Co., Inc., Reading, Mass., 1959.

Crombie, D. D., "Doppler Spectrum of Sea Echo at 13.56 Mc/s," Nature, 175, pp. 681-682, 1955.

Hasselmann, K., "Determination of Ocean Wave Spectra from Doppler Radio Return from the Sea Surface," Nature Phys. Sci., 229, pp. 16-17, 1971.

Herriot, John G., Methods of Mathematical Analysis and Computation, John Wiley & Sons, Inc., New York, 1963.

Johnstone, D. L. and G. L. Tyler, "Interpretation and Evaluation of a Second-Order Expression for High-Frequency Radar Cross Sections of Ocean Surfaces," Program and Abstracts for International Union of Radio Science annual meeting, Oct 1974, p. 64.

Jordan, Edward C., Electromagnetic Waves and Radiating Systems, Prentice-Hall, Inc., Englewood Cliffs, N.J., 1950.

Kinsman, Blair, Wind Waves: Their Generation and Propagation on the Ocean Surface, Prentice-Hall, Inc., Englewood Cliffs, N.J., 1965.

Phillips, O. M., "The Equilibrium Range in the Spectrum of Wind Generated Waves," J. Fluid Mech., 4, pp. 426-434, 1958.

Phillips, O. M., The Dynamics of the Upper Ocean, Cambridge University Press, London, 1966.

Pierson, Willard J., Jr. and Lionel Moskowitz, "A Proposed Spectral Form for Fully Developed Wind Seas Based on the Similarity Theory of S. A. Kitaigorodskii," J. Geophys. Res., 69, 24, pp. 5181-5190, 1964.

Ramo, Simon and John R. Whinnery, Fields and Waves in Modern Radio (2nd edition), John Wiley & Sons, Inc., New York, 1953.

Rice, Stephen O., "Reflection of Electromagnetic Waves from Slightly Rough Surfaces," Comm. Pure Appl. Math., 4, 1951.

Skolnik, Merrill I., Introduction to Radar Systems, McGraw-Hill Book Co., Inc., New York, 1962.

Sokolnikoff and Redheffer, Mathematics of Physics and Modern Engineering, McGraw-Hill Book Co., New York, 1958.

Stewart, R., private communication.

Stratton, Julius Adams, Electromagnetic Theory, McGraw-Hill Book Co., New York, 1941.

Teague, C. C., G. L. Tyler, J. W. Joy, and R. H. Stewart, "Synthetic Aperture Observations of Directional Height Spectra for 7s Ocean Waves," Nature Phys. Sci., 244, 137, pp. 98-100, Aug 1973.

Thomas, John B., An Introduction to Statistical Communication Theory, John Wiley & Sons, New York, 1969.

Tyler, G. L., W. E. Faulkerson, A. M. Peterson, and C. C. Teague, "Second-Order Scattering from the Sea: Ten-Meter Observations of the Doppler Continuum," Science, 177, 28 Jul 1972, pp. 349-351.

Tyler, G. L., C. C. Teague, R. H. Stewart, A. M. Peterson, W. H. Munk, and J. W. Joy, "Wave Directional Spectra from Synthetic Aperture Observations of Radio Scatter," Deep Sea Research, 21, pp. 989-1016, 1974.